Mode of action of a human cancer cell active toxin (Parasporin-3) from *Bacillus thuringiensis*

Barbara Domanska

Submitted for the award of Degree of Doctor of Philosophy

Department of Biochemistry

School of Life Sciences

University of Sussex

September 2016

Work not submitted elsewhere for examination

I hereby declare that this thesis has not been submitted in whole or in part to this or any other University for the award of a degree

Barbara Domanska

Dedication

To those who have the fear and do things anyway

Acknowledgements

I show gratitude to my supervisor, Dr Neil Crickmore, who is an excellent scientist and a remarkably just and considerate person, a sincere thank you for all the support and various opportunities. I give special thanks to Prof Michelle West for valuable advice and the use of tissue culture facilities, Dr Roger Phillips for assistance with the DIC microscopy, Prof Simon Morley, Prof George Kemenes, and Prof John Spencer for their advice. I thank Prof Jean-Louis Schwartz for a successful collaboration in the field of electrophysiology, as well as for the expertise and feedback received in this area. I thank Eva Fortea for conducting experiments with planar lipid bilayers.

I acknowledge the University of Sussex for giving me the opportunity to conduct my research and BBSRC for supporting me financially. I also thank the Society for Invertebrate Pathology (SIP) for a travel award to help cover the cost of the 48th SIP conference in Vancouver, Canada 2015 and the Research Development authorities at the University of Sussex for providing me with a grant to cover the cost of my research visit in Montreal, Canada 2016, where the electrophysiology experiments took place.

A special thanks to lab colleagues and friends. I thank Alicia Elhigazi who brought laughter into the lab and joy into my life, a big thank you for countless talks and support. I appreciate: Vidisha Krishnan, Heather Collins, Wided Souissi, Aminah Barqawi, Lazarus Joseph and others, whom I had the pleasure of meeting. I thank my amazing husband for looking after our kids, who made my escapes to the lab and writing possible and always believes in me, and my incredible mums, whose support was just invaluable. I thank God for this journey.

Abstract

Bacillus thuringiensis (*Bt*) crystal (Cry) proteins, used for decades as insecticidal toxins worldwide, are well known to be toxic to certain insects, but not to mammals. The three domain Cry toxins represent the biggest group with pore formation as a widely accepted model for insect killing. A novel group of Cry proteins has been identified known as parasporins. They do not show insecticidal or hemolytic activity, but exert a strong cytocidal effect against some human cancer cells. The preferential activity of parasporins has potential for anticancer drug design but at the same time the knowledge that some *Bt* toxins are able to kill mammalian cells may raise concerns about the use of *Bt*-based pesticides in the future. Out of 19 parasporins Parasporin-3 (PS-3) most closely resembles the commercially used insecticidal toxins and is toxic to a narrow range of human cancer cell lines. In this study the effect of recombinant PS-3 on the human hepatic cancer cell line HepG2 was investigated to elucidate its mode of action. Results are consistent with PS-3 being a pore forming toxin. The toxin induced: pore formation in artificial and biological membranes, irreparable membrane damage, cell swelling, rapid decrease in ATP levels and drop in metabolic activity. The toxin did not induce activation of caspases or oxidative stress. In response to the toxin, cells activated p38 MAPK, a conserved signalling pathway induced in host cells by pore forming toxins. PS-3 induced very stable lesions and p38 MAPK did not facilitate cell recovery. Identification of a proteinous receptor was unsuccessful, but the toxin interaction with the membrane was prevented by EGTA facilitated chelation of membrane associated cations, suggesting the existence of a cation dependent receptor.

List of abbreviations

A – ampere

BAPTA – 1, 2 – bis (o-aminophenoxy) ethane - *N,N,N',N'*-tetraacetic acid

BBMV - brush border membrane vesicle

bp - base pairs

BSA - bovine serum albumin

Bt – Bacillus thuringiensis

°C - degrees Celsius

cAMP - 3', 5' - cyclic adenosine monophosphate

CAPS – 3 - (cyclohexylamino) – 1 - propanesulfonic acid

Cry - crystal

Cyt – cytolytic

Da - Dalton

DIC - differential interference contrast

DMEM - Dulbecco's modified Eagle medium

DMF - *N, N* - dimethylformamide

DMSO - dimethyl sulfoxide

DNA - deoxyribonucleic acid

DPBS - Dulbecco's phosphate-buffered saline

DTPA – 2 - [Bis [2 - [bis (carboxymethyl) amino] ethyl] amino] acetic acid

DTT - dithiothreitol

EC_{50} - half maximal effective concentration

ECL - enhanced chemiluminescence

E.coli - *Escherichia coli*

EDTA – 2, 2', 2'', 2''' - (Ethane - 1, 2 - diyldinitrilo) tetraacetic acid

EGTA – ethylene glycol – bis (2 - aminoethylether) - *N,N,N',N'* - tetraacetic acid

F - farad

FCS – fetal calf serum

FITC - fluorescein isothiocyanate

FPLC - fast protein liquid chromatography

G - conductance

g – gram

HA - human influenza hemagglutinin

HEPES – 2 - [4 - (2 - hydroxyethyl) piperazin – 1 - yl] ethanesulfonic acid

HRP - horseradish peroxidase

Hz - hertz

I – current

l - litre

LB - Luria Bertani

M – molar concentration

m - meter

MβCD - methyl-β-cyclodextrin

MEM – modified Eagle medium

min – minute(s)

MW – molecular weight

NOG - N-octyl-β-D-glucoside

NP-40 – nonidet-P40

OD_{600} - optical density measured at 600 nm

PAGE - polyacrylamide gel electrophoresis

PBS – phosphate - buffered saline

PBS-T – phosphate - buffered saline with Tween - 20

PC - phosphatidylcholine

PCR – polymerase chain reaction

PE - phosphatidylethanolamine

PEG - polyethylene glycol

pI - isoelectric point

PI-PLC – phosphatidylinositol-specific phospholipase C

PKA – protein kinase A

PLB – planar lipid bilayer

PS-3 – Parasporin-3

PSG - penicillin, streptomycin, and glutamine

RFU – relative fluorescence units

RGB – resolving gel buffer

RIPA - radio immune - precipitation assay

RLU – relative luminescence units

RPMI - Roswell Park Memorial Institute medium

RT – room temperature

S – siemens

SDS - sodium dodecyl sulphate

SEM - standard error of the mean

SGB – stacking gel buffer

TBE – tris - borate EDTA

TBS – tris - buffered saline

TBS-T - tris - buffered saline with Tween - 20

TEMED - *N*,*N*,*N*′,*N*′-tetramethylethylenediamine

TX-100 - triton X-100

V – volt

Vr – reversal potential

Ω - ohm

Table of contents

1. Introduction

1.1 *Bt* and its toxins

Bacillus thuringiensis (*Bt*) is a gram positive bacterium belonging to the *Bacillus cereus* group, which among others includes: *B. cereus, B. thuringiensis* and *B. anthracis* (Rasko et al., 2005). What distinguishes *Bt* from other *Bacillus* species is the presence of a parasporal crystal produced during sporulation (Vilas-Boas et al., 2007). *Bt* was first isolated in Japan in 1901, but is ubiquitously present worldwide in many environments, mainly in soil. Thousands of strains have been isolated (Martin and Travers, 1989), and over 80 different serovars have been described (Lecadet et al., 1999).

Bt was initially recognised as an insect pathogen due to its parasporal crystal inclusions, which are toxic to insects in their larval stages. For this reason *Bt* toxins have been used as bio-pesticides across the world, both in the form of sprays and transgenically expressed in crop plants (Bravo et al., 2011). However studies have shown that some *Bt* toxins also possess toxic activity towards mites, protozoa, nematodes (Schnepf et al., 1998) and also to human cancer cells (Mizuki et al., 1999b). Insecticidal properties of *Bt* toxins are mainly attributed to the δ-endotoxins within the crystal inclusions produced during bacterial sporulation and classified into two families: Cry and Cyt (Hofte and Whiteley, 1989).

In 1989, Höfte and Whiteley proposed a nomenclature and classification for crystal proteins based on amino acid sequence homology as well as their host range (Höfte and Whiteley, 1989). This was later revised by Crickmore et al. A four rank

system was devised for *Bt* toxin classification by the *Bacillus thuringiensis* Toxin Nomenclature Committee. Proteins are classified based on the degree of pairwise amino acid identity and not structure, target specificity or mode of action. A different primary (e.g. Cry1, Cry2), secondary (e.g. Cry1A, Cry1B), tertiary (e.g. Cry1Aa, Cry1Ab), and quaternary (e.g. Cry1Aa1, Cry1Aa2) rank mean that proteins share less than 45%, 78%, 95%, and ≤100% pairwise identity respectively (Crickmore et al., 1998, Crickmore, 2016).

The family of Cry toxins represent around 300 different crystal proteins (Crickmore, 2016), which are specifically toxic to insects from different orders such as: Lepidoptera, Diptera, Coleoptera, and Hymenoptera (Palma et al., 2014a) and will be discussed more in section 1.2.

Cyt toxins have been classified into four families (Crickmore, 2016). In vivo they are mostly toxic to dipteran insects, but some of them are able to kill coleopteran species (Soberón et al., 2013). A synergistic mosquitocidal effect was demonstrated between Cyt and Cry toxins, indicating an important role of Cyt toxins in the pathogenicity of *Bt* strains (Crickmore et al., 1995). In vitro Cyt toxins possess a general cytolytic activity against various cultured cells including erythrocytes (Thomas and Ellar, 1983a). Cyt protoxins are solubilised and activated in the insect midgut environment to an active 25 kDa toxin (Thomas and Ellar, 1983b). Crystal structure data indicate the presence of a single domain comprising of α-helical layers wrapped around a β-sheet (Cohen et al., 2011, Cohen et al., 2008, Li et al., 1996). Cyt toxins associate with membranes via interaction with lipids rather than proteins (Thomas and Ellar, 1983b). Two modes of action were proposed, reviewed by Soberón et al. One

involves oligomerisation and formation of a β-barrel pore. In the second, called the detergent model, toxin does not insert into a membrane but aggregates near the cell surface and causes damage by affecting lipid packing (Soberón et al., 2013).

Apart from Cyt and Cry toxins, the third family of *Bt* toxins - called the vegetative insecticidal proteins (Vip) - represents proteins secreted from cells into the medium in a non-crystal form during vegetative growth rather than sporulation (de Maagd et al., 2003). Vips are classified into four families (Crickmore, 2016), reviewed recently by Chakroun et al. (Chakroun et al., 2016). Vip1 and Vip2 represent an A+B type binary toxin highly toxic to some coleopteran species (Warren et al., 1998). Vip3 toxins are active against a wide range of lepidopterans (Donovan et al., 2006), while the target of Vip4 remains unknown. Vip toxins undergo proteolytic cleavage in the insect midgut followed by different mechanisms of action. Vip1 binds to cell membrane and translocates toxic component Vip2 into the cytoplasm, most likely by receptor mediated endocytosis or via a pore created by Vip1, where it facilitates ADP-ribosylation of actin (Chakroun et al., 2016). Vip3 was demonstrated to induce pore formation in planar lipid bilayers (Lee et al., 2003).

The classification of *Bt* toxins based on sequence homology is presented graphically in Figure 1. Figure 2 shows the arrangement of *Bt* δ-endotoxins based on target specificity.

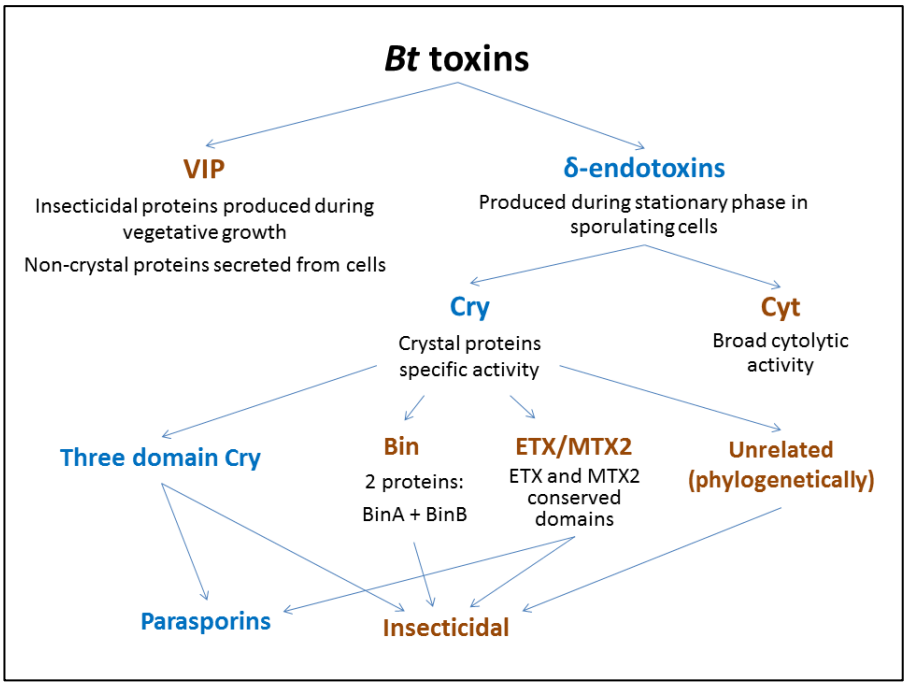

Figure 1 Classification of *Bt* toxins based on protein sequence homology.
The main virulence factors produced by *Bt* are δ endotoxins called Cry and Cyt. Some *Bt* strains additionally produce insecticidal non-crystal forming proteins Vips. Cry family consists of four phylogenetically different families: three domain, Bin, ETX/MTX2 and unrelated toxins.

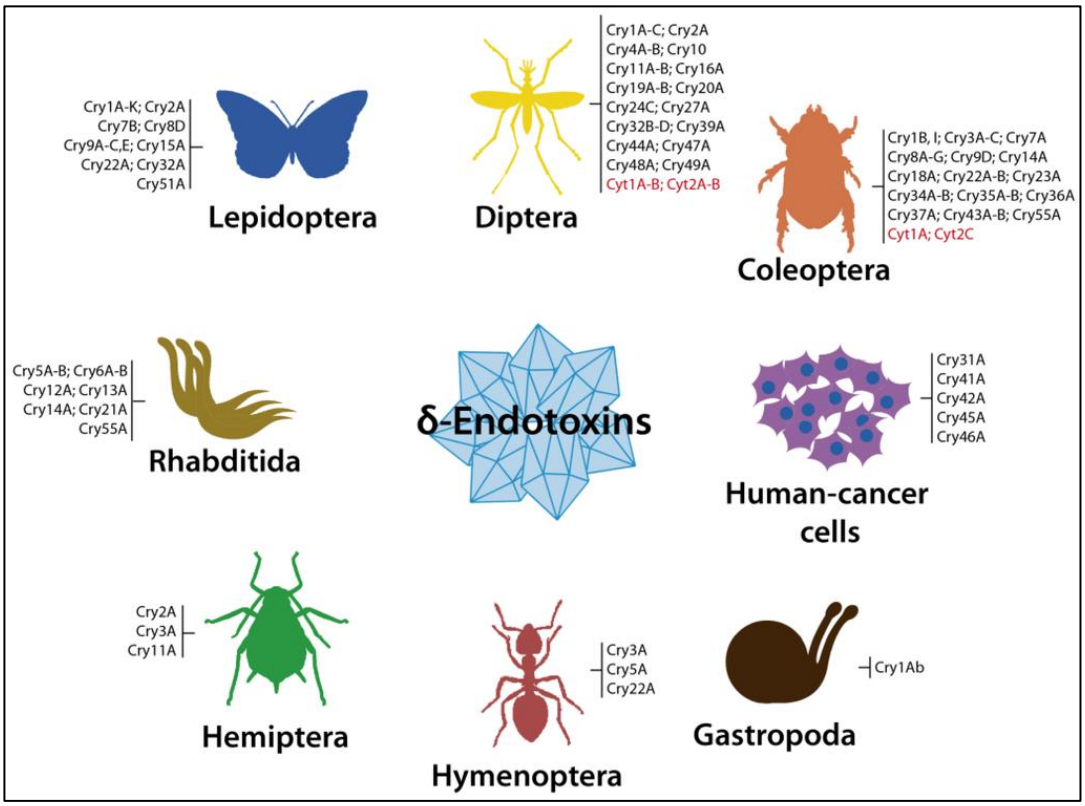

Figure 2 Diversity of hosts and *Bt* toxin organisation based on target specificity.
Host range and their pathogens showing *Bt* δ endotoxins (Cry and Cyt) grouped based on target specificity. Figure taken from Palma et al. (Palma et al., 2014a).

1.2 Introduction to Cry toxins

The name Cry derives from the fact that the proteins are contained in a parasporal crystal. They are synthesised during sporulation usually as protoxins which are then digested at the N- and/or C- terminus to form a toxic core (Schnepf et al., 1998). In some *Bt*, crystals can account for up to 25% of the dry weight of the sporulated cell (Agaisse and Lereclus, 1995). Although the Cry toxins are mainly found in parasporal crystals, some proteins have been found within the spore coat (Aronson et al., 1982). Genes encoding Cry toxins are thought to reside on large plasmids with many *Bt* strains containing multiple *cry* genes (Gonzalez et al., 1981).

To date, Cry toxins have been classified into 74 different types (Crickmore, 2016), which represent the largest group of insecticidal *Bt* toxins, with documented toxicity towards: lepidopterans (moths and butterflies), dipterans (flies), coleopterans (beetles), hemipterans (bugs, aphids and cicadas), hymenopterans (wasps, bees and ants), nematodes (worms), snails and cancer cells (Palma et al., 2014a). The main families within this group include: three domain, binary (Bin) and ETX/MTX2 toxins. Figure 3 shows a list of *Bt* toxins with colour coded families (list last updated August 2014).

Three-domain			ETX-MTX	Bin		Parasporin	
Cry1Aa	Cry2Aa	Cry8Aa	Cry15Aa	Cry31Aa	Cry40Aa	Cry58Aa	Cyt1Aa
Cry1Ab	Cry2Ab	Cry8Ab		Cry31Ab	Cry40Ba		Cyt1Ab
Cry1Ac	Cry2Ac	Cry8Ac	Cry16Aa	Cry31Ac	Cry40Ca	Cry59Aa	Cyt1Ba
Cry1Ad	Cry2Ad	Cry8Ad		Cry31Ad	Cry40Da	Cry59Ba	Cyt1Ca
Cry1Ae	Cry2Ae	Cry8Ba	Cry17Aa				Cyt1Da
Cry1Af	Cry2Af	Cry8Bb		Cry32Aa	Cry41Aa	Cry60Aa	Cyt2Aa
Cry1Ag	Cry2Ag	Cry8Bc	Cry18Aa	Cry32Ab	Cry41Ab	Cry60Ba	Cyt2Ba
Cry1Ah	Cry2Ah	Cry8Ca	Cry18Ba	Cry32Ba	Cry41Ba		Cyt2Bb
Cry1Ai	Cry2Ai	Cry8Da	Cry18Ca	Cry32Ca	Cry41Ca	Cry61Aa	Cyt2Bc
Cry1Ba	Cry2Aj	Cry8Db		Cry32Cb			Cyt2Ca
Cry1Bb	Cry2Ak	Cry8Ea	Cry19Aa	Cry32Da	Cry42Aa	Cry62Aa	Cyt3Aa
Cry1Bc	Cry2Ba	Cry8Fa	Cry19Ba	Cry32Ea			
Cry1Bd		Cry8Ga	Cry19Ca	Cry32Eb	Cry43Aa	Cry63Aa	Vip1Aa
Cry1Be	Cry3Aa	Cry8Ha		Cry32Fa	Cry43Ba		Vip1Ab
Cry1Bf	Cry3Ba	Cry8Ia	Cry20Aa	Cry32Ga	Cry43Ca	Cry64Aa	Vip1Ac
Cry1Bg	Cry3Bb	Cry8Ib	Cry20Ba	Cry32Ha	Cry43Cb		Vip1Ad
Cry1Bh	Cry3Ca	Cry8Ja		Cry32Hb	Cry43Cc	Cry65Aa	Vip1Ba
Cry1Bi		Cry8Ka	Cry21Aa	Cry32Ia			Vip1Bb
Cry1Ca	Cry4Aa	Cry8Kb	Cry21Ba	Cry32Ja	Cry44Aa	Cry66Aa	Vip1Bc
Cry1Cb	Cry4Ba	Cry8La	Cry21Ca	Cry32Ka			Vip1Ca
Cry1Da	Cry4Ca	Cry8Ma	Cry21Da	Cry32La	Cry45Aa	Cry67Aa	Vip1Da
Cry1Db	Cry4Cb	Cry8Na	Cry21Ea	Cry32Ma	Cry45Ba		
Cry1Dc	Cry4Cc	Cry8Pa	Cry21Fa	Cry32Mb		Cry68Aa	Vip2Aa
Cry1Ea		Cry8Qa	Cry21Ga	Cry32Na	Cry46Aa		Vip2Ab
Cry1Eb	Cry5Aa	Cry8Ra	Cry21Ha	Cry32Oa	Cry46Ab	Cry69Aa	Vip2Ac
Cry1Fa	Cry5Ab	Cry8Sa		Cry32Pa		Cry69Ab	Vip2Ad
Cry1Fb	Cry5Ac	Cry8Ta	Cry22Aa	Cry32Qa	Cry47Aa		Vip2Ae
Cry1Ga	Cry5Ad		Cry22Ab	Cry32Ra		Cry70Aa	Vip2Af
Cry1Gb	Cry5Ba	Cry9Aa	Cry22Ba	Cry32Sa	Cry48Aa	Cry70Ba	Vip2Ag
Cry1Gc	Cry5Ca	Cry9Ba	Cry22Bb	Cry32Ta	Cry48Ab	Cry70Bb	Vip2Ba
Cry1Ha	Cry5Da	Cry9Bb		Cry32Ua			Vip2Bb
Cry1Hb	Cry5Ea	Cry9Ca	Cry23Aa	Cry32Va	Cry49Aa	Cry71Aa	
Cry1Ia		Cry9Da		Cry32Wa	Cry49Ab		Vip3Aa
Cry1Ib	Cry6Aa	Cry9Db	Cry24Aa			Cry72Aa	Vip3Ab
Cry1Ic	Cry6Ba	Cry9Dc	Cry24Ba	Cry33Aa	Cry50Aa		Vip3Ac
Cry1Id		Cry9Ea	Cry24Ca		Cry50Ba	Cry73Aa	Vip3Ad
Cry1Ie	Cry7Aa	Cry9Eb		Cry34Aa			Vip3Ae
Cry1If	Cry7Ab	Cry9Ec	Cry25Aa	Cry34Ab	Cry51Aa	Cry74Aa	Vip3Af
Cry1Ig	Cry7Ba	Cry9Ed		Cry34Ac			Vip3Ag
Cry1Ja	Cry7Bb	Cry9Ee	Cry26Aa	Cry34Ba	Cry52Aa		Vip3Ah
Cry1Jb	Cry7Ca	Cry9Fa			Cry52Ba		Vip3Ai
Cry1Jc	Cry7Cb	Cry9Ga	Cry27Aa	Cry35Aa			Vip3Ba
Cry1Jd	Cry7Da			Cry35Ab	Cry53Aa		Vip3Bb
Cry1Ka	Cry7Ea	Cry10Aa	Cry28Aa	Cry35Ac	Cry53Ab		Vip3Ca
Cry1La	Cry7Fa			Cry35Ba			
Cry1Ma	Cry7Fb	Cry11Aa	Cry29Aa		Cry54Aa		Vip4Aa
Cry1Na	Cry7Ga	Cry11Ba	Cry29Ba	Cry36Aa	Cry54Ab		
Cry1Nb	Cry7Gb	Cry11Bb			Cry54Ba		Sip1Aa

Figure 3 A list of *Bt* toxins.
The figure lists *Bt* toxins according to their primary rank (proteins with the same quaternary rank are not listed) with colour-coded families. The majority of Cry toxins belong to the three domain Cry toxin family - depicted in blue. Two other families: Bin and ETX/MTX2 are coloured in pink and orange respectively. Cry toxins highlighted with other colours represent toxins unrelated to other Cry toxins and not classified into existing Cry toxin families. Additionally, parasporins are written in red. Figure was taken from Adang et al. (Adang et al., 2014).

The three domain Cry toxins represent the largest group of insecticidal *Bt* proteins, active mostly against Lepidoptera, Diptera, Coleoptera, Hemiptera and nematodes (Palma et al., 2014a). They share the five conserved blocks of amino acids in the sequence of the toxic core and a distinct three domain structure. Protoxins generally have two different lengths: around 70 and 130 kDa. The C-terminus of the protoxin often contains additional three conserved blocks 6-8, but is not required for toxicity (Schnepf et al., 1998). It is rich in cysteine residues and believed to be essential for crystal formation by facilitating the creation of the disulfide bonds between these residues within the crystals (Bietlot et al., 1990, Du et al., 1994).

Several crystal structures of the three domain toxins have been solved by X-ray crystallography: Cry1Aa, Cry1Ac, Cry2Aa, Cry3Aa, Cry3Bb, Cry4Aa, Cry4Ba, Cry5B and Cry8Ea (Li et al., 1991, Grochulski et al., 1995, Morse et al., 2001, Galitsky et al., 2001, Boonserm et al., 2006, Guo et al., 2009, Hui et al., 2012, Derbyshire et al., 2001, Boonserm et al., 2005). Examples of the three domain structure are shown in Figure 4.

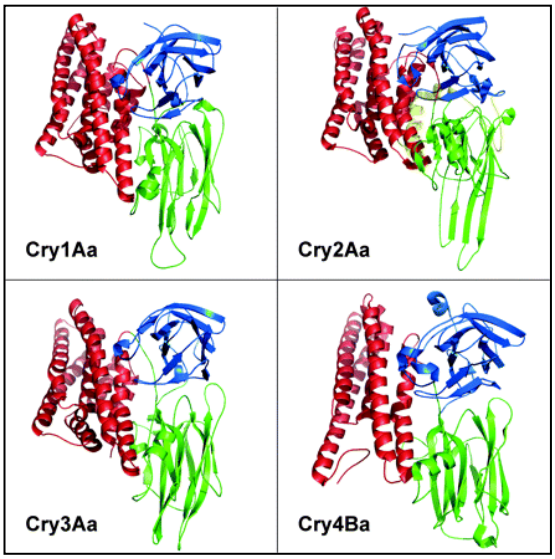

Figure 4 Architecture of the three domain Cry toxins.
Crystal structures of Cry1Aa, Cry2Aa, Cry3Aa and Cry4Ba showing the three domain structure common in some *Bt* Cry toxins. Domain I, II, and III are represented in red, green, and blue, respectively. Figure taken from Pigott and Ellar et al. (Pigott and Ellar, 2007).

Domain I, located at the N-terminus, is made up of 7-8 α-helices with a central hydrophobic α-helix 5. It is involved in membrane insertion and pore formation (Li et al., 1991). An umbrella model was postulated where α-helices 4 and 5 insert into the membrane by forming a hydrophobic hairpin, whereas the other α-helices lay flat on the surface of the cell membrane (Li et al., 1991). The middle domain II is comprised of three antiparallel β-sheets and plays an important role in receptor binding and specificity (Schnepf et al., 1998). At the base of domain II there are three flexible loops, with the second and the third one being principally involved in receptor recognition and binding (Adang et al., 2014). Domain III is a two antiparallel β-sheet sandwich that is also involved in receptor binding and possibly in pore formation (Li et al., 1991). It resembles a galactose binding domain and contains conserved blocks 3-5 (Adang et al., 2014).

The mechanism of action of the three domain Cry toxins is discussed in section 1.4. Cry toxin receptors are described in section 1.6.

The ETX/MTX2 family includes 11 members structurally very different from the three domain Cry toxins. They show sequence similarity to ETX - epsilon toxin from *Clostridium perfringens* and MTX2 - a mosquitocidal toxin from *Lysinibacillus sphaericus* (formerly *Bacillus sphaericus*) (Adang et al., 2014). Structurally this group is also related to aerolysin type β-pore forming toxins (PFTs) with elongated structures rich in β-sheets (Knapp, 2010); presented in section 1.3, Figure 5. Some toxins in this group, e.g. Cry23 and Cry37 exist as binary toxins, despite the lack of homology to Bin toxins (Palma et al., 2014a). MTX toxins are widely present in *L. sphaericus* strains and have mosquitocidal activities, but MTX related proteins found in *Bt* show toxicity

against some lepidopteran and coleopteran species (de Maagd et al., 2003). ETX forms β-barrel pores in the membranes of susceptible cells (Popoff, 2011). Due to structural homology ETX/MTX2 Cry proteins are believed to share a similar mode of action (Adang et al., 2014).

The class of binary toxins (Bin) comprises of 13 proteins. They resemble Bin toxins found in the mosquitocidal strains of *L. sphaericus*, which are composed of two homologous components: Bin A and Bin B, both required for full toxicity. After solubilisation and proteolytic activation in insect midgut, Bin B is required for receptor binding, which is followed by cell death facilitated most likely by pore formation (de Maagd et al., 2003). However toxin internalization was also observed (Opota et al., 2011) and the exact mode of action remains to be clarified (Berry, 2012). Contrary to Bin toxins from *L. sphaericus*, Bins found in *B. thuringiensis* strains show little homology between each other and their mechanism of action is unclear (Adang et al., 2014). E.g. Cry35 is toxic towards the coleopteran *Diabrotica virgifera virgifera* only in the presence of unrelated Cry34 (Ellis et al., 2002).

1.3 Introduction to parasporins

There are a great number of *Bt* strains with no known insecticidal activity (Meadows et al., 1992). Therefore researchers in the past began to look for other activities associated with these strains. In 1999 Mizuki et al. screened the activated toxins from 1744 *Bt* strains against human leukemic T-cells (MOLT-4). Hemolytic activity against sheep erythrocytes was tested as well. Out of 1684 strains with no hemolytic activity,

42 showed cytotoxic activity against these cancer cells. These strains did not show significant insecticidal activity when tested against 11 insect species of five orders: Lepidoptera, Diptera, Orthoptera (grasshoppers and crickets), Dictyoptera (cockroaches), and Isoptera (termites). Furthermore, a few proteins showed preferential activity, being able to discriminate between cancerous and healthy T cells, killing the former (Mizuki et al., 1999b). The results of this study revealed for the first time cytocidal activity of *Bt* Cry proteins against cancerous cells. After that report, further toxins with human cancer cell activity have been identified. A new group of *Bt* toxins was devised - named parasporins – described as: '*B. thuringiensis* and related bacterial parasporal proteins that are non-hemolytic but capable of preferentially killing cancer cells' (Katayama et al., 2005b) and their application in the medical field was suggested (Ohba et al., 2009, Mizuki et al., 1999a).

To date 19 parasporins have been discovered. They were classified into 6 families, parasporin (PS) 1-6, by the Committee of Parasporin Classification and Nomenclature based on the primary amino acid sequence of protoxins (http://parasporin.fitc.pref.fukuoka.jp/intro.html). Similarly to other Cry toxins, a novel parasporin is assigned a four rank name based on the degree of sequence identity to previously identified toxins (Crickmore et al., 1998). In addition to already classified parasporins, many *Bt* strains showing anticancer activities have been isolated around the world, e.g. LDC-391 from India (Poornima et al., 2010), 64-1-94 from Caribbean Islands (Gonzalez et al., 2011a), and *Bt*18 isolated in Malaysia (Nadarajah et al., 2008).

Anticancer activity of parasporins however does not mean that they do not affect normal cells at all. Initial studies on PS-1 reported low to moderate activity of

the native toxin against normal lung cells (Mizuki et al., 2000). Some cytopathic effects were observed in normal T-cells after exposure to recombinant PS-2 (Ito et al., 2004). Cytotoxicity was also induced in normal T-cells (Saitoh et al., 2006) and normal uterine UtSMC cells by recombinant PS-4 (Okumura et al., 2005), as well as UtSMC and normal lung MRC-5 cells by recombinant PS-5 (Ekino et al., 2014). Also, parasporins are not expected to have evolved to kill cancer cells, therefore their target insect(s), although currently unknown, may be present in nature. For example, Palma et al. already reported a novel Cry toxin related to PS-3 (40% pairwise identity), which possess specific toxic activity against the aphid *Myzus persicae* (Palma et al., 2014b).

Parasporins differ in many aspects. Some of them share the five conserved blocks and the three domain structure. However, in general homology with each other or with other proteins is low. Based on their molecular weight size parasporins can be divided into two groups. Parasporins processed to the active form of around 60 kDa include: PS-1, PS-3 and PS-6, which with varying degrees contain the five conserved Cry toxin blocks characteristic of three domain toxins. Parasporins 2, 4 and 5 are cleaved to a smaller mass fragment of around 30 kDa (details in Table 1). Parasporins target different cell lines and different levels are required for cytotoxicity. They also have different cytotoxic spectra; some are cytotoxic to a wide range of cancer cell lines, whereas others affect only a few of them. Sensitive cells do not seem to possess any obvious common characteristics responsible for susceptibility towards parasporin(s). More importantly, the mechanism of cell killing seems to be different. Also, different morphological effects have been observed after treatment with the same parasporin depending on the cell type. At present, only the cytotoxic effects of parasporins: 1, 2

and 4 have been closely examined, and each toxin appears to have a distinct mode of action (Ito et al., 2004, Ohba et al., 2009).

Parasporin-1 (Cry31Aa1 from strain A1190)

PS-1 presents cytocidal activity towards HeLa, HL-60, MOLT-4 and HepG2 cells (Katayama et al., 2005a). The toxin shows low (<25%) amino acid sequence homology to existing *Bt* proteins. It contains the five blocks conserved in three domain Cry toxins but sequence homology is low, particularly within the third block (Mizuki et al., 2000). Proteolytic cleavage resulted in two tightly associated polypeptides of 15 and 56 kDa (Katayama et al., 2005a). Its crystal structure was resolved at 1.76 Å resolution, but only incomplete data was released into the public domain. The protein showed a three domain structure common to insecticidal Cry toxins with an additional N-terminal region resembling that seen with Cry2Aa (PDB ID: 1I5P) (Akiba et al., 2005, Akiba and Okumura, 2016).

A novel mechanism of action was proposed for PS-1. The toxin seems to activate apoptotic signalling in HeLa cells causing rapid Ca^{2+} influx, without alterations in membrane permeability (Katayama et al., 2007). PS-1 decreased cell viability gradually. Cytopathic effects, like cell ballooning were observed only after 8 – 10 hours in susceptible HeLa and MOLT-4 cells, despite a relatively high toxin dose being used (10 μg/ml). This is the first parasporin reported that did not effectively compromise membrane integrity. The membrane of susceptible cells stayed polarized and impermeable to a small DNA binding dye within 30 minutes of PS-1 treatment. Also, there was no significant release of a big cytosolic marker (LDH) within 4 hours

(Katayama et al., 2007). Instead, within the first few minutes of treatment levels of intracellular Ca^{2+} increased, indicated by the intracellular calcium probe Fura-2. Calcium influx was from extracellular space as cytotoxicity was reduced in medium with low Ca^{2+} and it correlated with toxin dose and sensitivity levels of four cell lines tested. A set of various Ca^{2+} influx inhibitors were tested on PS-1 activity including voltage dependent Ca^{2+} channel antagonists. However only suramin, which inhibits G protein coupled receptors (GPCR), substantially reduced calcium influx and PS-1 cytotoxicity. Toxin also activated apoptotic signalling as indicated by increased caspase-3 levels and PARP cleavage in treated cells and inhibited protein and DNA synthesis. The authors proposed that PS-1 is not a pore forming toxin and its action involves the activation of GPCR, calcium influx and apoptosis resulting from disrupted calcium homeostasis (Katayama et al., 2007).

However, it is worth mentioning that a close homolog of PS-1 - designated as PS-1Aa2 or Cry31Aa2 (94% sequence identity) - was demonstrated to form pores in artificial membranes. Conductance values were not as big as the ones recorded for other Cry toxins (section 4.7), but the presence of ionic channels formed in the absence of cellular content and protein receptors may be a strong evidence of pore forming capacity of this group (Cry31A) of Cry toxins. Moreover, the same research group also reported Cry31Aa2 induced calcium oscillations, even in the absence of extracellular calcium and in non-cancer cell line HEK 293 (Gabriel Narvaez, 2014). Interestingly, the authors that revealed the PS-1 crystal structure proposed that the presence of the additional N-terminal region, which locks domain I, may be responsible for hindered pore formation of this particular toxin (Akiba et al., 2005, Akiba and Okumura, 2016).

In 2011 a patent application was published regarding the identification of a PS-1 receptor. In this document a tumor suppressor protein – beclin-1 – was reported as the PS-1 receptor in HeLa cells, based on experiments where anti-beclin-1 antibody suppressed toxin binding and cytotoxicity (Katayama et al., 2011).

Parasporin-2 (Cry46Aa1 from strain A1547)

PS-2 is highly cytotoxic to a wide range of cancer cell lines (Table 1), like MOLT-4, Jurkat, and HepG2 cells (Kitada et al., 2006); however the main cell line used in PS-2 research was HepG2. The activity of PS-2 was additionally tested in tumor slices. Tissues isolated from differentiated hepatocellular carcinoma and colon cancer were incubated with PS-2 resulting in cancerous but not non-neoplastic cells showing a cytopathic appearance (Ito et al., 2004, Kitada et al., 2006).

Immunofluorescence established toxin association with the plasma membrane of susceptible cells (Kitada et al., 2006). PS-2 induced rapid cell swelling and blebbing, disintegration of organelles and cytoskeleton in HepG2 cells. Swelling was observed in toxin treated MOLT-4 cells. Cell permeability assays measuring LDH release and PI staining demonstrated rapid membrane damage. Experiments with osmoprotective PEGs indicate that PS-2 induced the formation of large, up to 3 nm in diameter, pores (Kitada et al., 2006). Low doses of PS-2 induced caspase activation and DNA fragmentation in HepG2 cells; however a caspase inhibitor did not prevent cytotoxicity, indicating that the mode of action is primarily non-apoptotic (Ito et al., 2004).

PS-2 was targeted to the lipid rafts in HepG2 cells, where it required GPI -anchored proteins for oligomerization and cytotoxicity (Kitada et al., 2009, Okumura et

al., 2011). PS-2 formed ~200 kDa SDS-resistant membrane embedded oligomers in susceptible cells, a temperature dependent process that correlated with membrane permeability and was significantly inhibited by cholesterol depletion or membrane solubilisation (Abe et al., 2008). Further experiments that examined the effect of cholesterol depletion on cell viability showed only small contribution of cholesterol in cytotoxicity. Conversely, depletion of GPI-linked proteins with PI-PLC treatment significantly inhibited PS-2 activity due to decreased efficiency in binding and oligomerisation (Kitada et al., 2009).

The crystal structure of activated PS-2 was solved. The toxin is extremely elongated with dimensions of 115 x 30 x 29 Å. It has a track of serine and threonine residues exposed along the long axis, which is thought to play a role in oligomerisation and pore formation (Akiba et al., 2009b). The structure is different from the ones resolved for other three domain Cry and Cyt toxins. Based on primary amino acid sequence homology it does not belong to the ETX/MTX2 Cry toxin family (Figure 3), however structurally resembles one of them, as well as the proteins in the Toxin_10 family (which possess an additional beta trefoil motif in the head domain) and aerolysin-type β-PFTs (Figure 5), which supports a proposed pore formation activity of PS-2. It also shares structural similarity with hydralysin (Sher et al., 2005).

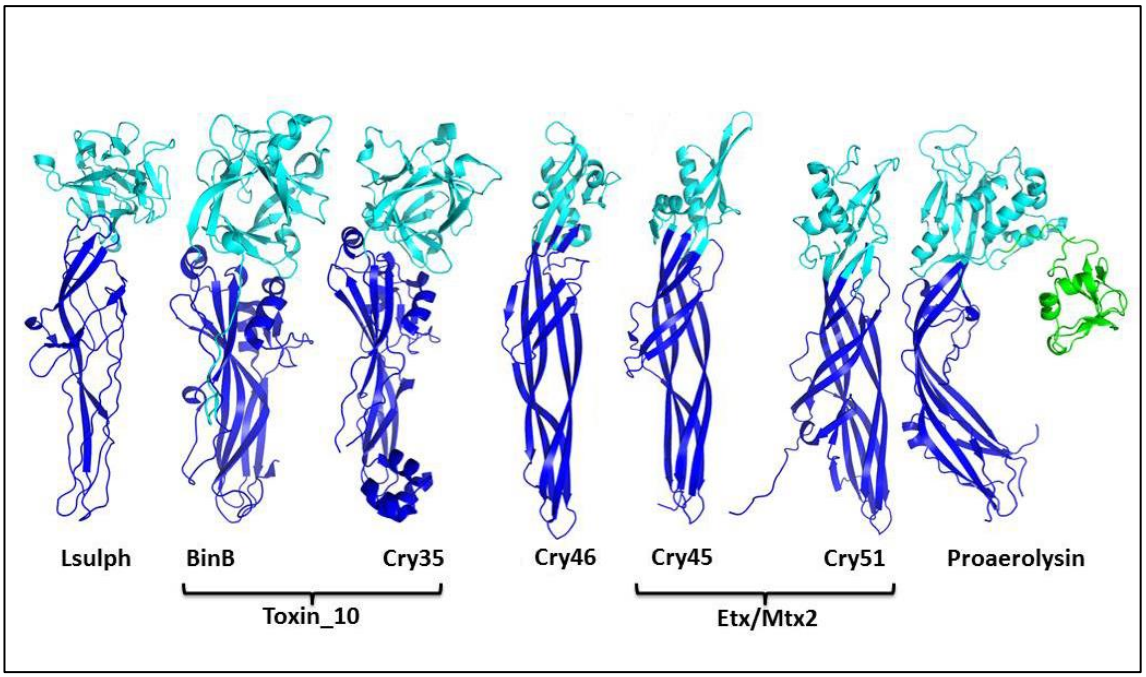

Figure 5 Crystal structure of PS-2 (Cry46) and its structural homologues.
PS-2 (Cry46) crystal structure was resolved at a resolution of 2.38 Å (PDB ID: 2ZTB). Its structural homologues include: Cry45 - a non-toxic protein related to PS-4 from A1470 *Bt* strain (PDB 2D42), Cry51 (PDB 4PKM) from *Bt*, BinB (PDB 3WA1) from *L. sphaericus*, Cry35 (PDB 4JP0) from *Bt*, lectin (Lsulph) from *L. sulphureus* (PDB 1W3A), and proaerolysin (PDB 1PRE) from *A. hydrophila*. Head domains are presented in light blue and tail domains in dark blue, with the extra domain in proaerolysin in green. Figure was edited from Berry et al. (Berry and Crickmore, in press).

Parasporin-3 (Cry41Aa and Cry41Ab from strain A1462)

Protein inclusions containing PS-3 were originally isolated from *Bt* strain designated 89-T-26-17 (later named A1462), from a soil sample in Tokyo, Japan (Mizuki et al., 1999b). This strain produced bi-pyramidal shaped crystals of differing sizes: 0.6-2 µm long, 0.4-1.1 µm wide (Yamashita et al., 2000). Genes encoding PS-3 were first identified and characterised in 2005 (Yamashita et al., 2005). DNA cloning and sequencing revealed the existence of two gene complexes, each comprised of three ORFs: ORF1, ORF2 and ORF3, located close to each other and orientated in the same direction. Putative ribosome binding sites were identified upstream of each ORF and no transcriptional terminator sequence was present in between the ORFs (Yamashita

et al., 2005). ORF1 encodes a hypothetical protein of 19 kDa (predicted MW). ORF2 codes for the 93 kDa (predicted MW) protein with cytocidal activities and contains the five conserved blocks (1-5) commonly found in Cry toxins and accountable for the three domain fold (Schnepf et al., 1998). Additionally, the C-terminus of the protein coded by ORF2 contains a sequence belonging to ricin superfamily (Yamashita et al., 2005), similar to that of *Clostridium botulinum* hemagglutinin HA-33 (Tsuzuki et al., 1990). 82 kDa (predicted MW) protein coded by ORF3 includes the additional three conserved blocks (6-8), lying outside the active toxic core in 130-140 kDa Cry protoxins, and believed to help facilitating crystallization and expression (Schnepf et al., 1998).

The two encoded toxins were designated as Cry41Aa1 and Cry41Ab1 by the *Bt* Toxin Nomenclature Committee (Crickmore, 2016). The deduced amino acid sequence of these two proteins uncovered a high degree of homology between them (87%, 88% and 99% homology between the proteins coded by ORFs: 1, 2 and 3 respectively). SDS PAGE analysis revealed that alkali solubilisation in the presence of DTT resulted in five major bands ranging from 88-180 kDa, while in the absence of DTT, solubilisation yielded only two 88 kDa proteins, indicating that the others stayed insoluble. Solubilized proteins did not possess cytocidal activity, unless treated with a protease. Proteinase K treatment cleaved 88 kDa protoxin to 64 kDa active toxin. N-terminal sequencing detected ORF2 sequence in the 88 and 64 kDa bands, whereas ORF3 sequence was found in 120 kDa band (Yamashita et al., 2005). Digests with other proteases (trypsin, chymotrypsin) resulted in two bands (around 64 and 80 kDa) and a lower cytocidal activity against MOLT-4 cells compared to activation with proteinase K (Yamashita et al., 2000).

In the initial screen of 1744 *Bt* parasporal proteins against human cells 124 µg/ml of activated PS-3 (in the study addressed as 89-T-26-17) showed cytotoxic activity against human leukemic T-cells (MOLT-4), but not to normal T-cells or human erythrocytes. It also showed little or no insecticidal activity against 11 insect species from five different orders (Mizuki et al., 1999b). In the succeeding study, dose response experiments with activated protein inclusions from A1462 against HeLa and MOLT-4 showed that EC_{50} for HeLa was 37.6, and >130 µg/ml for MOLT-4, whereas normal T-cells were unaffected even at a high 130 µg/ml dose (Yamashita et al., 2000). In the 2005 study, the cytopathic effect of purified Cry41Aa and Cry41Ab was tested individually using a broad range of mammalian cell lines (Figure 6).

Cell		Origin	EC_{50} (µg/ml)	
			Cry41Ab	Cry41Aa
Human				
	MOLT-4	Leukemic T cell	>10	>10
	Jurkat	Leukemic T cell	>10	>10
	HL60	Myeloid leukemia	1.32	1.25
	HeLa	Uterus cervix cancer	>10	>10
	TCS	Uterus cervix cancer	>10	>10
	Sawano	Uterus cancer	>10	>10
	HepG2	Hepatocyte cancer	2.80	1.86
	A549	Lung cancer	>10	>10
	CACO-2	Colon cancer	>10	>10
	T cell	Normal T cell	>10	>10
	UtSMC	Normal uterus	>10	>10
	HC	Normal hepatocyte	>10	>10
	MRC-5	Normal lung	>10	>10
Simian				
	Vero	African green monkey kidney	>10	>10
	COS-7*	African green monkey kidney	>10	>10
Murine				
	NIH3T3-3	Mouse embryo	>10	>10

Figure 6 Cytotoxicity of purified Cry41Aa and Cry41Ab proteins on mammalian cells.
Cytotoxicity of proteinase K activated, purified Cry41Aa and Cry41Ab was tested on various cell lines using an MTT cell viability assay 24 hours after toxin treatment. Figure was edited from Yamashita et al. (Yamashita et al., 2005).

Cry41Aa and Cry41Ab exhibited strong cytocidal activity only against HL-60 (myeloid leukaemia cancer) and HepG2 (liver cancer) cells with EC_{50} of 1.25 and 1.86 µg/ml respectively (for Cry41Aa). The other cells tested, including four human non-cancer cell types, were not affected by this toxin treatment. Decrease in viability (tested in an MTT assay) and membrane damage (assessed by LDH efflux assay) were more rapid in Cry41Aa treated cells, suggesting Cry41Aa was more toxic than Cry41Ab (Yamashita et al., 2005).

Morphological observations of compromised HepG2 cells (Figure 7) showed widespread swelling within one hour and a serious membrane damage within 24 hours detected with Trypan Blue staining (Yamashita et al., 2005). In the previous study, following application of high doses of PS-3, rapid cell swelling was also noted in HeLa and MOLT-4 cells, two cell lines reported later as non-susceptible to the toxin (Yamashita et al., 2005, Yamashita et al., 2000).

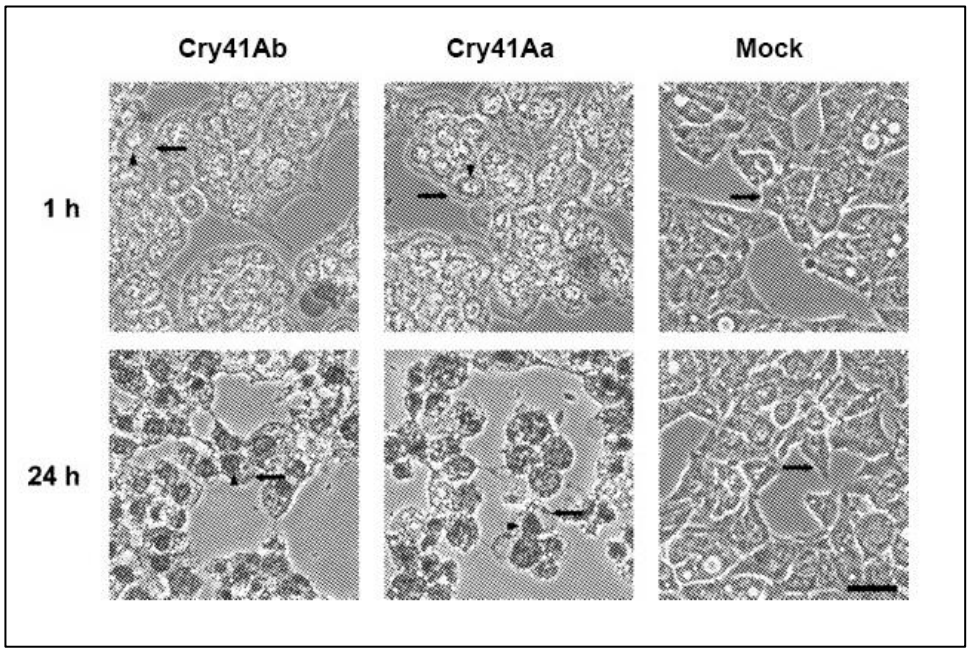

Figure 7 Morphological changes in HepG2 cells following PS-3 treatment.
The effect of Cry41Aa and Cry41Ab was recorded 1 and 24 hours post-treatment. Cells stained with Trypan Blue point to membrane damage (bar = 50 µm). Figure edited from Yamashita et al. (Yamashita et al., 2005).

As mentioned earlier, the *cry41Aa* gene exists as part of a three gene operon in the native A1462 strain. *cry41Aa* was expressed by Krishnan, et al. (Krishnan, 2013). PCR primers were designed to amplify the ORF2 and ORF3 and incorporate suitable restriction sites: a *Bam*HI 22 bp upstream from the ORF2 start codon and an *Xba*I 16 bp downstream of ORF3. These two ORFs and their ribosome binding sites were cloned into the *E. coli* - *Bt* expression vector pSVP27A (Crickmore and Ellar, 1992). This vector places cloned genes under the control of the promoter for the *Bt cyt1Aa* toxin gene. The resulting vector (pSVP2741Aa) was introduced into the acrystalliferous *Bt* strain 4D7 (Krishnan, 2013). In this work, the name Parasporin-3 (or PS-3) refers to the Cry41Aa protein, encoded by *cry41Aa* gene, expressed in the *Bt* 4D7 strain by Krishnan, et al. (Krishnan, 2013). Amino acid sequence of PS-3 ORF2 with conserved blocks and domains is presented in Figure 8.

Figure 8 Deduced amino acid sequence of PS-3 protoxin encoded by ORF2.
Putative domains marked with coloured boxes were identified based on sequence comparison with other three domain Cry toxins (Elhigazi et al. unpublished). Conserved blocs written in red are based on sequence comparison by Yamashita et al. (Yamashita et al., 2005). N- and C-terminal regions of the protoxin, incorporating a ricin type domain and most probably cleaved off by proteinase K, are positioned outside coloured boxes. Extra loop region in a blue box represents a region not found in other three domain Cry toxins.

According to Yamashita et al. cleavage by proteinase K occurs after alanine at position 60 and is prerequisite for toxicity (Yamashita et al., 2005). The N-terminal sequence analysis of trypsin cleaved PS-3 (upper band sequenced) may indicate that the cleavage takes place after arginine at position 63 (Souissi, unpublished). Similarly to many insecticidal Cry toxins, only a small portion of PS-3 is cleaved at the N-terminus with majority of processing done at the C-terminus (Schnepf et al., 1998).

Figure 9 shows predicted three dimensional structure of PS-3 protoxin generated by Phyre^2 (Kelley et al., 2015), viewed using UCSF Chimera 1.10.1 (Pettersen et al., 2004).

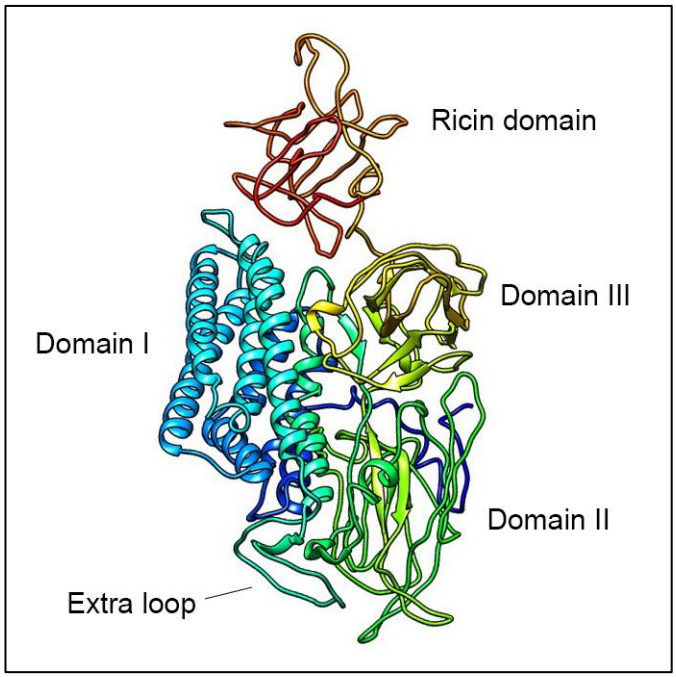

Figure 9 Structural model of PS-3 protoxin showing the three domain Cry toxin organisation.
Based on 13 templates 792 residues of PS-3 protoxin (96%) were modelled at >90% accuracy by Phyre^2. Domain I is represented by the blue helix bundle, domain II by the light green β-sheets and domain III by the yellow β-sandwich. C-terminal ricin domain is depicted in red and the unstructured extra loop of domain I is presented in light blue.

One notable aspect of this protein is that it is the only parasporin identified so far in which the five blocks are well conserved and is the most closely related to the insecticidal three domain Cry toxins. This poses a question whether similarity is also

reflected in their mode of action. Another feature of PS-3 is the presence of a ricin-type domain, which is not normally present in Cry toxins, as well as a short unstructured region located within domain I named the extra loop (Figure 8 and Figure 9). Whereas deletion of the 111 amino acids from the C-terminus containing the ricin domain did not abolish or decrease protein toxicity against HepG2 cells (Krishnan, 2013), the removal of 31 amino acids encoding the extra loop resulted in an unstable protein (Banani et al., unpublished). Furthermore, sequence comparison of PS-3 and insecticidal toxins identified a putative binding site, loop 3 in domain II of PS-3, which in insecticidal Cry toxins plays a major role in receptor binding (Pardo-Lopez et al., 2013a). Alanine scanning experiments, involving changing hydrophobic to alanine residues in this putative loop revealed that F509A and W511A mutations (but not Y514A) completely abolished PS-3 cytotoxicity. Further mutagenesis experiments showed that F509Y and W511F remained toxic contrary to F509W, F509S, and F509L. These results may indicate that amino acid with a single aromatic ring at position 509 and amino acid with aromatic rings at position 511 are important for the function of the toxin (Elhigazi et al., unpublished).

Parasporin-4 (Cry45Aa1 from strain A1470)

PS-4 exhibits toxicity mainly towards CACO-2, Sawano, and MOLT-4 cells (Okumura et al., 2005). Similar to PS-2, it does not contain the five conserved Cry blocks and showed low homology (<25%) to existing proteins. Structure of a close PS-4 homolog is presented in Figure 5. The authors suggested that PS-4 is an aerolysin type β-PFT due to high amount of β structure (51%) measured by a CD spectrum and a weak sequence

identity to β-PFTs like: α toxin from *C. septicum*, epsilon from *C. perfringens*, and aerolysin from *A. hydrophila* (Okumura et al., 2011).

A novel method of toxin activation in acidic conditions was described by Okumura et al. Toxin was solubilised in 10 mM HCl and activated with pepsin. While cytotoxic activity remained the same, the efficiency of a protein yield was 27 times higher compared to activation in alkaline conditions (Okumura et al., 2008, Okumura et al., 2006).

Within the first 10 minutes of PS-4 treatment swelling and membrane blebbing were observed in susceptible MOLT-4 cells. Over time shrinkage and disintegration of the nucleus occurred as early as 1 hour post-treatment and the cell burst within 24 hours. PS-4 induced membrane damage and formation of large pores in the membrane of MOLT-4 cells, as evidenced by the passage of 70 kDa dextrans and LDH efflux. Despite non-specific monomer binding observed in non-susceptible cells, SDS-resistant 90-200 kDa oligomers were detected only in susceptible cells, which increased in a time dependent manner after toxin treatment. Further research found little caspase activation following treatment with low or high doses of PS-4 and cholesterol independence (Okumura et al., 2011).

Interestingly, strain A1470 produces multiple proteins including PS-4 (Okumura et al., 2005), and a protein designated as PS-2Aa2, which differs from PS-2 (from strain 1547) by four amino acids (Okumura et al., 2013). It is consistent with the observation that inclusion proteins from A1470 strain were more toxic than recombinant PS-4 with EC_{50} towards MOLT-4 of 0.13 and 0.47 μg/ml respectively (Saitoh et al., 2006).

Parasporin-5 (Cry64Aa1 from strain A1100)

Out of 18 mammalian cell lines tested, PS-5 showed strong cytocidal activity (EC_{50} values below 0.1 μg/ml) against 5 human: MOLT-4, HepG2, TCS (uterus cervix cancer), HeLa, Sawano and 2 monkey kidney cell lines: COS7 and Vero. The 34 kDa protoxin was cleaved by proteinase K at the C-terminal to produce a 30 kDa toxin. Similarly to PS-2 and PS-4, the protein showed slight homology to aerolysin type β-PFTs (<35%). Microscopic observation revealed rapid cell swelling (MOLT-4) within the first hour of treatment. The mode of action is unknown, but it is predicted to act as a β-PFT, similarly to PS-4 (Ekino et al., 2014).

Parasporin-6 (Cry63Aa1, CP84 from strain M019)

Three cytotoxic proteins were isolated from strain M019. CP78A and CP78B were added into the PS-1 family based on sequence similarities. CP84 was assigned to a new parasporin-6 class. Trypsin activation of the 84 kDa protoxin produces two fragments (14 and 59 kDa), which together are toxic to HeLa and HepG2 cells. Interestingly, the N-terminus of the protoxin that shows structural homology to PS-1 is cleaved during the digestion step, and the resistant core partially resembles the three domain structure. It shows 56% sequence similarity with Cry2A toxin in the region of the five conserved blocks. After PS-6 treatment, cell swelling was apparent in both susceptible cell lines, with additional vacuole formation in HepG2 cells (Nagamatsu et al., 2010).

Table 1 presents a comparison of the best characterised parasporins so far: PS-1, PS-2, PS-3 and PS-4.

Table 1 Comparison of parasporins 1-4.

Human cell line origins: Jurkat (leukemic T-cell), HepG2 (liver cancer), Sawano (cervical cancer resistant to cisplatin treatment), MOLT-4 (acute lymphoblastic leukaemia), HL-60 (myeloid-granulocyte precursor in bone marrow- leukaemia), CACO-2 (epithelial colorectal adenocarcinoma cells), UtSMC (normal uterus smooth muscle cells), TCS (uterus cervix cancer).

	PS-1	PS-2	PS-3	PS-4
Native strain	84-HS-1-11; A1170	90-F-45-14; A1547	89-T-26-17; A1462	89-T-34-22; A1470
Cry designation	Cry31Aa1	Cry46Aa1	Cry41Aa1	Cry45Aa1
Serovar	*kurstaki*	*dakota*	Untypable	*shandongiensis*
Susceptible cancer cell lines (EC_{50} μg/ml):	HeLa (0.12), HL-60 (0.32), MOLT-4 (2.2), HepG2 (3)	Jurkat (0.015), HepG2 (0.023), Sawano (0.041), MOLT-4 (0.044), HL-60 (0.066)	HL-60 (1.25), HepG2 (1.86)	CACO-2 (0.12), Sawano (0.24), MOLT-4 (0.47), TCS (0.71), HL-60 (0.72), HepG2 (1.9)
Lethal dose used (μg/ml)	10	0.1	10	2-4
Activity towards normal cells (EC_{50} μg/ml)	Initial studies reported low to moderate activity against lung cells; UtSMC cells (>10)	T cells (0.148), hepatocytes (>10)	T cells (>10), hepatocytes (>10)	Significant activity against T cells of native and recombinant PS-4; recombinant PS-4 also cytotoxic to UtSMC
Activation enzyme	Proteinase K, trypsin	Proteinase K	Proteinase K	Proteinase K, pepsin
Protoxin (kDa)	81	37	88	31
Active fragment (kDa)	15 and 56 – heterodimer	30	64	27

Cleavage at a terminus	N	N and C	N and C	N and C
Conserved Cry toxin blocks	Blocks detected in 56 kDa fragment but low homology especially in block 3	Not present	Blocks 1-5 in the active fragment	Not present
Structural homology	Crystal structure resolved: similar to a three domain Cry toxin fold	Crystal structure resolved: similar to aerolysin type β-PFTs	Possibly similar to a three domain Cry toxin fold	Possibly similar to aerolysin type β-PFTs
Sequence homology	Low sequence homology to *Bt* proteins (<25%)	Low sequence homology to *Bt* proteins (<25%) and β-PFTs from other species. 41% sequence identity to hydralysin from *Ch. viridissima*	Low sequence homology to *Bt* proteins (<30%). 34% sequence identity with coleopteran active Cry3Ba. Presence of a ricin type domain	Low sequence homology to *Bt* proteins (<30%) and β-PFTs from other species
Apoptosis	Presence of apoptotic markers in HeLa cells treated with PS-1 (10 μg/ml); caspase inhibitor decreased cytotoxicity	Presence of apoptotic markers in HepG2 cells treated with low PS-2 dose, but caspase inhibitor did not prevent	Not assessed	Little caspase 3/7 activity, induced as a secondary effect by a high PS-4 dose

		cytotoxicity		
Morphology of susceptible cells	Granulation of the cytoplasm, swelling (MOLT-4 and HeLa), swelling (HepG2), fragmentation (HL-60)	Blebbing, disintegration of cytoskeleton and organelles (HepG2), swelling, vacuolation (MOLT-4)	Swelling within 1 hour and membrane rapture within 24 hours (HepG2)	Swelling and blebbing within 10 minutes, nuclear disintegration within 1 hour, membrane rupture within 24 hours (MOLT-4)
Membrane permeability	No membrane damage (PI, LDH) or depolarisation ($DiSC_3$)	Rapid membrane damage (PI, LDH) and depolarisation ($DiBAC_4$)	Rapid membrane damage (LDH, Trypan Blue)	Rapid membrane damage (LDH, flow cytometry)
Pore size	No small pores within 30 minutes (PI), no big pores within 4 hours (LDH)	Big (up to 3 nm) pores (PEGs)	Not assessed	Big pores (70 kDa dextrans enter MOLT-4 cells)
Oligomerization and cholesterol dependence	Not assessed	Formation of 200 kDa SDS resistant oligomers in HepG2 cells corresponded with cytolysis and decreased after depletion of cholesterol or GPI-anchored proteins	Not assessed	Formation of 90-200 kDa SDS resistant oligomers in CACO-2 and MOLT-4 but not in resistant HeLa cells. PS-4 activity is cholesterol independent

Receptor	Beclin-1	Possibly a GPI-anchored protein	Not identified	Not identified
References:	(Katayama et al., 2007, Katayama et al., 2005a, Mizuki et al., 1999a, Mizuki et al., 2000, Akiba et al., 2005, Katayama et al., 2011, Akiba and Okumura, 2016)	(Abe et al., 2008, Ito et al., 2004, Kim et al., 2000, Kitada et al., 2009, Kitada et al., 2006, Okumura et al., 2008, Akiba et al., 2009a)	(Mizuki et al., 1999a, Yamashita et al., 2000, Yamashita et al., 2005)	(Okumura et al., 2011, Okumura et al., 2005, Okumura et al., 2006, Lee et al., 2001, Okumura et al., 2008)

1.4 Different models of Cry toxin modes of action

The exact mechanism of insect killing by the Cry toxins has been the subject of discussion for a long time. Results gathered in this area are intriguing and often inconsistent. Conflicting theories result from the presence of many different insect targets, toxins and receptors that are currently under investigation and are further complicated by experimental artefacts.

Given that pore-facilitated cytolysis is a common strategy adopted by pathogenic bacteria, it is not a surprise that the most widely accepted model of Cry toxin mode of action is based on the colloid-osmotic lysis model, proposed first by Knowles and Ellar in 1987 (Knowles and Ellar, 1987). It is based on the action of the three domain δ-endotoxins on lepidopteran larvae. In order to exert toxicity, the *Bt* crystals have to be ingested by the larvae. They are solubilized inside their guts, usually in high pH (above 9.5). After that, the protoxin is cleaved by midgut proteases to the toxic core. Activated in this way toxin binds to a specific receptor in the gut brush border membrane. Following toxin-receptor interaction, toxin oligomerization occurs. In vitro studies support the hypothesis that oligomerization of monomeric Cry toxins does not occur spontaneously in a solution, suggesting that it requires interaction with the membrane (Güereca and Bravo, 1999). Following toxin insertion into the membrane, non-specific pores are formed. Generation of pores results in rapid changes in membrane potential, ion imbalance, influx of water, cell swelling, colloid-osmotic lysis of gut cells, and larval death (Knowles and Dow, 1993). Since the colloid-osmotic lysis model was proposed, many further studies provided additional

information in the aim to unravel the mechanism of toxicity, including e.g. the identification of receptors and crystal structures of different Cry toxins, including structures of toxin-receptor complexes. The main current models are presented below.

The Bravo Model

The Bravo model is based on Knowles and Ellar osmotic-lysis theory and involves experiments with insecticidal Cry1Ab and its interactions with *Manduca sexta* brush border membrane vesicles (BBMV). It suggests that Cry1A toxins require not one but two receptors for toxin action: cadherin-like protein (e.g. BT-R1) and aminopeptidase N (APN) (Bravo et al., 2004). The model proposes sequential binding of the activated monomers to these receptors. This hypothesis is based on co-immunoprecipitation experiments, which provide evidence that primary binding of Cry1Ab to BT-R1 is followed by binding to APN (Bravo et al., 2004). Binding to BT-R1 facilitates cleavage of α-helix 1 of the domain I by membrane-associated proteases, which is thought to expose a hydrophobic surface allowing toxin oligomerization into pre-pore structures (Gómez et al., 2002). Supportive data comes from Soberón et al., who demonstrated that genetically modified Cry1Ab and Cry1Ac lacking helix α-1 region (named Cry1AbMod and Cry1AcMod) are able to form oligomeric structures in vitro in the absence of cadherin receptor and exert toxicity in vivo in resistant insects with a mutated cadherin gene (Soberón et al., 2007). Finally, oligomerization greatly increases binding affinity to the second receptor APN, which directs oligomers into the lipid rafts facilitating insertion and tetrameric pore formation (Bravo et al., 2004). However, there is evidence that toxin monomers can also insert into the membrane.

Changes in the number of fluorophore labelled Cry1Aa monomers were monitored in the lipid bilayer system. The toxin entered the membrane as monomers before forming tetrameric pores, indicating that oligomerization could be occurring after toxin insertion by lateral diffusion of the monomers (Groulx et al., 2011). A simplified mechanism of the Bravo pore formation model is depicted in Figure 10 (top diagrams).

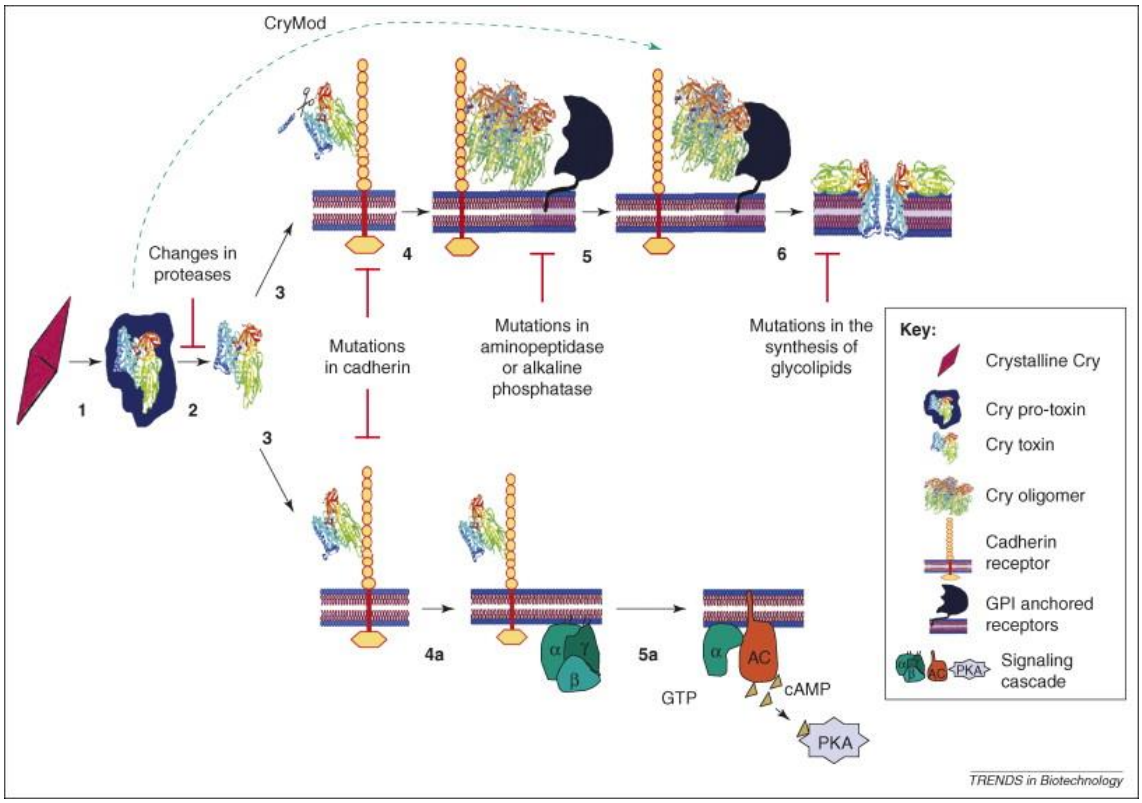

Figure 10 Two different models representing the mode of action of *Bt* Cry toxins.
Cry toxins are solubilised and cleaved by proteases followed by toxin monomer binding to a cadherin-like receptor (1, 2, and 3; steps shared in both models). Top diagrams (4-6) represent the Bravo model in which, after cadherin binding, a small portion of the toxin is cleaved, monomers are able to oligomerize, oligomers bind to the second GPI-anchored receptor, which facilitates membrane insertion and pore formation. Bottom diagrams (4a-5a) represent the signalling model according to Zhang et al., which proposes the involvement of adenylyl cyclase/protein kinase A signalling pathway. Figure was taken from Bravo et al. (Bravo and Soberón, 2008).

More recently, a 'ping pong' binding mechanism was suggested by Pacheco et al., where the Cry1Ab monomer first binds with low affinity to highly abundant APN through domain II loop 3. This is followed by binding with higher affinity to the second low-abundance receptor cadherin via loops in domain II (including loop 3). Cleavage of

α–helix 1 and oligomerization increase binding affinity to APN via domain III. Finally APN facilitates oligomer insertion in the membrane. Pacheco et al. showed that mutations in domain II loop 3 of Cry1Ab differentially affected binding to the two receptors depending on the oligomeric state of the toxin. Because binding of the monomeric - but not oligomeric - Cry1Ab mutants to APN was greatly reduced, this led to the conclusion that oligomerization involves conformational change which in turn affects receptor interaction. This 'ping pong' interaction with receptors (graphically shown in Figure 11) together with toxin oligomerization were proposed to be prerequisite for Cry1Ab toxicity towards *M. sexta* (Pacheco et al., 2009).

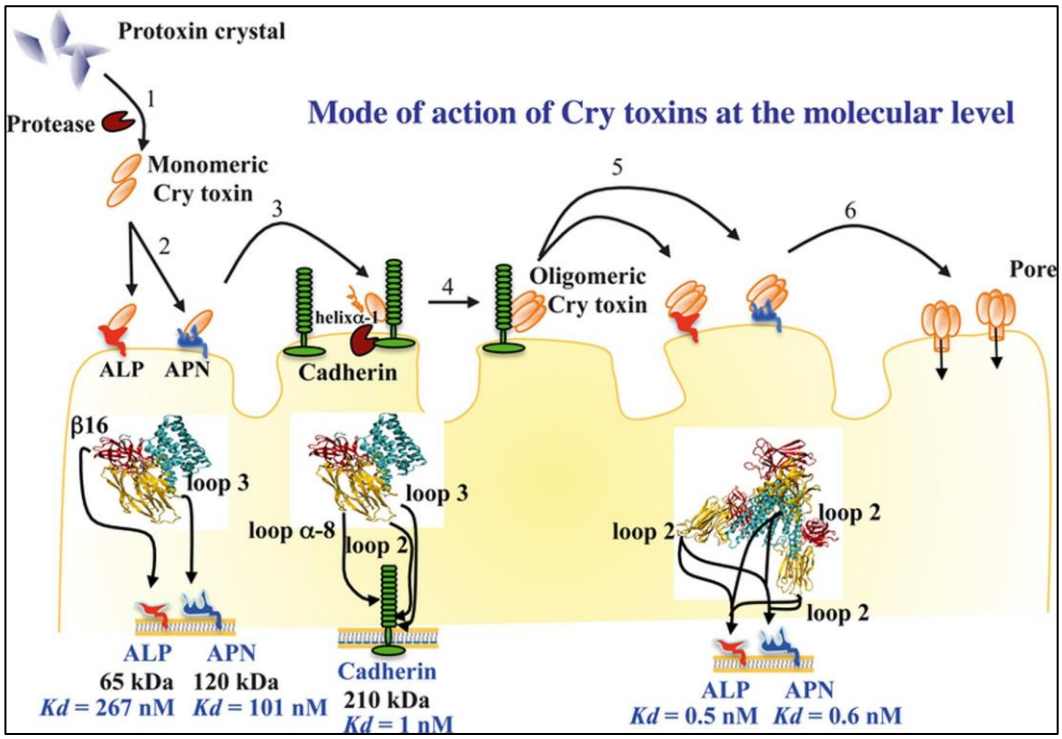

Figure 11 'Ping pong' mechanism suggested for Cry1A toxins in lepidopteran insects.
A 'ping pong' model suggests initial Cry1A toxin binding with a low affinity to ALP or APN receptors (APN in *Manduca sexta* or ALP in *Heliothis virescens*), followed by a high affinity interaction with cadherins that promotes cleavage of the N-terminal end of the toxin. After cleavage toxin monomers oligomerize into pre-pore structures that bind APN or ALP with high affinity resulting in pore formation. The figure was taken from Pardo-Lopez et al. (Pardo-Lopez et al., 2013b).

The Zhang model

Another mechanism proposed by Zhang et al., attributes toxic events solely to a signalling pathway, and not to pore formation. This group suggested that only the monomeric form of Cry1Ab can specifically bind to BT-R1 receptor and induce toxicity, and that toxin oligomers do not form lytic pores (Zhang et al., 2005). Further, the model states that the mode of action involves an adenylyl cyclase (AC), protein kinase A (PKA) signalling pathway (Zhang et al., 2006) as illustrated in Figure 10 (bottom diagrams) and Figure 12.

The model is based on experiments conducted using Cry1Ab toxin and transformed ovarian cells of the cabbage looper *Trichoplusia Ni*. The cell line, called S5, has been engineered to stably express BT-R1 receptor on the cell surface. Western blot experiments using anti-Cry1Ab antibody showed that only monomeric form of the toxin incorporated into the membranes of cells expressing BT-R1, whilst oligomeric forms were detected in membrane fractions of both susceptible and non-susceptible cells. Moreover blocking the receptor binding site prevented monomer but not oligomer incorporation in the membrane while inhibiting the toxicity. Monomer incorporation in S5 cells was rapid (5 minutes after treatment) and stable, whereas oligomer incorporation started appearing after 15 minutes and was dose dependent in both S5 and non-susceptible cells. Moreover, oligomers stayed incorporated in the membrane for a few generations without any toxic effects. All these results led to the conclusion that only toxin monomers can bind specifically and exert toxicity in susceptible cells (Zhang et al., 2005).

In the proposed model Zhang et al. further suggested that binding of the monomer to BT-R1, stimulates a G protein-coupled receptor (GPCR), which activates AC/PKA pathway. After activation of GPCR with extracellular ligand, a conformational change occurs in the attached heterotrimeric G protein complex on the intracellular side of the membrane. The $G_{\alpha s}$ subunit exchanges GDP for GTP, dissociates from the complex and binds to AC. Activated AC promotes the increase of a second messenger cAMP in cytoplasm, which in turns activates PKA. PKA regulates a wide range of cellular processes such as gene expression, protein phosphorylation, and conductance of ion channels (Lodish, 2008). The Zhang et al. model is based on the experiments, which show that cAMP and PKA levels increased in toxin treated S5 cells, cell permeable inhibitors of $G_{\alpha s}$ and AC considerably decreased cytotoxicity of Cry1Ab, whereas two PKA inhibitors completely prevented morphological changes (blebbing and swelling) and cellular death (Zhang et al., 2006). Zhang et al. additionally showed that Cry1Ab toxicity can be abolished by 5 mM EDTA cell pre-treatment in vitro. This effect was interpreted as Mg^{2+} depletion as supplementation with magnesium salt restored toxicity. Interestingly, EDTA prevented toxicity, but not the binding, as evidenced by the monomer and oligomer bands detected in western blot analysis of EDTA treated cells. The authors suggested the importance of Mg^{2+} ions in post-binding toxicity of Cry1Ab and imply that interaction with the receptor is not sufficient for full toxin action (Zhang et al., 2005). The authors support the AC/PKA signalling pathway model with the fact that Mg^{2+} is required in the mechanism of cAMP synthesis by AC as well as for stimulation of G protein (Sprang, 1997, Tesmer et al., 1999, Zimmermann et al., 1998).

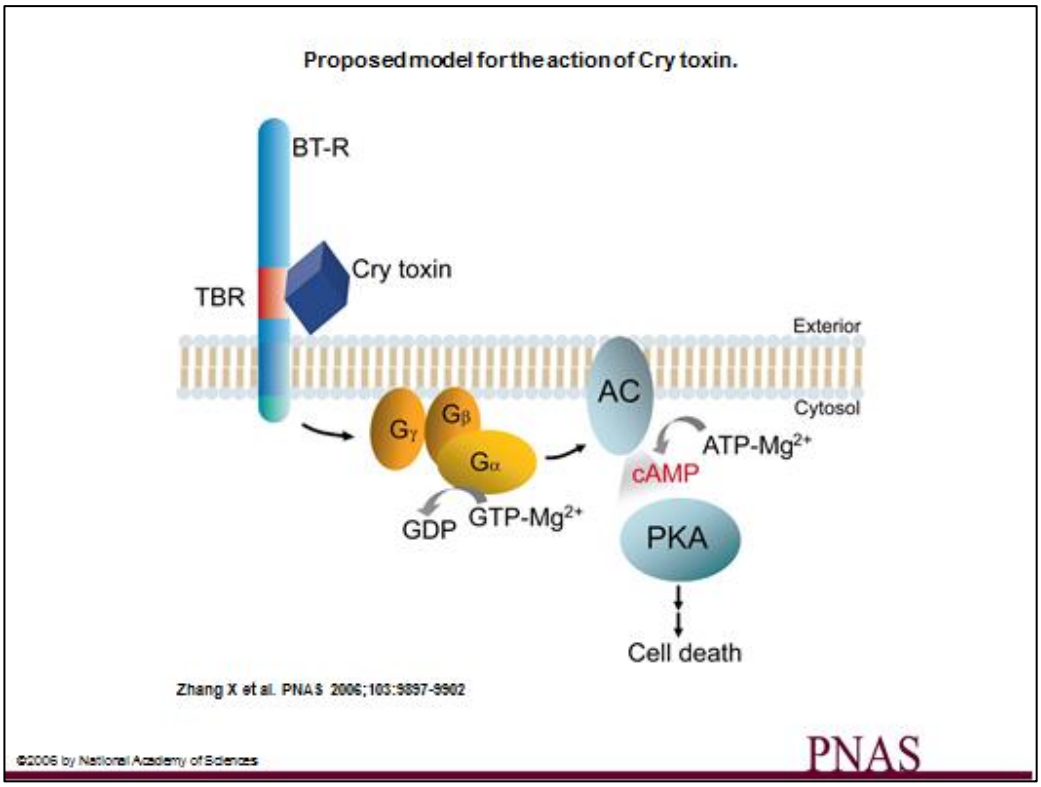

Figure 12 The Zhang model implicating AC/PKA signalling pathway in toxicity of Cry proteins.
The Zhang model postulates that it is the binding of the monomeric Cry1Ab toxin to cadherin receptor that leads to toxicity. Receptor binding results in G protein stimulation, which activates adenylyl cyclase and subsequent increase of cAMP in cytoplasm. Increased levels of cAMP activate protein kinase A, which phosphorylates target proteins leading to disruption of ion channels and cell death. Figure was taken from Zhang et al. (Zhang et al., 2006).

The Zhang model remains controversial and has been challenged (Kirouac et al., 2006, Vachon et al., 2012). Conclusions drawn by Zhang et al. are based on experiments that involved an engineered insect cell line, transformed to express BT-R1, which does not represent midgut environment of the susceptible insect larvae. Vachon et al. points to the fact that the amount of EDTA used by Zhang et al. was insufficient to effectively chelate all $MgCl_2$ present in the insect medium and that low pH of the medium affected the efficiency of ion chelating by EDTA and EGTA, leading to wrong conclusions about Mg^{2+} dependence. The authors note that factors like pH, ionic composition, temperature, presence of proteases influence experimental data and should be taken into account when drawing conclusions (Vachon et al., 2012). More

importantly the model contradicts the ability of Cry toxins to form pores, proven before by different research groups, both in insect epithelial membranes and artificial bilayers.

The Jurat-Fuentes interpretation

The interpretation of Cry toxin mode of action by Jurat-Fuentes et al. combines the Bravo and the Zhang models together. The authors suggest that both pore formation and signalling pathway leading to apoptosis may in cooperation play a role in toxicity and that the presence of one does not exclude the other. The model tries to explain the mode of action of Cry1Ac in *Heliothis virescens* larvae (Jurat-Fuentes and Adang, 2006a). The model of multiple binding sites for Cry1Ac was proposed in *H. virescens* (Van Rie et al., 1989). HevCaLP, a cadherin-like protein was proposed to be one of them as HevCaLP gene knockout was connected with Cry1Ac resistance in some resilient strains (Gahan et al., 2001). The second receptor was identified as a GPI-anchored alkaline phosphatase called HvALP. Decreased activity of alkaline phosphatase in brush border membrane proteins from resistant strains of *H. virescens* correlated with reduced levels of HvALP in these larvae (Jurat-Fuentes and Adang, 2004). In addition, actin was identified as a novel receptor in BBMV proteome of *M. sexta* and *H. virescens* (Krishnamoorthy et al., 2007, McNall and Adang, 2003), as well as intracellular phosphatases (Jurat-Fuentes and Adang, 2006a). The Jurat-Fuentes model proposes two mechanisms that are not mutually exclusive. Both of them may considerably contribute to cell death. In the first one, Cry1Ac associates with HevCaLP cadherin and after oligomerization binds the second receptor HvALP, which leads to

pore formation in lipid rafts. Pore formation causes cell death due to osmotic shock but may additionally activate some signalling pathways. The second mechanism proposes that binding to HevCaLP induces a signalling pathway regulated by intracellular phosphatases, which may activate intracellular apoptotic pathway. There also may be a direct interaction between Cry1Ac and actin. The interaction between actin and a cytosolic domain of cadherin via tyrosine phosphatases (catenin and actinin) was already demonstrated (Lilien and Balsamo, 2005). The authors suggested that actin, although it is a cytoskeleton protein, may interact with the cytosolic domain of cadherin or with the toxin itself after its conformational change (Jurat-Fuentes and Adang, 2006a, Pigott and Ellar, 2007). The model is graphically presented in Figure 13.

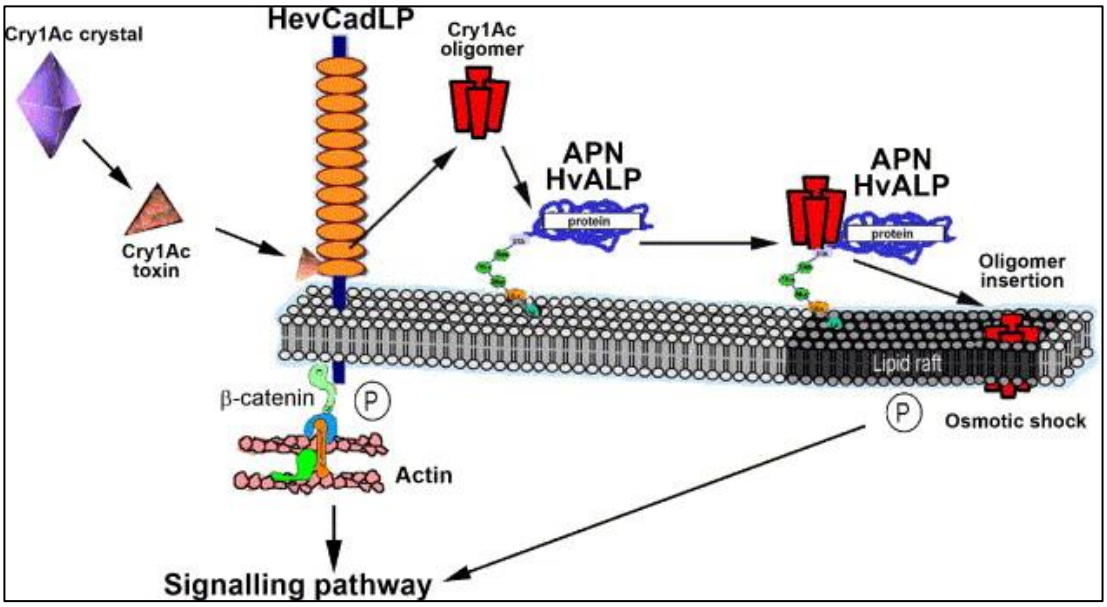

Figure 13 Proposed mechanisms of action of Cry1Ac toxin in *H. virescens.*
Following toxin processing in the insect midgut activated Cry1Ac binds to HevCaLP. Monomers oligomerize and bind to GPI-anchored HvALP receptor leading to membrane insertion and pore formation. Binding to cadherin may also exert toxicity via a signalling pathway after the interaction between cadherin intracellular domain and actin, which is regulated by phosphatases (P). Figure was taken from Jurat-Fuentes and Adang et al. (Jurat-Fuentes and Adang, 2006a).

1.5 Cellular responses to pore forming toxins

Cells have evolved different ways to cope with bacterial toxins. Attack on cell membranes by PFTs is a conserved mechanism and due to the widespread nature of PFTs, many of the host cellular responses overlap. Yet, some remain cell and toxin specific, additionally dependent on toxin concentration and time of exposure. When toxin concentration is high, cells die quickly as a result of rapid and irreversible membrane damage. However when the dose is sub-lytic, cells often produce signals promoting survival and repair.

Research has shown that one of the conserved responses to various PFTs is the phosphorylation of p38 mitogen-activated protein kinase (MAPK) (Ratner et al., 2006). The MAPK protein family comprises highly conserved serine/threonine kinases that are activated in response to extracellular signals and stresses, like osmotic shock, UV radiation, heat shock, ischemia, or DNA damage. MAP kinases can be classified into four subgroups: ERK (extracellular signal regulated kinase), JNK/SAPK (c-Jun N-terminal kinases or stress activated protein kinases), BMK1 (ERK/big MAP kinase 1) and p38. MAP kinases are activated by MAP kinase kinases (MKKs), with MKK3 and MKK6 being known p38 activators (Zarubin and Han, 2005). p38 is present in four isoforms: α, β, ϒ, and δ, but only α and β are ubiquitously expressed. Following stress, cytosolic p38 upon activation is translocated into the nucleus to access its nuclear substrates (Gong et al., 2010). When activated, p38 phosphorylates a broad range of proteins. The downstream targets may be as many as 200-300 and include: cytokines (TNF-α, interleukins), nuclear transcription factors and extracellular receptors (Zarubin and Han, 2005).

Phosphorylation of p38 was previously reported for: *Streptococcus aureus* streptolysin O, *Gardnerella vaginalis* vanginolysin, *B. anthracis* anthrolysin O, *S. pneumonia* pneumolysin, *Staphylococcus aureus* α-hemolysin, *Aeromonas hydrophyla* proaerolysin, Listeriolysin O, *Vibrio cholera* cytolysin, *Escherichia coli* hemolysin A (Fickl et al., 2005, Gelber et al., 2008, Huffman et al., 2004, Kloft et al., 2009, Ratner et al., 2006, Gonzalez et al., 2011b). p38 pathway was activated in experiments involving *C. elegans* treated with low doses of Cry5B toxin (Huffman et al., 2004). Activation of p38 MAPK was also shown in lepidopteran *M. sexta* and dipteran *A. aegypti* exposed to Cry1Ab and Cry11Aa respectively (Cancino-Rodezno et al., 2010).

In the studies with *C. elegans, M. sexta* and *A. aegypti* silencing of p38 MAPK pathway resulted in hypersensitivity to Cry toxins (Cancino-Rodezno et al., 2010, Huffman et al., 2004), suggesting a role in cellular defence. However, published data are contrasting. In a study by Husmann et al., it has been shown using the same target cell line that inhibition of p38 MAPK pathway impeded cellular recovery in cells exposed to *S. aureus* α toxin but not in cells exposed to streptolysin O (Husmann et al., 2006). Also, a specific p38 inhibitor prevented cell death in neural cells exposed to pneumolysin, implicating a role of p38 in facilitating apoptosis (Stringaris et al., 2002). Therefore, the p38 MAPK pathway - depending on a cell and toxin type - may exert different biological effects. Interestingly, a recent study by Guo et al. showed that MAPK genes can trans-regulate expression levels of ALP and ABCC genes (encoding Cry toxin receptors) in *Bt* resistant *P. xylostella* larvae. The authors suggested that MAPK signalling pathway could play an important role in insect resistance by altering expression levels of Cry toxin receptors (Guo et al., 2015).

The unfolded protein response (UPR) of the endoplasmic reticulum (ER) was identified as one of the downstream targets of p38 MAPK pathway in *C. elegans* (Bischof et al., 2008, Huffman et al., 2004). Under stressful conditions, like nutrient deprivation, disruption of Ca^{2+} or redox homeostasis, protein folding in the ER may be impaired, leading to accumulation of misfolded or unfolded proteins. Cells have evolved to deal with this threat by activating pathways that on the transcriptional and translational levels lead to a decrease in protein translation, degradation of misfolded proteins, and promotion of correct folding (Zhang and Kaufman, 2004). Loss of this pathway was demonstrated to cause hypersensitivity of *C. elegans* and mammalian cells to the attack of Cry5B and aerolysin, respectively and was functionally linked to upstream components of p38 pathway (Bischof et al., 2008).

It was shown that in addition to the p38 pathway some PFTs like proaerolysin and listeriolysin O specifically triggered activation of the ERK pathway. It was suggested that these two pathways helped to recover ion homeostasis as inhibition of either p38 or ERK by specific inhibitors significantly diminished the recovery of intracellular K^+ (Gonzalez et al., 2011b). Furthermore JNK MAPK was activated in experiments involving *C. elegans* and Cry5B toxin (Huffman et al., 2004). JNK MAPK was later shown to protect nematode cells from both small pore (Cry5B) and large pore (streptolysin O) inducing PFTs. Based on a genome-wide RNAi screen results, JNK and p38 MAPKs were suggested to play a paramount role in cellular protection of *C. elegans* against Cry5B (Kao et al., 2011).

Efflux of intracellular potassium, arising as a consequence of transmembrane pores, was shown to mediate various cellular responses. It was demonstrated that

potassium efflux promoted p38 activation after exposure to *S. aureus* α-toxin, *V. cholerae* cytolysin, streptolysin O, and *E. coli* hemolysin A (Kloft et al., 2009). Potassium efflux induced activation of the inflammasome and caspase-1 in aerolysin treated Chinese hamster ovary cells. Because caspase-1 positively regulates the Sterol Regulatory Element Binding Proteins (SREBPs) involved in membrane biogenesis, it is thought that this pathway promotes cell survival by assisting in membrane repair (Gurcel et al., 2006). Another consequence of potassium efflux is autophagy, which was observed in aerolysin treated HT29 cells. Although it did not restore ion homeostasis or help in membrane repair, its function was predicted to benefit cells in a quiescent state, where recycling cellular molecules and organelles via autophagy would help surviving low energy consumption state following a PFT attack (Gonzalez et al., 2011b). Autophagy was also observed in cells exposed to *S. aureus* α-toxin, *V. cholerae* cytolysin, *E. coli* haemolysin and streptolysin O. A similar conclusion was drawn, that autophagy promotes energy maintenance during recovery in cells affected by pore formation (Kloft et al., 2010). A significant increase in lipid droplet formation was observed in HeLa cells following cell treatment with: proaerolysin, listeriolysin O, streptolysin O, *S. aureus* α-haemolysin. Lipid droplets were beneficial to cells and their formation was abolished by ERK inhibitor in aerolysin treated cells. The authors suggested that - along with an arrest in protein synthesis - storing energy in lipid droplets represents a mechanism that puts the cells into a low energy consumption mode (Gonzalez et al., 2011b).

Hypoxia (low oxygen levels) and hypoxia response was identified as another protective mechanism in *C. elegans* against Cry21A, Cry5B and *V. cholerae* cytolysin. Loss of function of the main hypoxia response effector HIF-1 (hypoxia inducible factor

1) led to hypersensitivity of previously resistant nematodes. Moreover, the hypoxia pathway was shown to work upstream of UPR. The role of low amount of oxygen in pathogenicity and the role of UPR being the downstream effector of hypoxia response was suggested (Bellier et al., 2009).

Additionally, activation of the nuclear factor kappa B (NF-κB) pathway and production of inflammatory molecules was observed in immune cells exposed to the following PFTs: *S. aureus* α-toxin, aerolysin, pneumolysin, listeriolysin O, streptolysin O (Aroian and van der Goot, 2007). Antimicrobial peptides were released in *Spodoptera* larvae in response to Cry1Ca and Vip3 (Herrero et al., 2016). In other studies extensive cell vacuolization was noted after treatment with aerolysin or *S. marcescens* hemolysin (Abrami et al., 1998, Hertle et al., 1999). Listeriolysin O, perfringolysin O and pneumolysin caused Ubc9 degradation, decreasing the levels of protein SUMOylation and increasing at the same time infection efficiency. De-SUMOylation was shown to be independent of the calcium influx or MAPKs (Ribet et al., 2010).

Another pathway activated by PFTs is apoptosis, often mediated by uncontrolled influx of Ca^{2+} ions – a known apoptosis inducer. An apoptotic pathway was triggered by: *S. aureus* α-toxin in epithelial cells (Imre et al., 2012) and lymphocytes (Jonas et al., 1994), by listeriolysin in dendric cells (Guzmán et al., 1996), aerolysin in lymphocytes (Nelson et al., 1999), PS-2 like protein in HepG2 (Brasseur et al., 2015b), and PS-1 in HeLa cells (Katayama et al., 2007), however the pore forming nature of PS-1 (from strain A1190) has not been demonstrated.

Other mechanisms attributed to PFT-induced Ca^{2+} influx is a repair process based on exo- and endocytosis. The studies suggest that after plasma membrane injury

and calcium entry, lysosomal enzyme acid sphingomyelinase is released during exocytosis of lysosomes, where it converts sphingomyelin into ceramide. Ceramides form microdomains which in turn facilitate endosome formation. Endosomes internalise transmembrane pores by disruption of actin cytoskeleton and target them for degradation contributing to membrane repair. The model is based on experiments with cells permeabilized with streptolysin O, but similar processes were observed in mechanically injured cells (Idone et al., 2008, Tam et al., 2010). Vesicle trafficking pathways were also noted for *S. aureus* α-toxin, Cry5B and *V. cholerae* cytolysin; reviewed by Los et al. (Los et al., 2013).

Cellular processes triggered by PFTs are graphically presented in Figure 14.

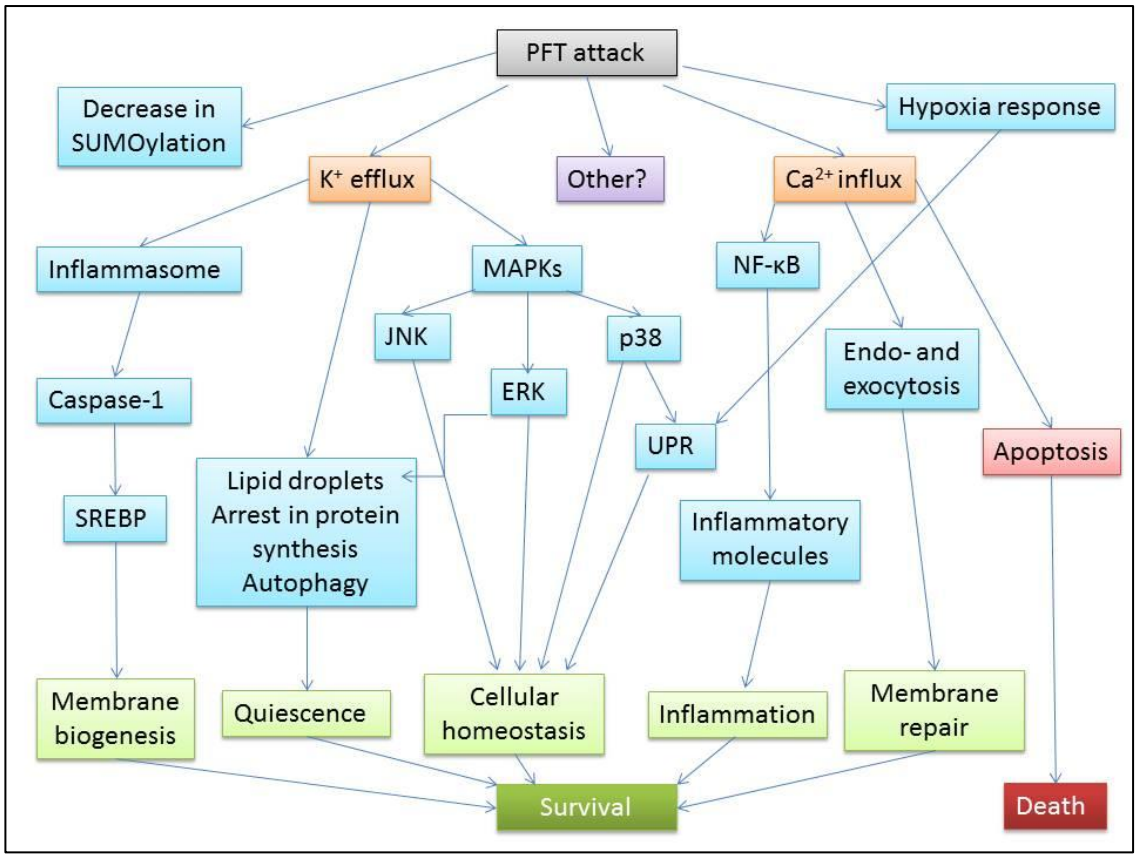

Figure 14 Cellular responses to PFTs.
Schematic diagram represents signalling pathways and cellular mechanisms triggered by pore formation.

In summary, despite the deceptively simple mechanism of action of PFTs, cellular responses upon pore formation remain complex and not fully characterised. Disrupting protective barrier of plasma membrane initiates numerous pathways arising mostly as a result of uncontrolled flow of ions.

1.6 Cry toxin receptors

Receptors have been shown to be critical determinants of specificity of Cry toxins. Receptor recognition has been done mostly by identification and characterization of toxin binding partners. However, correlation between binding and toxicity was not always consistent. For example, a positive correlation was demonstrated for Cry1Ab and Cry1Ba toxins (Hofmann et al., 1988), but not for Cry1Ac, where BBMV from naturally resistant *Spodoptera frugiperda* insect larvae showed high-affinity, saturable binding sites (Garczynski et al., 1991). Later on, Liang et al. separately analyzed the kinetics of reversible and irreversible binding of Cry1Aa, Cry1Ab and Cry1Ac and demonstrated that in these experiments only irreversible binding directly correlated with toxicity (Liang et al., 1995). Problems with binding studies additionally involve a high risk of false-positive results, which may arise as a result of: non-specific binding, conditions used (denatured versus non-denatured epitopes), similarity in protein size, posttranslational modification (which is the case for APNs) and erroneous exogenous expression. To separate putative from functional receptors, Table 2 presents reported Cry toxin binding partners, whereas Table 3 shows receptors confirmed to be responsible for susceptibility to the toxin. The best characterized classes of insecticidal Cry toxin receptors include: aminopeptidase N (APN), cadherin-like receptor and

alkaline phosphatase (ALP), reviewed extensively by Pigott and Ellar (Pigott and Ellar, 2007).

APN is a zinc binding metalloprotease that cleaves neutral amino acids from the protein N-terminus digesting dietary proteins (Wang et al., 2005b). The mature protein (90 - 170 kDa) is attached to the membrane by a glycosylphosphatidylinositol (GPI) anchor and is modified post-translationally by glycosylation. The presence of this carbohydrate has been demonstrated to be crucial for interaction with some Cry toxins, e.g. GalNAc – containing APN in Cry1Ac binding (Knight et al., 1994). Binding to APNs has been demonstrated for Cry1Aa, Cry1Ab, Cry1Ac, Cry11Ba, Cry1Ba, Cry1Ca and Cry1Fa. Functionality of APN as a receptor was confirmed for Cry1Aa, Cry1Ab, Cry1Ac, Cry1Ca and Cry11Ba (references in Table 2 and Table 3).

Cadherins are calcium-dependent, transmembrane proteins, playing a variety of roles including: cell adhesion, migration, and morphogenesis (Leckband and Prakasam, 2006). Their expression in insects is regulated temporarily and spatially, increasing during larval development. The exact role of insect cadherins remains unclear, however they are believed to help with the organization of midgut epithelial cells (Midboe et al., 2003). Toxin binding regions in cadherin occur near the membrane proximal extracellular domain and adjacent cadherin repeats (Pigott and Ellar, 2007). Cadherins have been shown to be important receptors for Cry1A toxins, especially in lepidopteran species, but not all of them. Binding was demonstrated for Cry1Aa, Cry1Ab, Cry1Ac, Cry11Aa and Cry4Ba; receptor functionality for Cry1Aa, Cry1Ab, Cry1Ac and Cry3Ba (references in Table 2 and Table 3).

Alkaline phosphatases (ALPs) represent another group of *Bt* Cry toxin receptors. Similarly to APNs, ALPs are zinc binding, GPI anchored proteins and undergo glycosylation. GalNAc-dependent binding was detected for Cry1Ac and *H. virescens* ALP (Jurat-Fuentes and Adang, 2004), but there is no indication of a general role for carbohydrates in the interaction with toxin. Binding to ALP was demonstrated for Cry1Ac, Cry11Aa, Cry4B, and Cry11Ba; APN conferring susceptibility - only for Cry11Ba (references in Table 2 and Table 3).

Some of other molecules that have been reported to interact with Cry toxins are ADAM 10 metalloprotease in *L. decemlineata* and sodium solute symporter in *T. castaneum* (Table 2). Interestingly binding partners have been identified for two parasporins. Glyceraldehyde-3-phosphate dehydrogenase (GAPDH) – an enzyme performing diverse functions in cell metabolism, transcription and apoptosis - was revealed as a binding partner for parasporin-like protein *Bt*18 in leukemic T-cells (Krishnan et al., 2010). Also, beclin-1 - a tumor suppressor with a role in the regulation of autophagy and cell death (Qu et al., 2003) - was identified as a PS-1 receptor in HeLa cells, based on experiments with anti-beclin-1 antibody that suppressed toxin binding and toxicity (Katayama et al., 2011).

The identification of genes involved in insect resistance to Cry toxins led to discovery of new putative receptors. ABCC2 transporter, was linked to resistance to Cry1A toxins in *H. virescens, B. mori, P. xylostella* and *T. ni* (Atsumi et al., 2012b, Baxter et al., 2011, Gahan et al., 2010). Functional studies confirmed the involvement of the transporter in Cry1A toxicity in *B. mori* and *S. exigua* (Table 3). Direct binding however was never demonstrated and therefore it is believed that the interaction between Cry

toxins and ABCC2 transporter may be of transient nature, e.g. toxin insertion into the membrane may be driven by the transport cycle of the ABC protein (Heckel, 2012).

Research on resistance mechanisms in *C. elegans* and forward genetic experiments, revealed four genes: *bre2, bre3, bre4* and *bre5*, which when mutated brought resistance towards nematocidal Cry5Ba. The *bre* genes encode glycosyltransferases, which are involved in the biosynthesis of glycosphinglipids. Most importantly, these glycolipids were found to be necessary for the toxin interaction with intestinal cells (Griffitts et al., 2005, Griffitts et al., 2003, Griffitts et al., 2001).

Comparison of transcripts from larval midgut cells from resistant and susceptible populations of *P. xylostella* was performed after exposure to DiPel (*Bt* pesticide containing: Cry1Aa, Cry1Ab, Cry1Ac, Cry2Aa). Among others, the following genes were identified: homologues of methylthiotransferase (CDKAL1), co-chaperone (SDF2L1), and metalloproteinase (PxHEL-1). RNAi-based silencing of these genes significantly increased the mortality of resistant but also susceptible insects (Ayra-Pardo et al., 2015). In another studies, among other proteins, actin was identified as intracellular binding targets in proteome analyses in *M. sexta* and *H. virescens* BBMVs (McNall and Adang, 2003, Krishnamoorthy et al., 2007). The exact role of these proteins remains unclear, but the data points to the significance of molecules other than classical receptors, and involved in cellular processes, in the toxin mode of action and resistance mechanisms.

To sum up, lepidopteran APNs and cadherins remain the best characterised Cry toxins receptors. Nevertheless, there is more and more data evidencing novel receptors as well as molecules influencing toxin binding and host susceptibility.

Table 2 Reported binding between Cry toxins and putative receptors.
Table presents putative Cry toxin receptors based on the results of binding assays. Species full names: *Anopheles (A.): quadrimaculatus, gambiae; Tribolium (T.) castaneum; Spodoptera (S.): frugiperda, exigua, litura; Drosophila (D.) melanogaster; Heliothis (H.) virescens; Aedes (A.) egypti; Ostrinia (O.) nubilalis; Caenorhabditis (C.) elegans; Helicoverpa (H.) armigera; Trichoplusia (T.) ni; Bombyx (B.) mori, Manduca (M.) sexta, Lymantria (L.) dispar, Epiphyas (E.) postvittana, Leptinotarsa (L.) decemlineata.*

Receptor	Origin	Toxin	Method	Reference
APN	*M. sexta*	Cry1Ac	Ligand blot	(Knight et al., 1994); (Sangadala et al., 1994);
APN	*M. sexta*	Cry1Aa, Cry1Ab, Cry1Ac	SPR	(Masson et al., 1995)
APN	*H. virescens*	Cry1Aa, Cry1Ab, Cry1Ac	SPR	(Luo et al., 1997)
APN	*H. virescens*	Cry1Ac, Cry1Fa	Ligand blot	(Banks et al., 2001)
APN	*B. mori*	Cry1Aa	Ligand blot	(Yaoi et al., 1999)
APN	*H. armigera* (expressed in *T. ni* cells)	Cry1Aa, Cry1Ab, Cry1Ac	Ligand blot	(Rajagopal et al., 2003)
APN	*M. sexta*	Cry1Ab	Ligand blot	(Denolf et al., 1997)
APN	*L. dispar*	Cry1Ac	Ligand blot, SPR	(Valaitis et al., 1997)
APN	*H. virescens*	Cry1Ac	Ligand blot	(Gill et al., 1995)
APN	*H. armigera* (expressed in *T. ni* cells)	Cry1Ac	Ligand blot	(Rajagopal et al., 2003)
APN	*E. postvittana* (expressed in *S. frugiperda* 9 cells)	Cry1Ac, Cry1Ba	Ligand blot	(Simpson and Newcomb, 2000)

APN	*S. litura* (expressed in *S. frugiperda* 21 cells)	Cry1Ca	Ligand blot, immunofluorescence	(Agrawal et al., 2002)
APN	*A. quadrimaculatus*	Cry11Ba	SPR	(Abdullah et al., 2006)
APN AgAPN2	*A. gambiae* (expressed in *E. coli*)	Cry11Ba	Competition assay, ligand dot blot, ELISA	(Zhang et al., 2008)
Cadherin BT-R1	*M. sexta*	Cry1Ab	Ligand blot	(Vadlamudi et al., 1993)
Cadherin BT-R1	*M. sexta* (expressed in COS-7 and HEK-293 cells)	Cry1Ab	Ligand blot	(Vadlamudi et al., 1995)
Cadherin BT-R1	*M. sexta* expressed in (*S. frugiperda* 21 cells)	Cry1Aa, Cry1Ab, Cry1Ac	Ligand blot	(Keeton and Bulla, 1997)
Cadherin BT-R(1a)	*M. sexta* (expressed in *D. melanogaster* S2 cells)	Cry1Aa, Cry1Ab, Cry1Ac	Ligand blot	(Hua et al., 2004)
Cadherin BT-R1	*M. sexta* (expressed in H5 *T. ni* cells)	Cry1Ab	Ligand blot	(Zhang et al., 2005)
Cadherin BTR175	*B. mori*	Cry1Aa	Immunoprecipitation	(Nagamatsu et al., 1998)
Cadherin BTR175b	*B. mori* (expressed in HEK-293 cells)	Cry1Aa	Immunofluorescence	(Ikawa et al., 2000)
Cadherin HevCaLP	*H. virescens*	Cry1Aa	Ligand blot	(Jurat-Fuentes et al., 2004)
Cadherin HevCaLP	*H. virescens* (expressed in *E. coli*)	Cry1Ab, Cry1Ac	SPR	(Xie et al., 2005)

Cadherin OnBT-R1	*O. nubilalis*	Cry1Ab	Ligand blot	(Flannagan et al., 2005)
Cadherin BTR harm	*H. armigera* (expressed in *E. coli*)	Cry1Ac	Binding assay	(Wang et al., 2005a)
Cadherin AaeCad	*A. aegypti* (expressed in *E. coli*)	Cry11Aa	Ligand blot	(Chen et al., 2009)
Cadherin SeCad1b	*S. exigua*	Cry1Ac	Ligand blot	(Chen et al., 2014)
Cadherin AgCad1	*A. gambiae* (expressed in *D. melanogaster* S2 cells)	Cry4Ba	Ligand blot	(Hua et al., 2008)
ALP HvALP	*H. virescens*	Cry1Ac	Ligand blot	(Jurat-Fuentes and Adang, 2004)
ALP	*M. sexta*	Cry1Ac	Ligand blot	(McNall and Adang, 2003)
ALP	*A. aegypti*	Cry11Aa	Immunofluorescence, Ligand blot	(Fernandez et al., 2006)
ALP	*A. aegypti*	Cry4B	Ligand blot	(Buzdin et al., 2002)
ALP AgALP1	*A. gambiae* (expressed in *E. coli*)	Cry11Ba	Ligand blot, ELISA	(Hua et al., 2009)
ALP	*H. armigera*	Cry1Ac	Ligand blot	(Sarkar et al., 2009)
APN (TcAPN-I), E-cadherin (TcCad1), sodium solute symporter (TcSSS)	*T. castaneum*	Cry3Ba	Ligand blot	(Contreras et al., 2013)

Glycolipids	*C. elegans*	Cry5B	TLC overlay, supported lipid bilayers	(Griffitts et al., 2005)
Metalloprotease ADAM 10	*L. decemlineata*	Cry3Aa	Ligand blot	(Ochoa-Campuzano et al., 2007)
GAPDH	Leukemic T-cells (CEM-SS)	Cytotoxic Cry toxin Bt18	Ligand blot, immunofluorescence	(Krishnan et al., 2010)
Beclin-1	HeLa cells	PS-1	Photo-reactive chemical crosslinking, competition assay	(Katayama et al., 2011)
Actin	*M. sexta*	Cry1Ac	2 dimensional electrophoresis, mass spectrometry	(McNall and Adang, 2003)
Actin	*H. virescens*	Cry1Ac	2 dimensional electrophoresis, mass spectrometry	(Krishnamoorthy et al., 2007)

Table 3 Reported functional Cry toxin receptors.
The table presents a list of studies that have reported a positive correlation between presence of the receptor and toxicity/pore formation. Species full names: *Anopheles (A.): quadrimaculatus, gambiae; Tribolium (T.) castaneum; Spodoptera (S.): frugiperda, exigua, litura; Drosophila (D.) melanogaster; Heliothis (H.) virescens; Aedes (A.) egypti; Ostrinia (O.) nubilalis; Caenorhabditis (C.) elegans; Helicoverpa (H.) armigera; Trichoplusia (T.) ni; Bombyx (B.) mori, Manduca (M.) sexta, Lymantria (L.) dispar.*

Receptor	Origin	Toxin	Method	Reference
APN	*M. sexta*	Cry1Ac	Permeability: Rb+ efflux assay	(Sangadala et al., 1994);
APN	*H. virescens*	Cry1Aa, Cry1Ab, Cry1Ac	Permeability: Rb+ efflux assay	(Luo et al., 1997)

APN	*M. sexta* reconstituted in PLBs	Cry1Aa, Cry1Ac, Cry1Ca	PLB experiments	(Schwartz et al., 1997)
APN	*M. sexta* (expressed in *D. melanogaster*)	Cry1Ac	Feeding bioassay	(Gill and Ellar, 2002)
APN	*S. litura*	Cry1Ca	RNAi, feeding bioassay	(Rajagopal et al., 2002)
APN AgAPN2	*A. gambiae* (expressed in *E. coli*)	Cry11Ba	Competition assay, feeding bioassay	(Zhang et al., 2008)
Cadherin BT-R1	*M. sexta* (expressed in COS-7 and HEK-293 cells)	Cry1Ab	Morphological changes tracked by immunofluorescence	(Dorsch et al., 2002)
Cadherin BT-R(1a)	*M. sexta* (expressed in *D. melanogaster* S2 cells)	Cry1Aa, Cry1Ab, Cry1Ac	Flow cytometry, propidium iodide	(Hua et al., 2004)
Cadherin BT-R1	*M. sexta* (expressed in H5 *T. ni* cells)	Cry1Ab	Permeability: Trypan Blue	(Zhang et al., 2005)
Cadherin BT-R1	*M. sexta* (expressed in *S. frugiperda* 9 cells)	Cry1Aa	Whole cell patch clamping	(Nagamatsu et al., 1999)

Cadherin BTR175b	*B. mori* (expressed in HEK-293 cells)	Cry1Aa	Permeability: LDH assay	(Tsuda et al., 2003)
Cadherin HevCaLP	*H. virescens* (expressed in *D. melanogaster* S2 cells)	Cry1Aa, Cry1Ab, Cry1Ac	Flow cytometry, propidium iodide	(Jurat-Fuentes and Adang, 2006b)
Cadherin OnBT-R1	*O. nubilalis* (expressed in *S. frugiperda* 9 cells)	Cry1Ab	Microscopic observation	(Flannagan et al., 2005)
Cadherin SeCad1b	*S. exigua*	Cry1Ac	RNAi, feeding bioassay	(Chen et al., 2014)
E-cadherin (TcCad1), sodium solute symporter (TcSSS)	*T. castaneum*	Cry3Ba	RNAi, feeding bioassay	(Contreras et al., 2013)
ALP AgALP1	*A. gambiae* (expressed in *E. coli*)	Cry11Ba	Competition assay, feeding bioassay	(Hua et al., 2009)
Glycolipids synthesised with the help of glycosyltransfe-rases encoded by: *bre2, bre3, bre4, bre5* genes.	*C. elegans*	Cry5B	Immunofluorescence, chase assay, feeding bioassay	(Griffitts et al., 2003)

ABCC transporter ABCC2	*S. exigua*	Cry1Ca, Cry1Ac	RNAi, feeding bioassay	(Park et al., 2014)
ABCC transporter ABCC2	*B. mori*	Cry1Ab	Germline transformation	(Atsumi et al., 2012a)
ABCC transporter BmABCC2	*B. mori* (expressed in *S. frugiperda* 9 cells)	Cry1Ab, Cry1Ac	Permeability: LDH assay, cell swelling assay	(Tanaka et al., 2013)
ABCC transporter HevABCC2	*H. virescens* (expressed in *S. frugiperda* 9 cells)	Cry1Aa, Cry1Ab, Cry1Ac	Viability assay	(Bretschneider et al., 2016)
Homologues of methylthiotrans-ferase (CDKAL1), co-chaperone (SDF2L1), metalloproteinase (PxHEL-1)	*P. xylostella*	DiPel: Cry1Aa, Cry1Ab, Cry1Ac, Cry2Aa	RNAi, feeding bioassay	(Ayra-Pardo et al., 2015)
Beclin-1	HeLa cells	PS-1	Beclin-1 polypeptide competition assay	(Katayama et al., 2011)

2. Objectives

Overall, this project aims to uncover the mechanism of action of a human cancer cell active toxin – parasporin-3, also known as Cry41Aa. Different features of PS-3 toxic action were investigated on susceptible HepG2 cells, like the presence of apoptotic and necrotic markers, changes in cell morphology, effect on metabolic activity and membrane permeability. The toxin's ability to form pores in planar lipid bilayers was also assessed. Activation of certain signalling pathways was evaluated to gain basic understanding of cellular responses to the toxin. Aiming to increase knowledge about toxin specificity, PS-3 was tested on cell lines not examined before. Finally, this work attempted to identify a PS-3 receptor predicted to be present on susceptible cells, which is thought to play a pivotal role in cytotoxicity.

3. Materials and methods

3.1 Materials

Bacterial strains and plasmids

E. coli DH5α - a high efficiency transformation strain, used for routine cloning.

E. coli GM2163 – a dam^-/dcm^-, chloramphenicol resistant strain used to obtain non-methylated DNA for transformation of *Bt* 4D7.

Bt 4D7 - a crystal minus strain, derivative of *Bt* subspecies *kurstaki*, obtained from the Bacillus Genetic Stock Centre.

Bt pSVP2741Aa – a recombinant 4D7 strain expressing *cry41Aa* PS-3 gene (Krishnan, 2013) using *E.coli* - *Bt* expression shuttle vector pSVP27A, ampicillin and chloramphenicol resistant, under the control of the *cyt1A* promoter (Crickmore et al., 1994, Crickmore and Ellar, 1992).

Bt pSVP2741Aa-ΔR-HA - a recombinant 4D7 strain expressing *cry41Aa* with ricin sequence deleted and HA tag sequence introduced (Etherington et al., unpublished).

Buffers

5 x TBE buffer: 108 g of tris, 55 g of boric acid, 40 ml of 0.5 M EDTA, 2 l of dH_2O, pH 8.0.

RGB: 18.18 g tris, 0.4 g SDS, 100 ml of dH_2O, pH 8.8.

SGB: 6.06 g tris, 0.4 g SDS, 100 ml of dH_2O, pH 6.8.

5 × SDS running buffer: 7.6g tris-HCl, 36g glycine, 2.5g SDS, 250 ml of dH_2O.

2 × protein gel sample loading buffer: 2 g SDS, 6 mg EDTA, 20 mg Bromophenol Blue, 5 ml of RGB, 50 ml glycerol, 100 ml of dH_2O.

Coomassie Blue stain: methanol, dH_2O, acetic acid (10:9:1 v/v/v), Brilliant Blue R-250 (0.25%, w/v).

De-staining buffer: methanol, dH_2O, acetic acid (10:9:1, v/v/v).

10 × PBS: 80 g of 1.37 M NaCl, 2 g of 27 mM KCl, 14.4 g of 100 mM Na_2HPO_4, 2.4 g of 18 mM KH_2PO_4, 1 l of dH_2O, pH 7.4.

NP-40: 150 mM NaCl, 1.0% NP-40 or Triton X-100, 50 mM tris, pH 8.0.

RIPA: 150 mM NaCl, 1.0% NP-40 or Triton X-100, 0.5% sodium deoxycholate, 0.1% SDS, 50 mM tris, pH 8.0.

Dry blot buffer: 39 M glycine, 48 mM tris, 0.0375% SDS, 20% methanol.

Chemiluminescent detection solution: 10 ml of 100 mM tris pH 8.5, 3 µl of H_2O_2, 25 µl of 14.7 mg/ml p-coumaric acid, 50 µl of 88.6 mg/ml luminol.

Coupling buffer: 50 mM tris, 5 mM EDTA-Na, pH 8.5.

Patch clamp NaCl buffer: 140 mM NaCl, 5 mM KCl, 1.1 mM $MgCl_2$, 1.1 mM $CaCl_2$, 10 mM HEPES (pH 7.4).

Patch clamp KCl buffer: 140 mM KCl, 1.1 mM $MgCl_2$, 0.1 mM EGTA, 10 mM HEPES (pH 7.4).

PLB KCl buffer: 150 mM KCl, 1 mM $CaCl_2$, 10 mM HEPES, (pH 7.5).

Reagents and enzymes

Reagents obtained from Sigma - Aldrich: SDS, tris base, tris-HCl, CAPS, sodium pyruvate, 1-thioglycerol, sodium carbonate, Brilliant Blue R-250, hydrogen peroxide, BSA fraction V, PEGs: 1000, 2000, 4000, DMSO, sodium deoxycholate, ammonium persulfate, Bromophenol Blue, β-mercaptoethanol, TEMED, acrylamide/bis-acrylamide 30%, chloramphenicol, etoposide, EGTA, *p*-coumaric acid, luminol, sodium orthovanadate, sodium arsenite, PI-PLC, MβCD, trypsin, α-chymotrypsin, pepsin, proteinase K, lysozyme, menadione. The following were purchased from AnalaR BDH: glucose, NaCl, NaOH, Ponceau S, NP-40, TX-100, EDTA, $CaCl_2$, ethanol, sodium acetate, sodium hydrogen carbonate. Chemicals obtained from Thermo Fisher Scientific: FITC, glycine, methanol, 1-butanol, KCl, glycerol, mono-potassium phosphate, di-potassium phosphate, acetic acid, $MgCl_2$. Microcystin and SB202190 were purchased from Calbiochem; mono-sodium phosphate from Laboratory FSA Supplies. Pre-stained Protein Ladder (7-175, 11-245 and 10-230 kDa), 1 Kb DNA ladder, *Dpn*I, T4 DNA ligase were from New England Biolabs. *Hae*III was obtained from Promega. BSA, PKi (14-22 amide, myristoylated), 8-bromo-cAMP were obtained from Torcis.

Chloramphenicol was prepared as 5 mg/ml stock solution in ethanol, diluted further in LB agar to 5 µg/mL. Etoposide was prepared as 50 mM stock solution in DMSO and diluted to 0.1 mg/ml in tissue culture medium. EGTA and EDTA were prepared as a 55 mM stock solution in dH_2O (pH adjusted to 8), diluted in culture medium accordingly. $CaCl_2$ and $MgCl_2$ were dissolved in dH_2O to make 280 mM stock

solutions and later diluted to 5 mM. PI-PLC aqueous solution from *Bacillus cereus* was diluted directly in culture medium to obtain the desired concentration. MβCD was prepared as a 37.55 mM stock solution in dH_2O, diluted in culture medium to 1 - 5 mM. *p*-coumaric acid was diluted in DMSO to 14.7 mg/ml stock, then diluted in 100 mM tris to 36.7 µg/ml. Luminol was diluted in DMSO to 88.6 mg/ml stock, then diluted in 100 mM tris to 443 µg/ml. Stock of 8-bromo-cAMP was made up and used on the same day by dissolving the powder in dH_2O to 10 mg/ml. 5 mM H-89 stock was a gift from Prof George Kemenes. PKi was diluted to 1 mg/ml in dH_2O and this stock was frozen in small aliquots. PEGs were made in 25 mM tris, 150 mM NaCl, pH 8.0 as 330 mM stock solution, later accordingly diluted in DMEM. Menadione was dissolved in DMSO to 100 mM, diluted later in dH_2O. 5 mg/ml stock of HA peptide was prepared in dH_2O, later diluted in PBS. FITC was dissolved in DMF to 10 mg/ml, and then further diluted to desired concentration in DMF. Complete Mini EDTA-free Protease Inhibitor Coctail Tablet (Roche) was prepared and diluted according to the manufacturer's instruction. ECL Protein Biotinylation Module (Amersham) and SulfoLink Coupling Resin (Thermo Scientific) – were used according to manufacturer's instruction.

Antibodies

Rabbit monoclonal antibody against phospho-p38 (Thr180+Tyr182) and rabbit polyclonal antibodies against phospho-ERK, total p38 and total ERK were from Cell Signaling Technology (9215S, 9101S, 9212 and 9102 respectively). Second vial of rabbit monoclonal antibody against phospho-p38 (Thr180+Tyr182) was from Thermo Fisher Scientific (MA5 15182). The following primary antibodies were purchased from Abcam:

rabbit monoclonal against CD59 (ab126777), chicken polyclonal anti – HA tag HRP (ab1190), rabbit monoclonal anti-CREB phospho S133 (ab32096), rabbit polyclonal anti-N-cadherin (ab95440), anti-Fluorescein HRP (ab19492). Secondary HRP conjugated goat anti-rabbit antibody was purchased from Abcam (ab97051).

Cell lines

HepG2, human hepatocyte carcinoma cell line was purchased from ECACC, Salisbury, UK. HeLa, lymphoblastoid (GM12878, IB4) and Burkitt's lymphoma (MUTU1, BL31) cells were gifts from Dr Michelle West (University of Sussex, UK). HL-60 cell line was a gift from Dr Helen Stewart (University of Sussex, UK). Another batch of HL-60 cells was purchased from ECACC, Salisbury, UK. Cell lines used in electrophysiology experiments were provided by Prof Jean-Louis Schwartz (University of Montreal, Canada).

Culture media, reagents and plasticware

DMEM (high glucose), Advanced DMEM (high glucose), DMEM (high glucose, no phenol red), DMEM (low glucose), RPMI 1640, MEM, PSG, DPBS, DPBS with Ca^{2+} and Mg^{2+}, trypsin/EDTA (0.05% trypsin and 0.53 mM EDTA), Trypan Blue (0.4%) were obtained from Gibco (Life Technologies); FCS, 40 µm Nylon Mesh Cell Strainer, Nalgene 2.0 mL cryogenic vials, Trypan Blue HyClone (0.2 µm filtered) were from Fisher Scientific. 25, 75 and 175 cm^2 flasks; 60 mm dishes; 6, 12, 24 and 96-well clear and black-walled clear flat bottom plates were obtained from Nunc (Nunclon surface treated). Poly-D-Lysine treated 96-well white and black wall clear bottom plates (3843) and cell scrapers (1.8 cm) were from Corning.

Cell assay kits

The following cell assay kits manufactured by Promega were used:

- CellTiter-Blue Cell Viability Assay,
- CellTiter-Glo Luminescent Cell Viability Assay,
- RealTime-Glo Cell Viability Assay,
- ApoTox-Glo Triplex Assay,
- Caspase-Glo 3/7 Assay,
- CellTox Green Cytotoxicity Assay,
- CytoTox-Glo Cytotoxicity Assay,
- ROS-Glo H_2O_2 Assay.

3.2 Methods

Storage of cells and proteins

For long-term storage cancer cells were kept in liquid nitrogen at - 197°C and for short-time storage at - 80°C in complete medium with 10% glycerol. For bacterial strains long-term storage was in LB with 15% glycerol at - 80°C and short-term on appropriate agar plates at 4°C. Toxins were stored at - 20°C.

Bacterial growth conditions

Bt transformants were grown on high nutrient LB (Gerhardt, 1994) agar plates supplemented with chloramphenicol (5 µg/ml) for 3 - 4 days at 30°C. *E.coli* DH5α transformants were grown on LB agar plates containing ampicillin (100 µg/ml) and GM2163 transformants on chloramphenicol plates (5 µg/ml). *E.coli* and *Bt* cells prior to transformation were grown on LB plates without antibiotic overnight at 37°C. Before transformation bacterial strains were grown in LB broth shaking at 37°C.

Agarose gel electrophoresis

1% agarose gel was prepared in TBE buffer and heated until dissolved. After brief cooling 0.5 µl of Gel Red dye (Biotium) was added, and gel was left to solidify. A mixture of the DNA and a loading buffer (5:1 v/v) was loaded per lane, alongside a 1 kB DNA ladder. Gel was run at 120 V in TBE buffer for 30 min. The bands were visualised using Image Lab 4.0.1 software (Bio-Rad).

PCR

Bt pSVP2741Aa-ΔR-HA plasmid was used as a template in the mutagenesis experiment. The PCR programme named PFU Ultra 10 Kb involved the following steps: initial denaturation at 98°C for 2 min, 30 cycles of denaturation at 92°C for 40 seconds, 30 cycles of annealing at 63°C for 8 min, 30 cycles of elongation at 68°C for 5.5 min and final extension at 68°C for 5 min. The primers used to create the mutation were obtained from Eurofins Genomics at a concentration of 10 pmol/µl each:

Forward primer: 5'- GCAATTGAATTCATTCCGCTAAGTCC – 3'

Reverse primer: 5' - GTCAATCCAAATAGGCCCG – 3'

PCR mixture (50 µl total volume) contained: 1 µl of forward and reverse primers each, 1 µl of template DNA, 25 µl of the PfuUltra II Hotstart PCR Master Mix (Agilent) and 22 µl of dH_2O. PCR product was purified using QIAquick kit and visualised on a gel.

Purification of DNA from a bacterial culture

Purification of DNA from a bacterial culture was done using QIAprep kit (QIAgen). Briefly, the area of 1 cm^2 of freshly grown *Bt* cells was scraped and re-suspended in P1 buffer containing dissolved lysozyme (10 mg/ml). This mixture was incubated at 37°C for 30 min. For *E.coli* cells the lysozyme incubation step was omitted. Next, 250 µl of buffer P2 was added to the tubes and they were inverted until solution became clear. Then, 350 µl of buffer N3 was added and tubes were mixed by inverting until solution went cloudy. Tubes were spun at 17,000 x g for 10 min. Supernatant was applied to spin column. Tubes were spun briefly at 17,000 x g and flow-through was discarded. 500 µl of PB buffer was added, followed by a brief spin at 17,000 x g. Supernatant was discarded. Next, samples were washed with 750 µl of PE buffer, followed by a brief centrifugation. Flow-through was discarded and samples centrifuged again at 17,000 x g to remove residual buffer. Spin columns were placed in clean 1.5 ml tubes. Finally, after 1 min incubation, DNA was eluted in 30 µl of EB buffer (10mM tris-Cl, pH 8.5) by brief centrifugation at 17,000 x g.

Purification of PCR products

Amplified PCR products were purified using QIAquick kit (QIAgen) according to manufacturer's instruction.

DNA Digestion

*Dpn*I enzyme was used to digest the methylated DNA prior to transformation into *E.coli* DH5α to remove template DNA. 1 µl of *Dpn*I was added to 45 µl of PCR product. This mixture was incubated for 1 hour at 37C. *Hae*III enzyme was used to digest plasmids to confirm that the purified DNAs were the right constructs. Digestion tube contained: 1 µl of DNA, 7.5 µl of dH_2O, 1 µl of Buffer C, 0.5 µl of *Hae*III enzyme. Tube was incubated for 30 min at 37°C. Experimental restriction banding patterns were compared with the pattern predicted by the NEBcutter (Vincze et al., 2003).

DNA ligation

After digestion with *Dpn*I and purification using QIAquick kit, PCR product was self-ligated. Ligation mixture included: 8.5 µl of purified DNA, 1 µl of ligase buffer, 0.5 µl of T4 ligase enzyme. The tube was left at RT overnight.

Bacterial Transformation

Bacterial strain was inoculated in 100 ml LB broth and incubated with shaking at 37°C until OD_{600} 0.4-0.8 (about 2 – 3 hours). Cell suspension was then centrifuged at 15,000

x g for 10 min at 4°C. The broth was discarded and the pellet was washed with 100 ml of cold water and centrifuged again. The supernatant was discarded and pellet was re-suspended in 1 ml of cold water. Cells were transferred to a microcentrifuge tube and spun briefly at 16,873 x g. Supernatant was poured off and the cells were re-suspended in 200 µl of cold water. 1 µl of the DNA was mixed with 50 µl of cell suspension and this mixture was placed into a pre-chilled 2 mm electroporation cuvette. Cuvette was slotted into a Gene Pulser II (Bio-Rad) set to 1.8 kV, 200 Ohms, 25 µF and electro-transformation was induced. Cells were washed with 0.5 ml of LB broth, transferred into a clean bottle and incubated for 1 hour at RT. No DNA transformation was performed as a negative control. After incubation the mixture was then plated out on appropriate antibiotic supplemented plates and incubated overnight at 37°C. The next day plates were analysed for colonies followed by DNA purification.

Verification of mutation

Purified DNA from colonies after transformation into *E. coli* DH5α and *Bt* 4D7 was sequenced to confirm presence of the correct mutation by Eurofins Genomics. This was done using the primer: 5'- CATCATATGGATA - 3'.

Protein harvesting

Sporulation and crystal production was assessed under a light microscope (Leica DMLS). Sporulated cells were aseptically scrapped off the plate and suspended in 30 ml of cold dH_2O. The cells were lysed by repeated sonication at 150 Watt (four cycles of 1 min) on ice. The pellet was collected by centrifugation at 12,000 x g for 10 min at 4°C

and re-suspended in 1 ml of dH_2O. Crystal/spore mixture was analysed under the light microscope.

Protein solubilisation and activation

Pellet containing parasporal inclusions was solubilized in 50 mM sodium carbonate (pH 10.5) in the presence of 5 mM dithiothreitol (DTT) at 37°C for 1 hour (1:1 v/v ratio of pellet to buffer). Sample was then spun down at 16,873 x g for 5 - 10 min and supernatant containing solubilized protein was treated with a protease. 10 mg/ml of trypsin solution in dH_2O was used for activation at the ratio of 1:10 (v/v) enzyme to supernatant at 37°C for 1 hour. Sometimes proteinase K solution (0.1 mg/ml) was used instead. After digestion, Complete mini EDTA-free protease inhibitor was added to stop further proteolysis.

Protein dialysis and concentration

The proteins were dialysed overnight before being used in cell assays to remove traces of DTT and other low molecular weight contaminants. The dialysed samples were analysed using SDS-PAGE. For small volumes this was done using a 10 kDa MW cut - off Micro DispoDialyzer (Harvard Apparatus). For bigger volumes (>100 µl) 12 kDa MW cut - off Dialysis Tubing Cellulose Membrane (D9777-100FT Sigma) was used. Samples were dialysed usually against 1 litre of either 50 mM Na_2CO_2 (pH 7.4), PBS (pH 7.4), 25 mM tris-HCl 150 mM NaCl (pH 7.4), or 10 mM CAPS (pH 10.4) at 4°C using a magnetic stirrer. For dialysis, buffer exchange and sample concentration Vivaspin500 and Vivaspin6 columns (GE Healthcare) were used.

Protein purification

Sephacryl S-200 High Resolution (Amersham) resin was used for gel filtration. A glass column was filled with 15 ml of resin and equilibrated with appropriate buffer (5 times the column volume). Most common buffers used for sample elution were: 50 mM Na_2CO_3 (pH 7.4), 25 mM tris-HCl 150 mM NaCl (pH 7.4), or PBS (pH 7.4). Generally 0.5 ml of the solubilized or protease treated protein was applied to the equilibrated column and sample was eluted with around 10 ml of the buffer. Collected fractions (0.5 - 1 ml) were analysed for protein content using Bio-Rad protein assay and SDS-PAGE.

Proteins were also purified and separated by the means of Resource Q 1 ml (GE Healthcare Life Sciences), a strong anion exchange column connected to ÄKTA Purifier FPLC System. Toxins were first dialysed overnight against 10 mM CAPS (pH 10.4) using 12 kDa MWCO Dialysis Tubing Cellulose Membrane, spun and 0.22 μM filtered before injection. Sample was injected in 10 mM CAPS (pH 10.4) and elution was achieved with a gradient of NaCl (0 to 1 M) over 20 minutes at a flow rate of 1 ml/minute. 0.5-1 ml fractions were collected and analysed using Bio-Rad protein assay and SDS-PAGE.

Protein concentration

Protein concentration was determined by the Bradford method (Bradford, 1976) using a Bio-Rad Protein Assay Kit (Bio-Rad) with BSA as the standard. All presented concentrations represent final concentrations used (unless stated otherwise). The assay involves the addition of Coomassie Brilliant Blue G-250 to a protein solution,

which in acidic conditions binds to basic amino acids and can be measured at 595 nm with a spectrophotometer. The mixture was incubated for 5 - 10 min at RT before measurement. Concentration of the unknown sample was determined by comparing its absorbance value against a plotted BSA standard curve. The standard curve showed near linear response (R^2=0.9975) over 0 - 1 mg/ml BSA concentration range.

Protein analysis by SDS-PAGE

Proteins were resolved in 7.5 - 12% separating gels depending on the fragment size by SDS-PAGE based on method described by Laemmli (Laemmli, 1970) using Mini-PROTEAN® II Electrophoresis Cell (Bio-Rad). Samples were mixed with 2 or 4 x sample loading buffer additionally supplemented with reducing agent β- mercaptoetanol (5%), boiled for 3-5 min, and spun. Supernatant samples were loaded on the gel and run at 200 V for approximately 35 min using a tris - glycine buffer. Gels were stained with Coomassie blue staining and de-stained. Molecular masses of proteins were estimated by comparison with molecular standards (New England BioLabs).

Microscopy

Nikon Eclipse TS100 inverted microscope was used for routine cell viability observation and post-treatment monitoring of swelling. For DIC morphological observation cells were seeded in the Chambered 1.0 Borosilicate Coverglass slide (Lab-Tech) at the density of 2.97 x 10^4 cells per chamber well and cultured overnight. For detailed DIC cell examination using purified toxins, cells were seeded in 1 µ-Slide 8 well coated (Collagen IV) Microscopy Chamber (ibidi) at the density of 1.54 x 10^4 cells per well and

cultured overnight. The next day cells were observed using Zeiss Axiovert 200M motorized inverted microscope with 63x air objective.

Cell culture conditions

The cells were maintained under the conditions recommended by the supplier. For adherent cells, culture medium DMEM with high glucose (4.5 g/l) was supplemented with 10% FCS, and with 1% PSG (100 U/ml penicillin, 100 µg/ml streptomycin, 292 µg/ml L-glutamine). Suspension cells were cultured in RPMI 1640 supplemented with 10% FCS and 1% PSG. For the culture of BL31 cells, RPMI 1640 was additionally supplemented with sodium pyruvate (100 nM) and 1-thioglycerol (100 nM).

The cells were routinely cultured in sterile polystyrene 75 cm^2 flasks (Nunc) in standard cell culture conditions (37°C and 5% CO_2 humidified air). Medium was changed twice a week. When adherent cells reached confluency (between 70-80%) they were washed with DPBS and detached by trypsinization (trypsin/EDTA containing 0.05% trypsin and 0.53 mM EDTA) at 37°C for 5 - 10 minutes. This was followed by spinning (100 - 200 x g for 5 min). Adherent cells were dispersed by banging and re-suspension in fresh medium. Cells were counted and split depending on the desired seeding ratio.

For electrophysiology experiments HepG2 cells were cultured in DMEM and low glucose (1 g/l). HeLa cells were cultured in MEM. Both media were supplemented with 10% FCS and 1% PS (10 U/ml penicillin, 10 µg/ml streptomycin). Media were buffered with 25 mM HEPES and cultured in the absence of CO_2 in non-coated 60 mm plastic dishes.

Cell assays

Fluorescent and luminescent cell assays were performed in 96-well plates. Each well received 90 µl of cell suspension at a density of 5,000 or 22,500 cells per well (equivalent to 5.5 x 10^4 or 25 x 10^4 cells/ml) in complete DMEM (DMEM supplemented with FCS and PSG) and cultured overnight under standard cell culture conditions (unless specified otherwise). After incubation, each well received 10 µl of treatment. In most cases mock control wells contained 90 µl of cell suspension and 10 µl of the appropriate buffer. The following control buffers were used: for non-purified, dialysed toxins - Na_2CO_3 (7.4 pH), for gel filtered toxin - 25 mM tris-HCl, 150 mM NaCl (pH 7.4), for ÄKTA purified toxin - PBS (7.4 pH). For background fluorescent/luminescent control 100 µl of appropriate cell culture medium was aliquoted. Additionally, whenever possible, to test for possible interference between analyte and culture medium, a control containing 90 µl of medium only and 10 µl of treatment was set up. Generally, each treatment was tested in triplicate (three technical replicates).

The viability of the cells was measured using CellTiter-Blue, generally after 24 hours of treatment. For CellTiter-Blue assays cell density and incubation time with the reagent were optimised for each cell line. 20 µl of the reagent was added at the end of toxin exposure period and the reading was taken after additional 2 hours (end-point method). Fluorescence was measured with a green filter with excitation wavelength at 525 nm and emission wavelength range of 580-640 nm. For RealTime-Glo cell viability assay 'Continuous – Read Method: Reagent Addition at Cell Plating' was selected.

CellTox-Green and CytoTox-Glo assays were used for evaluation of cytotoxicity by measuring changes in membrane permeability. CytoTox-Glo assays were done

according to the manufacturer's protocol. For CellTox-Green assays 'Express, No-Step Addition at Seeding Method' was selected. In brief: to 5 ml of cell suspension 10 µl of CellTox Green dye was added and then 90 µl of the mixture was dispensed into each well and allowed to adhere overnight. The next day each well received 10 µl of treatment followed by the desired incubation length. Fluorescence was measured before the treatment and at different time-points post-treatment using a blue filter with excitation wavelength at 490 nm and emission wavelength range of 510-570 nm.

Caspase 3/7 levels were assessed in compromised cells over 8 hour period using ApoTox-Glo Triplex Assay and over 24 hour period using Caspase-Glo 3/7 Assay. The former was performed according to the manufacturer's protocol. The latter was multiplexed with CellTiter-Blue for simultaneous assessment of cell viability. At the end of each treatment 20 µl of CellTiter-Blue reagent (for this assay diluted 1:4 v/v in DPBS) was added to each well and the reading was taken after 1.5 hours. After that 100 µl of Caspase-Glo 3/7 reagent was added to each well and the luminescence readings were taken after brief orbital mixing and 30 min incubation at RT.

The fluorescent and luminescent readings were performed using GloMax - Multi Detection System (Promega) according to each assay instructions. After the readings were acquired, the CellTox-Green values before toxin treatment were subtracted from the readings after treatment in that same well. In the case of other cell assays fluorescent or luminescent signal in the background control wells was subtracted from each experimental value.

Trypan Blue exclusion method was used for additional assessment of cell viability (Mehdizadeh, 1991). HL-60 (25 x 10^4 cells/ml) or HepG2 (20 x 10^4 cells/ml)

cells were grown in a 96-well plate and incubated with either PS-3 (12 µg/ml) or buffer only for 3 or 24 hours. The medium was removed from HepG2 and cells were trypsinized (100 µl of trypsin/EDTA) for 10 min at 37°C, followed by the addition of 100 µl of 0.4% Trypan Blue dye aqueous solution. In case of HL-60 cells, 100 µl of Trypan Blue was added straight in the wells containing 100 µl of cell suspension. Viable cells were counted after 10 min incubation with Trypan Blue.

In experiments with metal chelators 90 µl of cell suspension (containing 25 x 10^4 cells/ml) were pre-treated with a chelator for 30 min (unless specified differently) followed by toxin treatment for 3 hours. After that CellTiter-Blue reagent was added and the reading was taken after additional 2 hours. If metal salts were used they were added 10 min before toxin addition.

Statistical analysis and data presentation

Cell assay results were expressed as means ± SEM for each experimental triplicate (unless stated otherwise). To establish PS-3 $EC_{50,}$ Probit Regression analysis was performed in SPSS software version 22.0 (IBM, 2013). For statistical comparison of treatments in salt supplementation experiments, Post-Hoc analysis applying a Bonferroni adjustment was carried out in SPSS. Dose-response curves in chapter 5 were performed using nonlinear regression analysis and the equation 'Dose-response – Stimulation, log (agonist) vs. response - Variable slope' in GraphPad Prism version 7.00 for Windows, GraphPad Software, La Jolla California USA, www.graphpad.com.

Planar lipid bilayer

Preparation of planar lipid bilayers involved creating a lipid mixture containing: phosphatidylethanolamine (PE), phosphatidylcholine (PC) and cholesterol (Avanti Polar Lipids) in a ratio of 7:2:1 (w/w/w). Lipids were first dried with N_2 to evaporate chloroform and then dissolved in n-decane, at a final concentration of 20 µg/ml. 1 ml of KCl buffer (150 mM KCl, 1 mM $CaCl_2$, 10 mM HEPES, pH 7.5) was added to each of the custom made disposable chambers. A 250 µm diameter hole present at the junction of both chambers was painted with the lipid mixture using a blunt end glass pipette. However, only the central area of around 100 µm in diameter created a functional bilayer. Chambers were connected to the electrodes through conducting agar bridges and placed inside a Faraday cage to decrease electrical interference. Voltage was applied to the cis chamber (trans chamber was grounded). Membrane activity was recorded for 30 minutes before toxin was added to ensure that there was no contamination. Capacitance of the membrane was between 180 - 200 pF and the painted membranes remained stable for a few hours. PS-3 was dosed at a starting concentration of 4 µg/ml, later increased to 8 µg/ml, and current was recorded at different applied voltages. At the end of each of the three experiments, concentration of KCl in the cis chamber was increased to 450 mM to test if the pore was more cation or anion selective. All experiments were performed at RT. Voltage was applied using Axopatch – 1D (Molecular Devices). Detected current was recorded and amplified by the same instrument and converted into a digital signal with Axon Digidata 1440A (Molecular Devices). Currents were filtered at 5 kHz and digitized at 50 kHz. Recordings were analysed using pCLAMP 10.5 (Molecular Devices). To measure the conductance,

20 to 25 current jumps were recorded for each voltage and averaged. Currents were plotted versus applied voltages (I/V curves) and the data points were fitted by linear regression. Mean conductance (G) was read from the slope of each I/V curve regression line. Probability of channel opening was evaluated from recordings by digital analysis of the distribution of all current values and plotted for each voltage as a histogram using pCLAMP 10.5 software.

Patch clamping

Cells were seeded at a low density on 24 mm circular glass coverslips inside 35 mm dishes, usually 24 - 48 hours before the experiments. Just before patching, cells were washed three times with appropriate buffer and mounted inside a coverslip holder that was fitted to the stage of an inverted microscope (IMT-2, Olympus). 1 ml of either NaCl (140 mM NaCl, 5 mM KCl, 1.1 mM $MgCl_2$, 1.1 mM $CaCl_2$, 10 mM HEPES, pH 7.4) or KCl buffer (140 mM KCl, 1.1 mM $MgCl_2$, 0.1 mM EGTA, 10 mM HEPES, pH 7.4) was added. Pipettes were prepared using a Narishige glass capillary puller in a two-step heating process. Two types of pipettes were used: borosilicate LG16 (Warner Instruments) for some of single channel recording and soda lime 200 (Kimble Chase) for single channel and whole cell recordings. The heater was set to 84/77 for borosilicate and 84/74 for soda lime pipettes. The following configurations were used in patch clamp experiments: cell attached, whole cell, inside out (explained in section 4.7). Pipettes were mounted inside a holder attached to an automatic micromanipulator. Electrical connection between the pipette and the amplifier was via Ag/AgCl pellets. Bath solution was grounded. In some experiments, the pipette was

first filled with appropriate buffer, followed by toxin addition on top to allow slow diffusion towards the tip of the pipette. In other experiments, the toxin was added straight to the bath. The filled pipettes had the resistance of around 4 MΩ and the resistance of the seal was in the range of 2 - 10 GΩ. In the whole cell mode a voltage of - 20 mV was applied to ease the transition from the cell attached into the whole cell mode. Currents were induced by a set of seventeen 1 second depolarizing potential steps from −20 to 140 mV (10 mV increments). Current values between 0.95 – 1 s were analysed at each voltage, counting from the beginning of each recording. Values were corrected for the averaged baseline current measured just prior to the applied potential. Current – voltage curves in the whole cell experiments were generated from each data set for each time point and conductance was calculated from the slope of regression line of each I/V curve. In the single channel experiments, with excised patches conductance was calculated using G = I/V equation. Similar conductance values were grouped and mean conductance calculated. In the cell attached mode the data points were plotted and reversal potential (Vr) calculated from the intersection of the voltage axis with the linear regression at zero current. Conductance was calculated using: G=I/(V-Vr) equation to correct for the intracellular voltage. Similar conductance values were grouped and mean conductance calculated. All experiments were performed at RT. Voltage was applied using Axopatch – 1D (Molecular Devices). Detected current was amplified and converted into a digital signal with Axon Digidata 1550 (Molecular Devices). Currents were filtered at 10 kHz and digitized at 50 kHz. Recordings were analysed using pCLAMP 10.6 (Molecular Devices).

Cell lysis prior to western blot

For western blot experiments, cells were plated inside 6, 12, 24-well plates or 60 mm dishes. In general, cells were lysed with either RIPA, NP-40 (1 ml of lysis buffer per 2.8 x 10^7 cells) or 1.5% NOG (1 ml of lysis buffer per 2 x 10^7 cells). Each lysis buffer contained protease inhibitors: Complete protease inhibitor mixture, 1 mM EGTA, 1 mM EDTA and phosphatase inhibitors: 2 mM sodium orthovanadate and 1 µM microcystin.

Cell lysis for ligand blots with biotinylated PS-3, HA-tagged PS-3 and N-cadherin, pCREB western blots:

HepG2 and HeLa cells were seeded at the density of 3.5 x 10^6 cells/ml in 60 mm dishes (14 x 10^6 cells/dish) unless specified differently. The next day medium was removed; cells were washed twice with cold DPBS and lysed with RIPA, NP-40 or NOG as described above. Lysed cells were incubated on ice with swirling for 30 min. RIPA cell extracts were transferred into tubes and sonicated on ice 3 x 10 sec. at 21% output (Sonics, The Vibra-Cell). Lysates were spun at 16,873 x g for 15 - 60 min at 4°C. Supernatant was collected and frozen down for further analysis.

Cell lysis for p38, ERK western blots:

HepG2 or HeLa cells were seeded at the density of 25 x 10^4 cells/ml in 6 well-plates (75 x 10^4 cells/dish). When cells reached >70% confluency (often the next day) they were exposed to sodium arsenite, buffer, or toxins for 15 - 30 min before being washed twice with DPBS. Intact cells were gently scraped, spun at low speed (200 x g) and supernatant was discarded. Pellet containing intact cells was re-suspended in 100 µl of

NP-40 with protease and phosphatase inhibitors (1 ml of lysis buffer per 7.5 x 10^6 cells). Samples were vortexed for 10 seconds, left on ice shaking for 20 minutes and spun at 16,873 x g for 15-30 min at 4°C. Supernatant was collected, diluted 3 - 5 times and protein concentration measured using the Bradford method. In case of HL-60, the cells were harvested on the same day. 1 x 10^6 cells were placed in each test tube containing 1 ml. Cells were treated and the tubes were placed in the incubator slightly open. After 30 min incubation supernatant was removed by gentle spin and the cells were gently washed with 1 ml of DPBS. After a gentle centrifugation DPBS was removed and the pellet was lysed with 100 µl of NP-40 buffer as described above.

Cell lysis for western blots with HA-tagged PS-3 - modified protocol:

HepG2 cells were seeded at the density of 40 x 10^4 cells/ml in 6 well-plates (1.2 x 10^6 cells/dish). Cells were exposed to concentrated HA-PS-3 (60 µg/ml) for 20 min and washed three times with DPBS. Fresh DMEM was added and cells were incubated for additional 40 min at 37°C. After that the medium was gently removed and cells were lysed in 250 µl of either RIPA or NP-40 with inhibitors (1 ml of lysis buffer per 4.8 x 10^6 cells). Cells were scraped, transferred into tubes, shaken on ice for 30 min and spun at 16,873 x g for 15 min at 4°C.

Western blot

Western blot protocol was optimised for each experiment.

p-p38, t-p38, p-ERK, t-ERK, CD59, p-CREB, N-cadherin western blots:

Between 5-30 µg of protein were loaded per well. The proteins were resolved on SDS-PAGE gels (7.5 - 12%). The gel was soaked in dry blot buffer gently rotating for 10 min. Proteins were transferred to a nitrocellulose membrane (HyBond ECL or Bio-Rad, pore size 0.45 µm) using a Bio-Rad Trans-Blot Semi-Dry Transfer Cell system (100 mA for 60 min). Membrane was washed for 5 min with PBS and then blocked with PBS containing 0.02% Tween-20 (PBS-T) and 3% BSA for 1-3 hours at RT. Membranes were washed 3 x 10 min with PBS-T. Probing was done overnight at 4°C by incubating the membranes with rocking in a fresh blocking solution containing 3% BSA and primary antibody diluted in PBS-T (1:1000 v/v dilution for antibodies against total and phosphorylated ERK and p38; 1:50000 v/v dilution for anti-CD59 antibody). In p CREB and N-cadherin western blots both blocking and incubation with primary antibody (1 µg/ml final) was done using 5% non-fat dry milk instead of BSA. The next day the membranes were washed 3 x 10 min with PBS-T, followed by 1 hour incubation with an appropriate horseradish peroxidase-conjugated secondary antibody diluted 1:2000 v/v in PBS-T containing 5% non-fat dried skimmed milk. Finally, the membranes were washed again (3 x 10 min, PBS-T) and soaked in the chemiluminescent detection solution and exposed to X-ray film (FUJI medical X-ray film).

<u>Biotin labelled PS-3 western and ligand blots:</u>

In western blots with biotin labelled toxin, blocking was done for 1 hour using supplied blocking reagent diluted to 5% in PBS with Tween-20 (0.1%). Membrane was rinsed with PBS-T twice followed by 1 hour incubation with biotinylated toxin diluted in PBS-T gently shaking at RT. Next, membrane was washed three times with PBS-T, first for 15 then twice for 5 min and incubated with Streptavidin – HRP (1 in 1500 v/v) in PBS-T for

another hour at RT. After 3 x 15 min washes signal was detected using supplied enhanced luminol-based chemiluminescent detection (ECL).

HA-PS-3, HA-PS-3 (K668A), FITC-PS-3 western and ligand blots:

Protocol was modified in a way that blocking was done for 1-2 hours at RT with PBS-T containing 5% non-fat dry milk (in experiments with FITC-PS-3 blocking was done using 3% BSA). In toxin ligand blot experiments the membranes were then washed and incubated with different amounts of tagged PS-3 diluted in PBS-T or PBS usually for 1 hour at RT. Incubation with FITC-PS-3 was done in the dark. After washes, the membrane was incubated with appropriate antibody (either anti HA-tag HRP conjugated; 0.5 µg/ml or anti FITC-HRP conjugated; 7.5 µg/ml) for 1 hour at RT in PBS-T 5% Milk, followed by washes and ECL detection.

Native western blots:

PAGE gels were cast as in SDS-PAGE, except SDS was omitted in gels and running buffers. Non-reducing (without β-mercaptoethanol) and non-denaturing (without SDS) 5 x sample loading buffer was used and samples were not boiled before loading. Gels were run at 100 - 150 V for about 1 - 2 hours.

Pull down

Pull down with anti-HA agarose slurry:

Pull down was carried out as recommended by the manufacturer (Pierce). Briefly 100 µl of anti HA agarose slurry was placed in a tube and washed with TBS. Roughly 50 - 150 µg of HA tagged protein was added to pelleted resin and samples were incubated

for varying amounts of time on a rocking platform either at RT or 4°C. Next, cell extract (containing between 150 - 350 µg of protein) was added and the tube was incubated with rotation for the designated period of time. After incubation resin was washed three times with TBS with 0.05% Tween-20. Finally HA-tagged protein was eluted with 50 µl of either 0.1 M glycine (pH 2.4) or 3 M NaSCN. When using glycine, supernatant containing eluted protein was neutralized with 1:10 volume with 0.1 M tris pH 9.5. Elution step was repeated twice.

Coupling of cysteine residues and pull down with SulfoLink resin:

Toxin coupling was carried out as recommended by the manufacturer (Thermo Fisher Scientific). Briefly 100 µl of agarose slurry was placed in a tube and washed four times with the coupling buffer. Roughly 50 - 150 µg of ÄKTA purified toxin concentrated and dialysed against coupling buffer was added to pelleted resin and samples were incubated with rocking at RT for 15 min. Next, non-specific binding sites on the resin were blocked to avoid cell extract proteins with reactive –SH groups binding to the beads. 50 µl of 50 mM L-cysteine-HCl solution in coupling buffer was added to the resin and incubated for 15 min at RT rotating, followed by a 30 min additional incubation without mixing. Next, resin was washed and incubated with cell extract (containing between 150 - 350 µg of protein) rotating for 1 hour at RT. After incubation resin was washed three times with coupling buffer and samples (supernatant and pellet) were analysed using SDS-PAGE.

Biotinylation

ECL Protein Biotinylation kit (Amersham) was used according to manufacturer's instruction. Briefly 40 µl of biotinylation reagent was incubated per 1 mg of activated toxin in 40 mM bicarbonate buffer for 1 hour at RT shaking. Next, sample was applied to a pre-equilibrated column and eluted with PBS.

FITC labelling

PS-3 was trypsin activated, gel filtered and eluted in 50 mM sodium carbonate buffer (pH 8.5). Molar concentration of PS-3 was calculated based on Beer-Lambert law which relates concentration of a solute to its absorbance (Wood, 1983): $A = \varepsilon c l$, were A = absorbance, ε = molar extinction coefficient, c = concentration and l = light path-length. Given this equation, concentration can be calculated: $c = A/\varepsilon l$. ε is related to protein's tryptophan (W), tyrosin (Y) and cysteine (C) amino acid composition. At 280 nm, ε can be calculated as follows: $\varepsilon = (nW \times 5500) + (nY \times 1490) + (nC \times 125)$, where n stands for the number of each residue. In the PS-3 sequence after trypsin cleavage the following are most likely present: W=24, Y=45 and C=6. ε was calculated as 199,800, and protein absorbance at 280 nM was 7.664. Molar concentration of activated PS-3 came up as 38.358 µM. 50 µl of activated PS-3 was mixed gently with 25 µl of 1534 µM solution of FITC (to achieve 20 fold excess of the dye). Mixture was incubated in the dark for 1 hour, then excess dye and DMF was removed and buffer exchanged into 50 mM sodium carbonate (pH 8.0) via at least five washes with a Vivaspin500 column.

4. Protein characterization and cytotoxic effects

4.1 Introduction

Conditions for toxin solubilisation and digestion used by the research group that first characterised PS-3 involved a 1 hour incubation at 37°C in 50 mM sodium carbonate 1 mM EDTA (10.5 pH), followed by a 90 minute treatment with proteinase K (10 µg/ml) in the presence of 10 mM DTT reducing agent at 37°C (Yamashita et al., 2005). Here a characterization of recombinant PS-3 was carried out in order to find the optimum conditions for protein solubilisation, digestion and purification.

Many attempts were made to purify PS-3. Mono S HR 5/5 (strong cation exchange) and Phenyl Sepharose 6 Fast Flow column (hydrophobic interaction chromatography) proved unfruitful (data not shown). Successful purification (but not separation of toxic fragments) was achieved with the gel filtration resin Sephacryl S-200. In gel filtration molecules in solution are separated according to their sizes and shapes as they pass through a column packed with a chromatographic medium. Sephacryl is a hydrophilic composite gel made by covalently cross-linking allyl dextran with N,N'-methylene bisacrylamide, that allows for protein purification in the range from 5,000 to 250,000 Daltons for globular proteins (Biotech, 2010). Successful purification and separation of toxic fragments was achieved with a 1 ml Resource Q column (strong anion exchange, GE Healthcare Life Sciences) connected to an ÄKTA Purifier – FPLC System. In anion exchange chromatography, negatively charged molecules are attracted to a positively charged solid phase. Ionic interaction between

the oppositely charged sample molecule and the column resin retains the sample, which is later eluted by increasing salt concentration. The predicted pI of PS-3 protoxin calculated by Compute pI/Mw Expasy tool (Elisabeth Gasteiger, 2005) is 6.18 and only slightly changes when proteolytically cleaved toxin sequence is input. Close to neutral pI should make PS-3 suitable for both cation and anion exchange methods. However because PS-3 fragments were previously successfully separated using anion exchange (Yamashita et al., 2005) and because previous attempts to use cation exchange purification failed, anion exchange method was optimised to separate PS-3 fragments.

Cell based assays were used to measure viability of PS-3 treated cells in vitro. Metabolic activity and ATP levels were used as viability indicators. Trypsin activated Cry1Ca was tested as a negative control in these and other cell assays for two reasons. It shares a similar three domain Cry toxin fold with PS-3 while having activity against lepidopteran insects and no known human cytocidal activity. Secondly, Cry1Ca was expressed in the same acrystalliferous *Bt* strain as recombinant PS-3. Most of the cell assays were performed with susceptible HepG2 cells. Additionally, the effect of PS-3 was assessed on cellular viability of other cell lines not examined before, like Burkitt's lymphoma and lymphoblastoid cells.

Measurement of cell membrane integrity in compromised cells was achieved using two cytotoxicity cell assays. CellTox-Green assay, using a non-toxic small cyanine dye (~661 Da), allows for continuous assessment of membrane permeability for up to 72 hours in the same set of cells. The dye is excluded from viable cells, whereas in cells with compromised membranes it binds to the minor grove of the DNA producing a fluorescent signal proportional to the amount of cells with disrupted membranes.

Another membrane permeability assay, CytoTox-Glo measures a distinct protease activity associated with a cytotoxic marker, which is released from cells that have lost membrane integrity. The substrate cannot cross the intact membrane of live cells but in the presence of the released protease generates a stable luminescent signal. Scientists speculate that the cellular protease responsible for this reaction is consistent with tripeptidyl peptidase II (Niles et al., 2007), which is a relatively big 138 kDa protein. Osmotic swelling resulting from toxin induced membrane damage was recorded using a differential interference contrast (DIC) microscope.

Additionally, changes in membrane permeability were monitored in electrophysiology experiments using both artificial bilayers and biological membranes. Electrophysiology allows the measurement of electrical properties of a membrane. In a simplified model, the membrane represents a charge storing capacitor separating two current conducting solutions. In the presence of a pore, ions driven by the electrochemical gradient pass through the pore and current can be detected. The current is directly proportional to the voltage potential as described by Ohm's law: I=V/R, where V is potential, I current and R resistance (Millikan et al., 1917). The planar lipid bilayer (PLB) technique has been widely used to study the properties of pores induced by Cry toxins (Lorence, 1995, Peyronnet et al., 2001, Rausell et al., 2004, Schwartz et al., 1993, Schwartz et al., 1997, Slatin et al., 1990a, Walters et al., 1993). The advantage of the PLB method is having a simplified system with total control over experimental conditions like lipid composition, pH and ionic concentration. For this study, the most significant is the fact that being receptor-free, the PLB method enabled evaluation of the innate pore forming ability of PS-3. Patch clamp recordings from cells exposed to Cry toxins have been previously documented (Schwartz et al.,

1991, Stumpff et al., 2007). However in contrast to PLBs, biological complexity of the cell membrane and the presence of endogenous channels are the main reasons why this technique has not been fully exploited in the studies of PFTs. Here, the whole cell and single channel patch clamp experiments were attempted and conductance levels compared with each other and with values obtained in PLB experiments.

PEGs are linear, generally non-toxic to cells polyethers, but they act like spherical molecules in aqueous solutions (Scherrer and Gerhardt, 1971). Pore diameter can be estimated from the smallest PEG that is excluded from the cells and prevents osmotic swelling (Sabirov et al., 1993). Using this approach pore size was estimated for various proteins, including *Bt* toxins: Cry1C (Peyronnet et al., 2002), PS-2 (Kitada et al., 2006). This method was also applied to estimate the size of PS-3 induced primary lesions.

4.2 Optimizing conditions for solubilisation and digestion

The coding region of the *cry41Aa* gene was cloned from *Bt* A1462 strain and expressed in the acrystalliferous 4D7 *Bt* strain (Krishnan, 2013). Crystals of the recombinant PS-3 were observed during sporulation (Figure 15).

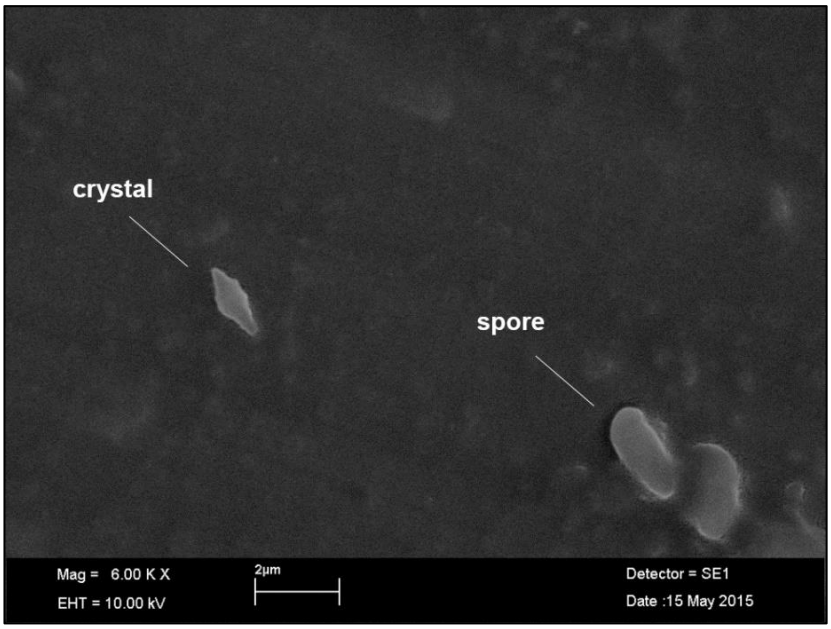

Figure 15 Scanning electron micrograph of PS-3 crystal and spores expressed in *Bt* 4D7 strain.
Sonicated suspension containing spores and PS-3 crystals was spread over a metal stub, dried overnight and coated with gold. The next day sample was visualised using transmission electron microscopy.

Crystals had a bi-pyramidal shape similar to Cry1 toxins. Figure 16 shows PS-3 samples before and after solubilisation and post-activation resolved on an SDS-PAGE gel.

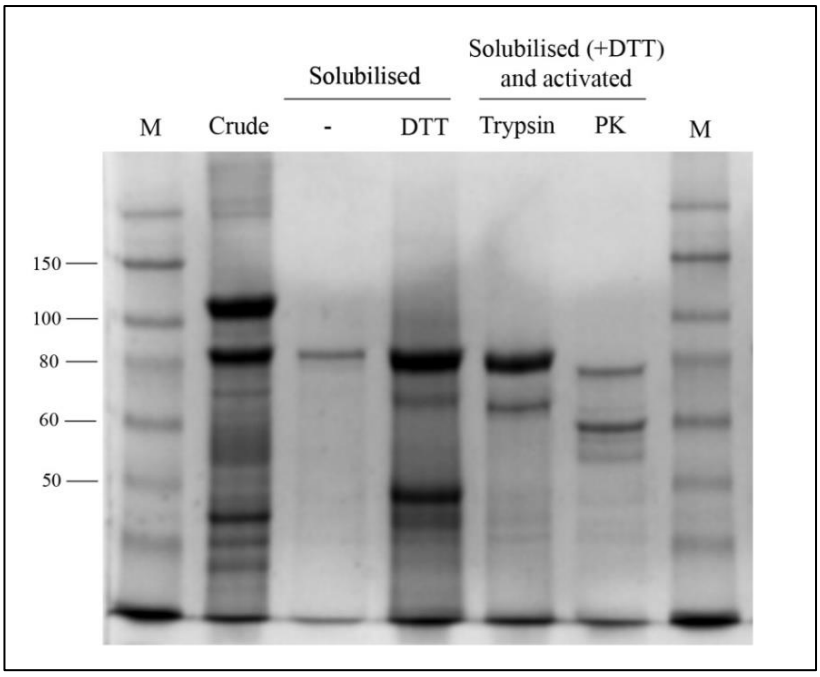

Figure 16 SDS-PAGE analysis of alkali solubilisation and activation of PS-3.
PS-3 samples were run on a 7.5% SDS-PAGE gel: protein marker (M), crude solution before solubilisation, PS-3 solubilized in the presence or absence of DTT (5 mM), solubilised protoxin activated with 1 mg/ml trypsin or 0.01 mg/ml proteinase K (PK).

An 80 kDa protein representing PS-3 was clearly visible in the crude sample after three days of growth. The 120 kDa band (Figure 16, lane 2) represents the protein coded by ORF3, normally degraded during solubilisation. Proteinase K and trypsin activated toxin forms are presented for comparison. They showed different digestion patterns. The relatively big difference in size between the lower and higher MW fragments after toxin activation can be attributed to the C-terminal cleavage since the extent of N-terminal removal was previously demonstrated to be small (Yamashita et al., 2005).

Independent solubilisation and proteolysis

Before this optimization, PS-3 had been solubilized and trypsin digested in a single tube for 1 hour at 37°C. This process resulted in a single band of around 80 kDa on a gel. However, when solubilisation and trypsin activation were performed separately (1 hour at 37°C each) two main bands appeared: around 80 and 65 kDa (Figure 17).

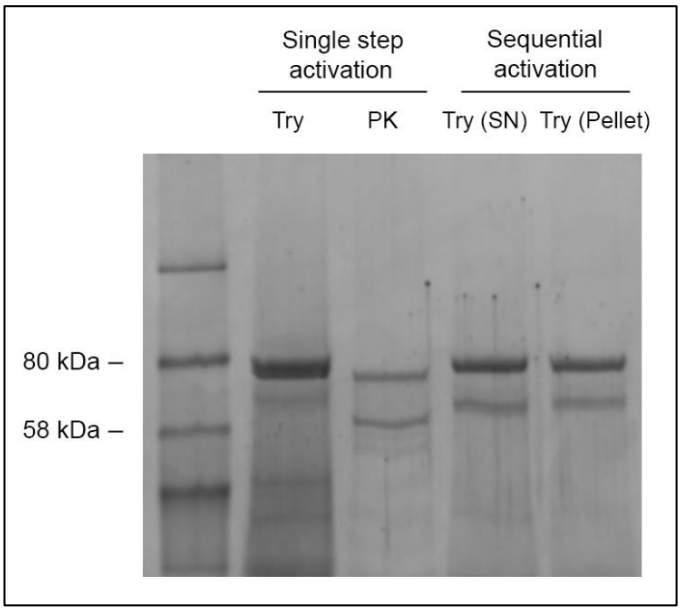

Figure 17 The effect of sequential activation on toxin processing.
PS-3 was incubated in 50 mM sodium carbonate (10.5 pH) with 5 mM DTT and trypsin (1 mg/ml) or proteinase K (0.01 mg/ml) for 1.5 hour at 37°C (Try and PK) or incubated first in 50 mM sodium carbonate/5 mM DTT for 1 hour at 37°C and then with the protease for another hour at 37°C. Samples were run on a 7.5% SDS-PAGE gel. Try (SN) and Try (Pellet) represent supernatant and total of solubilised toxins respectively after trypsin activation.

The effect of sequential activation was tested on protein cytotoxicity (Figure 18).

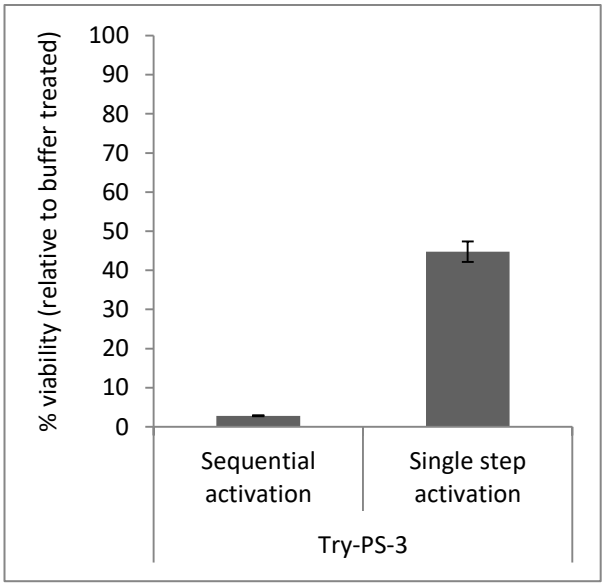

Figure 18 The effect of sequential activation on PS-3 cytotoxicity.
PS-3 was solubilized and trypsin treated either separately (sequential activation) or at the same time (single step activation). HepG2 cells were seeded at density 5.5 x 10^4 cells/ml. The next day cells were treated with non-purified PS-3 either sequentially activated (96 μg/ml) or activated in a single step (98 μg/ml). Viability was measured 24 hours later using CellTiter-Blue.

Consecutive solubilisation and digestion altered toxin processing and significantly increased toxicity in case of trypsin activated PS-3. Separate solubilisation and proteolysis did not improve cytotoxicity or processing of proteinase K digested proteins (data not shown). PS-3 fragments after proteinase K digestion showed similar 75 and 60 kDa fragments regardless of the activation method (Figure 17).

Endogenous proteolysis of protoxin

High molecular weight proteins including ORF3 degraded upon alkali solubilisation of PS-3 (Figure 16). Also, PS-3 protoxin showed some degree of cytotoxic activity in presented later viability (Figure 39) and membrane permeability (Figure 45 and Figure 46) assays implying some processing of the protoxin. To test that, PS-3 was solubilised

in the presence or absence of protease inhibitors. Purified samples were run on an SDS-PAGE gel (Figure 19) and tested on HepG2 cells (Figure 20).

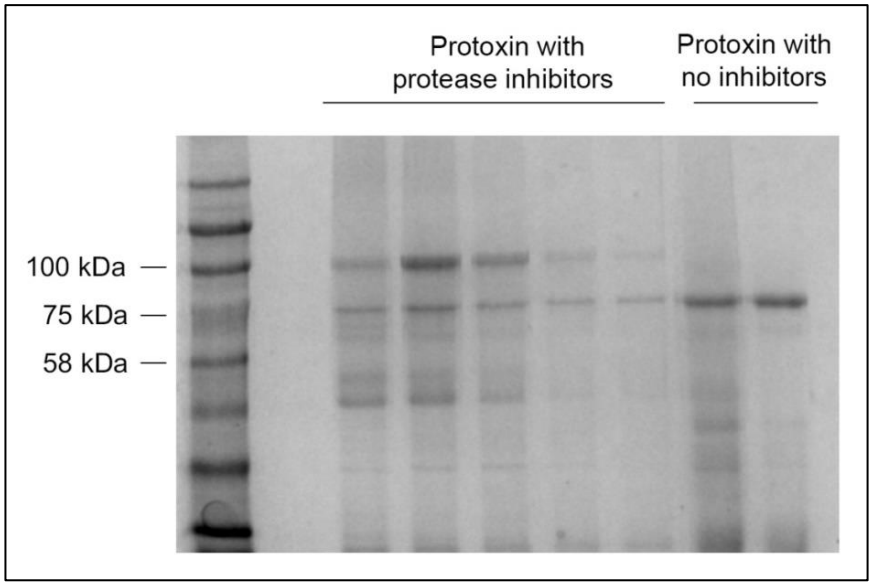

Figure 19 The effect of protease inhibitors on protoxin solubilisation.
Toxin crude suspension was solubilised in 50 mM sodium carbonate (pH 10.5) with 5 mM DTT for 1 hour at 37°C either in the presence or absence of protease inhibitors. After 1 hour protease inhibitors were added to stop proteolysis in a sample containing protoxin without previously added inhibitors and both proteins were purified. Fractions collected were run on a 10 % SDS-PAGE gel.

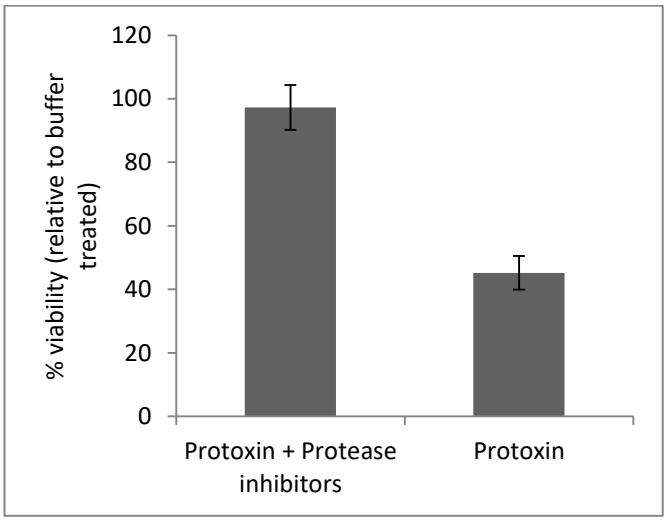

Figure 20 The effect of protease inhibitors on protoxin cytotoxicity
HepG2 cells were seeded at the density of 20 x 10^4 cells/ml together with CellTox-Green dye in a black 96-well plate. The next day cells were treated with purified protoxin incubated previously with (56 µg/ml) or without (58 µg/ml) protease inhibitors. After cytotoxicity was measured (data presented in Figure 46) CellTiter-Blue reagent was added and viability was measured 28 hours after toxin exposure.

Experiments with protease inhibitors showed that protoxin processing occurs due to proteolysis by the endogenous proteases present in the crude sample and that this processing is responsible for protoxin induced drop in cell viability (Figure 20) and membrane damage (Figure 46). They also suggest that protoxin is not processed in culture medium in the presence of cells.

The effect of DTT

Concentration-dependent effects of DTT were assessed on solubilisation and activation of PS-3 (Figure 21) as well as toxicity (Figure 22).

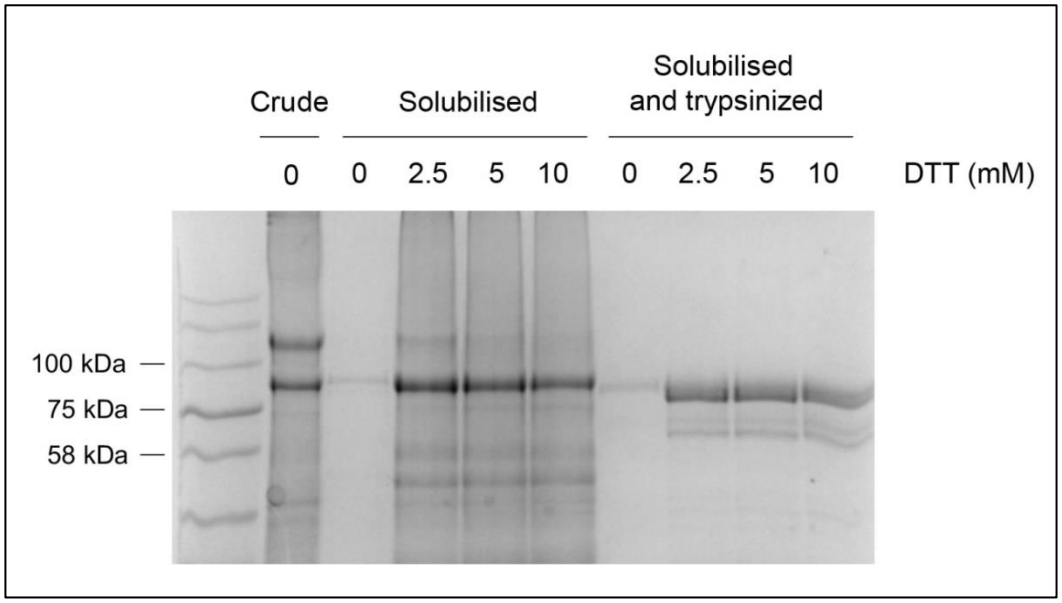

Figure 21 The effect of DTT on PS-3 solubilisation and trypsinization.
Sonicated crude suspension of PS-3 was solubilized in the presence of different DTT concentrations (0, 2.5, 5, or 10 mM) followed by trypsin digest (1 mg/ml). Samples at different stages of activation were run on a 7.5% SDS-PAGE gel.

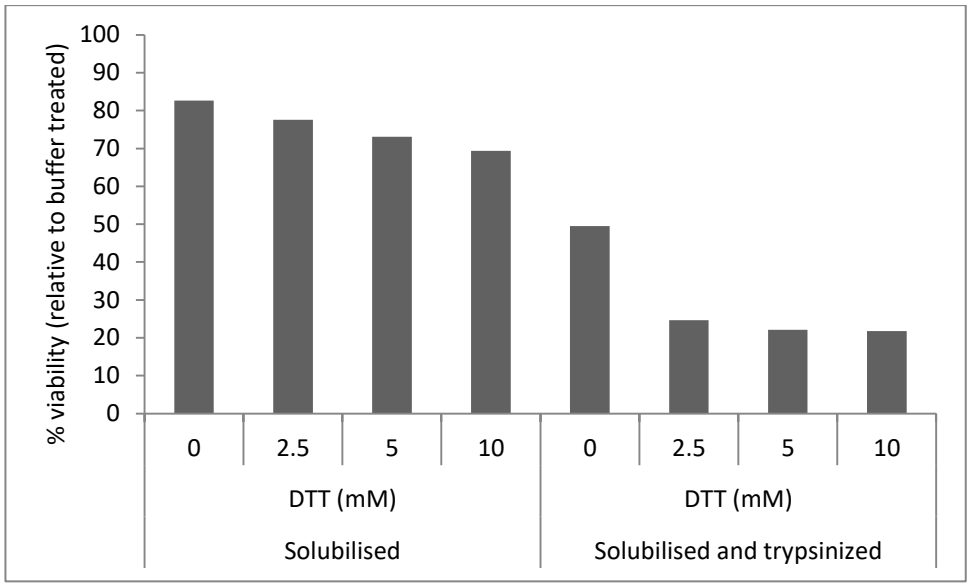

Figure 22 The effect of DTT assisted activation on PS-3 cytotoxicity.
HepG2 cells were seeded at density 25 x 10^4 cells/ml. The next day cells were treated with samples presented in Figure 21: PS-3 solubilized in the presence of different DTT concentrations (0, 2.5, 5, or 10 mM) followed by trypsin digest (1 mg/ml). The effect on cell viability was measured 6 hours later using CellTiter-Blue. Data come from only one technical replicate.

The presence of DTT greatly increased solubilisation yield and was prerequisite for effective trypsin cleavage. The presence of as little as 2.5 mM DTT significantly increased PS-3 cytotoxicity. Similar toxin processing was obtained whether DTT was added at solubilisation or at proteolysis step (data not shown). Efficient solubilisation in the presence of DTT was confirmed by obtaining no protein bands on an SDS-PAGE gel after pellet re-solubilisation (data not shown). Addition of 1 mM EDTA to 50 mM sodium carbonate buffer during solubilisation did not influence toxin processing (data not shown), but its effect on toxicity was not assessed.

The effect of pH

Solubilisation and activation of PS-3 was tested at pH 8 (Figure 23) in the hope that the number of sample dialysis steps during purification could be reduced and to provide an

optimum pH for proteolytic digestion which for trypsin is 7-9 (Sipos and Merkel, 1970) and 7.5-12 for proteinase K (Ebeling et al., 1974).

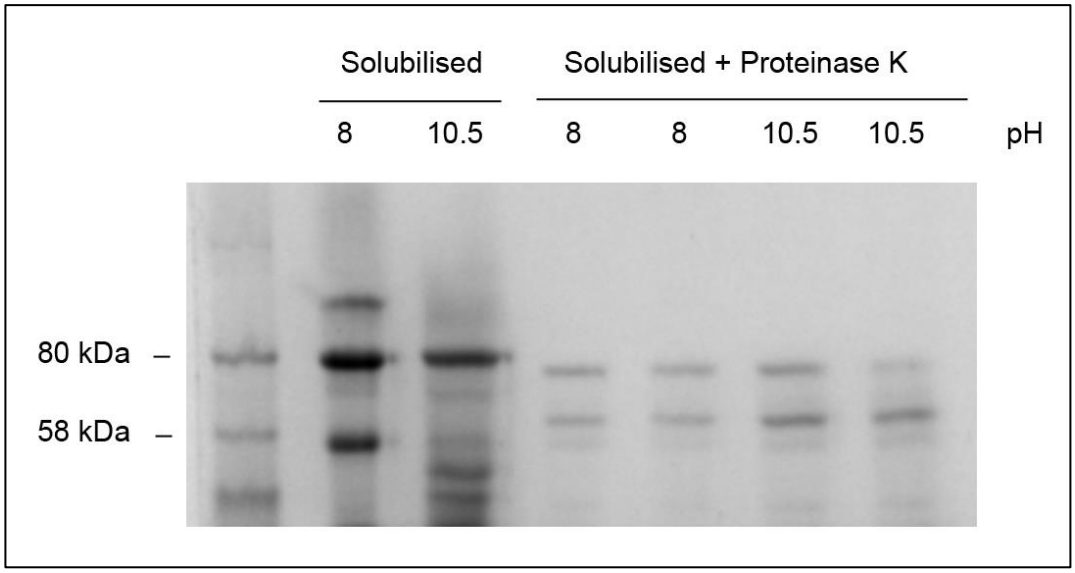

Figure 23 The effect of pH on solubilisation and activation of PS-3.
PS-3 was solubilised for 1 hour at 37°C in 50 mM sodium carbonate/5 mM DTT at pH 8 or 10.5. This was followed by 1 hour proteinase K digest (0.01 mg/ml) at 37°C (in duplicates). Supernatant samples were run on a 7.5% SDS-PAGE gel.

pH 10.5 was slightly more efficient for toxin solubilisation and proteinase K digestion than pH 8, also when trypsin was used for processing (data not shown). Experiments where activation was done at pH 6 showed similar to pH 8 results, whereas solubilisation in 20 mM sodium acetate 1 M NaCl, pH 5 was ineffective (data not shown). Interestingly, solubilisation at lower pH (6-8) seemed to inhibit the degradation of protein coded by ORF3. Also, solubilisation and trypsin activation of PS-3 was relatively well attained in 10 mM CAPS (pH 10.4), but was not practiced due to lower protein stability during storage (data not shown).

Generally *Bt* inclusion bodies are solubilized in alkaline conditions, mimicking the high pH of the digestive juice of most insects. However, a few studies demonstrated efficient solubilisation and activation of *Bt* Cry inclusions using acidic

buffers while retaining similar cytotoxic activities to the alkali-treated toxins (Koller et al., 1992, Okumura et al., 2006). Solubilising PS-4 in 10 mM HCl and digesting it with pepsin (200 µg/ml, activity 1:10,000) resulted in about 25 fold higher protein yield in comparison to alkaline solubilisation and proteinase K treatment (Okumura et al., 2006). To test whether PS-3 can be activated in acidic conditions, PS-3 crude sample was solubilised in HCl, followed by pepsin treatment (Figure 24).

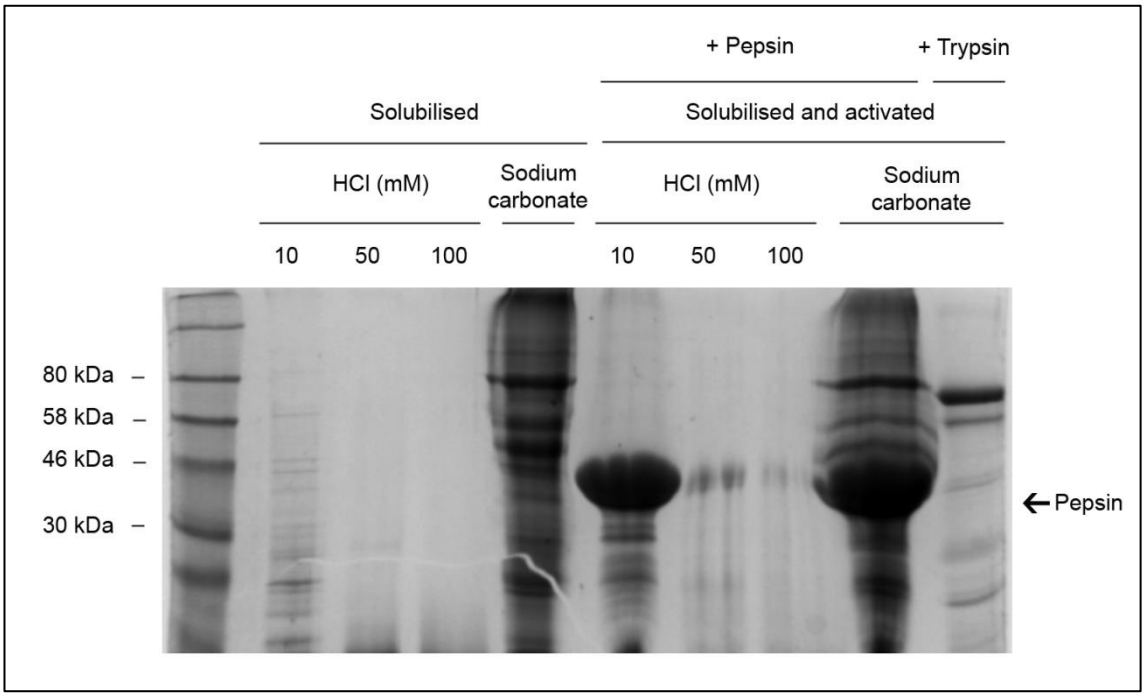

Figure 24 Solubilisation and pepsin treatment of PS-3 at low pH.
PS-3 toxin was solubilised for 1 hour at 37°C in either 50 mM sodium carbonate (pH 10.5) or 10, 50 or 100 mM of HCl (pH around 2). After that, samples were spun and supernatant was digested for 1 hour at 37°C with either trypsin (1 mg/ml) or pepsin (33 µg/ml, activity 1:60,000). Supernatant samples were run on a 12% SDS-PAGE gel.

Acidic solubilisation followed by pepsin digest did not result in higher MW bands that could represent the toxin (the 35 kDa band represents pepsin, degraded at higher HCl concentrations); samples were not tested for toxicity against HepG2.

Protein stability

Changes in protein stability were assessed because protease inhibitors had not been routinely added to the toxin samples before. Protease treated PS-3 (trypsin or proteinase K) was incubated for 24 hours either at room temperature or 37°C with or without protease inhibitors (Figure 25).

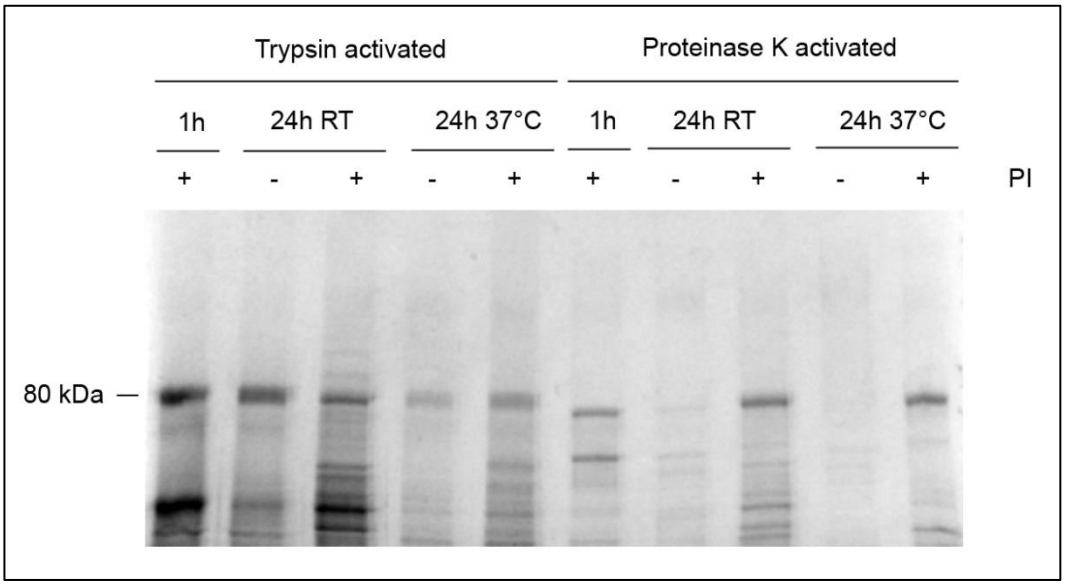

Figure 25 Assessment of PS-3 stability in the presence or absence of protease inhibitors.
Trypsin or proteinase K activated PS-3 was incubated for 1 or 24 hours at RT or 37°C in the presence or absence of protease inhibitors (PI). Samples were run on a 7.5% SDS-PAGE gel.

Protease inhibitors considerately slowed down the rate of toxin degradation, which was greater at 37°C than at RT. However, inhibitors did not preserve the lower band of proteinase K activated PS-3 suggesting its instability.

For the purpose of cation exchange purification activated toxin was dialysed overnight against low pH (3) or high salt concentration (3M NaCl) buffer. SDS-PAGE analysis confirmed that PS-3 was structurally stable in these conditions (data not shown).

Proteolytic processing

Solubilized toxin was treated with various concentrations of proteases to identify the dose that would result in optimum toxin processing; also to examine possible toxin degradation at a high dose of the protease used. PS-3 protoxin was activated with different concentrations of trypsin or proteinase K (Figure 26 and Figure 27 respectively) and activated toxins were tested on HepG2 cells (Figure 28 and Figure 29).

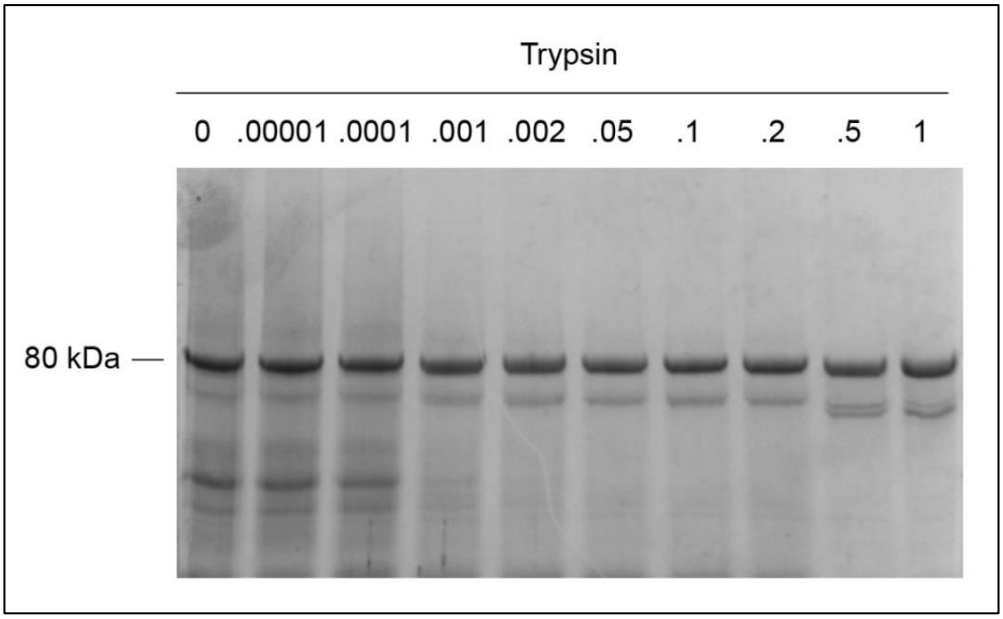

Figure 26 Dose dependent effect of trypsin activation on toxin processing.
Solubilised protoxin was digested for 1 hour at 37°C with trypsin to achieve the following final concentrations: 0.005, 0.01, 0.5, 0.2, 0.3, 0.6, 1 mg/ml. Protease inhibitors were added and samples were run on a 7.5% SDS-PAGE gel.

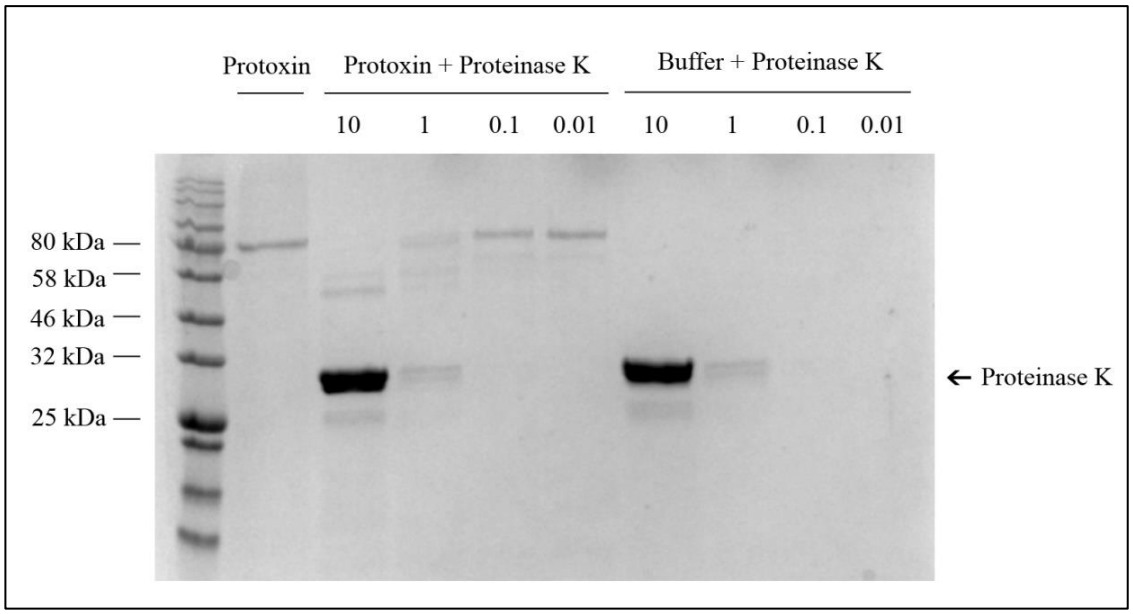

Figure 27 Dose dependent effect of proteinase K activation on toxin processing.
Purified solubilised protoxin was digested for 1 hour at 37°C with proteinase K to achieve the following final concentrations: 0.01, 0.1, 1, 10 mg/ml. After proteolytic digestion samples were run on a 12% SDS-PAGE gel.

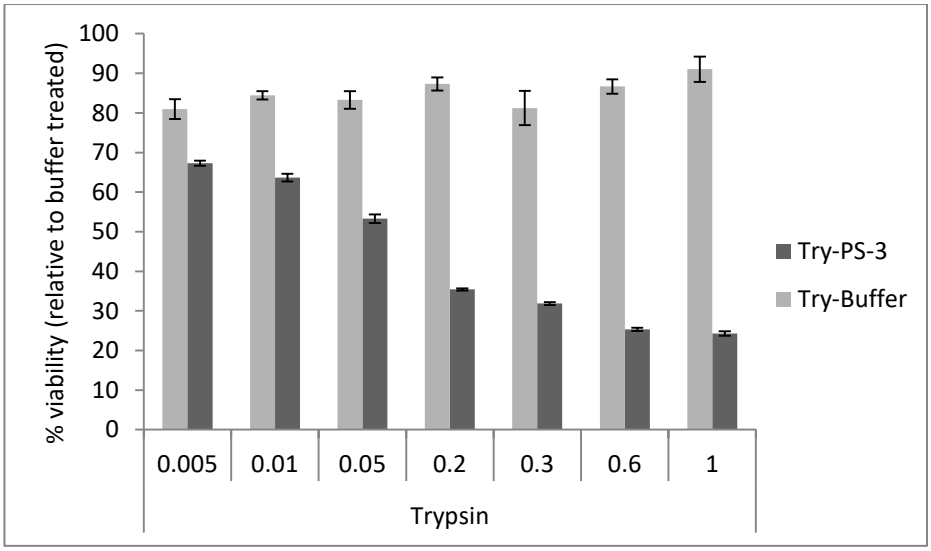

Figure 28 Dose dependent effect of toxin activation by trypsin on HepG2 cell viability.
Purified protoxin (100 µg/ml) was processed for 1 hour at 37°C with trypsin at the following final concentrations: 0.005, 0.01, 0.05, 0.2, 0.3, 0.6, 1 mg/ml. After that protease inhibitors were added to each sample. HepG2 cells were seeded at density 25 x 10^4 cells/ml. The next day cells were treated with trypsin activated samples. Control cells were treated with respective concentrations of trypsin dissolved in buffer. After 24 hour incubation cell viability was measured using CellTiter-Blue assay.

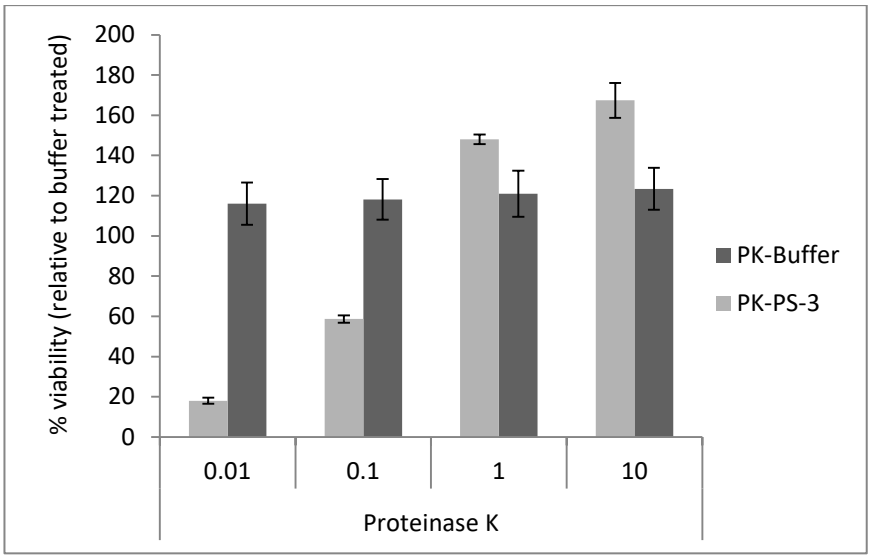

Figure 29 Dose dependent effect of toxin activation by proteinase K on HepG2 cell viability.
Purified protoxin (100 µg/ml) was processed for 1 hour at 37°C with proteinase K at the following final concentrations: 0.01, 0.1, 1, 10 mg/ml. After that protease inhibitors were added to each sample. HepG2 cells were seeded at density 25 x 10^4 cells/ml. The next day cells were treated with proteinase K activated samples. Control cells were treated with respective concentrations of proteinase K dissolved in buffer. After 24 hour incubation cell viability was measured using CellTiter-Blue assay.

The SDS-PAGE results showed that PS-3 was very resistant to degradation when treated with trypsin up to 1 mg/ml, whereas it degraded when proteinase K was used at concentration ≥1 mg/ml, breaking down to low MW bands. PS-3 was stable even in the presence of 10 mg/ml of trypsin or chymotrypsin (data not shown).

Although proteinase K activated toxin showed more toxicity compared with trypsin processing (also shown in Figure 39), this activity greatly decreased when higher proteinase K concentrations were used (≥1 mg/ml). Trypsin activated PS-3, on the contrary, resulted in a cytotoxic effect when processed with higher enzyme doses. For these reasons, trypsin was used as a preferred choice for proteolytic treatment.

4.3 Protein purification

Toxin was purified using size exclusion resin as detailed in the method section. Sample before purification and purified fractions were run on an SDS-PAGE gel (Figure 30). Toxicity of PS-3 before and after purification was assessed (Figure 31).

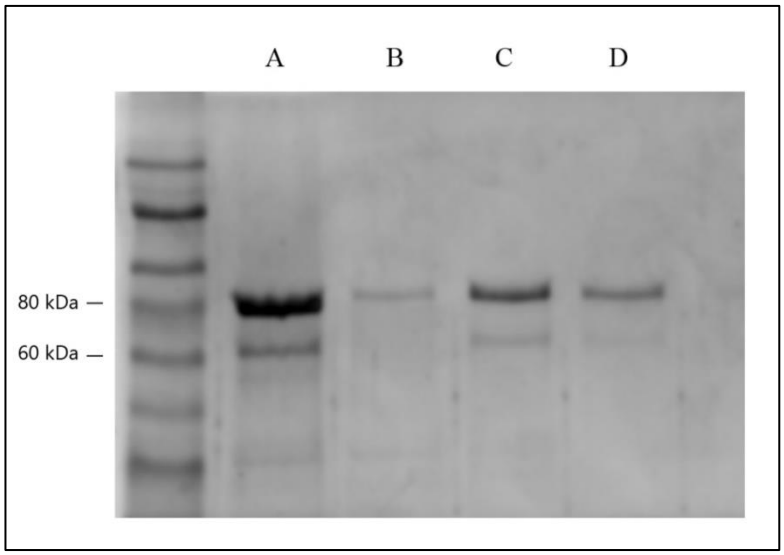

Figure 30 Purification of PS-3 by Sepharose gel filtration.
PS-3 was purified from DTT and other small MW contaminants using gel filtration as described in the method section. Trypsin activated toxin before and fractions collected after purification were run on a 7.5% SDS-PAGE gel: A) toxin before purification; B), C) and D) collected fractions of purified toxin.

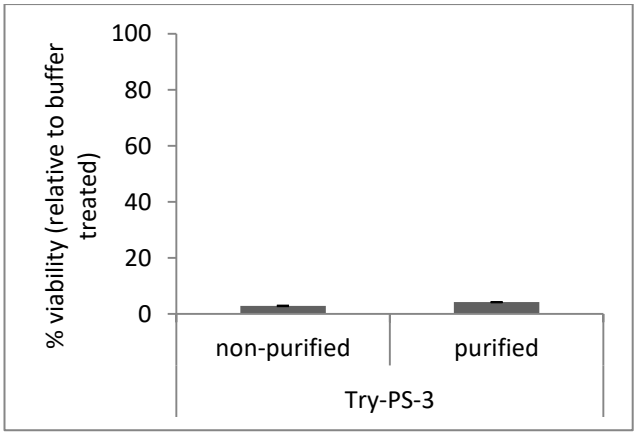

Figure 31 Comparison of PS-3 toxicity before and after gel filtration.
HepG2 cells were seeded at density 5.5 x 10^4 cells/ml. The next day cells were treated with trypsin activated PS-3 before (96 µg/ml) or after gel filtration (6 µg/ml). Cell viability was measured 24 hours later using CellTiter-Blue.

Gel filtration did not allow for separation of the lower 65 kDa band (Figure 30, C). In general, gel purified toxins – despite dilution - had similar cytotoxicity to non-purified PS-3. Gel filtration was used to purify most toxins used in the cell assays. 8 ml stocks of gel filtered PS-3 and Cry1Ca (120 µg/ml each) were mass prepared and band intensities were compared on an SDS-PAGE gel as shown in Figure 32. Gel filtration was also used for purifying PS-3 protoxin, ricin deleted PS-3, HA-tagged PS-3, biotin labelled and FITC labelled PS-3.

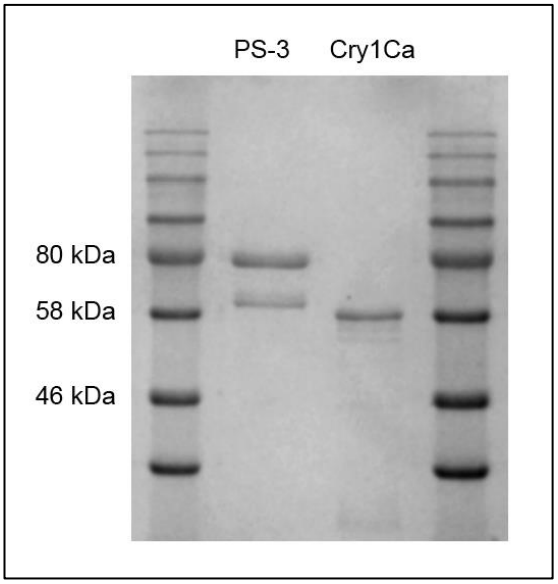

Figure 32 Gel purified stocks of PS-3 and Cry1Ca.
Trypsin activated PS-3 and Cry1Ca toxins were purified by gel filtration. Fractions containing purified toxins were combined together to create 8 ml stocks at 120 µg/ml concentration. A sample from each stock was run on a 10% SDS-PAGE gel for comparison.

Anion exchange chromatography was applied in an attempt to separate PS-3 fragments. Toxin was dialysed overnight against 10 mM CAPS (pH 10.4) as described in the methods section. Elution was achieved with an increasing gradient of NaCl (0 to 1 M). Upper band of protease treated PS-3 was eluted earlier than the bottom one, indicating a stronger ionic interaction between the more processed toxin and the column. Figure 33 shows separated toxin fragments on SDS-PAGE gels.

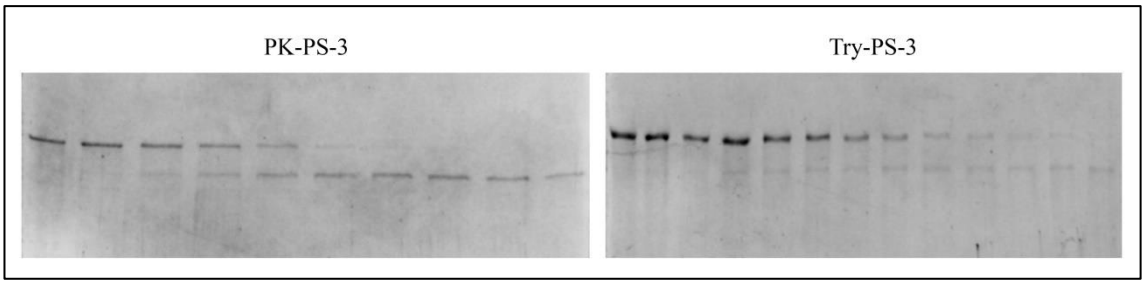

Figure 33 Separation of PS-3 bands using anion exchange chromatography.
Fragments of proteinase K (PK-PS-3) and trypsin activated PS-3 (Try-PS-3) were ÄKTA separated and purified using 10 mM CAPS (pH 10.4) buffer and an increasing gradient of NaCl (0 to 1 M). 0.8 ml fractions were collected and run on 10% SDS-PAGE gels.

Figure 34 and Figure 35 show sample elution profiles of proteinase K and trypsin activated toxins respectively.

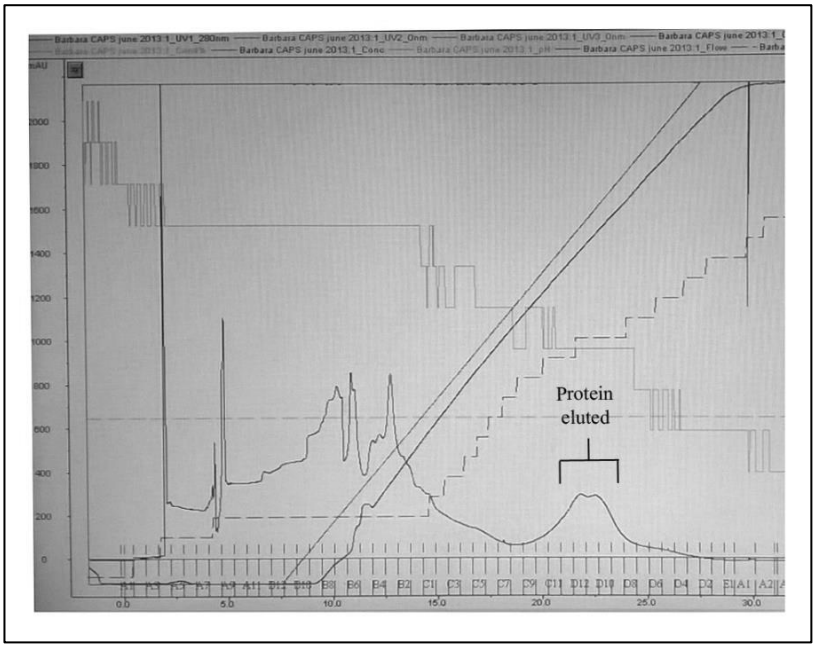

Figure 34 Elution profile of proteinase K activated PS-3.
Proteinase K activated PS-3 was ÄKTA purified. Toxin was eluted in 10 mM CAPS (pH 10.4) buffer as a double peak at ~750 mM NaCl.

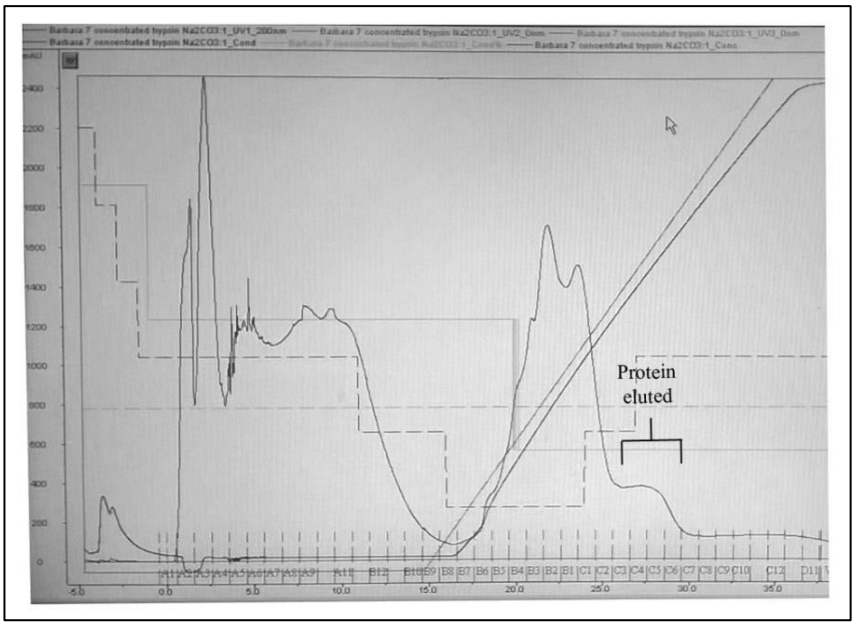

Figure 35 Elution profile of trypsin activated PS-3.
Trypsin activated PS-3 was ÄKTA purified. Toxin was eluted in 10 mM CAPS (pH 10.4) buffer mainly as a single peak at ~750 mM NaCl.

Selected fractions were desalted, concentrated and had buffer exchanged. Protein concentration was equalized and fragments were run on a gel (Figure 36). Toxicity of purified fragments was assessed on HepG2 cells (Figure 37 and Figure 38).

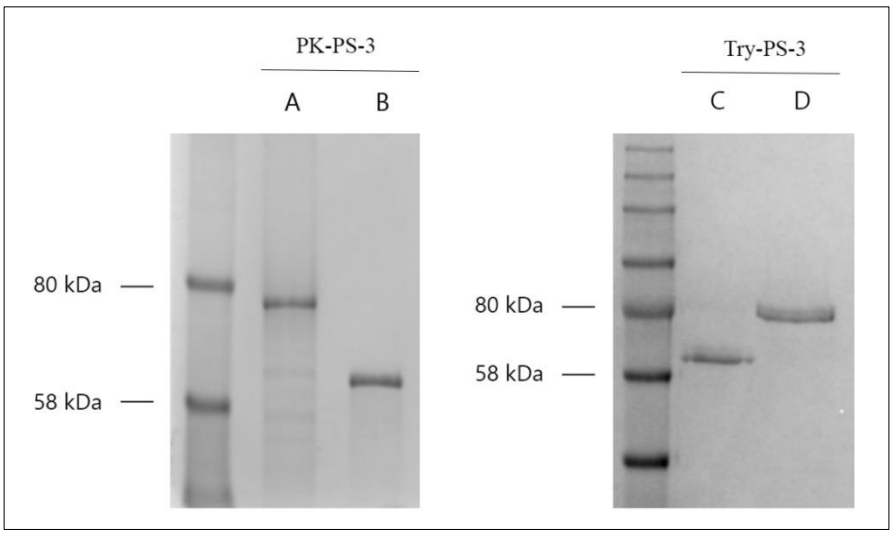

Figure 36 SDS-PAGE analysis of ÄKTA separated PS-3 fragments.
Proteinase K and trypsin activated PS-3 fragments were separated using ÄKTA. Samples were desalted, concentrated, and the buffer was changed to 25 mM tris-HCL 150 mM NaCl pH 7.4 (proteinase K activated toxin) or PBS pH 7.4 (trypsin activated toxin). Protein concentration was equalized to 100 µg/ml and samples were run on 7.5% SDS-PAGE gels: A) upper 75 kDa and B) lower 60 kDa bands of proteinase K activated toxin; C) lower 65 kDa fragment and D) upper 80 kDa fragment of trypsin activated toxin.

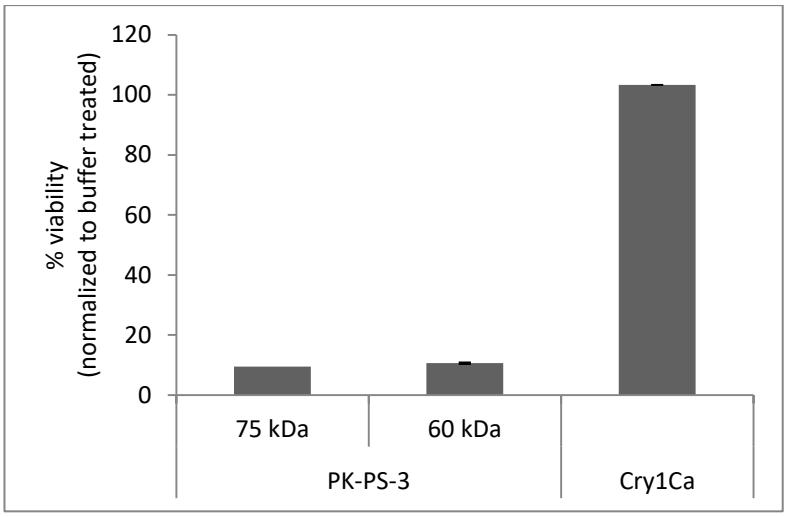

Figure 37 Toxicity of PS-3 separated bands after proteinase K digestion.
HepG2 cells were seeded at density 5.5 x 10^4 cells/ml. The next day cells were treated with proteinase K activated ÄKTA separated toxins: 60 kDa and 75 kDa (10 µg/ml). The effect on cell viability was measured 24 hours later using CellTiter-Blue.

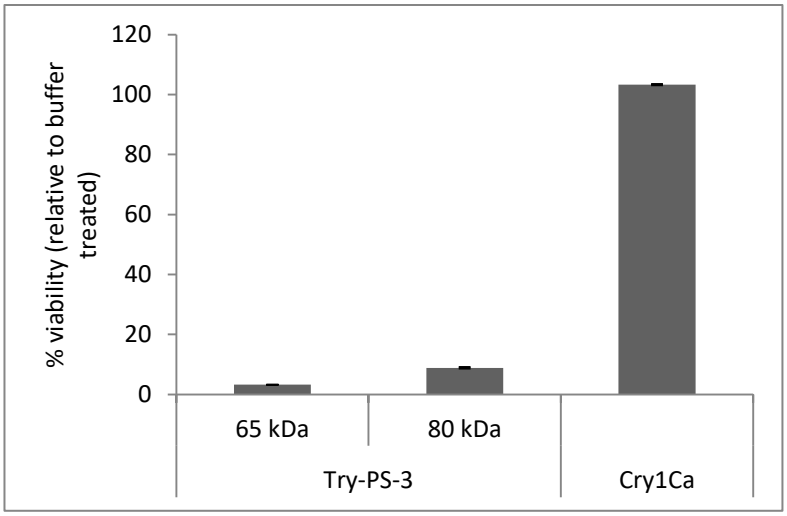

Figure 38 Toxicity of PS-3 separated bands after trypsin digestion.
HepG2 cells were seeded at density 25 x 10^4 cells/ml. The next day cells were treated with trypsin activated ÄKTA separated toxins: 65 kDa and 80 kDa (10 µg/ml). The effect on cell viability was measured 24 hours later using CellTiter-Blue.

Both lower and higher MW proteins after proteolytic activation with either trypsin or proteinase K were cytotoxic.

4.4 Assessment of cell viability

Estimation of metabolic activity

The majority of cell viability assays presented in this thesis was carried out using CellTiter-Blue. It is a fluorometric method estimating the number of viable cells by measuring metabolic activity. It uses the non-toxic and cell permeable resazurin dye, which is reduced by cellular enzymes in viable cells into highly fluorescent resorufin (O'Brien et al., 2000). Non-viable cells do not reduce the indicator dye. When reagent was added at the same time as toxin or incubated with cells for much longer than 2 hours, artefacts were often noted where high fluorescent signal did not correlate with immense cell death (data not shown). For this reason CellTiter-Blue was incubated with cells for no more than 2 hours and was always used as an endpoint reagent.

Initially experiments aimed to confirm the cytotoxic property of PS-3 on HepG2 cells after 24 hours as shown in Figure 39.

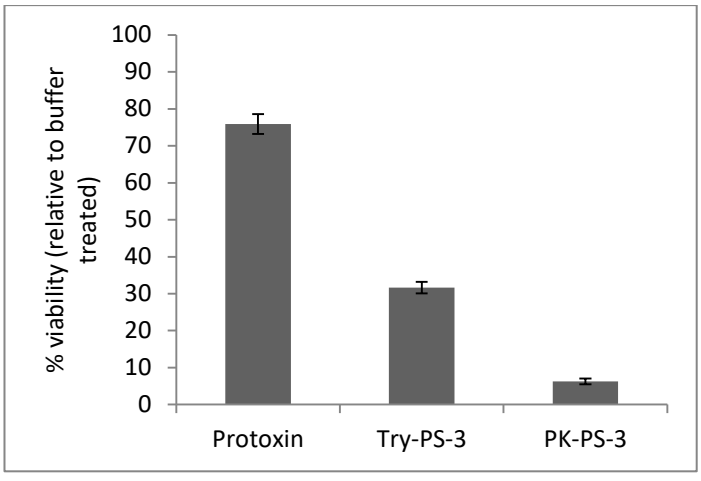

Figure 39 HepG2 cell viability after 24 hour exposure to toxins.
HepG2 cells were seeded at density 25 x 10^4 cells/ml. The next day cells were treated with non-purified, dialysed toxins: protoxin (100 µg/ml), trypsin treated PS-3 (100 µg/ml) and proteinase K treated PS-3 (50 µg/ml). Viability was measured 24 hours later using CellTiter-Blue.

A 24 hour incubation with proteinase K or trypsin digested toxin resulted in a significant decrease in cell viability. Reduction was greater in cells treated with proteinase K PS-3 even though smaller concentration was used. Protoxin showed moderate effect on cell viability as observed before.

Next, a 28 hour time course viability experiment was designed to establish how long it takes for the toxic effects to occur (Figure 40).

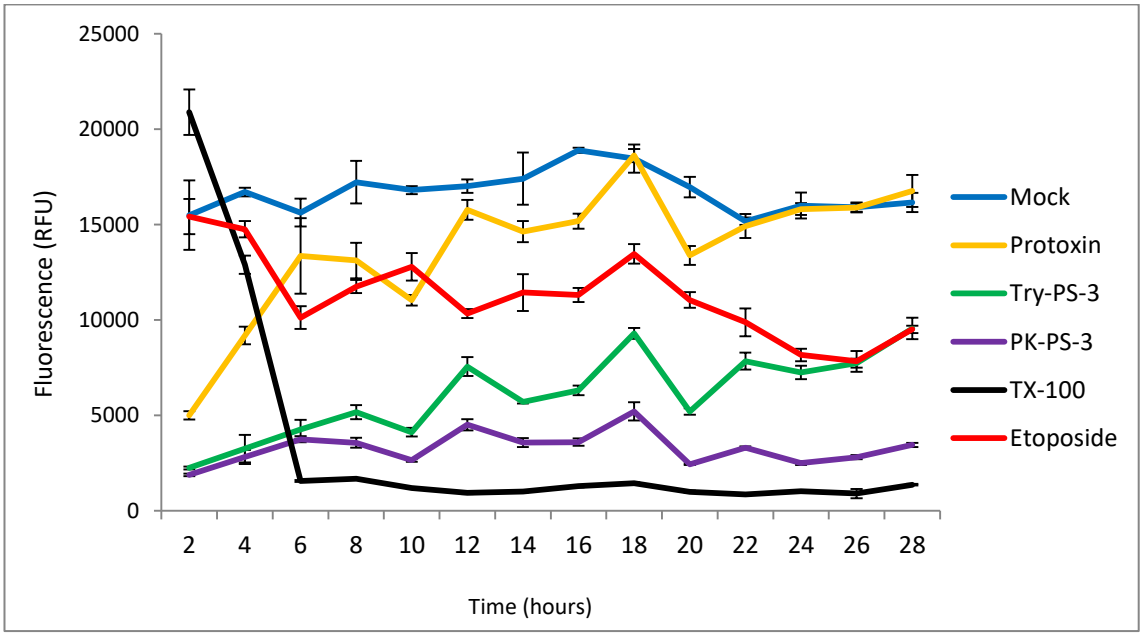

Figure 40 Time course experiment of HepG2 cells exposed to different forms of PS-3 over 28 hours.
HepG2 cells were seeded at density 25 x 10^4 cells/ml. The next day cells were treated at different time-points with non-purified, dialysed toxins: protoxin (100 µg/ml), trypsin treated PS-3 (100 µg/ml), proteinase K treated PS-3 (50 µg/ml), etoposide (100 µg/ml), Triton X-100 (0.01%) or buffer (mock). 20 minutes after the last toxin dose (2 hour time point), CellTiter-Blue was added to all cells and the fluorescence was measured for all time points after another 2 hours.

Proteinase K and trypsin activated PS-3 performed consistently, with viability readings increasing for Try-PS-3 towards the end of the time-course. PS-3 significantly affected cell viability within the first two hours, which was confirmed later using a real-time viability cell assay (Figure 182 and Figure 183). The viability of cells treated with protoxin was low initially. With time metabolic activity measurements of protoxin

treated cells increased, reaching after 24 hours the control levels. However, this rapid cell recovery seems unlikely and other factors like technical variables may have contributed to this effect. Etoposide and Triton X-100 showed the expected patterns of reduced viability associated with the different cytopathic effects they cause (rapid and severe viability decrease in case of Triton X-100, a detergent used for cell permeabilization and lysis, and gradual decrease in case of apoptosis inducer etoposide).

Estimation of ATP levels

Total ATP levels were measured in compromised cells as a second marker of cell viability (Figure 41).

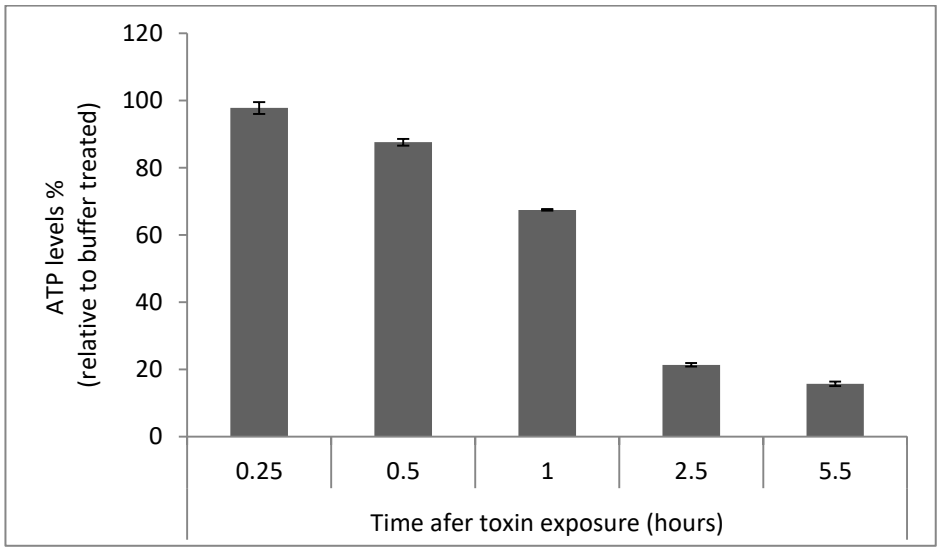

Figure 41 Assessment of ATP levels in HepG2 cells after exposure to PS-3.
HepG2 cells were seeded at the density of 25 x 10^4 cells/ml, in a white wall 96-well plate. The next day cells were dosed with PS-3 (12 µg/ml) or buffer. Luminescence was measured at different time points using CellTiter-Glo assay.

ATP levels were significantly reduced after the first 2.5 hours of toxin exposure.

Assessment of viability after a brief toxin exposure

Viability was assessed in HepG2 cells transiently exposed to PS-3 to determine how toxicity depends on the time, during which cells stay in contact with toxin molecules (Figure 42). Also toxin efficiency was tested by exposing different sets of cells to the same single toxin dose to check if there was a limitation in the amount of toxin that would reflect in viability levels (Figure 43).

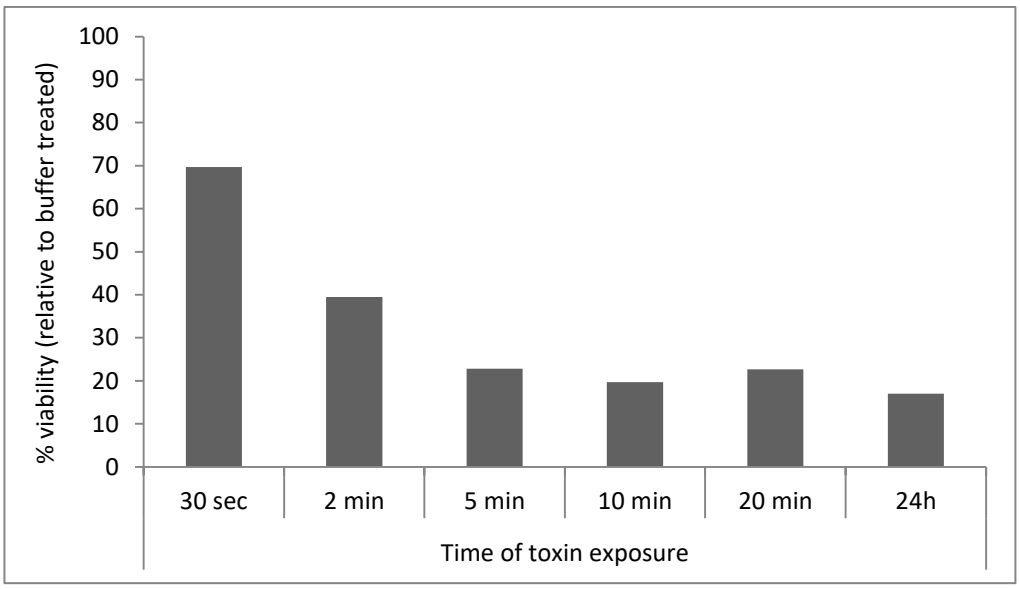

Figure 42 HepG2 cell viability in response to a brief or continuous toxin exposure.
HepG2 cells were seeded at the density of 25 x 10^4 cells/ml. The next day cells were exposed to PS-3 (12 µg/ml) transiently for 0.5, 2, 5, 10 or 20 minutes or continuously for 24 hours. After transient treatment cells were washed once with DPBS and incubated in toxin free medium. Viability was measured using CellTiter-Blue 24 hours after toxin treatment. Data come from one technical replicate.

Within the first 5 minutes PS-3 toxicity seemed to be dependent on the time of exposure, but not after that. This effect may result from diffusion time it takes for the toxin to reach the cell membrane. Experiment was repeated with similar outcome (data not shown).

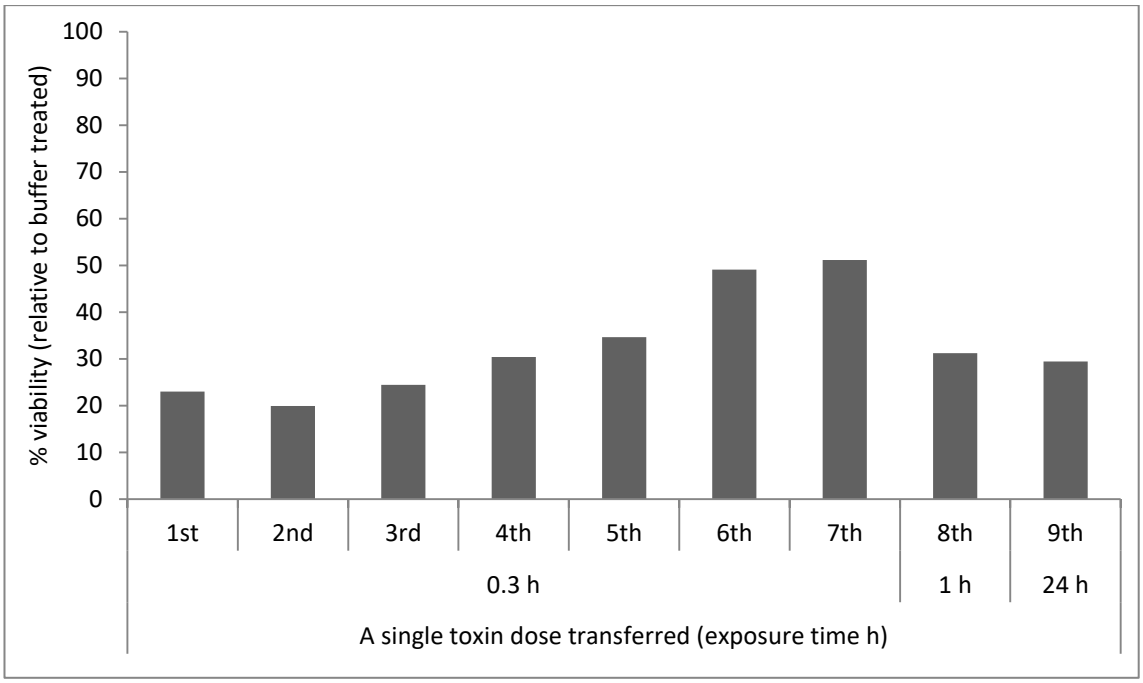

Figure 43 HepG2 cell viability after exposure to a single toxin dose transferred from one well to another.
HepG2 cells were seeded at the density of 25 x 10^4 cells/ml in a 96-well plate. The next day the 1st well was dosed with PS-3 (12 µg/ml) for 20 minutes. After 20 minutes, medium from the 1st well was removed and transferred to the 2nd one (previously emptied) for another 20 minutes. Fresh medium was placed in the 1st well. The transfer was repeated eight times. The last two times toxin medium containing the toxin was kept with the cells for longer: 1 and 24 hours for well 8th and 9th respectively. Viability was measured using CellTiter-Blue 24 hours after first toxin exposure. Data come from one technical replicate.

Results of the second experiment revealed high toxin potency to affect the cells. If PS-3 acts by binding and inserting into the membrane, it may indicate that the amount of toxin required to trigger toxicity is not limiting in this assay. Experiment was repeated with similar outcome (data not shown).

4.5 Estimation of EC_{50}

Figure 44 presents a dose response curve for HepG2 cells treated with different concentrations of PS-3 for 24 hours.

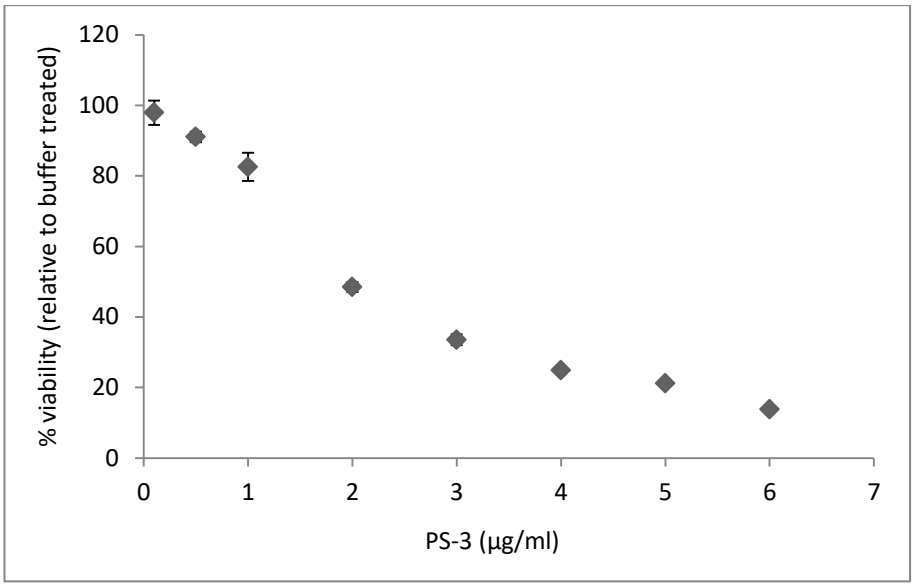

Figure 44 Dose response curve for HepG2 cells treated with PS-3.
HepG2 cells were seeded at the density of 25 x 10^4 cells/ml. The next day cells were incubated with different doses of PS-3 (trypsin digested, purified, 0.1 - 6 µg/ml). Fluorescence was measured after 24 hours using CellTiter-Blue. EC_{50} = 2.17 µg/ml.

Half maximal effective concentration (EC_{50}) value was determined as 2.17 µg/ml by Probit analysis using SPSS software.

4.6 Assessment of membrane damage using cytotoxic markers

Membrane permeability to a small marker

The effect of PS-3 on HepG2 membrane permeability to a small DNA binding dye was assessed over a 34 hour period using the CellTox-Green cytotoxic assay (Figure 45).

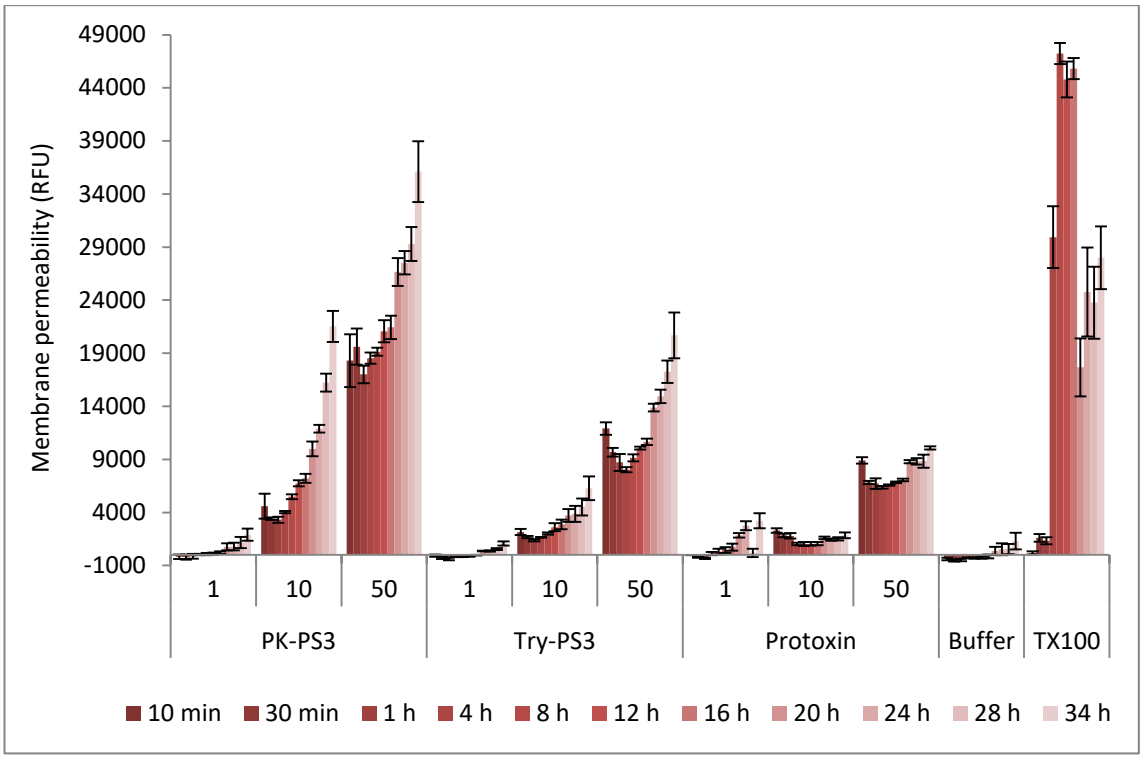

Figure 45 Analysis of membrane permeability to a small marker in HepG2 cells exposed to PS-3 over 34 hours. HepG2 cells were seeded at the density of 25 x 10^4 cells/ml in the presence of CellTox-Green dye in a black 96-well plate. The next day cells were treated with Triton X-100 (0.01%), buffer, or non-purified, dialysed toxins: trypsin or proteinase K activated PS-3 or protoxin (1, 10, or 50 µg/ml). Fluorescence was measured at different time points after toxin addition.

The fluorescent signal indicating membrane damage increased in a dose dependent manner. In cells treated with high toxin doses significant increase in permeability was noted after initial 10 minutes, with values gradually increasing with the toxin incubation time. PS-3 digested with proteinase K had greater impact on membrane permeability than trypsin digested toxin, consistent with CellTiter-Blue viability data (Figure 39). Unexpectedly high signal levels were obtained for protoxin treated cells, indicating significant membrane damage, even though microscopic observation did not show cell swelling. The experiment was repeated when stocks of purified PS-3, Cry1Ca and protoxin had been prepared. Also, to define the source of protoxin toxicity, its

effect on membrane permeability was additionally assessed after pre-treatment with protease inhibitors (Figure 46).

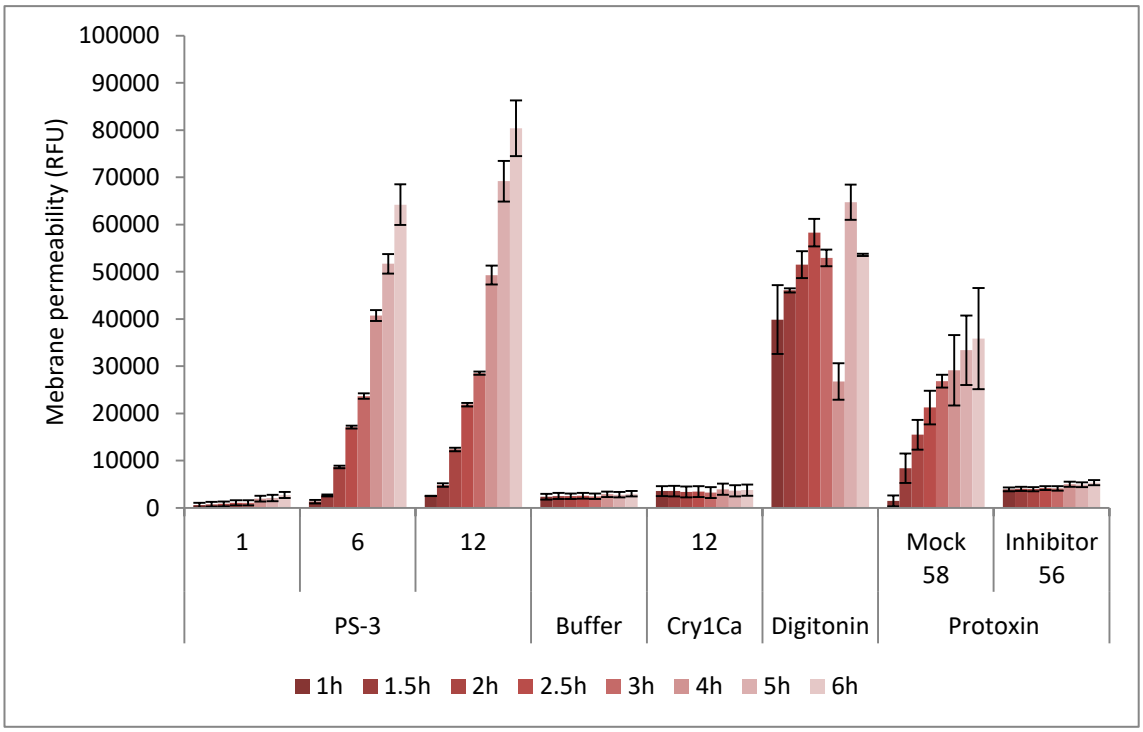

Figure 46 Analysis of membrane permeability to a small marker in HepG2 cells exposed to PS-3 over 6 hours. HepG2 cells were seeded at the density of 25 x 10^4 cells/ml in the presence of CellTox-Green dye, in a black 96-well plate. The next day cells were treated with digitonin (13 µg/ml), buffer, purified toxins: trypsin activated PS-3 (1, 6 or 12 µg/ml), Cry1Ca (12 µg/ml), or protoxin incubated previously with (56 µg/ml) or without protease inhibitors (58 µg/ml). Fluorescence was measured at different time points after toxin addition.

Purified PS-3 activated with trypsin increased membrane permeability in a time and dose dependent manner. Inhibiting native proteases during solubilisation step also inhibited protoxin associated membrane damage.

Membrane permeability to a large marker

The effect of purified PS-3 was assessed on HepG2 membrane permeability to a big protease marker over a 6 hour period using CytoTox-Glo cytotoxic assay (Figure 47).

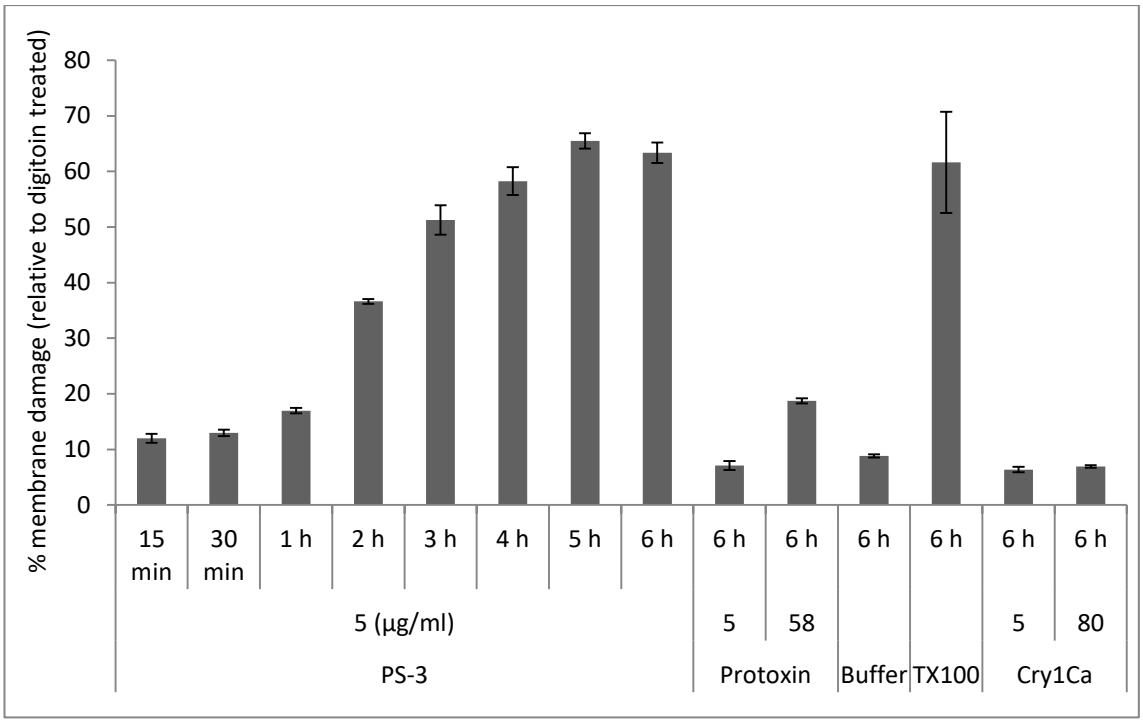

Figure 47 Analysis of membrane permeability to a big marker in HepG2 cells exposed to PS-3 over 6 hours.
HepG2 cells were seeded at the density of 25 x 10^4 cells/ml in a white 96-well plate. The next day cells were treated with TX-100 (0.01%), buffer, purified toxins: trypsin activated PS-3 (5 µg/ml), Cry1Ca (5 or 80 µg/ml), or protoxin (5 or 58 µg/ml). Luminescence was measured at different time points after toxin addition. After the measurement, digitonin solution was added to all cells (43.7 µg/ml) and 15 minutes later another reading was taken to determine the total cytotoxicity from remaining live cells using CytoTox-Glo. All data were background-subtracted and plotted as a percentage of the digitonin treated cells.

Compromised cells showed time-dependent membrane damage, similar to that created by membrane permeabilizing agent TX-100. Interestingly, damage caused by protoxin (at 58 µg/ml) relative to trypsin activated PS-3 was smaller in CytoTox-Glo assay compared with CellTox-Green assay (Figure 46), pointing to a possibility that pores created by protoxin may be of smaller size or less stable compared with the activated form of toxin.

4.7 Assessment of membrane damage using electrophysiology

Since the discovery of the patch clamp technique by Neher and Sakmann (Neher and Sakmann, 1976) it has been possible to study the behaviour of ion channels. The technique allows high resolution recordings of current in excised patches as well as in intact membranes. In principle, a membrane patch is isolated electrically from the external buffer by pressing a glass pipette containing electrolyte solution onto the cell membrane. Currents flowing through the channels in this patch can be recorded by an electrode mounted inside the pipette and connected to the amplifier. Experiments in this cell attached mode have the advantage of recording channel activity with functioning cellular metabolism; however the resting potential of the cell (Vr) remains unknown. One possibility to work with excised membrane patches is in the inside out configuration. After establishing the cell attached mode, the glass pipette is pulled off the cell to create a patch with intracellular side exposed to the bath solution. Because of the strong seal formed prior to pulling, the current passing through the patch will flow into the pipette and can be recorded. The advantage of this method is the control over ionic composition of the buffer on both sides of the patch. Both configurations can be used to measure single channel activity. Whole cell mode is achieved from the cell attached configuration by applying a strong suction to rapture the membrane patch, but without affecting the seal between the outside membrane and the pipette rim. The solution in the pipette equilibrates over time with the cytoplasm. Whole cell currents are much bigger as they result from opening of numerous channels simultaneously. However this technique, opposite to single channel recording, lacks

the sensitivity to characterise the properties of a single channel. Instead it is used to observe macroscopic currents in the membrane of the entire cell. Figure 48 summarises the patch clamp modes used in this study.

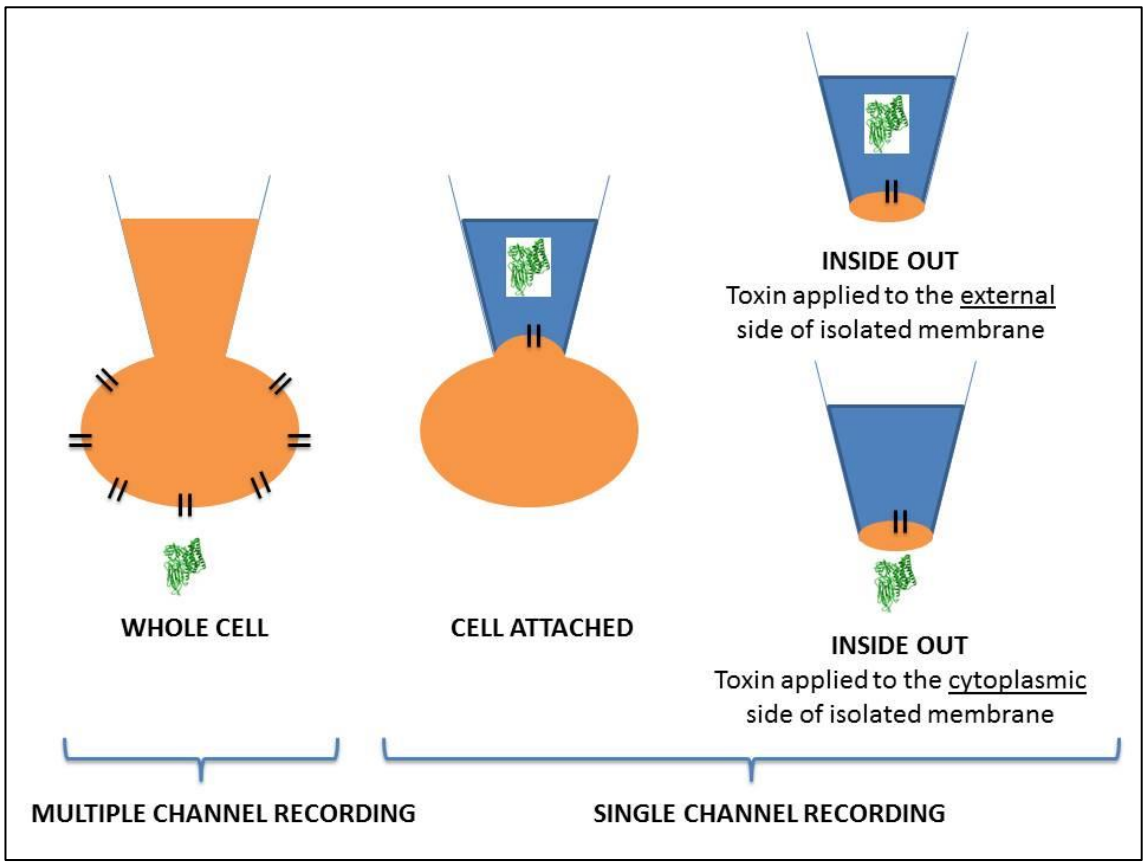

Figure 48 Schematic drawing of patch clamp configurations used in this study.
The four methods used to study PS-3 in patch clamp system. In a cell attached configuration a pipette is attached to the cell membrane by applying a mild suction to obtain a tight seal. After the seal is established, the inside out mode can be achieved by firmly pulling the pipette off isolating a membrane patch. In this configuration, cytoplasmic side of the membrane is exposed to the buffer in the bath while external one to the medium in the pipette. Depending to which side the toxin is added, both sides of the membrane can be tested. Whole-cell configuration is obtained from the cell attached mode by applying a brief and strong suction. The membrane is raptured and the buffer in the pipette comes into contact with the cytoplasm. The whole cell patch clamping records currents flowing through multiple channels across the entire membrane of the cell, while the other modes allow recordings from a single channel.

The experiments were performed under voltage clamp conditions. Two basic physiological buffers were used: 140 mM NaCl, 5 mM KCl, 1.1 mM $MgCl_2$, 1.1 mM $CaCl_2$, 10 mM HEPES, pH 7.4 (named NaCl buffer) and 140 mM KCl, 1.1 mM $MgCl_2$, 0.1 mM EGTA, 10 mM HEPES, pH 7.4 (named KCl buffer). The solution inside and outside

of the pipette was determined by the desired method of patch clamping, e.g. working in the whole cell mode required the pipette solution to have ionic composition close to that of the cytoplasm (like KCl buffer). In single channel experiments, with the exception of the cell attached mode where the pipette solution differed from the content on the other side of the membrane, working under symmetrical conditions (the same buffer in the bath and in the pipette) was the preferred choice. In the majority of patch clamp experiments a high resistance seal (2 - 10 GΩ), which reduces the current noise, was achieved. A higher chloride conductance was observed in dividing hepatocytes suggesting swelling activated conductance in proliferating liver cells (Wondergem et al., 2001). For this reason, non-dividing cells with well-developed pseudopods were targeted for patching.

Whole cell patch clamping

Whole cell patch clamping was used to observe macroscopic current activity in HepG2 and control cells during exposure to PS-3. The recordings were obtained before toxin addition and every 5 minutes for at least 20 minutes after toxin treatment. Resting membrane potential of hepatocytes is in the range of − 30 to − 40 mV due to the high basal chloride conductance (Moule and McGivan, 1990). Therefore, before the whole cell configuration was achieved, a holding potential of - 20 mV was applied to the pipette (close to the resting membrane potential of HeLa and HepG2 cells). KCl buffer was used in the pipette, and NaCl buffer in the bath. NaCl buffer was used as extracellular solution to avoid cell depolarization and because KCl solution, with 0.1 mM EGTA and no calcium, most likely would not permit toxicity, according to data

presented in Figure 100. Currents were induced by a set of seventeen 1 second depolarizing step potentials from −20 to 140 mV from a holding potential of − 20 mV. Figure 49 shows an example of the whole cell raw data of the current traces prior to analysis.

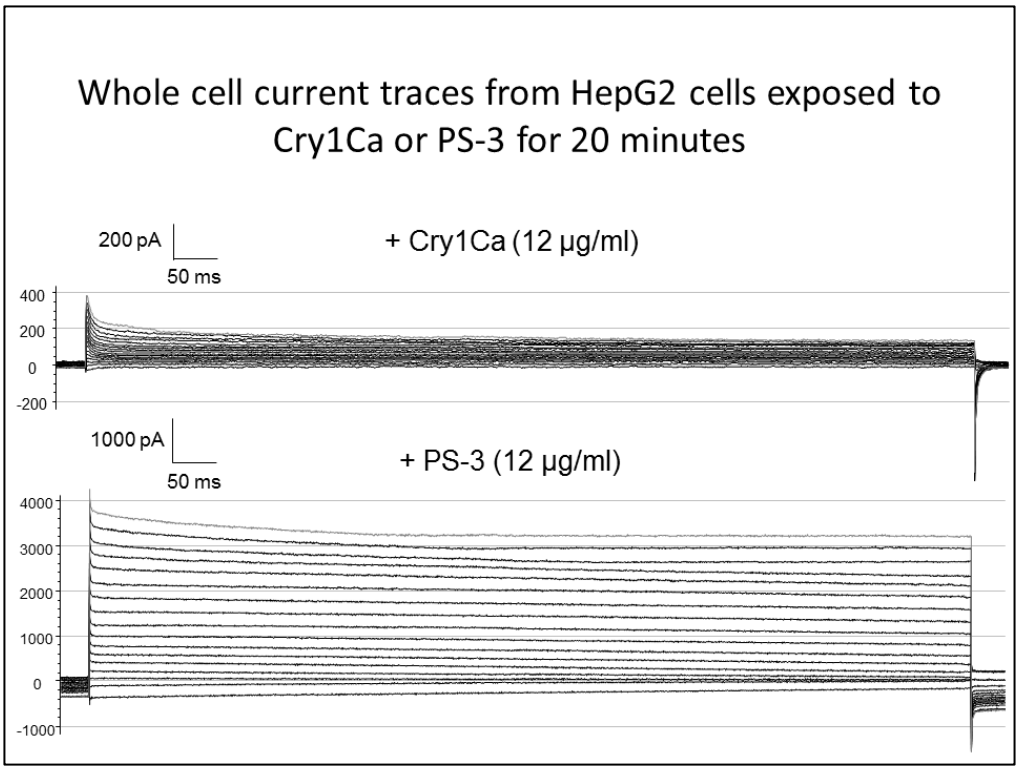

Figure 49 An example of the whole cell current traces from HepG2 cells exposed to Cry1Ca or PS-3.
The raw data traces of the whole cell current prior to baseline correction and I/V curve generation. The top and lower traces were obtained with the HepG2 cells in the NaCl buffer exposed for 20 minutes to Cry1Ca (12 µg/ml) or PS-3 (12 µg/ml) respectively in the whole cell mode using soda lime glass pipettes. Currents were induced by a set of seventeen 1 second depolarizing potentials from −20 to 140 mV from a holding potential of -20 mV. Traces were not baseline corrected.

Figure 50 shows a set of current – voltage relationships (I/V curve) of HepG2 cells exposed to PS-3 in time-course experiments. Digitonin treated HepG2 cells served as a positive control (Figure 51). HepG2 cells exposed to Cry1Ca and HeLa or CHOK1 cells exposed to PS-3 were tested as negative controls (Figure 52). Signal was baseline corrected and - with the exception of digitonin treated cells – lines represent the average of 3 experiments (three different cells patched).

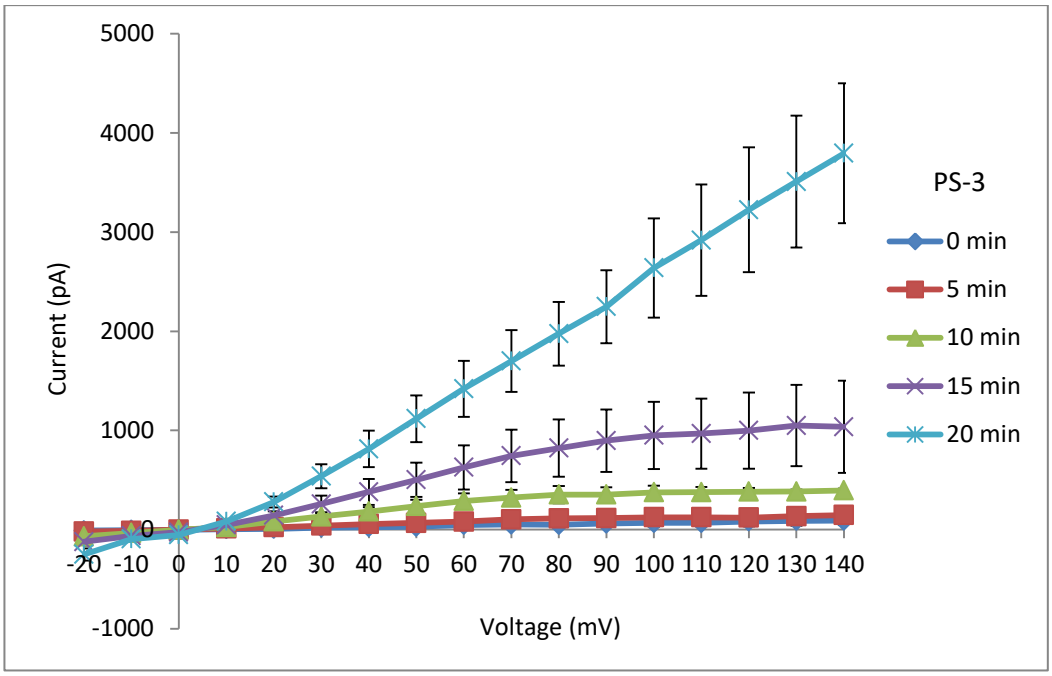

Figure 50 Whole cell patch clamp recordings from a time course experiment of HepG2 cells exposed to PS-3. HepG2 cells were seeded at the density of 5 x 10^4 cells/ml on the glass coverslip inside the 35 mm petri dish. The next day whole cell patch clamp recordings from a single cell were reported at 0, 5, 10, 15, 20 minutes after PS-3 (12 µg/ml) addition to the bath containing NaCl solution. Currents were induced by a 1 second set of depolarizing potentials from −20 to 140 mV from a holding potential of −20 mV. Error bars indicate the standard error of the mean. The lines show the mean currents from three representative experiments from three different cells patched.

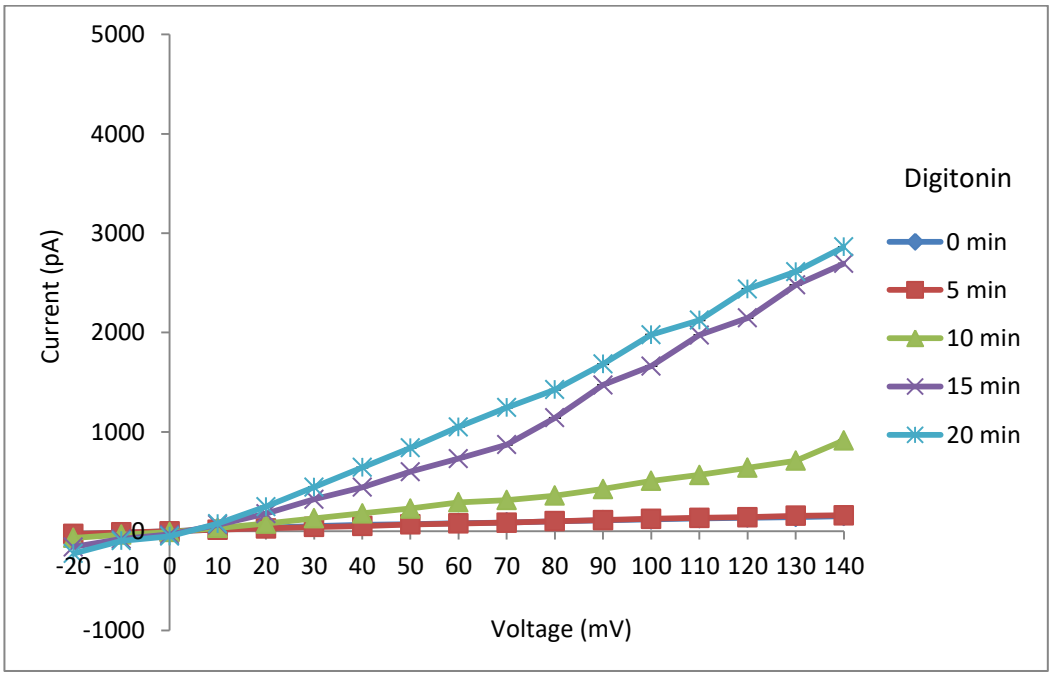

Figure 51 Whole cell patch clamp recordings from a time course experiment of HepG2 cells exposed to digitonin. HepG2 cells were seeded at the density of 5 x 10^4 cells/ml on the glass coverslip inside the 35 mm petri dish. The next day whole cell patch clamp recordings from a single cell were reported at 0, 5, 10, 15, 20 minutes after digitonin (13 µg/ml) addition to the bath containing NaCl solution. Currents were induced by a 1 second set of depolarizing potentials from −20 to 140 mV from a holding potential of −20 mV. Data come from a single patch clamp experiment.

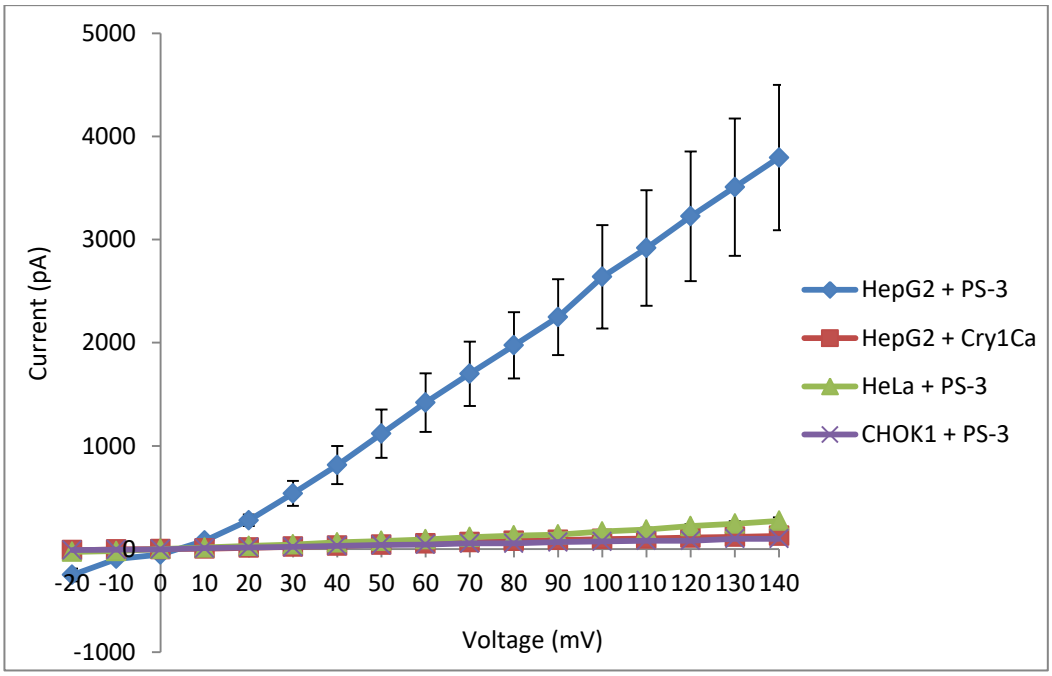

Figure 52 Whole cell patch clamp recordings from various cell types in response to treatment with PS-3 or Cry1Ca. HepG2, HeLa, CHOK1 cells were seeded at the density of 5 x 10^4 cells/ml on the glass coverslip inside the 35 mm petri dish. The next day whole cell patch clamp recordings from a single cell were reported 20 minutes after the addition of PS-3 (12 µg/ml) or Cry1Ca (12 µg/ml) to the bath containing NaCl solution. Currents were induced by a 1 second set of depolarizing potentials from −20 to 140 mV from a holding potential of −20 mV. Error bars indicate the standard error of the mean. The lines show the mean currents from three representative experiments from three different cells patched.

PS-3 induced large currents in HepG2, unlike Cry1Ca. In PS-3 and digitonin treated HepG2 cells at 20 minute time point currents increased proportionally with increased voltage applied, in accordance with the Ohm's law. PS-3 did not induce large currents in HeLa or CHOK1 despite a high toxin dose used in these experiments (12 µg/ml) at 20 minutes, but also at 5, 10, 15 and 30 minutes after treatment (data not shown). Conductance values were low also in HepG2 cells treated with PS-3 in the presence of 2 mM EGTA (Figure 91). In general, whole cell patch clamp results align with those obtained in membrane permeability cell assays (Figure 46 and Figure 47). To sum up, conductance levels were calculated from the slope of linear regression line of each I/V curve in the whole cell experiments at 10 and 20 minute time points and presented together in Table 4.

Table 4 Conductance levels calculated for the whole cell patch clamp experiments.
Conductance (nS) was calculated from the slope of linear regression line of individual whole cell I–V relationship for 10 and 20 minute time point (number of patches: n = 3, except for HepG2 cells treated with digitonin, mean +/- SEM). Conductance for HepG2 cells exposed to PS-3 in the presence of EGTA was calculated from data presented in Figure 91.

	Time (min)	Patch No.			Mean	SEM
		1	2	3		
CHOK1 + PS-3	10	9.4	7.6	3.4	**6.8**	1.8
	20	9.8	5.7	5.9	**7.1**	1.3
HeLa + PS-3	10	10.3	19.6	14.3	**14.7**	2.7
	20	21.8	17.3	15.7	**18.3**	1.8
HepG2 + Cry1Ca	10	7.9	6.2	6.8	**7.0**	0.5
	20	10.5	11.4	5.8	**9.2**	1.7
HepG2 + Digitonin	10	**55.5**	-	-	**-**	-
	20	**199.6**	-	-	**-**	-
HepG2 + EGTA + PS-3	10	19.1	5.5	11.8	**12.1**	3.9
	20	16.2	6.1	15.3	**12.5**	3.2
HepG2 + PS-3	10	28.3	29.3	37.6	**31.7**	2.9
	20	247.1	361.5	192.2	**266.9**	49.9

A significant increase in the whole cell conductance, to a few hundred nS, was observed only in HepG2 cells exposed to PS-3 or digitonin.

Single channel activity in biological membranes

Single channel activity was recorded from HepG2 and HeLa membranes exposed to PS-3. However, results may not be representative because of too few experiments performed and conditions not fully optimised. For these reasons, except for conductance, other channel characteristics were not analysed. Figures displaying recorded traces show channel activity uncorrected for leakage of the seal. In the cell attached mode the toxin was applied inside the pipette in NaCl buffer. In the inside out mode the toxin was applied either inside the pipette or in the bath, exposing external

or cytoplasmic side of the membrane to the toxin respectively. In the inside out configuration both NaCl and KCl buffers were used under symmetrical conditions.

Activation of endogenous channels in HepG2 cells was first monitored in the absence of PS-3 in the inside out mode for 10 minutes (Figure 53).

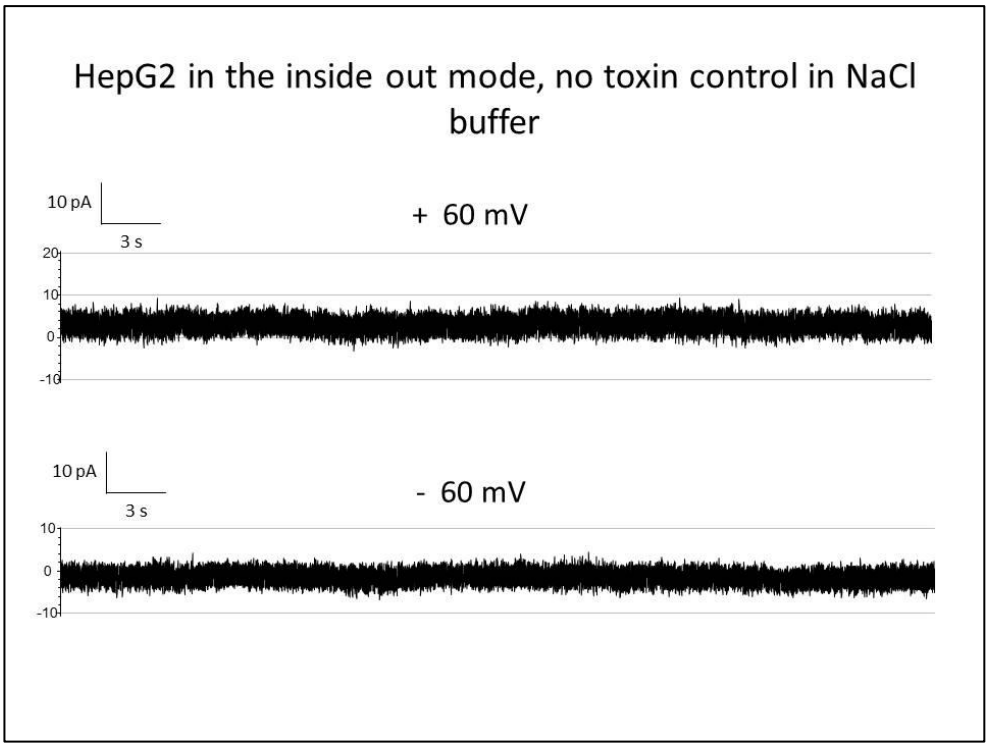

Figure 53 Single channel patch clamp recordings from HepG2 cells in the inside out mode in NaCl buffer.
Single channel activity was recorded at 9 minutes after establishing the seal at + 60 mV (upper trace) and at - 60 mV (lower trace) from HepG2 in the inside out configuration using soda-lime glass pipettes and NaCl buffer. Records were filtered at 120 Hz.

Membrane showed no channel activity at voltages applied in the range of - 60 to + 60 mV for 10 minutes until the seal was lost.

Figure 54 and Figure 55 show single channel recordings from HepG2 cells in the inside out mode after PS-3 was applied to the cytoplasmic and external side of the membrane respectively in the presence of KCl buffer. Figure 56 shows recordings after exposing external side of HepG2 cell membrane to PS-3 in NaCl buffer.

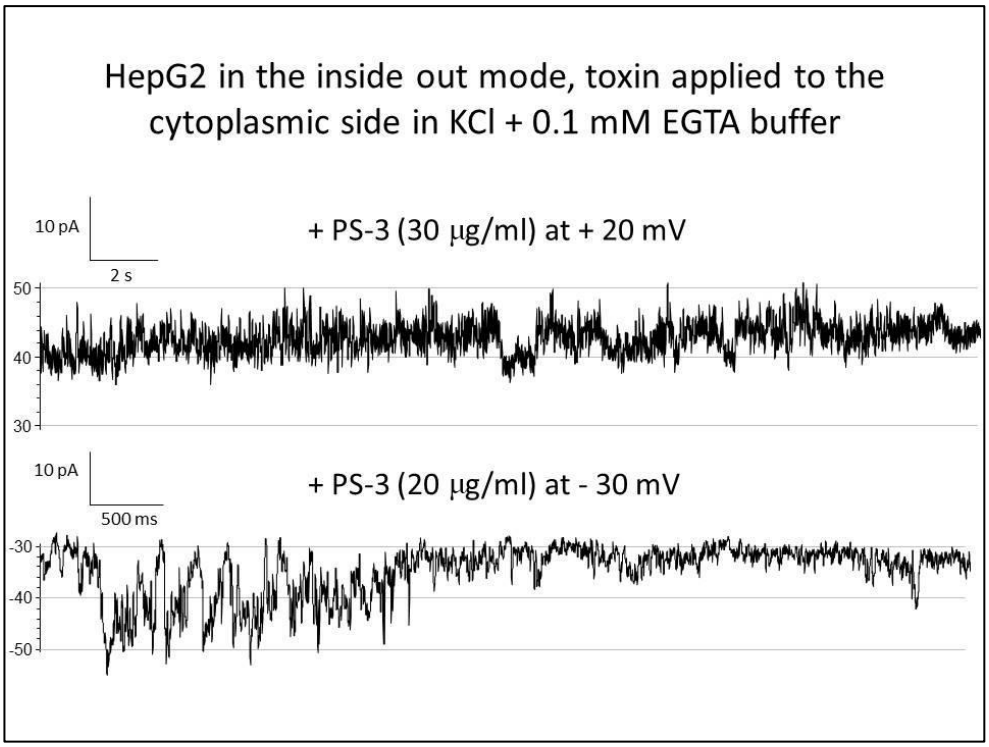

Figure 54 Single channel patch clamp recordings from HepG2 cells in the inside out mode after PS-3 was applied to the cytoplasmic side of the membrane in KCl buffer.
Single channel activity was recorded at +20 mV (upper trace) and -30 mV (lower trace) from HepG2 in the inside out configuration (two independent experiments) using LG16 borosilicate glass pipettes and KCl buffer. Channel activity started around 2 hours after toxin addition (either 30 or 20 μg/ml) to the bath. Records were filtered at 100 Hz.

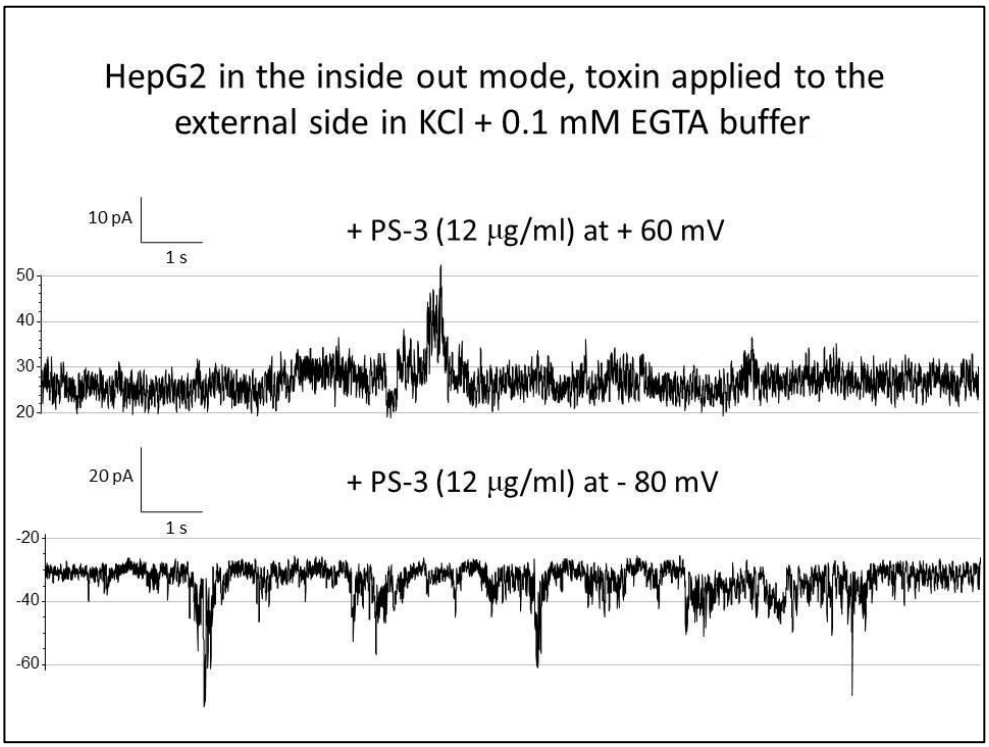

Figure 55 Single channel patch clamp recordings from HepG2 cells in the inside out mode after PS-3 was applied to the external side of the membrane in KCl buffer.
Single channel activity was recorded at +60 mV (upper trace) and -80 mV (lower trace) from HepG2 in the inside out configuration from two independent experiments using soda-lime glass pipettes and KCl buffer. Channel activity started around 20 minutes after addition of PS-3 (12 μg/ml) to the pipette. Records were filtered at 100 Hz.

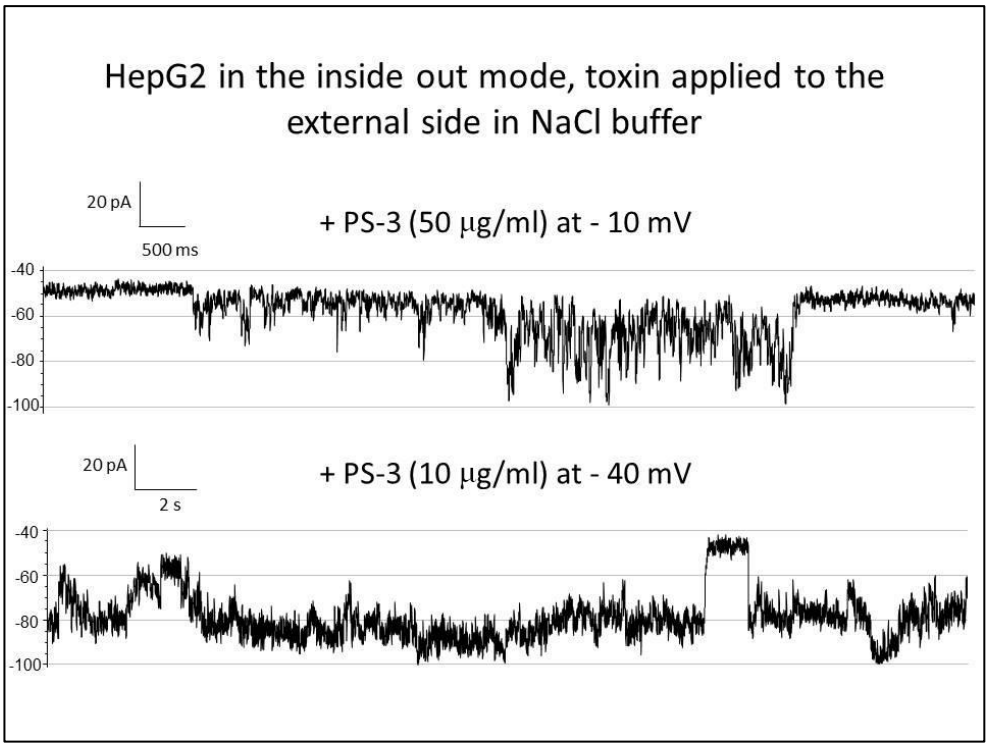

Figure 56 Single channel patch clamp recordings from HepG2 cells in the inside out mode after PS-3 was applied to the external side of the membrane in NaCl buffer.
Single channel activity was recorded at - 10 mV (upper trace) and -40 mV (lower trace) from HepG2 in the inside out configuration from two independent experiments using soda-lime glass pipettes and NaCl buffer. Channel activity started around 10 minutes after addition of PS-3 (50 or 10 µg/ml) to the pipette. Records were filtered at 100 Hz.

Exposing both cytosolic and external side of the HepG2 membrane to PS-3 resulted in channel activity, regardless of the buffer used. The aim of including 0.1 mM EGTA in KCl buffer was to chelate potential metal cations, specifically Ca^{2+}, resulting from buffer contamination to prevent activation of Ca^{2+} activated ion channels. However, because it was noted that the cell swelling was delayed in KCl buffer compared with NaCl buffer, a single channel experiment was attempted in KCl buffer without EGTA (Figure 57), on the assumption that EGTA may have decreased toxin activity, as evidenced in chapter 5.

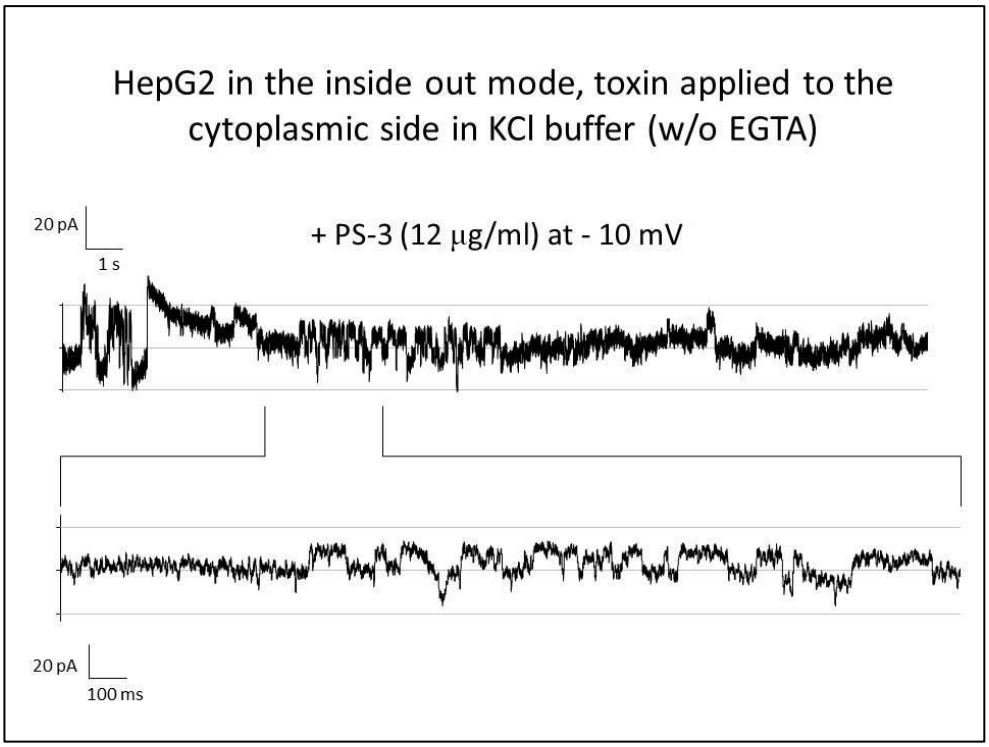

Figure 57 Single channel patch clamp recordings from HepG2 cells in the inside out mode after PS-3 was applied to the cytoplasmic side of the membrane in KCl buffer without EGTA.
Single channel activity was recorded at -10 mV (upper and lower trace) from HepG2 in the inside out configuration using soda-lime glass pipette and KCl buffer without EGTA from a single experiment. Channel activity started around 1.5 hours after addition of PS-3 (12 μg/ml) to the bath. Records were filtered at 80 Hz.

The absence of EGTA seemed to have increased the HepG2 membrane conductance compared to results in KCl buffer with EGTA (Figure 54 and Table 5); however these experiments may not be representative and results should not be generalized. Moreover lack of 0.1 mM EGTA in the buffer did not increase the cell swelling rate (data not shown).

Next, channel activity was monitored in HepG2 cells in the cell attached mode in the absence of PS-3 for 27 minutes to test the activation of endogenous channels in the absence of toxin (Figure 58).

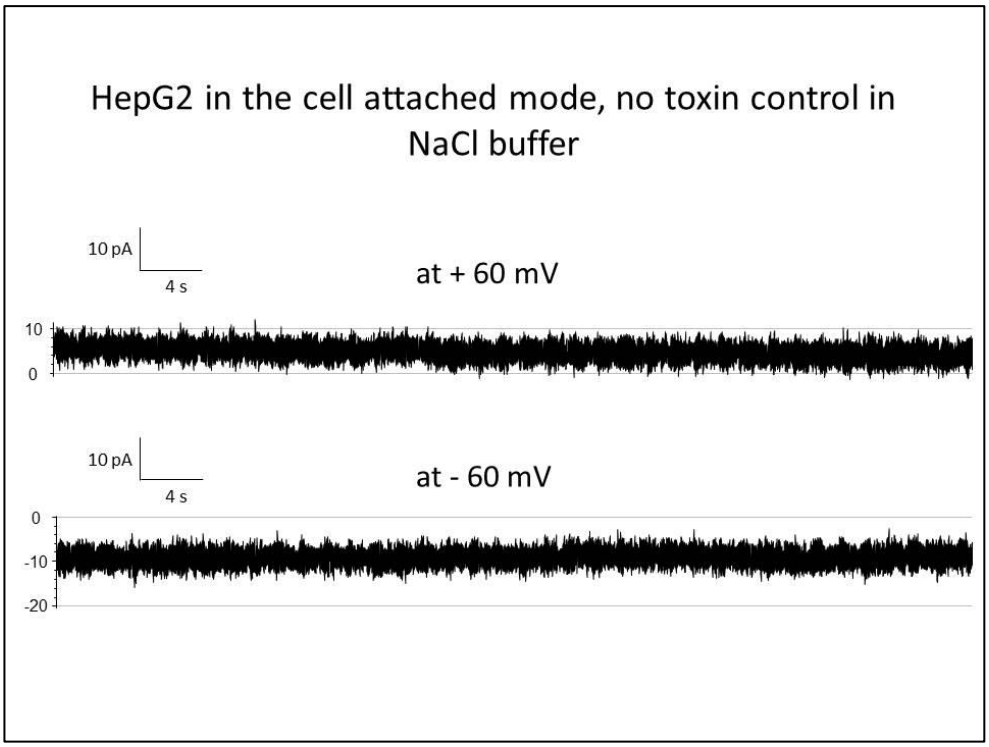

Figure 58 Single channel patch clamp recordings from HepG2 cells in the cell attached mode in NaCl buffer. Single channel activity was recorded at 26 minutes after establishing the seal at + 60 mV (upper trace) and at - 60 mV (lower trace) from HepG2 in the cell attached configuration using soda-lime glass pipettes and NaCl buffer. Records were filtered at 100 Hz.

Membrane showed no channel activity at voltages applied in the range of - 60 to + 60 mV for 27 minutes until the seal was lost.

Channel activity was then recorded in HepG2 cells in the cell attached mode in the presence of PS-3 (Figure 59).

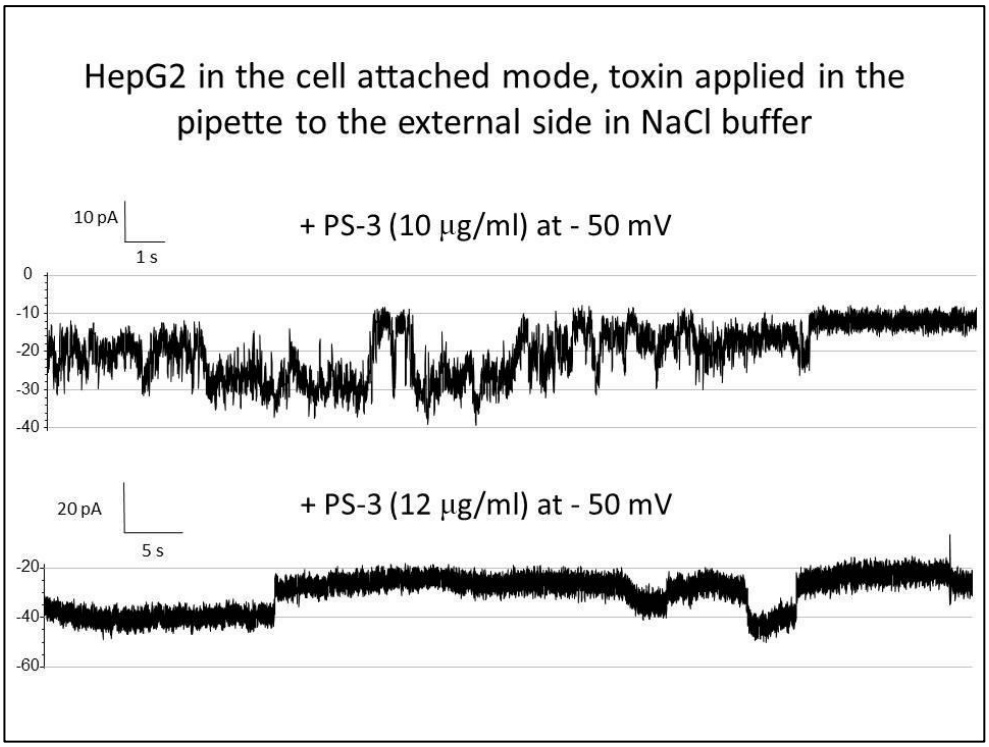

Figure 59 Single channel patch clamp recordings from HepG2 cells in the cell attached mode after PS-3 was applied in the pipette to the external side of the membrane in NaCl buffer.
Single channel activity was recorded at -50 mV (upper and lower trace) from HepG2 cells in the cell attached configuration from two independent experiments using soda-lime glass pipettes and NaCl buffer. Channel activity started around 15 minutes after addition of PS-3 (10 or 12 μg/ml) to the pipette. Records were filtered at 100 Hz.

Similar to the inside out mode, there was a single channel activity in PS-3 treated HepG2 cells in the cell attached configuration.

Next, negative controls were examined that included recordings in the cell attached mode from: HeLa cells exposed to PS-3 (Figure 60), HepG2 cells exposed to PS-3 but pre-treated with 2 mM EGTA (Figure 61), and HepG2 cells exposed to Cry1Ca (Figure 62).

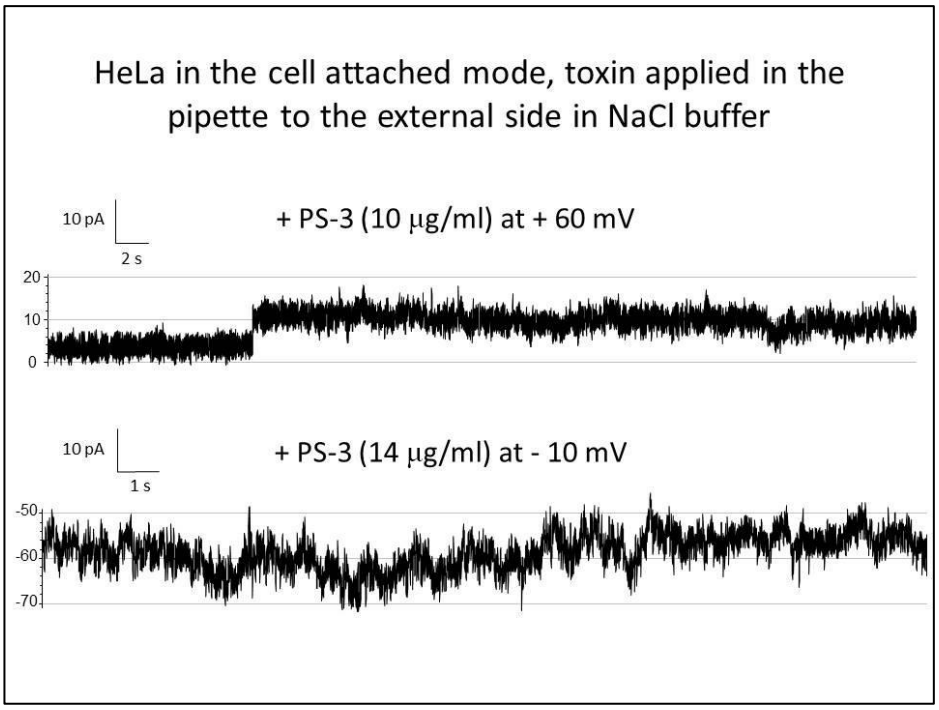

Figure 60 Single channel patch clamp recordings from HeLa cells in the cell attached mode after PS-3 was applied in the pipette to the external side of the membrane in NaCl buffer.
Single channel activity was recorded at + 60 mV (upper trace) and – 10 mV (lower trace) from HeLa in the cell attached configuration from two independent experiments using soda-lime glass pipettes and NaCl buffer. Channel activity started around 15 and 30 minutes after addition of 14 and 10 μg/ml of PS-3 respectively to the pipette. Record representing upper trace was filtered at 40 Hz and lower trace was filtered at 100 Hz.

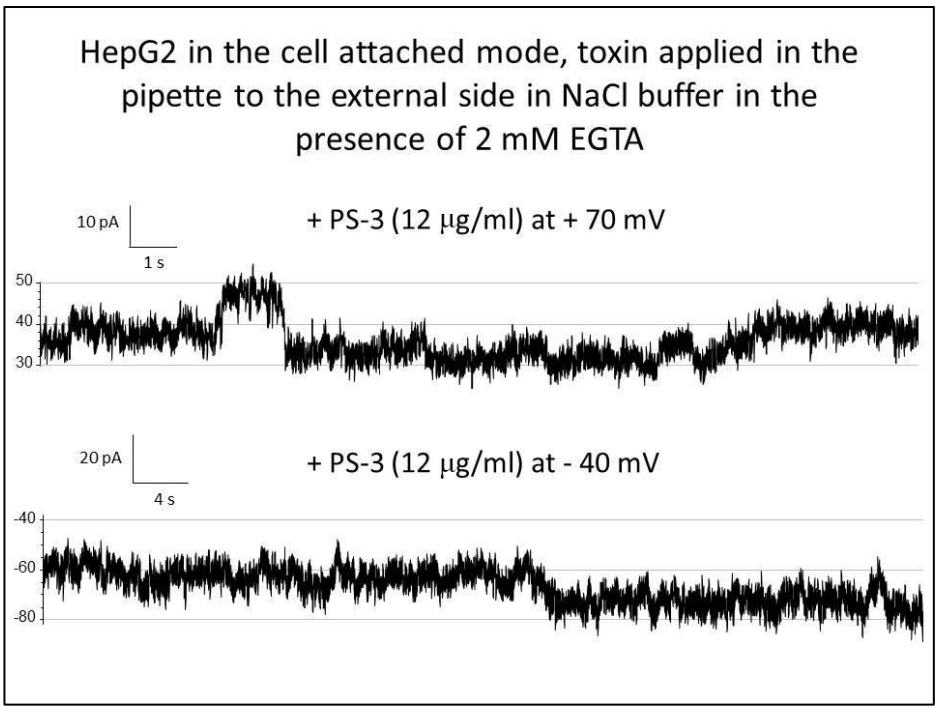

Figure 61 Single channel patch clamp recordings from HepG2 cells pre-treated with 2 mM EGTA in the cell attached mode after PS-3 was applied in the pipette to the external side of the membrane in NaCl buffer.
HepG2 cells were pre-treated with 2mM EGTA in NaCl buffer for 10 minutes before establishing a cell-attached mode. Single channel activity was recorded at + 70 mV (upper trace) and at - 40 mV (lower trace) from two independent experiments using soda-lime glass pipettes. Channel activity started around 10 minutes after addition of PS-3 (12 μg/ml) to the pipette. Records were filtered at 80 Hz.

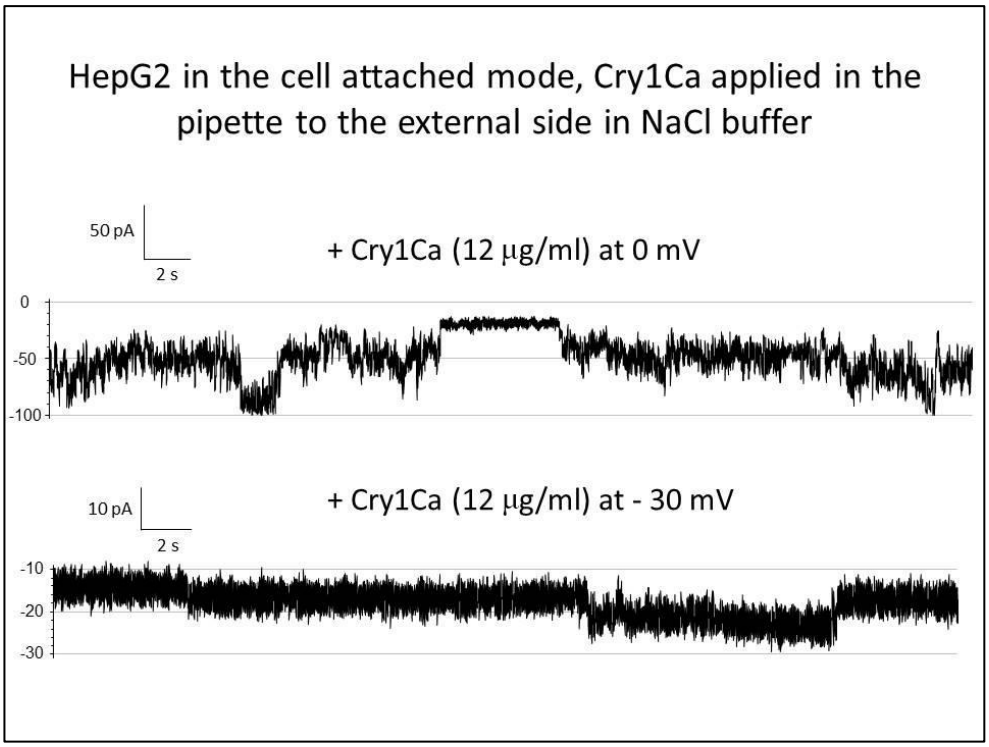

Figure 62 Single channel patch clamp recordings from HepG2 cells in the cell attached mode after Cry1Ca was applied in the pipette to the external side of the membrane in NaCl buffer.
Single channel activity was recorded at 0 mV (upper trace) and at - 30 mV (lower trace) from HepG2 in the cell attached configuration using soda-lime glass pipettes and NaCl buffer from a single experiment. Channel activity started around 5 minutes after addition of Cry1Ca (12 µg/ml) to the pipette. Records were filtered at 80 Hz.

Unexpectedly, some channel activity was present in HepG2 cells exposed to Cry1Ca, PS-3 treated HeLa cells, as well as HepG2 cells treated with PS-3 in the presence of 2 mM EGTA. Channel opening was also evident in resistant HepG2 cells (with developed resistance to ≤ 50 µg/ml of PS-3) when exposed to PS-3 at 14 µg/ml, in both inside out and cell attached modes (data not shown).

The main characteristic of ion channels is conductance. It provides information on the ease at which current flows through a pore and can predict the efficiency of pore formation. Average conductance levels in single channel recordings were estimated by looking at the open channel amplitudes in the inside out (Table 5) and cell attached (Table 6) configurations. Current amplitudes were measured for clear and

instantaneous channel openings (an example in Figure 63). Jumps smaller than 5 pA were not analysed. Conductance was calculated as described in the methods section.

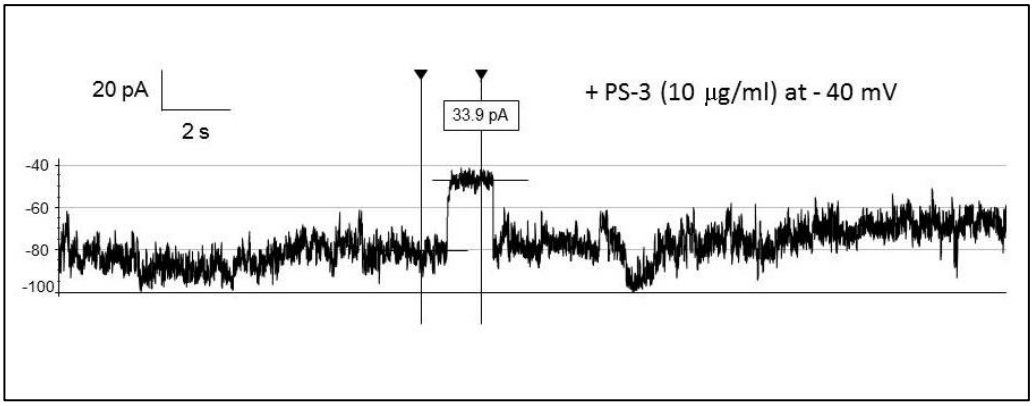

Figure 63 An example of current jump analysis performed in single channel recordings.
An example of a signal channel current analysis from HepG2 cell in the inside out mode with PS-3 (10 µg/ml) applied to the external side in NaCl buffer. Single channel openings are marked by downward current deflections at – 40 mV. The size of manually selected current jump was generated by pCLAMP 10.6.

Table 5 Average single channel conductance levels in the inside out configuration.
Average single channel conductance levels (pS) were calculated using the G=I/V equation, by analysing the current amplitudes for the period for which the channel was open at a given voltage in the inside out mode. Similar conductance values were averaged. Traces were filtered at 80 - 100 Hz before analyses. Number of cells patched/experiments is in brackets; NOB refers to the number of observations of certain current amplitude.

HepG2 cytoplasmic side + PS-3 (20-30 µg/ml) in KCl (four exp.)		
Mean	SEM	NOB
99.8	5.7	10
154.8	5.5	8
220.8	18.6	4
396.3	17.6	4
533.0	13.0	2
673.0	38.9	3

HepG2 external side + PS-3 (12 µg/ml) in KCl (one exp.)		
Mean	SEM	NOB
125.9	6.4	8
248.8	6.9	8
346.9	15.1	7
440.8	14.8	4
558.0	12.7	5
665.3	46.8	3

HepG2 cytoplasmic side + PS-3 (12 µg/ml) in KCl w/o EGTA (one exp.)		
Mean	SEM	NOB
431.8	18.1	5
589.4	15.8	8
820.7	13.6	7
955.5	8.9	11

HepG2 external side + PS-3 (50 µg/ml) in NaCl (one exp.)		
Mean	SEM	NOB
256.6	8.6	10
343.3	12.6	8
444.2	9.8	10
536.3	11.7	8

1349.5	55.7	32
2535.8	67.9	13
3539.0	75.5	10
5020.0	820.0	2

HepG2 external side + PS-3 (10 µg/ml) in NaCl (one exp.)		
Mean	SEM	NOB
384.0	28.3	5
654.2	16.8	10
763.4	13.6	5
922.3	37.7	3

631.9	10.9	7
738.9	7.6	15
845.3	9.6	10
951.3	9.8	6
1354.9	64.2	17
2576.7	77.4	9
3415.0	111.1	10
4467.9	67.5	16
5180.0	64.4	4

Table 6 Average single channel conductance levels in the cell attached configuration.
Average single channel conductance levels (pS) were calculated using the $G=I/(V-V_r)$ equation as described in the methods section, by analysing the current amplitudes for the period for which the channel was open at a given voltage in the cell attached mode. Similar conductance values were averaged. Traces were filtered at 80 - 100 Hz before analyses. Number of cells patched/experiments is provided in brackets; NOB refers to the number of observations of certain current amplitude.

HepG2 external side + PS-3 (10-14 µg/ml) in NaCl (three exp.)		
Mean	SEM	NOB
78.3	5.0	44
138.6	4.8	86
225.7	6.0	38
350.4	8.2	13
439.6	9.9	5
563.9	52.2	2

HeLa external side + PS-3 (10-14 µg/ml) in NaCl (two exp.)		
Mean	SEM	NOB
91.6	3.2	7
143.8	7.3	17
227.6	3.2	3
447.1	0.0	2
549.0	12.0	7
649.5	11.4	4
824.8	42.3	3
942.6	18.5	3

HepG2 external side + Cry1Ca (12 µg/ml) in NaCl (one exp.)		
Mean	SEM	NOB
91.6	3.2	7
143.8	7.3	17
227.6	3.2	3
447.1	0.0	2
549.0	12.0	7
649.5	11.4	4

HepG2 external side + PS-3 (12 µg/ml) in NaCl + 2 mM EGTA (two exp.)		
Mean	SEM	NOB
86.8	3.3	8
161.3	13.4	18
246.1	9.7	18
336.2	16.0	11
435.6	7.7	9
501.2	12.5	3

824.8	42.3	3
942.6	18.5	3
173.3	3.8	3
242.2	10.1	9
361.8	10.2	8
458.1	11.8	9
556.7	8.7	12
650.0	6.1	18
728.1	10.3	8
843.8	7.4	15
939.9	7.9	12
939.9	7.9	12
2557.5	61.8	26
3275.0	140.0	5
4512.5	196.3	4

Many conductance levels were present indicating more than one channel opening simultaneously, involving more than one type of channel or different substates of a single channel population. It was observed that generally channel activity was stronger at negative than at positive voltages (data not shown). This difference may have resulted from potential dependent changes in the number of channels or opening probability. Typically, channel activity increased with the time of the experiment often to a point where distinct levels of channel opening could not be easily established (e.g. Figure 62 upper trace). In most cases the recordings were stopped due to a lost seal, usually after large channel activity indicating membrane instability. This was possibly due to high toxin concentration and an increased tendency of its aggregation in the membrane environment. The cells in the cell attached mode did not show swelling or lysis at the end of experiments most likely because of local toxin application. Swelling of the cells in the whole cell mode was delayed, probably due to a basic biological buffer used and relatively low temperature (RT), which may have underestimated the real conductance.

Increased conductance could be attributed to the Cry toxin action, but also to the endogenous channels present in the cell membrane and activated either by the toxin or patching procedure. Most likely ion channel candidates include:

- Stretch-activated channels (Bear, 1990), as slight horizontal movements of the micromanipulator holding the glass pipette was noticed, which could have affected measurements in the cell attached and the whole cell modes;
- Ca^{2+}-activated channels (Chen et al., 1997), e.g. in the inside out experiments NaCl buffer rich in Ca^{2+} could have activated calcium channels;
- Voltage-gated ion channels (Chen et al., 1997), as some channels may have been activated by the applied voltage;
- Other endogenous channels, which activity was not blocked by inhibitors, e.g. K^{+} channels blocked by ATP (Liu et al., 2003).

However, micromanipulator movements did not correlate with increased channel activity, most experiments were performed with 0.1 mM EGTA present to chelate free Ca^{2+} and in the first few minutes of the recordings, channel activity was tested by applying relatively high positive and negative voltages (usually in the range of +50 to -50 mV). Quality of the seal was monitored often during the recordings and in the case of its deterioration it would result in increased leakage currents or membrane breakage rather than channel openings. Also channel activity in all experiments started after time needed for the toxin to diffuse in the buffer and reach the membrane and was not seen in the absence of toxin. Therefore the more probable cause of increased conductance in membranes exposed to PS-3 was either pore formation per se, or toxin directly influencing opening of endogenous channels or both.

Some of the ion channels have been characterised in HepG2 cells and in mammal hepatocytes. Characterization of ion channels in HepG2 was performed by Chen et al. (Chen et al., 1997). In the inside out mode, the conductance values were 18.9 in KCl and 19.8 pS in NaCl solution, not far from the ones measured in the cell attached mode: 22.2 in KCl and 19.7 pS in NaCl solution. Inside out experiments demonstrated that these channels were calcium and voltage dependent as well as cationic with low selectivity for a particular cation (Chen et al., 1997). Malhi et al. found that the whole cell currents from HepG2 in the absence of ATP (K^+ channel inhibitor) were low and ATP-sensitive K^+ channels in these cells required drug stimulation by potassium channel openers for full channel activation indicating decreased basal activity of these channels in HepG2 (Malhi et al., 2000). In rat hepatocytes a stretch activated channel of 16 pS conductance was identified, activated by suction as well as cell swelling induced by osmotic shock (Bear, 1990). Also in rat hepatocytes, single channel patch clamp studies identified calcium independent K^+ and Cl^- channels with an inward conductance of 55 and 30 pS and an outward conductance of 25 and 10 pS respectively (Breit et al., 1997). In guinea-pig hepatocytes a Cl^- channel with a conductance of 7.4 pS was present (Koumi S, 1994) as well as calcium activated K^+ channels with 20 pS single channel conductance (Capiod and Ogden, 1989). Conductance levels reported for hepatocytes and hepatoma cells are relatively low. Therefore, the most plausible explanation for large conductance values observed in single channel patch clamp experiments with PS-3 is channel formation de novo.

Contrary to PLB experiments, data on single channel activity induced by Cry toxins using the patch clamp technique is scarce. In one study, the effect of Cry1C was investigated on the single channel activity in SF-9 cultured lepidopteran cells using cell

attached (toxin added to the bath) and inside out patch clamp configurations. A voltage dependent anionic channel was observed 10 minutes after toxin treatment (EC_{50} dose) with a similar conductance of 26 pS in both cell attached and inside out configuration (with cytoplasmic side of the membrane exposed to the toxin). Interestingly, the initial response to Cry1C involved calcium influx via voltage dependent calcium channels, which demonstrated for the first time a role of ion channels in the cellular response to Cry toxins (Schwartz et al., 1991). A different Cry toxin Cry1Ac induced a large conductance (a few nS) in cell attached and inside out configurations in intact midgut cells of *M. sexta* larvae, activity that was not seen before exposure to toxin (Peyronnet et al., 2004). In another study, the activity of Cry1Ab (100 ng/ml) was assessed in ruminal sheep epithelium cells using whole cell and single channel configurations of the patch clamp technique. Although sheep ruminal cells, like other mammalian cells, are thought to be naturally resistant to Cry toxins, and viability of these cells were not affected by the toxin dose used in electrophysiology experiments, the conductance increased significantly in almost half of the cells tested in whole cell experiments and Cry1Ab induced single channel activity of conductance over 500 pS in outside out patch clamp configuration. The authors interpreted these results as toxin induced pore formation, pointing to similar Cry toxin behaviour in PLB experiments in the absence of receptors (Stumpff et al., 2007).

Generally, when PS-3 was added to the bath, a much higher dose was used (20-30 µg/ml) and more time (1 - 2 hours) was required to start channel activity, compared to the dose (10 - 14 µg/ml) and time (5-15 minutes) when toxin was added inside the pipette. This was probably caused by the differences in the rate of toxin diffusion, faster in experiments where toxin was put in the pipette due to a lesser distance to the

membrane patch and a smaller buffer volume. Also, due to almost vertical position of the pipette and gravitation force, applied toxin was able to reach the membrane patch quicker than in the bath. In both cases the membrane patch had roughly the same surface area of around 0.25 μm^2, with differing buffer volumes: 1000 µl in the bath, 50 µl in soda lime and 70 µl in borosilicate glass pipette.

In the inside out mode, channel conductance was similar when PS-3 was applied to the external or cytoplasmic side of the membrane. It may mean that the presence of the receptor did not affect the conductance, but the assumption that the external side of the patch contained the receptor may be wrong. If a physiological density of the receptor in the HepG2 membrane is small, it may have happened that it was not present in the patch. In case of more than one molecule critical for activity, the probability of having them both inside the patch would be even smaller. Another explanation of the data could come from the high toxin dose used, in which case the benefits of having the receptor would be unnoticed due to spontaneous toxin insertion regardless of the exposed membrane side.

In the inside out mode with PS-3 applied to the external side, there was a difference in conductance depending on the buffer composition. The values were higher in the NaCl, compared to KCl buffer. Interestingly, large difference in conductance was also noted between KCl buffer with and without 0.1 mM EGTA. The solutions differed not only in NaCl, KCl and EGTA but also in $CaCl_2$ concentration. It is possible that these differences could be influenced by selective ionic conduction or by the effect these ions may have on the membrane.

Selectivity of channels recorded in single channel patch clamp experiments in the presence of PS-3 remains unknown due to lack of substitution experiments. Endogenous conductance in hepatocytes is considerably driven by chloride ions. A study by Graf et al. showed that chloride accounts for 25%–80% of hepatocyte membrane conductance (Graf et al., 1987), which increases by 30 – 100 fold as a result of cell swelling (Meng and Weinman, 1996). Moreover, channels formed by Cry1C in SF-9 cells were anionic with high selectivity to Cl^- ions (at slightly acidic pH), but this effect was pH dependent (Schwartz et al., 1991). On the other hand a role of cations in passing current cannot be excluded, especially that PS-3-induced channels in PLBs were cationic (shown later in section 4.7), with K^+ being the candidate as in the hydrated form it is smaller than hydrated Na^+. To add to complexity, in the cell attached experiments NaCl buffer generates a potential due to asymmetric ion concentration inside and outside the membrane. After a pore is open ion movement that takes place will depend not only on the applied voltage and pore selectivity (like in symmetrical experiments with excised patches), but also on the voltage across the membrane and ionic gradient (Na^+, K^+ and Cl^- being the main players). Moreover, some ions due to the gradient will run in the opposite directions (Na^+, K^+), in which case the overall current and conductance may be underestimated.

In the cell attached mode, conductance in HepG2 cells exposed to PS-3 was not lowered compared to the values in the excised-patch mode, despite physically intact membrane and active cell metabolism during the experiments. Assuming that membrane activity in single channel patch clamp experiments was caused directly by the toxin, and not by endogenous channels, it is difficult to explain increased conductance in experiments involving negative controls. Conductance values in the cell

attached configuration were high regardless of the Cry toxin (PS-3 or Cry1Ca) or cell line (HepG2 or HeLa) used. Also, previously established resistance (explained in chapter 5) was insignificant as relatively high conductance values were recorded in EGTA pre-treated HepG2 cells exposed to PS-3 as well as in toxin-resistant HepG2 cells treated with PS-3 in two independent experiments (data not shown). These conductance levels do not match huge differences in conductance in the whole cell recordings, where for example Cry1Ca didn't induce large currents in HepG2 (similar to PS-3 in the presence of 2 mM EGTA or PS-3 in HeLa cells). Comparison of currents between the whole cell and single channel recordings is complex. Whereas in the patched membrane a full opening of one (sometimes two or more) channel can be recorded, in the whole cell experiment the overall current is dependent not only on the current value recorded at a single channel level but also on the number of channels and their opening probability. When comparing whole cell and cell attached single channel experiments another consideration has to be taken into account. In the former, the intracellular voltage is clamped to the pipette voltage, because there is an electrical continuum between the pipette and the interior of the cell. In the latter, the voltage across the membrane patch is the difference between the pipette voltage and the intracellular voltage (Vr), which is controlled by the electrochemical gradient that exists across the entire cell membrane. Another difference is the size of the exposed membrane material. Despite being in contact with the toxin, the size of the patch in the single channel experiments may be too small for the cell to respond properly. The patch is ~0.2 μm^2 - considerably smaller than the cell surface area normally exposed to toxin in the whole cell experiments, which may be around 300 μm^2 (assuming 0.25 µm patch radius and 7 µm cell radius). So, even though a high toxin concentration was in

the pipette (12 μg/ml), because it was applied only locally, the cell either did not detect the damage, detected it but did not react, or detected and tried to repair it but because the patch was isolated by the glass it could not. Also, it has been calculated that in the single channel experiments with the toxin in the pipette, 0.0085 nM of toxin was exposed to the membrane patch of around 0.2 μm^2, whereas in the whole cell experiments 0.17 nM was exposed to around 300 μm^2 (assuming that only half of the cell's surface is exposed to the treatment). This means that in the whole cell experiments the surface area of the membrane was ~ 1500 times larger with only 20 times more toxin molecules in the buffer, increasing the number of toxin molecules per surface area in single channel experiments. It may be that in the single channel experiments high doses of Cry toxins like PS-3 or Cry1Ca spontaneously inserted in the membrane independently of the membrane nature, similarly to experiments in artificial lipid bilayers devoid of any protein component, as suggested before (Stumpff et al., 2007). Increased conductance was previously observed in excised patches of non-susceptible sheep epithelial membranes exposed to Cry1Ab (Stumpff et al., 2007). In this study where high toxin dose was used, membrane patches (even in the cell attached mode) may represent an environment similar to that in PLB experiments, which would explain large conductance values in all of the single channel patch clamp experiments. Variation in conductance values between single channel recordings may simply reflect how well the toxin inserts into the membrane at a given time/experiment resulting in different efficiencies of pore formation.

To sum up, the data suggest that a substantial single channel activity arose most likely as a result of Cry toxin induced pore formation and in non-whole cell readings was independent of membrane origin and/or receptor presence most likely as

a result of the high doses used. However, due to time constraints single channel recordings presented here may not be representative, with two (in some cases only one) individual recordings per condition tested. Therefore, conclusions from these studies should be approached with caution.

Single channel activity in planar lipid bilayers

Planar lipid bilayer technique is another electrophysiological method that allows the testing of the activity of pore forming molecules. In this method, first described by Mueller and colleagues, an artificial phospholipid bilayer is created separating two aqueous solutions (Mueller et al., 1963). The advantage of this method is a more simplified environment than at the cell level with a total control over buffer and lipid composition. In PLB experiments lipid mixture consisted of PE, PC and cholesterol. PE is found in the inner cytoplasmic leaflet, whereas PC is more commonly found in the outer leaflet. Cholesterol present in animal cell membranes was added to improve membrane integrity and fluidity. No protein components were present.

All PLB experiments were conducted by Eva Fortea as described in the methods section. Briefly, a lipid membrane was painted inside a plastic holder in between two chambers named cis and trans. 1 ml of buffer (150 mM KCl, 1 mM $CaCl_2$, 10 mM HEPES, pH 7.5) was added to both chambers resulting in symmetrical conditions. Current trace was monitored for 30 minutes prior to toxin addition to insure no channel activity, e.g. due to contamination. PS-3 (4-8 μg/ml) was added to the cis chamber and activity was recorded at different applied voltages. Three experiments were performed. Example traces are shown in Figure 64 and Figure 65.

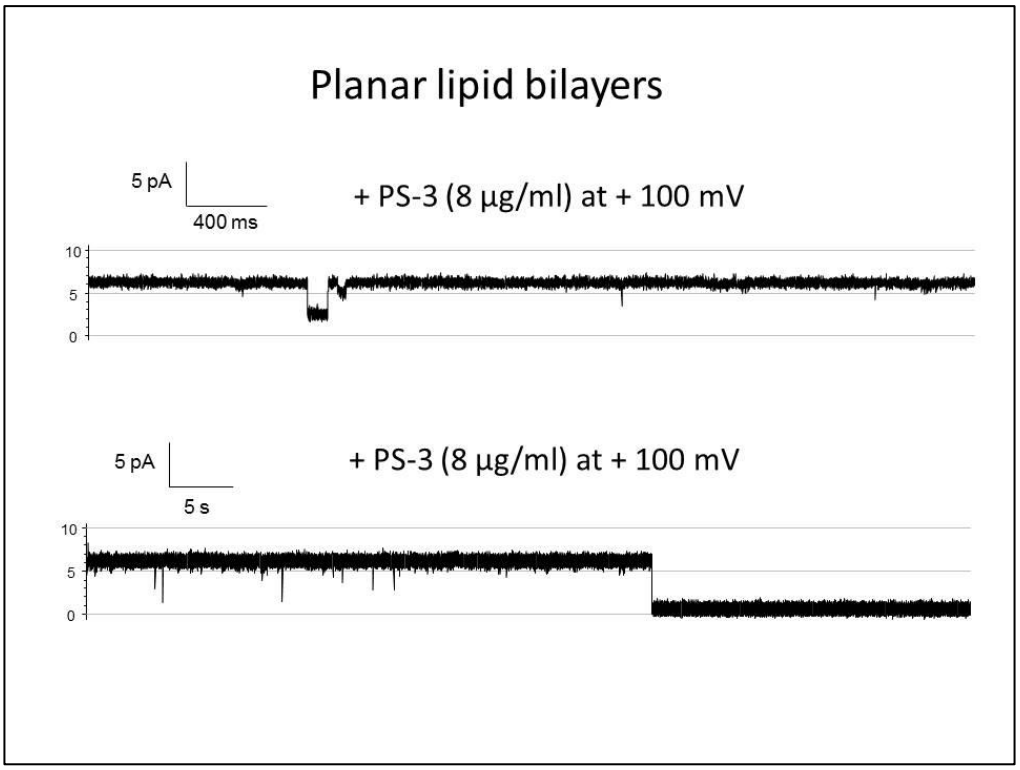

Figure 64 Example of a single channel recording in planar lipid bilayer after PS-3 application at positive voltage. Single channel activity was recorded at +100 mV (upper and lower traces) from PLB in KCl buffer after addition of PS-3 (8 µg/ml) to the cis chamber. Records were filtered at 200 Hz. The trace is representative of three experiments.

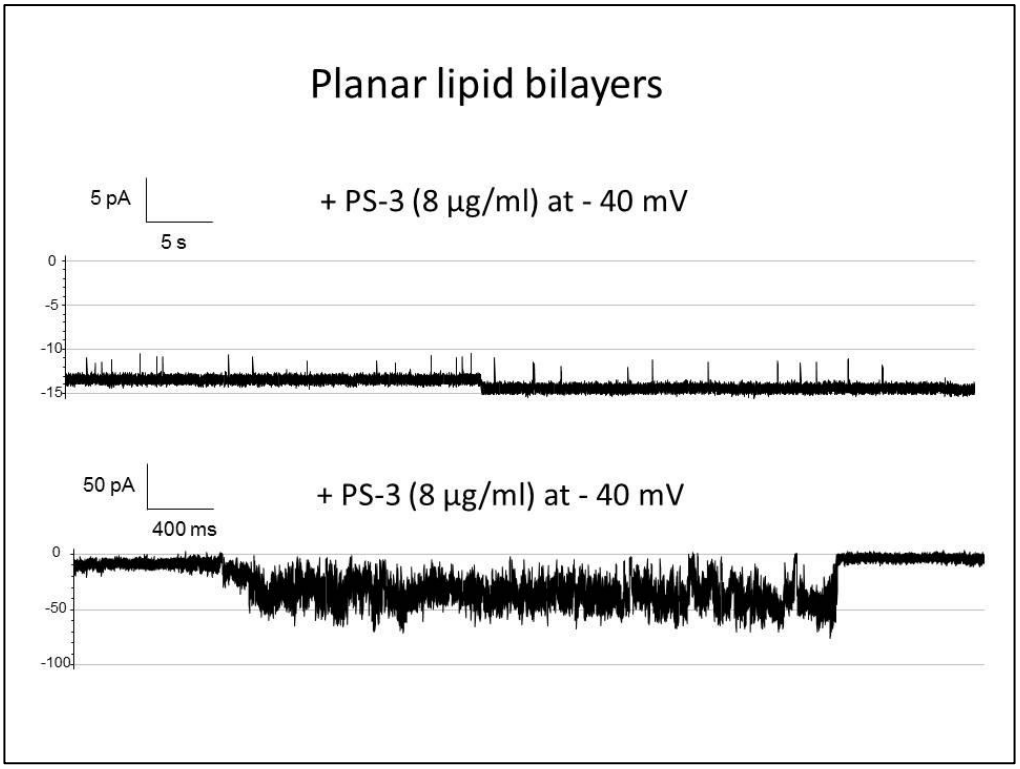

Figure 65 Example of a single channel recording in planar lipid bilayer after PS-3 application at negative voltage. Single channel activity was recorded at - 40 mV (upper and lower trace) from PLB in KCl buffer after addition of PS-3 (8 µg/ml) to the cis chamber. Records were filtered at 200 Hz. The trace is representative of three experiments.

Channel openings were longer and clearer with greater pore stability compared with single channel patch clamp recordings, however not always (Figure 65, bottom trace).

Conductance was calculated to estimate the efficiency of pore formation. Around 20-25 current jumps were averaged for each conductance value. Points representing similar conductance values were grouped together. Mean conductance within a group was read from a slope of a linear regression. Figure 66, Figure 67 and Figure 68 present current-voltage relation calculated for each experiment.

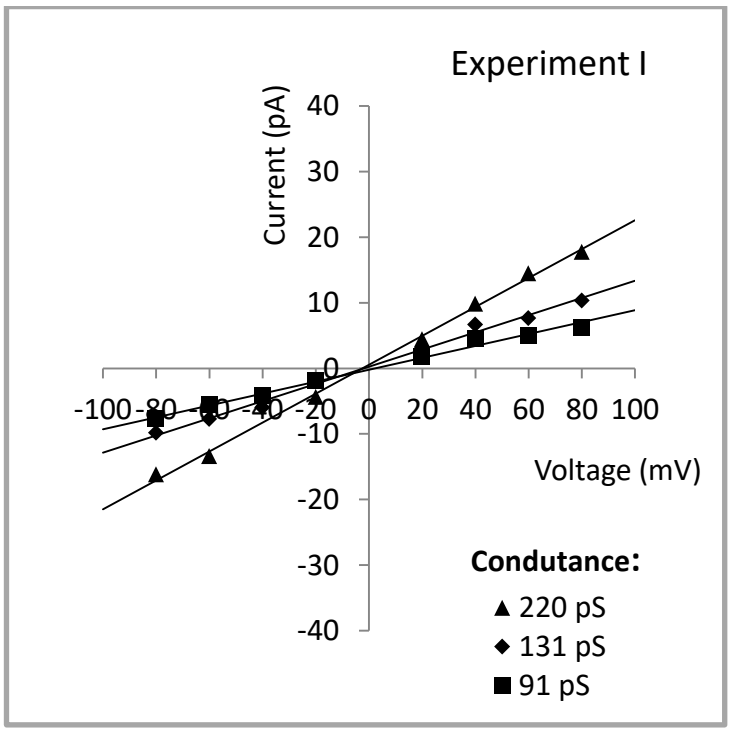

Figure 66 Single channel current – voltage relationship for PS-3 in planar lipid bilayers (experiment I).
Current–voltage (I/V) characteristics of single-channel activity in 150/150 mM KCl (cis/trans) buffer (n=20-25) at different voltages after PS-3 (8 µg/ml) was added to the cis side. Conductance was calculated (G=I/V) and data points fitted by linear regression. Mean conductance values were deduced as the slopes of the linear regressions on the data points as 91, 131, and 220 pS.

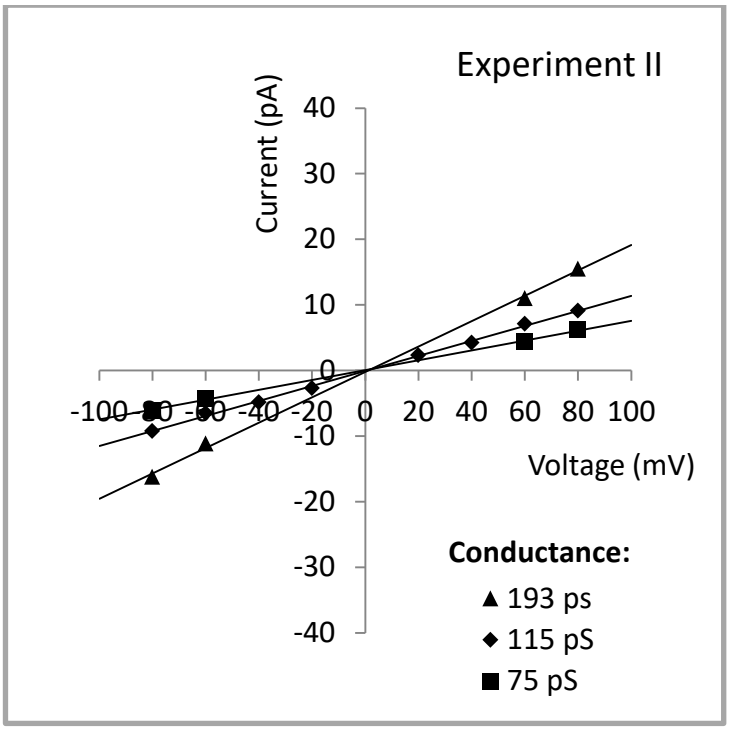

Figure 67 Single channel current – voltage relationship for PS-3 in planar lipid bilayers (experiment II).
Current–voltage (I/V) characteristics of single-channel activity in 150/150 mM KCl (cis/trans) buffer (n=20-25) at different voltages after PS-3 (8 µg/ml) was added to the cis side. Conductance was calculated (G=I/V) and data points fitted by linear regression. Mean conductance values were deduced as the slopes of the linear regressions on the data points as 75, 115, and 193 pS.

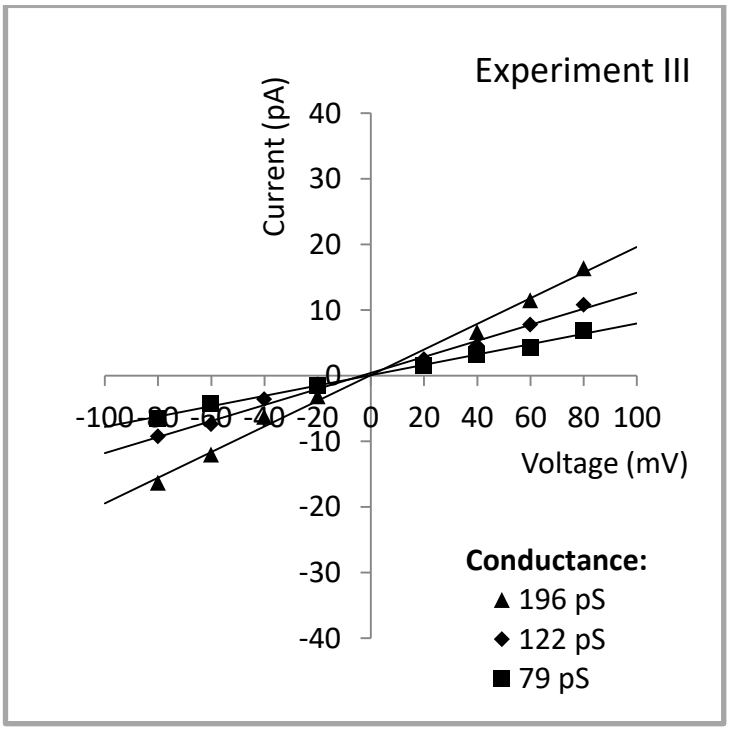

Figure 68 Single channel current – voltage relationship for PS-3 in planar lipid bilayers (experiment III).
Current–voltage (I/V) characteristics of single-channel activity in 150/150 mM KCl (cis/trans) buffer (n=20-25) at different voltages after PS-3 (8 µg/ml) was added to the cis side. Conductance was calculated (G=I/V) and data points fitted by linear regression. Mean conductance values were deduced as the slopes of the linear regressions on the data points as 79, 122, and 196 pS.

The results from the three experiments were consistent. Multiple conductance levels were observed. There was no rectification (non-linear current–voltage relation) as the conductance did not change with different voltages applied. Interestingly, there was a numerical relation of the two lowest conductance states to the highest conductance (roughly two add up to the third). This may result from two separate channel populations that open and close independently of each other, but when they open simultaneously, the highest conductance is achieved. Alternatively, the results may represent different sub-states of a single population of channels, when one channel type may have more than one open conformation, which results in different conductance values.

For comparison, in PLB experiments, under symmetrical 150 mM KCl conditions at pH 9.0, the main conductance for Cry1Ac was 461 pS, 350 pS for Cry1B, 90 pS for Cry1C, and 450 pS for Cry1Aa (Schwartz et al., 1997). Under symmetrical 150 mM KCl, pH 9.0 conditions conductance induced by nematocidal Cry5B was 125 pS and less (Kao et al., 2011). In 300 mM KCl, pH 9.7 conductance levels for Cry1Ac and Cry3A ranged from 200 pS to 4000 pS (Slatin et al., 1990a). In 300 mM KCl, pH 9.5 a 21.5 kDa α-helical region of Cry1Ac induced a range of conductance values up to 600 pS (Walters et al., 1993). A homolog of PS-1 – PS-1Aa2 (Cry31Aa2) formed pores that had several levels of conductance: 11, 16 and 21 pS in 150 mM KCl buffer (Gabriel Narvaez, 2014).

Importantly, incorporation of membrane material from susceptible insects into PLBs promoted activity of Cry toxins. In PLBs enriched in brush border membranes, conductance induced by Cry1Aa increased 8 fold to 85 - 420 pS (Peyronnet et al., 2001) and conductance induced by Cry1C increased from 31 - 76 pS to 50 – 752 pS, reaching

as high as 1900 pS (Lorence, 1995) compared to receptor free phospholipid bilayers. However in experiments where PLBs were reconstituted with GPI-linked receptor complex the conductance by Cry1Ac did not increase and by Cry1Aa even decreased, but it took significantly less Cry1Ac and Cry1Aa toxin to trigger channel activity compared with non-enriched lipid membranes (Schwartz et al., 1997).

Comparison of conductance was attempted between PLB and single channel inside out recordings in KCl, due to similar buffer composition and detection sensitivity levels in these methods. Composition of the membrane was the main difference; with artificial membrane being a simple, neutral bilayer, and biological membrane – asymmetric, packed with protein components and most likely negatively charged. Conductance ranging from 100 to 600 pS was obtained in patch clamp system - values being much higher than in PLB experiments (100 – 200 pS). The difference cannot be explained by the presence of toxin receptor as high values were observed with PS-3 exposed to both extracellular and intracellular sides. Bigger conductance values observed in single channel patch clamp compared with PLB experiments may be due to different lipid composition, presence of the protein component in general, or other factors influenced by the biological origin of the membrane. Also, higher toxin dose was used in patch clamp (12-30 µg/ml) compared to PLB experiments (4-8 µg/ml). Another explanation, mentioned before when comparing whole cell with other single channel experiments, is that in PLB experiments the probability of toxin hitting the bilayer is much smaller with toxin being in the bath compared with the toxin in the pipette in the patch clamp experiments, even though membrane surface in PLB is larger than in the patch. Calculations suggest (assuming 50 µm radius of the functional painted membrane) that in the PLB experiments the surface area of the membrane

was ~ 40,000 times larger with only 13 times more toxin molecules in the buffer. Also, the vertical position of PLB painted in the sidewall of the chamber does not promote contact with the protein. On the contrary, patch system where the toxin is in the pipette is much more sensitive as area is reduced by a patch pipette and toxin is concentrated in a very small area by diffusing down directly towards the membrane.

To study selectivity of channels in the PLB system, concentration of KCl was increased from 150 to 450 mM in the cis chamber. Conductance in these asymmetric conditions was calculated as previously (Figure 69).

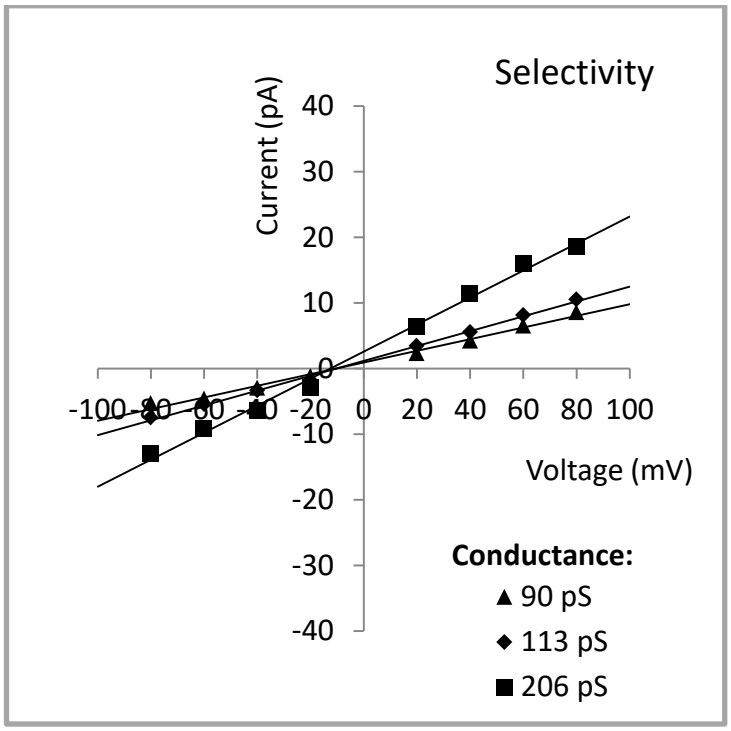

Figure 69 Single channel current – voltage relationship for PS-3 in planar lipid bilayers in asymmetric conditions (experiments I, II and III).
Current–voltage (I/V) characteristics of single-channel activity in 450/150 mM KCl (cis/trans) buffer (n=20-25) at different voltages after PS-3 (8 µg/ml) was added to the cis side. Conductance was calculated (G=I/V) and data points fitted by linear regression. Mean conductance values were deduced as the slopes of the linear regressions on the data points as 90, 113, and 206 pS.

Selectivity (P_{K^+}/P_{Cl^-} value) was calculated using Goldman-Hodgkin Katz potential equation (Hodgkin and Horowicz, 1959), which relates ions permeability across the

membrane and reversal potential (Table 7). Reversal potential (Vr) calculated below represents the potential at which there is no current passing through a pore.

Table 7 Selectivity and reversal potential calculated in PLB experiments I, II and III with PS-3 in asymmetrical conditions.
Selectivity (PK^+/PCl^-) and reversal potential (Vr) were calculated in planar lipid bilayer experiments I, II and III with PS-3 in asymmetrical (450/150 mM KCl cis/trans) conditions.

	I	II	III	Mean	SEM
Vr (mV)	-10.5	-9.5	-12.9	**-10.97**	1.0
P_{K^+}/P_{Cl^-}	2.35	2.15	2.93	**2.48**	0.23

Under asymmetrical conditions the channel conductance remained in the similar pS range and the reversal potential shifted to – 10.97 mV (± 1 mV). P_{K^+}/P_{Cl^-} value was 2.48 (± 0.23) indicating a slight selectivity to cations. Cationic channels in PLBs were also observed by Cry1B, Cry1Ac, Cry3A (Schwartz et al., 1997, Slatin et al., 1990b, Walters et al., 1993), by monomeric and oligomeric Cry1Ab (Rausell et al., 2004), as well as by Cry1Aa and Cry1Ac in *M. sexta* BBMV (Kirouac et al., 2002). A small P_{K^+}/P_{Cl^-} value is in agreement with the general thought that pores created by Cry toxins are weakly specific as these proteins did not evolve with the host insect membrane, which is also undoubtedly true for cancer cells.

Channel activity is a stochastic process with probabilities of opening and closing. The opening probability can be determined from single channel recordings by a simple analysis of the distribution of all the current values plotted as a histogram (called all-points histogram or amplitude histogram). A peak at 0 current represents a channel at the shut level and a peak at any other value, positive or negative depending on the voltage applied, represents a channel at an open level. The area under the peak is proportional to the time that a channel spends in each conformation. Amplitude

histograms were generated for each of the three experiments (Figure 70, Figure 71 and Figure 72).

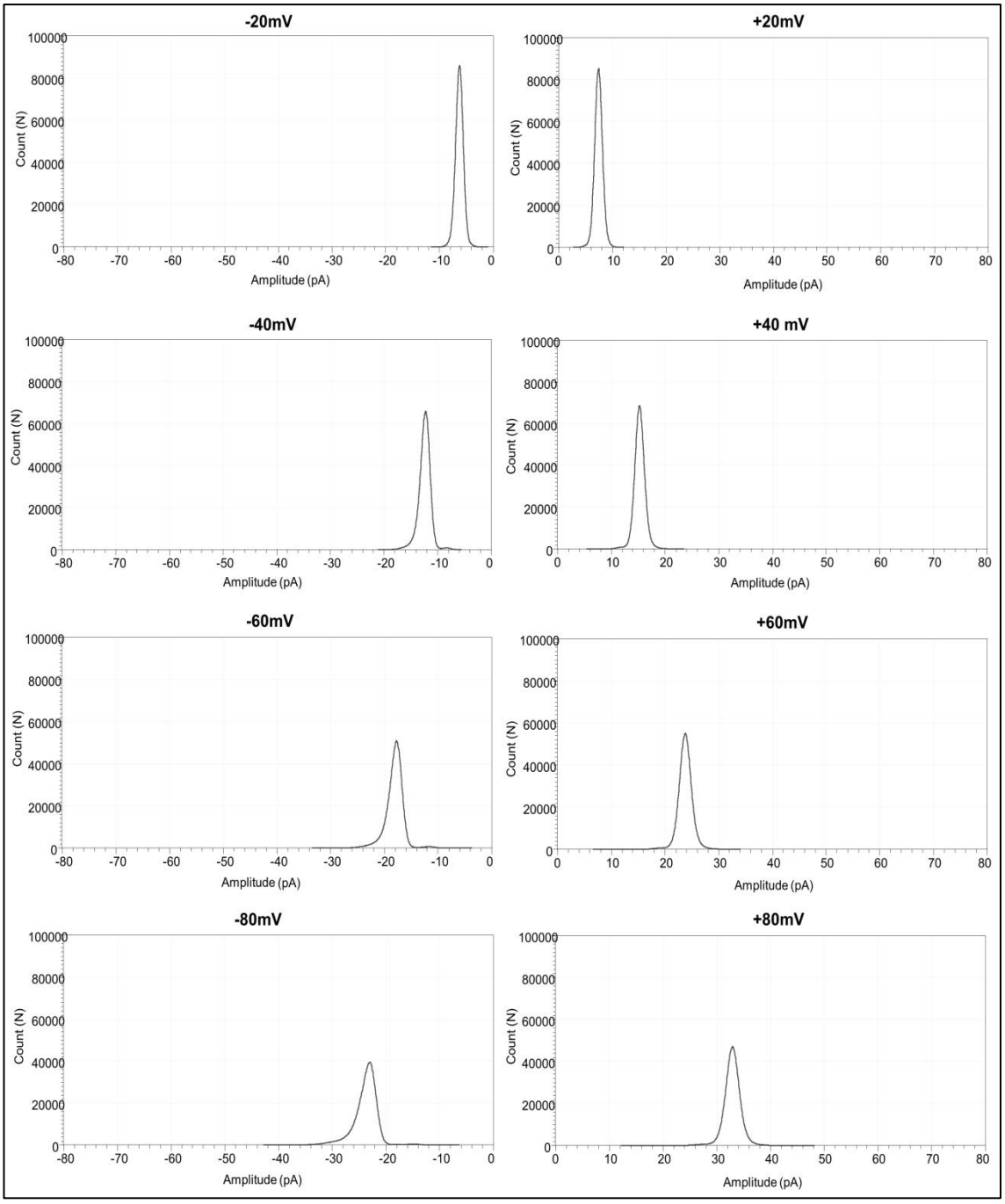

Figure 70 Amplitude histogram of channel openings obtained in the presence of PS-3 in PLBs in experiment I. Data presented in the histogram were collected at +/- 20, 40, 60, and 80 mV in PLBs in the presence of PS-3 (8 µg/ml) and were not Gaussian fitted. Count (N) represents the number of observed events of channel conductance and amplitude represents the value of a current jump in pA. Histogram plots were obtained for 1 minute current recordings generated by Clampfit 10.5, using 0.05 bin width. The bars have been removed for clarity.

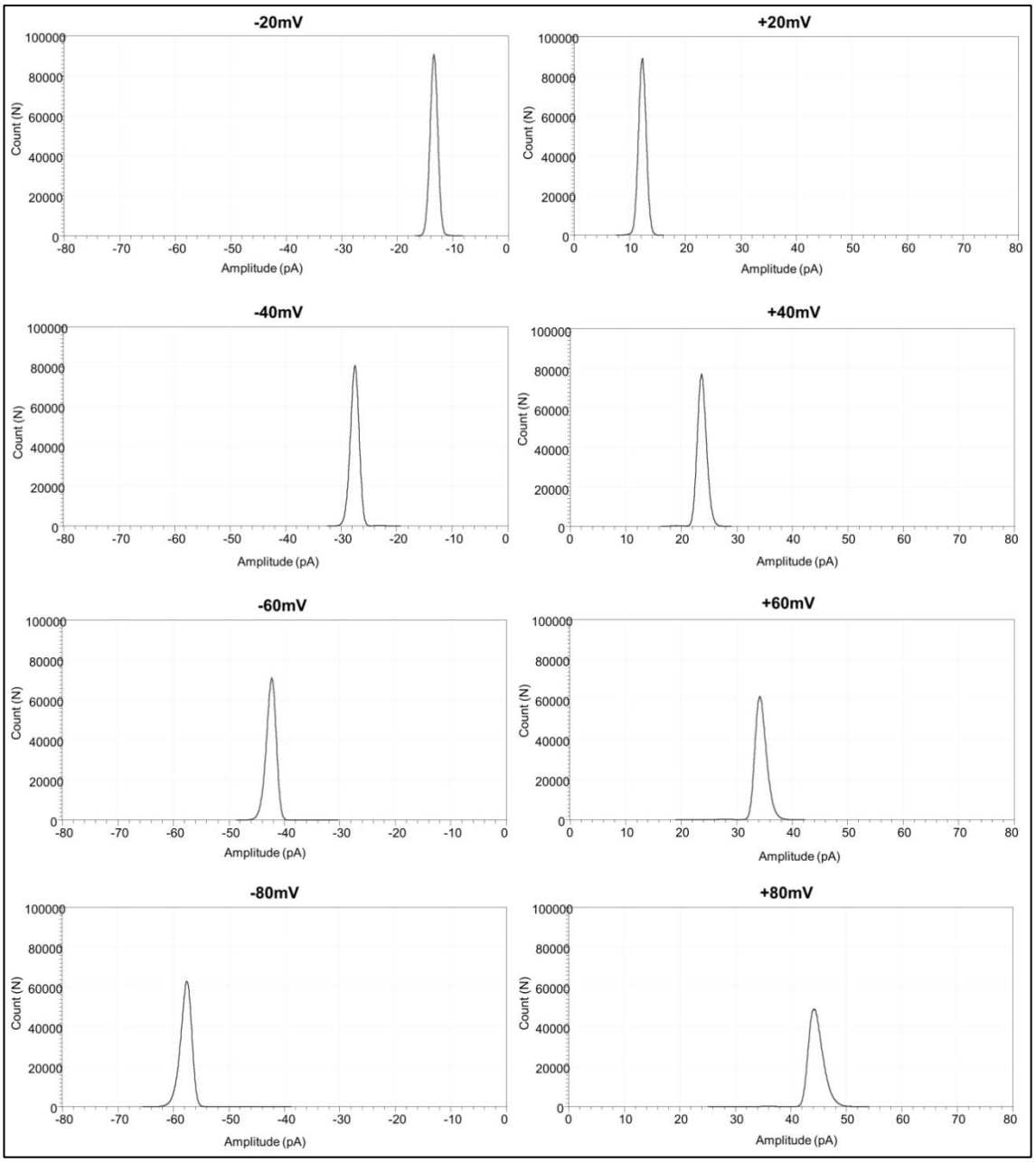

Figure 71 Amplitude histogram of channel openings obtained in the presence of PS-3 in PLBs in experiment II. Data presented in the histogram were collected at +/- 20, 40, 60, and 80 mV in PLBs in the presence of PS-3 (8 µg/ml) and were not Gaussian fitted. Count (N) represents the number of observed events of channel conductance and amplitude represents the value of a current jump in pA. Histogram plots were obtained for 1 minute current recordings generated by Clampfit 10.5, using 0.05 bin width. The bars have been removed for clarity.

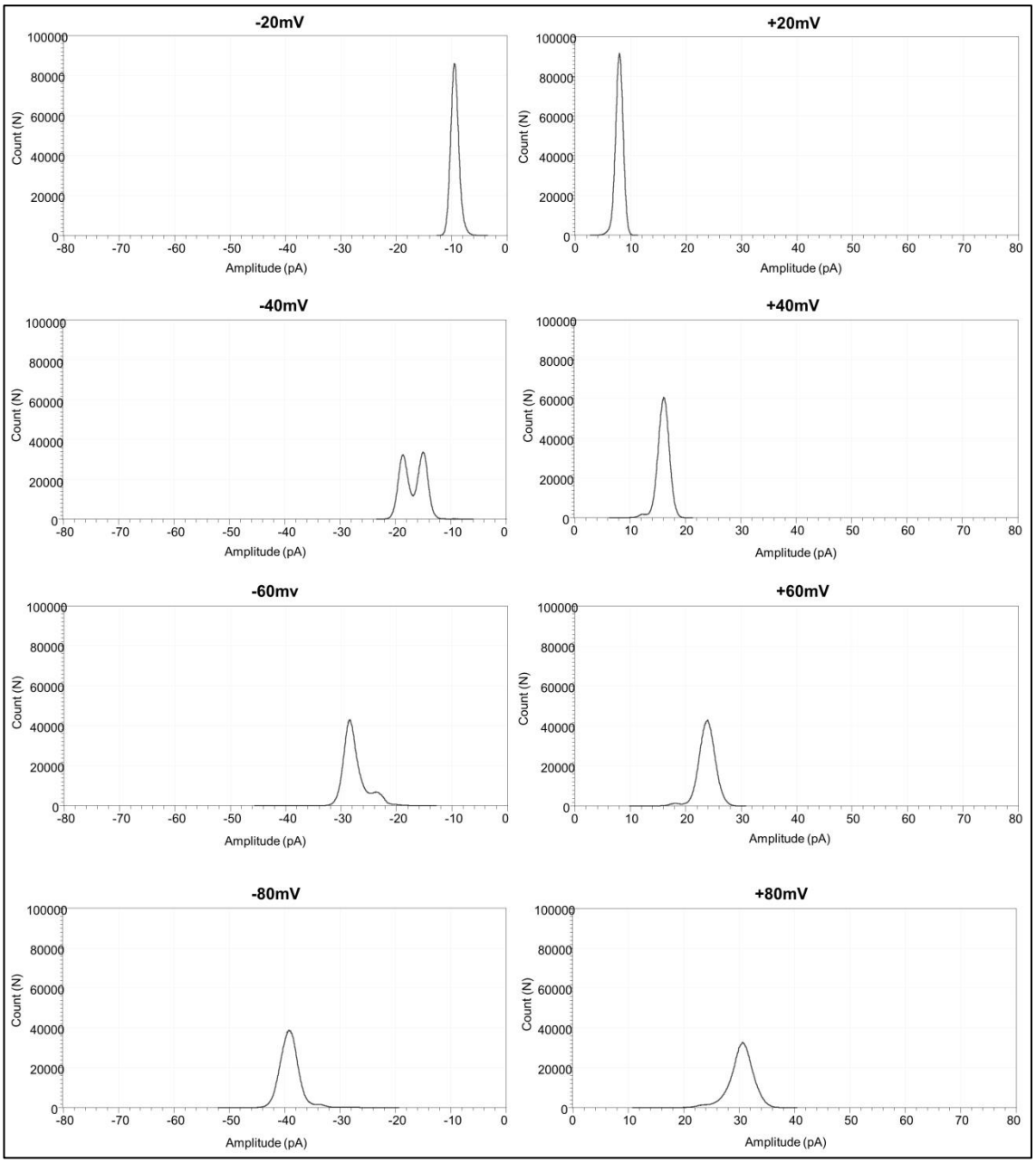

Figure 72 Amplitude histogram of channel openings obtained in the presence of PS-3 in PLBs in experiment III. Data presented in the histogram were collected at +/- 20, 40, 60, and 80 mV in PLBs in the presence of PS-3 (8 µg/ml) and were not Gaussian fitted. Count (N) represents the number of observed events of channel conductance and amplitude represents the value of a current jump in pA. Histogram plots were obtained for 1 minute current recordings generated by Clampfit 10.5, using 0.05 bin width. The bars have been removed for clarity.

All amplitude histograms showed that opening probability at different voltages was close to 100%. This was previously observed for oligomeric structures of Cry1Ab compared with the monomeric toxin (Rausell et al., 2004), but in general does not occur for *Bt* Cry toxins and implies the creation of very stable pores by PS-3.

Amplitude currents were not identical at positive and negative voltages. In experiments II and III, channels seemed to pass more current at negative compared to positive voltages. This shift was opposite in experiment I, where higher current was observed at positive voltages. These data, although not consistent, may point to some kind of voltage dependency, however they represent only 1 minute recordings and no rectification was observed previously (Figure 66, Figure 67 and Figure 68). Also, by comparing current values for the three experiments at a given voltage, it can be speculated that the number of pores was different in each experiment as currents are not the same, with smaller currents in experiment I and III and larger in II.

4.8 Estimation of pore size

The size of pores formed by PS-3 was estimated using various osmoprotectants in an assay that measures the release of a big (138 kDa) proteinous marker. Technically, pore blocking accomplished by some osmoprotectants should also prevent the release of cytotoxic marker to the cell medium leading to decreased luminescence. Reading was taken 3 hours after toxin exposure (Figure 73) as prolonged cell exposure to some osmoprotectants (especially high MW PEGs after 24 hours) led to cell rounding and disintegration reflecting in low viability readings (data not shown). Changes in permeability to osmoprotectants over time were not anticipated because osmoprotectants added before toxin would prevent swelling and further expansion of pores. Nevertheless the experiment was repeated extending toxin exposure time from 3 to 6 hours to test that (Figure 74). Hydrodynamic radii data were taken from references (Scherrer and Gerhardt, 1971, Schultz and Solomon, 1961).

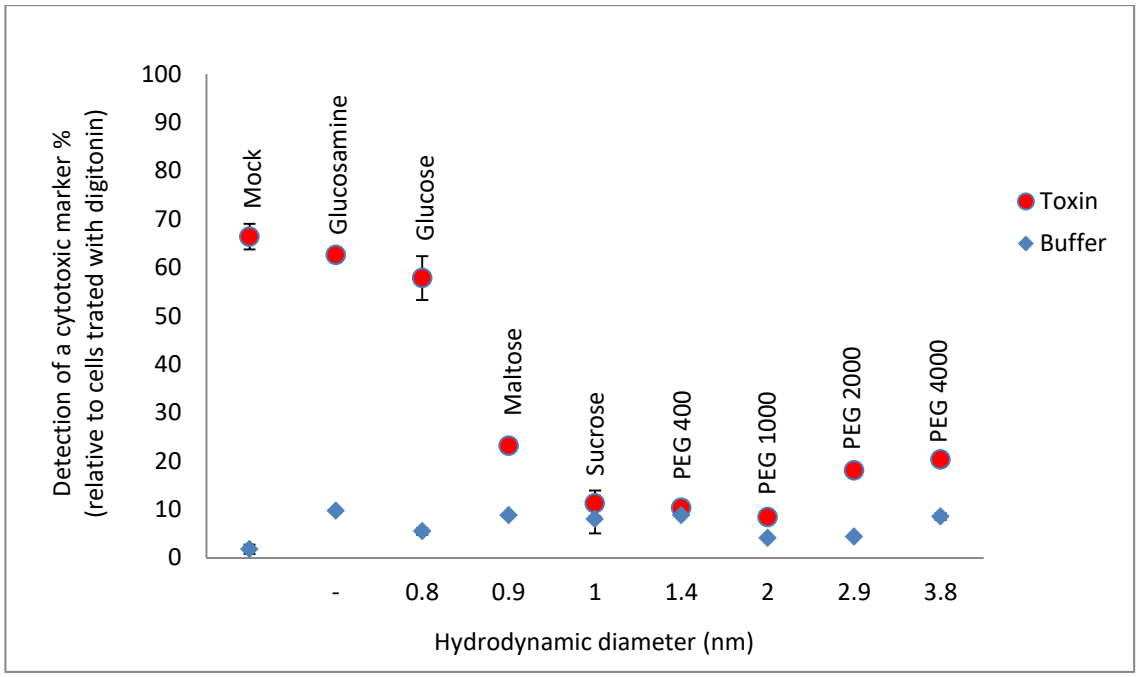

Figure 73 The effect of osmoprotectants on HepG2 membrane permeability 3 hours after exposure to PS-3.
HepG2 cells were seeded at the density of 25 x 10^4 cells/ml in a white 96-well plate. The next day cells were treated with various osmoprotectants (30 mM) or mock (dH_2O) for 10 minutes. This was followed by the addition of either trypsin activated PS-3 (55 µg/ml) or buffer. Luminescent reading was taken 3 hours later using CytoTox-Glo cell assay. All data were plotted as the percentage of digitonin treated cells (12 µg/ml).

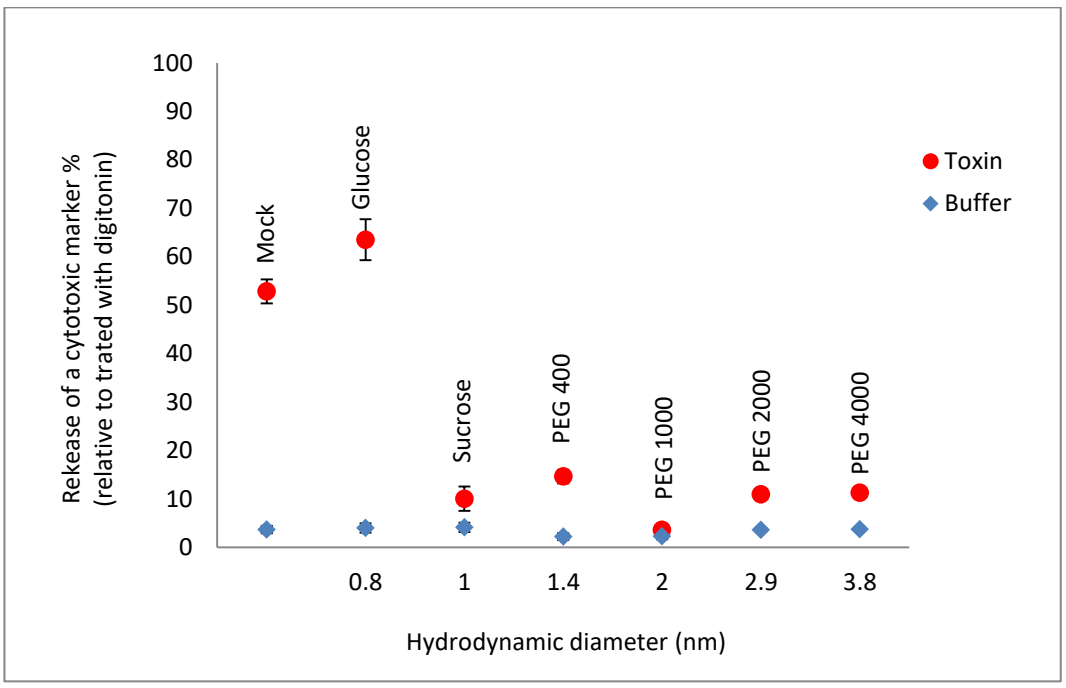

Figure 74 The effect of osmoprotectants on HepG2 membrane permeability 6 hours after exposure to PS-3.
HepG2 cells were seeded at the density of 25 x 10^4 cells/ml in a white 96-well plate. The next day the cells were treated with various osmoprotectants (30 mM) or mock (dH_2O) for 10 minutes. This was followed by the addition of either PS-3 (55 µg/ml) or buffer. Luminescent reading was taken 6 hours later using CytoTox-Glo cell assay. All data were plotted as the percentage of digitonin treated cells (12 µg/ml).

In the toxin's presence, the membrane was permeable to the small sugars but mostly impermeable to disaccharides and bigger molecules. Osmoprotectants showed little toxicity in the absence of PS-3 (assessed as membrane permeability). Swelling was assessed visually at the end of both experiments. It was present only in cells treated with toxin, toxin and glucose as well as toxin and glucosamine, but not in other treatments. Cells treated with digitonin rapidly disintegrated.

Although CellTiter-Blue reagent cannot indicate cell swelling inhibition (being cell permeable), it was used to assess the effect of high MW PEGs on cell metabolic activity and whether pore blocking itself could prevent viability decrease (Figure 75).

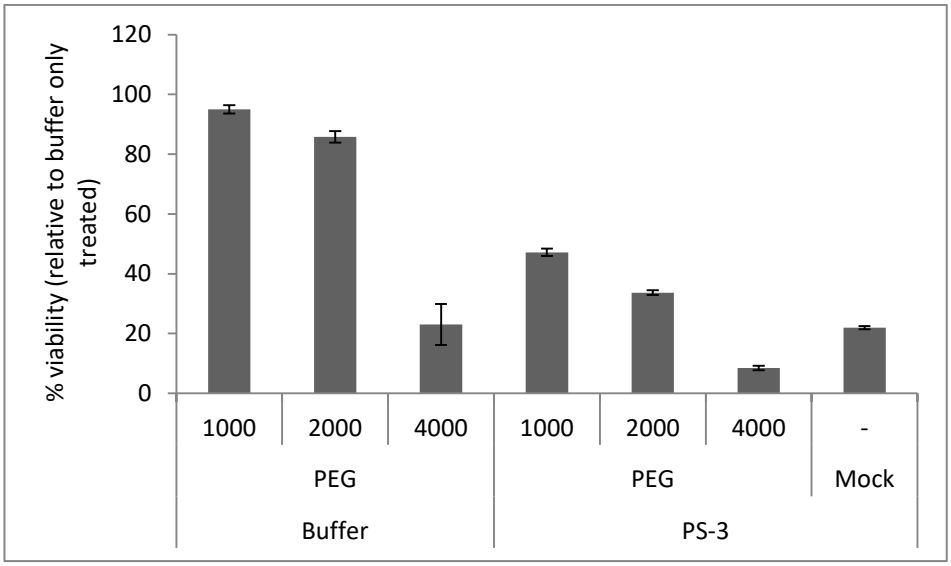

Figure 75 The effect of high MW PEGs on cell viability in the presence or absence of PS-3.
HepG2 cells were seeded at the density of 25 x 10^4 cells/ml. The next day cells were pre-incubated for 1 hour with 30 mM of either PEG 1000, 2000, 4000 or water, before PS-3 (10 µg/ml) or buffer was applied. Cell viability was measured 5 hours after toxin treatment using CellTiter-Blue.

PEG 4000 significantly decreased cell viability after 6 hours. High MW PEGs did not efficiently protect the cells from PS-3 elicited viability decline, although PEGs 1000 and 2000 seemed to slightly reduce the activity of the toxin.

4.9 Microscopic observation of susceptible cells

Cytotoxic effect of PS-3 and morphological changes in HepG2 cells were observed by differential interference contrast (DIC) microscopy. This method allows good visualization of cell morphology for unstained specimens. Pictures taken during initial experiments with non-purified PS-3, presented in Figure 76 and Figure 77, show progressive swelling and cell deterioration over time. Figure 78 shows results of a similar experiment repeated using lower cell density and lower dose of purified toxin in order to better visualise single cell swelling.

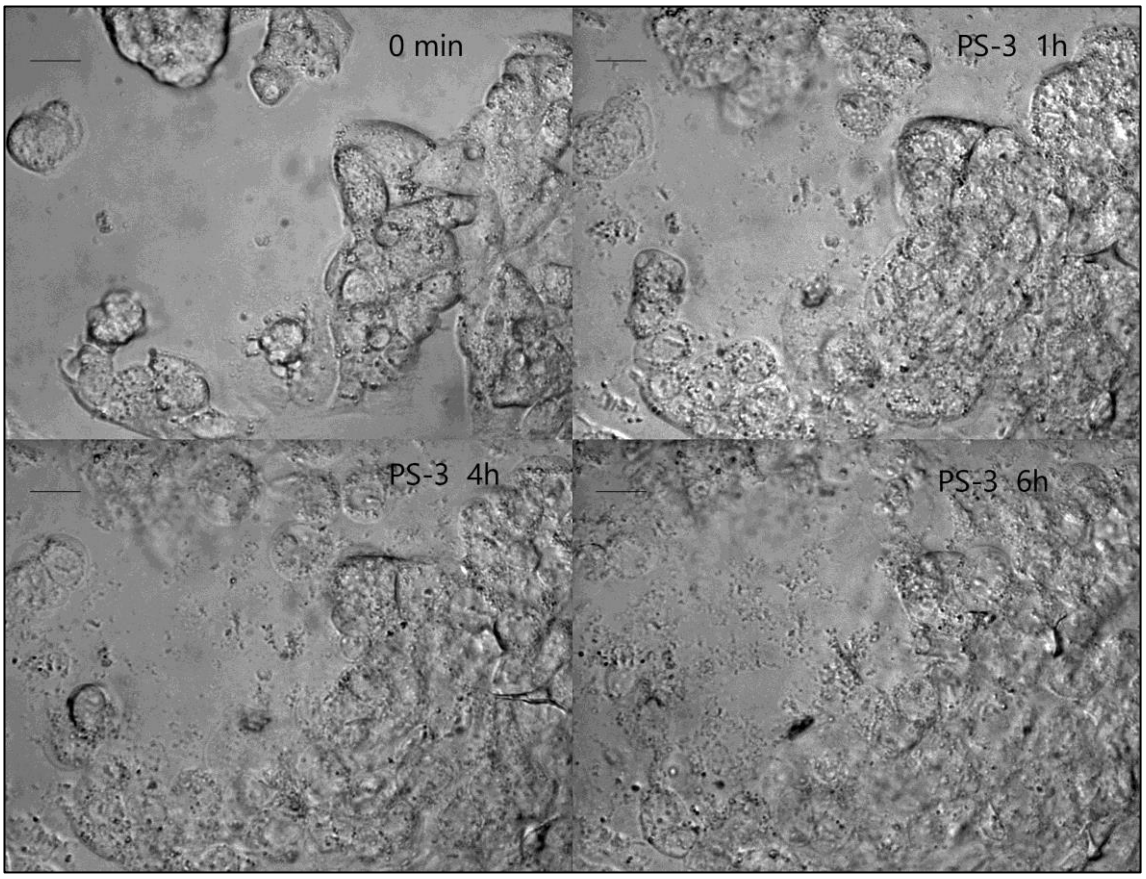

Figure 76 DIC microscopic analysis of HepG2 cell morphological changes after PS-3 exposure.
HepG2 cells were seeded at the density of 25 x 10^4 cells/ml in a microscope chamber slide. The next day cells were treated with non-purified dialysed trypsin activated PS-3 (100 µg/ml). Pictures were taken at 1, 4 and 6 hour time points after treatment using Zeiss Axiovert 200M, 63x DIC objective; scale bar 20 µm.

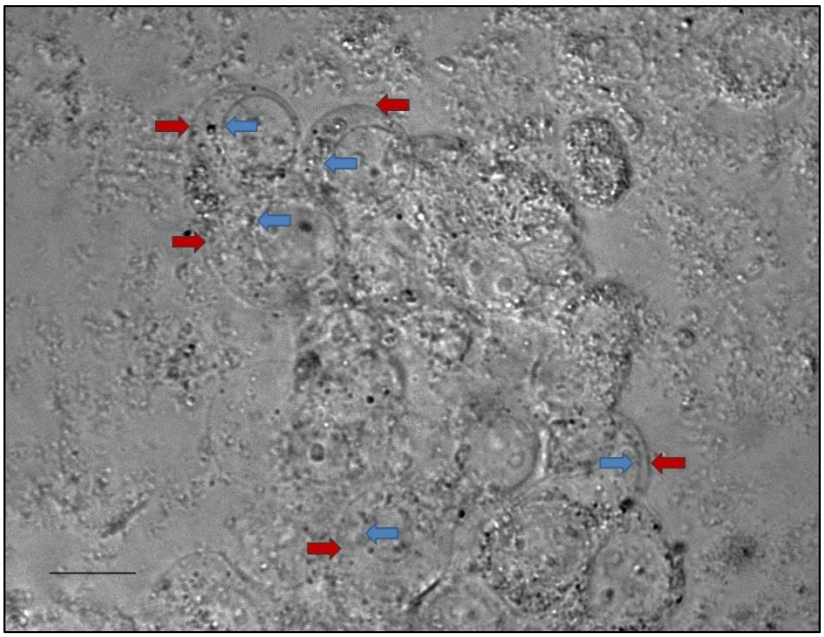

Figure 77 DIC microscopic analysis of HepG2 cellular and nuclear swelling after PS-3 exposure.
HepG2 cells were seeded at the density of 25 x 10^4 cells/ml in a microscope chamber slide. The next day cells were treated with non-purified, dialysed trypsin activated PS-3 (100 µg/ml). After 6 hours swelling of plasma membrane (indicated by red arrows) and nuclei (blue arrows) were apparent. Picture was taken with Zeiss Axiovert 200M, 63x DIC objective; scale bar 20 µm.

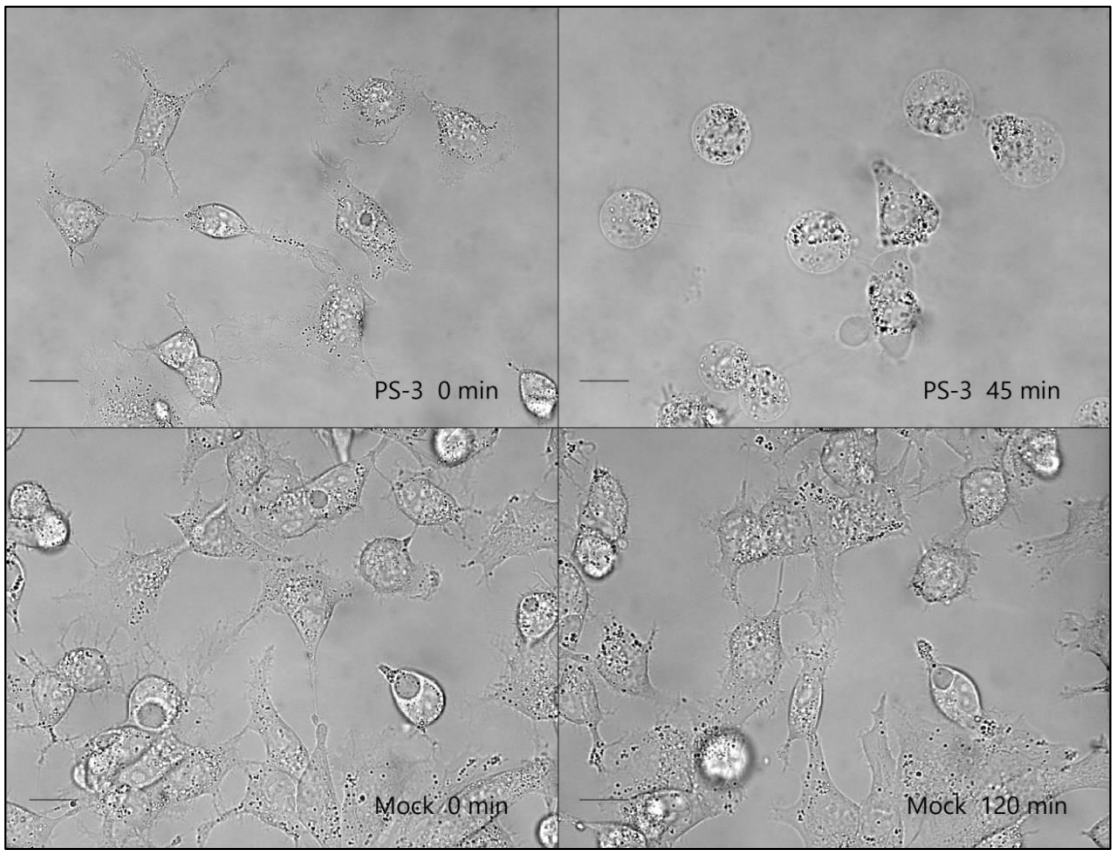

Figure 78 DIC microscopic analysis of HepG2 single cell swelling after PS-3 exposure.
HepG2 cells were seeded at the density of 5 x 10^4 cells/ml in a microscope chamber slide. The next day cells were treated with either buffer or purified trypsin activated PS-3 (5.5 µg/ml). Pictures were taken at different time points using Zeiss Axiovert 200M, 63x DIC objective; scale bar 20 µm.

Cell swelling as well as nuclear swelling was clearly observed in toxin treated cells within the first few hours. The rate of swelling was dose dependent, but generally compromised cells showed first signs of swelling after 20 minutes and the great majority of them become swollen within the first hour. By the end of 6 hours after exposure to toxin, cell disintegration and accumulation of debris was visible. Buffer treated cells showed no cytopathy. Also, cells treated with Cry1Ca (26 µg/ml) exhibited no morphological change (data not shown).

Interestingly, low temperature precluded PS-3 toxicity. 96-well plate containing HepG2 cells was pre-chilled for 30 minutes at 4°C. After that toxin was added (12 µg/ml) and plate was placed back at 4°C for another 4 hours. Cells were monitored during this time and no swelling was observed. When after 4 hours the plate was transferred into the 37°C incubator, majority of cells became swollen within an hour (data not shown). Longer than 4 hour cell incubation at 4°C damaged the cells and was not practiced. Temperature dependent rate of swelling was most likely caused by changes in the membrane fluidity affecting toxin interaction with the membrane, which was pointed out before in the context of PLB experiments (Stumpff et al., 2007).

4.10 Analysis of PS-3 cytotoxicity against other cell lines

The cytotoxic activity of purified trypsin activated PS-3 was tested against several human cultured cells. Cell lines and their origins are listed in Table 8. The cell density and incubation time with CellTiter-Blue reagent were optimized for each cell line (data not shown).

Table 8 Cell lines used in viability assays to assess PS-3 toxicity
Cell lines and their origins used in viability assays for the assessment of PS-3 cytotoxicity.

Cell line:	Origin:
HepG2	Hepatocyte cancer
HeLa	Uterus cervix cancer
Mutu1	Burkitt's lymphoma (EBV positive)
BL31	Burkitt's lymphoma (EBV negative)
IB4	Lymphoblastoid (B cells transfected with EBV)
GM12878	Lymphoblastoid (B cells transfected with EBV)
HL-60	Acute myeloid leukaemia

B lymphocytes

PS-3 was tested against several cell lines that have not been examined before, like cancerous Burkitt's lymphoma and non-cancerous lymphoblastoid cells (Figure 79). Since these cells easily undergo apoptosis when induced by therapeutic drugs (Loni et al., 2001), it was of interest to assess if PS-3 would trigger cell death. Susceptible (HepG2) and resistant (HeLa) cell lines were tested for comparison.

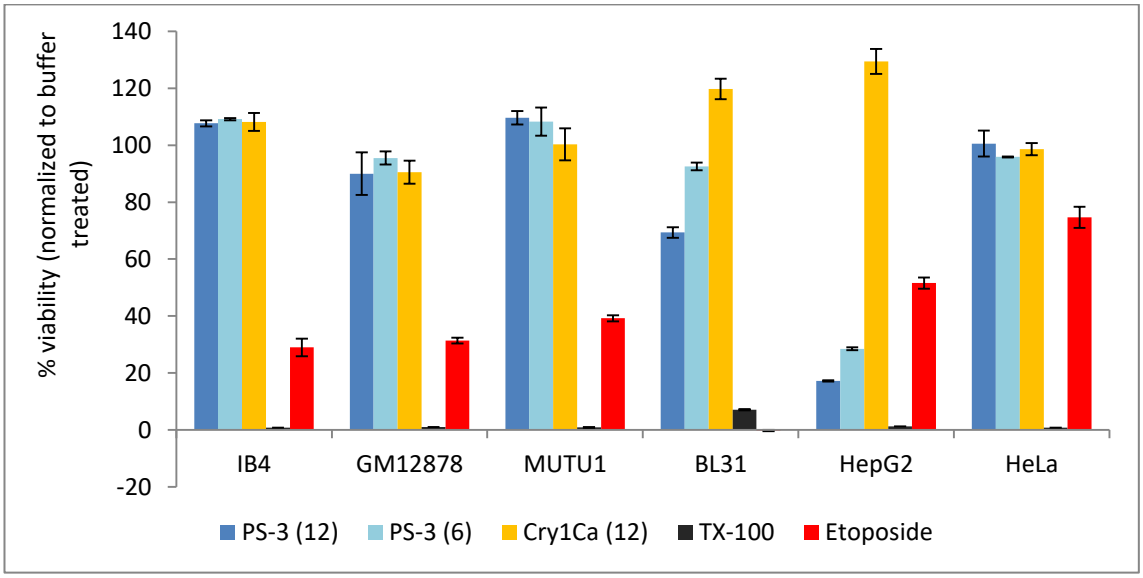

Figure 79 Viability analysis of various cultured cells after exposure to PS-3.
Cells were plated at 25 x 10^4 cells/ml, HepG2 and HeLa - 24 hours before the experiment, the other cell lines - on the day of the experiment. Cells were treated with trypsin activated, purified PS-3 (6 or 12 µg/ml), buffer, Cry1Ca (12 µg/ml), Triton X-100 (0.01%) or etoposide (100 µg/ml). Cell viability was assessed using CellTiter-Blue after 24 hour incubation with toxins.

The results confirmed narrow toxicity spectrum of PS-3. Only HepG2 cells showed high susceptibility towards the toxin. BL31 cells showed some decrease in viability; however the effect was relatively smaller compared to HepG2 cells considering the high toxin dose used. Moreover, no swelling was observed in PS-3 treated BL31 cells. None of the cell lines showed susceptibility towards Cry1Ca.

HL-60

Assessment of HL-60 susceptibility was studied in detail since this cell line has been previously shown to be the most sensitive to PS-3 with EC_{50} of 1.25 µg/ml (Yamashita et al., 2005). Toxicity of trypsin activated PS-3 was determined on HL-60 cells obtained from two independent sources as shown in Figure 80 and Figure 81.

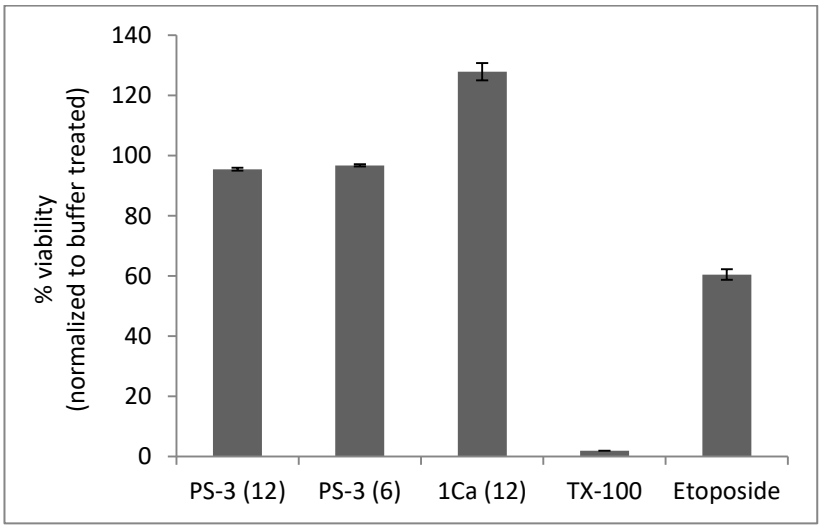

Figure 80 The effect of PS-3 on HL-60 of unconfirmed status.
HL-60 cells were plated at the density of 25 x 10^4/ml and treated with purified trypsin activated PS-3 (6 or 12 µg/ml), Cry1Ca (12 µg/ml), TX-100 (0.01%) or etoposide (100 µg/ml). Cell viability was assessed using CellTiter-Blue after 24 hour incubation with toxins.

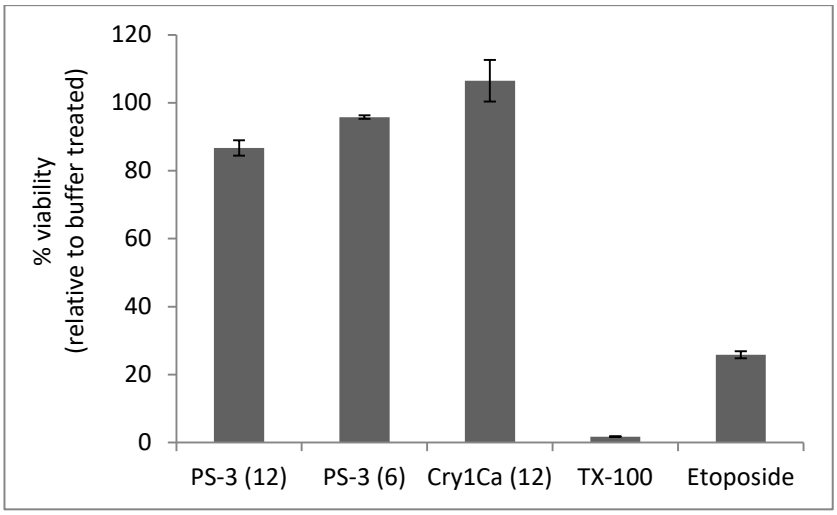

Figure 81 The effect of PS-3 on HL-60 purchased from ECACC.
HL-60 cells were plated at the density of 25 x 10^4/ml and treated with purified trypsin activated PS-3 (6 or 12 µg/ml), Cry1Ca (12 µg/ml), TX-100 (0.01%) or etoposide (100 µg/ml). Cell viability was assessed using CellTiter-Blue after 24 hour incubation with toxins.

Surprisingly, the viability of HL-60 cells was not greatly reduced after 24 hours. These results correlated with microscopic observation, where only a small percentage of the cells were swollen.

To further assess the toxin's impact on HL-60, membrane permeability was measured in HL-60 cells exposed to PS-3 (Figure 82). HepG2 data were included for comparison. To obtain more informative data per well about cell well-being, cytotoxic assay was multiplexed with CellTiter-Blue for additional assessment of cell viability after 30 hour exposure to toxins (Figure 83).

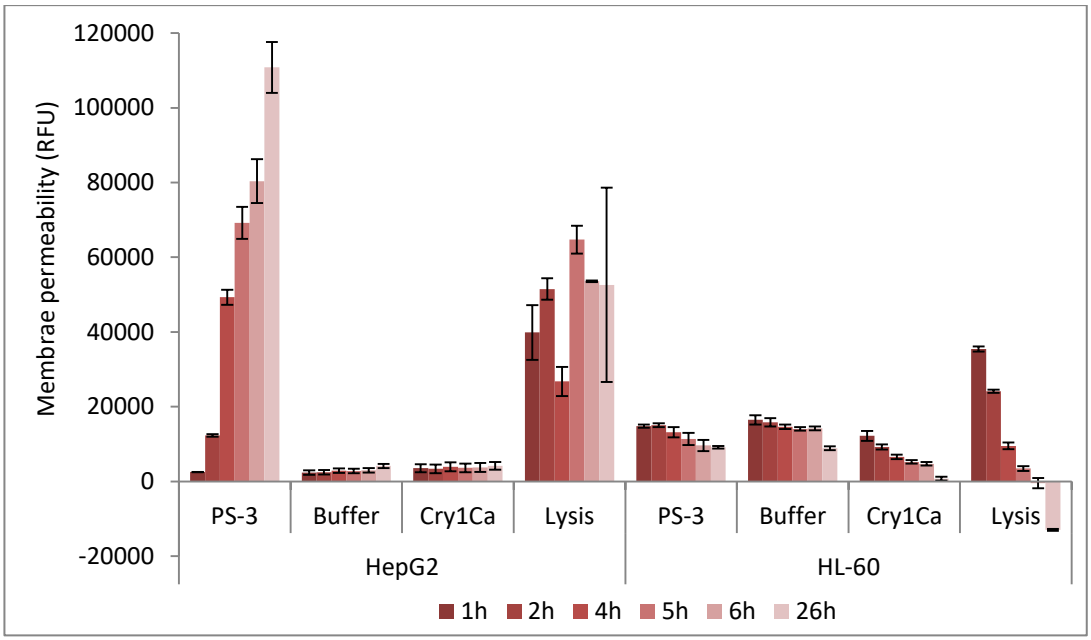

Figure 82 Analysis of membrane permeability in HL-60 and HepG2 cells exposed to PS-3 over 26 hour period. Cells were seeded at the density of 25 x 10^4 cells/ml in the presence of CellTox-Green dye in a black 96-well plate. HL-60 cells were seeded on the day of the experiment and HepG2 one day before. Cells were treated with buffer, lysis solution (provided by the manufacturer), or purified toxins: trypsin activated PS-3 (12 µg/ml) or Cry1Ca (12 µg/ml). Fluorescence was measured at different time points after toxin addition using CellTox-Green assay.

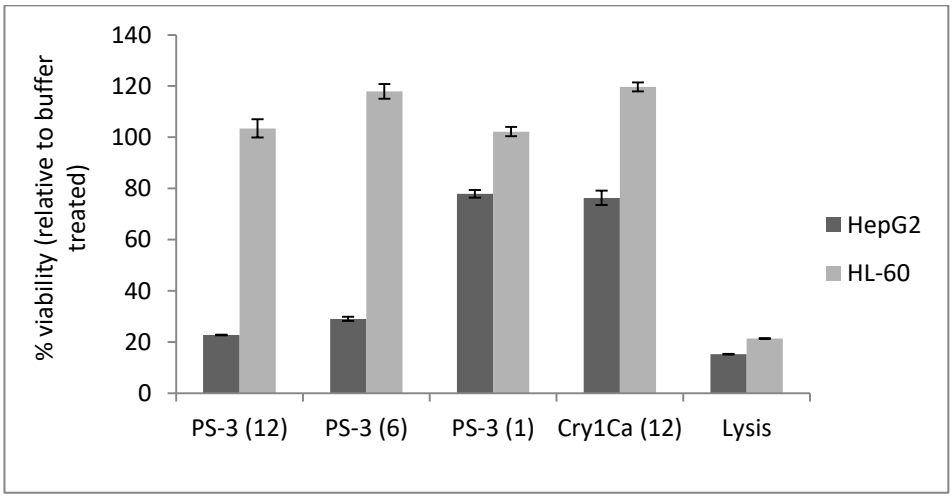

Figure 83 Viability of HL-60 and HepG2 cells used in the CellTox-Green experiment after 30 hour exposure to PS-3. Cells were seeded at the density of 25 x 10^4 cells/ml in the presence of CellTox-Green dye in a black 96-well plate; HL-60 on the day of the experiment and HepG2 one day before. Cells were treated with buffer, lysis solution, or purified toxins: trypsin activated PS-3 (1, 6 or 12 µg/ml) or Cry1Ca (12 µg/ml). After membrane damage was measured using CellTox-Green assay, CellTiter-Blue reagent was used to assess cell viability 30 hours after toxin treatment.

Trypsin activated PS-3 did not affect HL-60 cell viability within 30 hours, nor did it compromise membrane integrity. Only a small number of HL-60 cells showed swelling.

Additionally, Trypan Blue exclusion assay was performed to assess cell viability. HL-60 and HepG2 cells were treated with either PS-3 (12 μg/ml) or buffer only for 3 or 24 hours, followed by the addition of Trypan Blue and cell count. In wells containing compromised HepG2, the number of viable cells was drastically reduced after 3 hours. In PS-3 treated HL-60 cells the cell count was high after 3 and 24 hours and comparable to the 24 hour control wells. Even though some HL-60 cells were swollen after 3 and 24 hour treatment, they excluded the blue dye (data not shown).

HeLa

As presented in Figure 79 HeLa cells showed resistance to 12 μg/ml toxin treatment, and for this reason was used as a negative cell line control in western blot experiments in chapter 7. The mechanism of resistance was questioned in an experiment, where HeLa cells were treated with high doses of PS-3 (Figure 84).

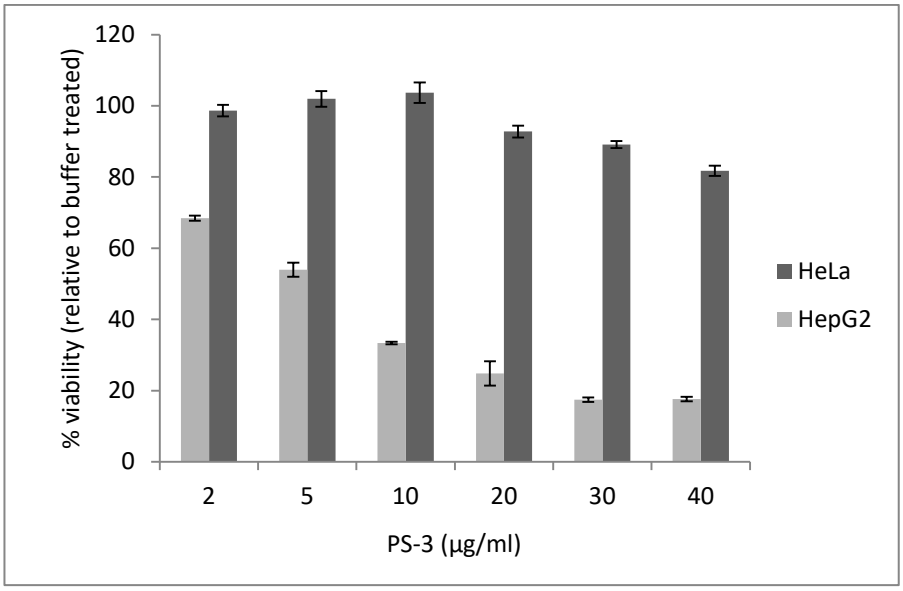

Figure 84 The effect of high concentration of PS-3 on HeLa and HepG2 cells after 6 hour treatment.
HeLa were seeded at 15 x 10^4 cells/ml and HepG2 at 25 x 10^4 cells/ml density. The next day cells were dosed with different concentrations of purified trypsin activated PS-3. Viability was measured 6 hours later using CellTiter-Blue.

0.4 mg/ml dose of PS-3 caused a 20% loss of viability in HeLa cells. Moreover some swelling was observed in toxin treated HeLa cells that was directly proportional to the PS-3 dose. These results indicate that the HeLa resistance can be overcome by increasing toxin concentration.

4.11 Discussion

Protoxin triggered low levels of cytotoxicity. It was revealed to undergo a proteolytic processing by the endogenous proteases present in the crude sample, as including protease inhibitors at solubilisation step supressed both protoxin associated viability decline and membrane damage in HepG2 cells. The role for native proteases in protoxin processing was postulated before for PS-2 (Kim et al., 2000). Experiments with PS-2 showed that this toxin was not activated by cellular proteases or by itself during the incubation with susceptible HepG2 cells (Kitada et al., 2006). Similarly Cry1Aa in the presence of BBMV from *M. sexta*; once activated, it did not need further proteolysis for activity (Kirouac et al., 2006). However there is a strong evidence of Cry1Ab cleavage after interaction with membrane receptor BT-R1 (Bravo et al., 2004, Gómez et al., 2002). PS-3 protoxin was not activated by HepG2 proteases, but further processing of active form of the toxin was not assessed. The presence of DTT greatly increased solubilisation yield and was prerequisite for effective activation with trypsin. Protease inhibitors considerately slowed down the rate of PS-3 degradation and were used at the end of toxin activation.

In general HepG2 cells were more sensitive towards toxin activated with proteinase K than with trypsin. The results of viability assays with ÄKTA purified trypsin and proteinase K activated toxins should not be directly compared with each other since different cell density and high toxin dose were used. The difference in toxicity between trypsin and proteinase K treated samples is most likely a consequence of different proteolytic cleavage by these two enzymes. Smaller size fragments after proteinase K digestion correspond with broad proteolytic activity of this enzyme compared to narrow substrate specificity of trypsin, which acts only on lysine and arginine residues. It is in accordance with the fact that the C-terminally truncated 30 kDa PS-2 killed CACO-2 and Sawano cells more efficient than the non-truncated 31 kDa protein. Also, in HepG2 cells, killing occurred significantly quicker with more processed PS-2 (Kitada et al., 2006). Despite proteinase K activating PS-3 more efficiently, trypsinization was chosen as a preferred method of activation, because trypsin did not degrade toxin at higher concentrations compared with proteinase K. Similarly, PS-1 digested with a high dose of proteinase K lost cytotoxicity to HeLa, but not when activated with a high dose of trypsin (Katayama et al., 2005a). Also, trypsin is one of the major proteases contributing to protein digestion in lepidopteran midguts (Terra and Ferreira, 1994) and has been widely used to process Cry toxins in vitro.

ÄKTA purification allowed for separation of the toxin bands. The fact that both lower and higher MW proteins (and arisen from digestion with either proteinase K or trypsin) showed toxic effect, confirms that all fragments contain the toxic core. For this reason bands were not separated for cell assays and size exclusion chromatography was used as a preferred method to make stocks of purified toxins.

Regardless of the activation method, PS-3 significantly affected cell viability within the first few hours. Protoxin caused moderate decrease in viability. There was a good correlation between measurement of metabolic activity (CellTiter-Blue assay) and ATP levels (CellTiter-Glo) in susceptible cells. EC_{50} was calculated as 2.17 μg/ml, which is similar to 1.86 μg/ml calculated for PS-3 by Yamashita et al. (Yamashita et al., 2005). Membrane permeability cytotoxic cell assays showed concentration and time dependent cytotoxicity of PS-3. After exposure to toxin, membrane became rapidly permeable to both small and big size markers. Toxin induced decrease in metabolic activity and ATP levels, swelling, and membrane damage followed similar time courses in susceptible cells, extensively affecting cells after 2 hours.

Results from electrophysiology experiments were discussed in detail in section 4.7. To conclude, a significant increase in the whole cell conductance was observed in HepG2 cells exposed to PS-3 (266.9 nS), but not in toxin treated HeLa (18.3 nS) or HepG2 exposed to Cry1Ca (9.2 nS) cells. Experiments in planar lipid bilayer system ultimately confirmed pore forming nature of PS-3. Toxin induced very stable channels with an opening probability close to 1 and conductance ranging between 75 – 220 pS with no rectification. The pore was slightly cationic selective and seemed to be voltage dependent. In single channel patch clamp experiments multiple conductance levels were observed, indicating the presence of different channel populations or different sub-states of a single channel population. Membrane activity was recorded after toxin exposure to either side of the membrane as well as in the cell attached mode. These channels were not seen in the absence of toxin and because of high conductance values obtained (100 - 5000 pS) and low conductance levels reported for hepatocytes and hepatoma cells, channel activity can be most likely attributed to Cry toxin induced

channel formation de novo. Large conductance values observed in all of the single channel patch clamp experiments did not reflect differences observed in the whole cell experiments between different treatments. The most plausible explanation for that is that membrane patches (even in the cell attached mode) do not represent a good model that would reflect cells natural susceptibility/resistance due to a high toxin dose used, but instead behave similar to PLBs, where any PFT at high enough dose would create a pore and increase conductance.

Experiments with osmoprotectants showed that the compromised membrane was permeable to the simple sugars like glucose or glucosamine but mostly impermeable to the disaccharides like sucrose or maltose, suggesting the creation of small primary lesions with estimated pore diameter <1 nm. This is smaller than previously estimated for some Cry toxins. Maximal radius of Cry1C was between 1 - 1.3 nm (Peyronnet et al., 2002) and that of Cry1Ac 1.2 – 1.3 nm (Carroll and Ellar, 1997). However the former experiments were performed in planar lipid bilayers in the absence of receptors and the latter with BBMV devoid of cellular content and at relatively high pH. Other experiments based on Trypan Blue exclusion method in *Ch. fumiferana* cells resulted in the detection of smaller pores. Channel radii induced by var. *kurstaki* P1 were less than 0.6 nm and vars. *aizawai* and *israelensis* between 0.6 - 1.0 nm (Knowles and Ellar, 1987). The size of PS-3 induced pores was also close to other pore forming toxin CyaA, a hemolysin from *B. pertussis*, which forms pores of 0.6 - 0.8 nm in diameter (Benz et al., 1994). These results are consistent with PS-3 forming discrete pores rather than causing a non-specific detergent-like membrane disruption.

Although PEGs in the toxin's presence inhibited detection of membrane damage, they did not fully prevent cells from decreased viability reassuring that - contrary to EGTA action (explained in chapter 5) - PEGs did not prevent toxin interaction with the membrane but only inhibited swelling arising as a result of membrane damage. It also implies that inhibition of swelling itself is not capable of fully rescuing HepG2 cell viability after PS-3 treatment.

Question however remains how a small pore diameter estimated using osmoprotectants (<1 nm) can allow for the passage of 138 kDa protease detected clearly in CytoTox-Glo assay, if the pore can be blocked by much smaller disaccharides. The possibility exists that the CytoTox-Glo substrate diffuses into the cell through toxin induced pores before the protease leaks out due to much smaller size. However, the manufacturers assure that substrate processing is inefficient inside the cells and predict that potential contribution of luminescence from intracellular processing of the substrate is small. More likely, primary lesions created by the toxin and cellular swelling induced membrane stretching. This in turn may have disrupted toxin arrangement in the membrane leading to radial expansion of pores – a process that would explain the changes in permeability presented in Figure 47, but would not have occurred when cells are protected from swelling by osmoprotectants.

Untreated HepG2 cells are polygonal in shape, generally arranged in monolayers. After toxin administration, the cells swelled and eventually detached from the bottom. This is consistent with the insect cells losing the ability to regulate the osmotic pressure and lysis due to osmotic shock after exposure to Cry toxins. After breaking open, often yellow granules were released from HepG2 cells treated with

proteinase K activated PS-3 (data not shown). These may possibly be lipid droplets. The literature shows that 15% of HepG2 cells have these dispersed in the cytoplasm (Bouma et al., 1989). Also, lipid droplet formation was documented as one of the cellular responses to PFTs (Gonzalez et al., 2011b).

PS-3 was tested against some additional cell lines that have not been examined before, like Burkitt's lymphoma and lymphoblastoid cells. None of them showed significant susceptibility towards the toxin, confirming narrow toxicity spectrum of PS-3. Surprisingly, HL-60 cells were mostly unaffected by trypsin activated PS-3. However, the same cells were significantly affected by proteinase K activated PS-3 (Souissi et al. unpublished), highlighting the role of toxin activation in specificity. Similarly, truncated at the C-terminus PS-2 killed Sawano and CACO-2 cells much more efficiently than the non-truncated form of the toxin (Kitada et al., 2006).

Interestingly, high dose of PS-3 (40 μg/ml final) caused a 20% reduction in HeLa cell viability, which was accompanied by swelling. These results indicate that the resistance of HeLa cells can be overcome by increasing toxin concentration. In fact, cytocidal activity of a high dose of PS-3 against HeLa cells has been previously documented (Yamashita et al., 2000). The toxin most likely affects HeLa cells by spontaneous insertion, similarly to how other Cry toxins can spontaneously form pores in artificial lipid bilayers devoid of receptors when present at a high enough dose (Schwartz et al., 1993, Slatin et al., 1990b). These results suggest the capacity of PS-3 for pore formation even in the absence of the receptor. This is also supported by the fact that high dose of PS-3 (40 μg/ml) overcame 2 mM protective effect of EGTA, inducing cell swelling and lowering viability by 40 % (Figure 88, chapter 5).

5. Role of divalent cations in binding and toxicity

5.1 Introduction

Ions play many distinct roles both in cellular metabolism and extracellular processes. A large number of proteins coordinate cofactors - often metal ions - which facilitate specific functions (e.g. enzymatic activity) or help stabilize structures. Moreover, ion homeostasis and regulation of ionic gradients are critical for the proper functioning of cells. In the case of PFTs, cations not only participate in ionic imbalance created after membrane damage (Knowles and Ellar, 1987), but may also control toxin binding and pore formation (Kirouac et al., 2006).

The two most commonly used non-specific chelators of metal ions are EGTA and EDTA. They have been widely used to test the roles of extracellular cations in the activities of various proteins including Cry toxins. Using this approach Zhang et al. showed that in the presence of the EDTA (but not EGTA) the toxicity of Cry1Ab on S5 cells was prevented (Zhang et al., 2005). EDTA also inhibited pore formation by Cry1Aa, Cry1Ac and Cry1Ea in isolated insect BBMV (Kirouac et al., 2006). Ca^{2+} was shown to be indispensable for the activity of PS-1. Cytotoxicity of PS-1 was substantially inhibited when HeLa cells were cultured in low-Ca^{2+} medium. This effect was reversed with the addition of Ca^{2+} but not Mg^{2+}. Extra– and intracellular increases in Ca^{2+} augmented Cry1C toxicity in Sf9 fall armyworm *S. frugiperda* cells in a dose-dependent manner, possibly via a Ca^{2+} dependent intracellular pathway (Monette et al., 1997). Toxicity of *Bt* var. *entomocidus* against the cotton leafworm *S. littoralis* was enhanced by calcium

and zinc salts (Salama et al., 1985). However, experiments with Cry1 toxins showed some contradictory results; for example, in osmotic swelling assays using *M. sexta* BBMV, Ca^{2+} reduced the rate of pore formation by Cry1Ac, but enhanced pore formation by Cry1Ca (Fortier et al., 2005). Moreover there are reports of synergistic effects of EDTA and Dipel in resistant *P. xylostella* larvae (Liu and Tabashnik, 1997)

To test the involvement of divalent ions in PS-3 toxicity, various cell treatment methods were developed that involved the use of different chelators and metal salts. Experiments with chelators were carried out over a time period of 5 hours as 24 hour cell exposure to 2 mM EGTA showed around 20% lowered viability (data not shown). There was no loss of viability within the first 5 hours, however it was noted that in the presence of >2 mM EDTA or EGTA cells showed some rounding over time (more so in case of EDTA than EGTA).

5.2 Exploration of the protective EGTA effect

HepG2 cells were pre-incubated with either EGTA or EDTA, followed by toxin administration and viability examination. Additionally Ca^{2+} and Mg^{2+} salts were added to some wells before the toxin to test if the chelator effect could be reversed (Figure 85). Addition of EGTA, EDTA, $CaCl_2$, $MgCl_2$ separately or a combination of a chelator and metal salt did not decrease cell viability within 5 hours (data not shown).

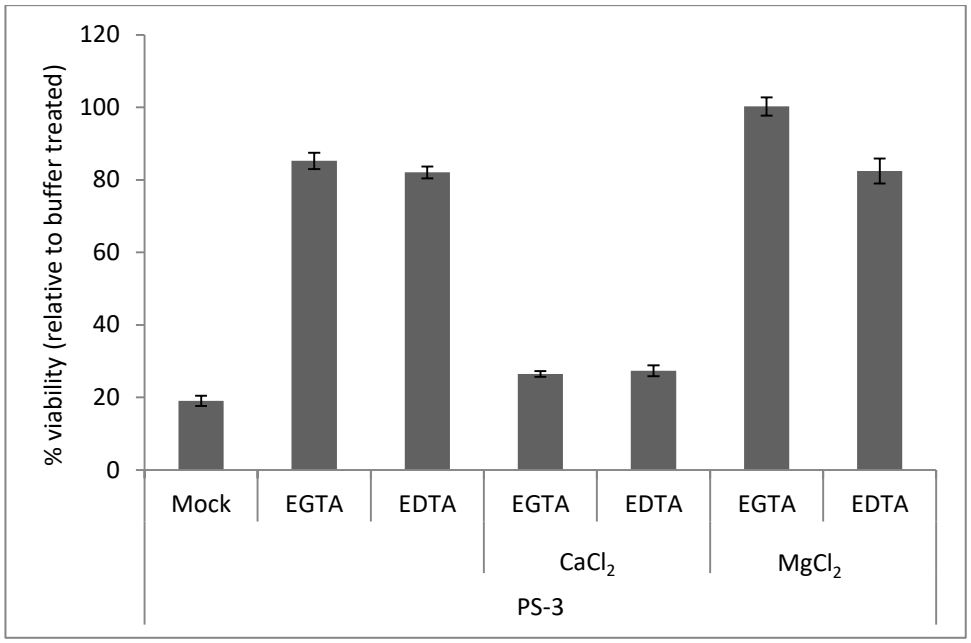

Figure 85 The effect of chelating agents on viability of PS-3 treated HepG2 cells.
HepG2 cells were seeded at the density of 25 x 10^4 cells/ml. The next day cells were pre-incubated with 5mM of either EGTA or EDTA or water (mock) for 30 min followed by the addition of toxin (12 µg/ml). $CaCl_2$ or $MgCl_2$ was added (5 mM) to some wells 10 minutes before the toxin. The readings were taken 5 hours after toxin addition using CellTiter-Blue assay.

Both EDTA and EGTA significantly reduced cytotoxicity of PS-3. Also, no cell swelling was observed. In comparison pre-incubation with EDTA or EGTA did not prevent cellular damage by 0.01% Triton X-100 (data not shown). Interestingly Ca^{2+}, but not Mg^{2+}, restored PS-3 cytotoxicity. Experiments with proteinase K activated toxin yielded comparable results (data not shown). It is consistent with EGTA's high affinity for calcium but negligible affinity for magnesium ions. Concentrations of bound and free Ca^{2+} and Mg^{2+} were calculated in the presence of 2 mM EGTA using the Chelator algorithm (Schoenmakers et al., 1992). Results presented in Table 9 show that EGTA bound 99.94 % of Ca^{2+}, but only 0.003 % of Mg^{2+} and point to a paramount role of calcium ions in the toxin's action.

Table 9 Calculation of Ca^{2+} and Mg^{2+} concentrations from given total metal concentrations in the EGTA presence.
Ca^{2+} and Mg^{2+} concentrations were calculated in the presence of 2 mM EGTA at pH = 7.4, 37° C and 0.165 N ionic contribution. Total ion concentrations were selected to match ion levels present in DMEM formulation. Calculations were performed using Ca/Mg/ATP/EGTA calculator v1, available online: maxchelator.stanford.edu.

Name	Total (M)	Free (M)	Bound (M)	% Bound
Ca^{2+}	0.0018	9.666e-7	0.001799	99.94
Mg^{2+}	0.0008	0.000799	3.160e-8	0.003
EGTA	0.002	0.000184	0.001815	90.78

Next, the minimal concentration of $CaCl_2$ that can counteract the effect of 2 mM EGTA was estimated (Figure 86).

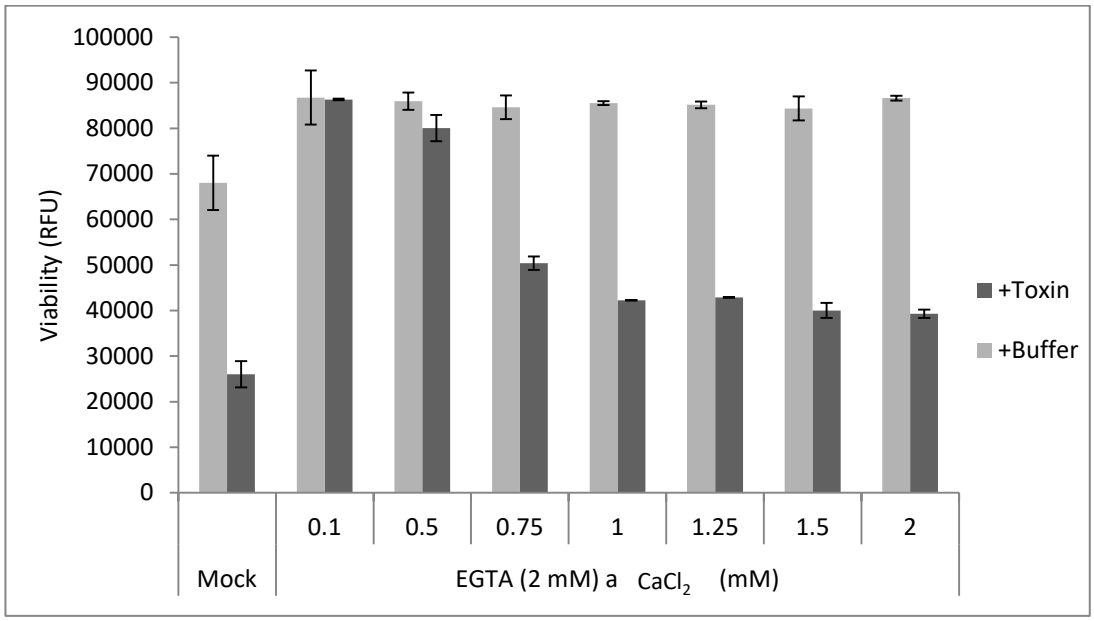

Figure 86 Analysis of reversal of the 2 mM EGTA effect by $CaCl_2$.
HepG2 cells were seeded at the density of 25 x 10^4 cells/ml. The next day cells were dosed with 2 mM EGTA and 20 minutes later supplemented with various concentrations of $CaCl_2$ for another 10 minutes, followed by PS-3 (10 µg/ml) administration. Viability was measured 5 hours after treatment using CellTiter-Blue assay.

Addition of ≥1 mM of $CaCl_2$ counteracted the 2 mM EGTA effect.

It was assessed whether the addition of $CaCl_2$ after toxin treatment would reinstate toxicity as efficiently as when calcium ions were added first (Figure 87).

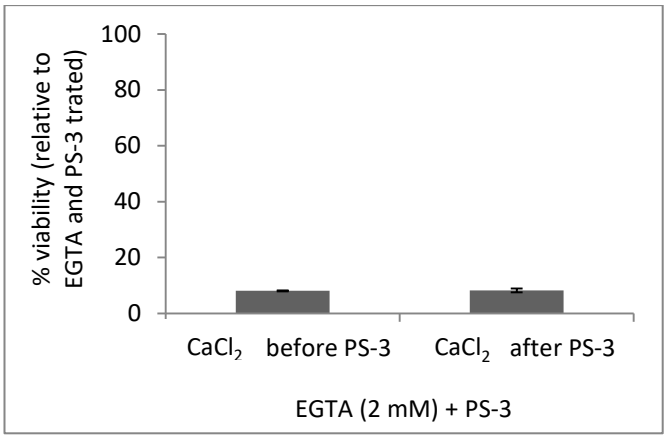

Figure 87 Analysis of PS-3 activity in EGTA treated HepG2 cells with $CaCl_2$ added before or after the toxin.
HepG2 cells were seeded at the density of 25 x 10^4 cells/ml. The next day cells were pre-incubated with 2 mM EGTA 35 minutes before the toxin (12 µg/ml) administration. 2 mM $CaCl_2$ was added 30 minutes before or after the toxin. Viability was measured 5 hours after treatment using CellTiter-Blue assay.

The presence of calcium ions, regardless of whether they were added before or after the toxin, had the capacity to restore PS-3 toxicity in EGTA treated cells.

Knowing that 2 mM EGTA is sufficient to block the activity of PS-3 at 12 µg/ml, it was hypothesised that adding toxin in excess could inflict damage in the presence of EGTA. Cells were treated with 2 mM EGTA and higher PS-3 doses (Figure 88).

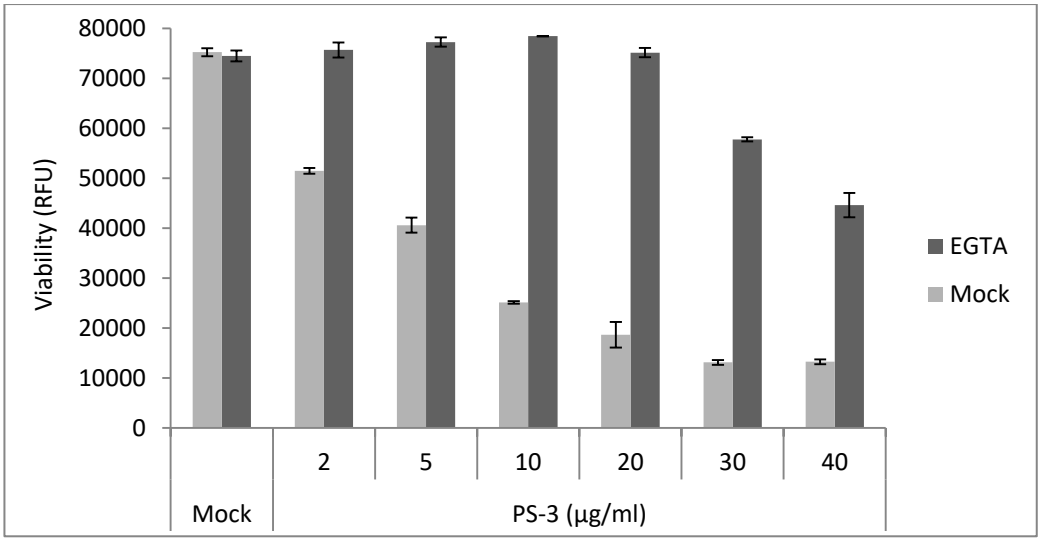

Figure 88 The effect of high doses of PS-3 on HepG2 cell susceptibility in the presence of 2 mM EGTA.
HepG2 cells were seeded at the density of 25 x 10^4 cells/ml. The next day cells were treated with 2 mM EGTA or water (mock). 10 minutes later cells were treated with different concentrations of PS-3 or buffer. Viability was measured 5 hours after toxin treatment using CellTiter-Blue assay.

High concentrations of PS-3 (>30 μg/ml) overcame 2 mM protective effect of EGTA. Cells treated with EGTA and >30 μg/ml toxin showed signs of swelling and decreased viability.

An experiment was performed to find out if there is a competition between PS-3 and EGTA when both of these components are added at the same time and if toxicity could be reversed by late EGTA administration (Figure 89).

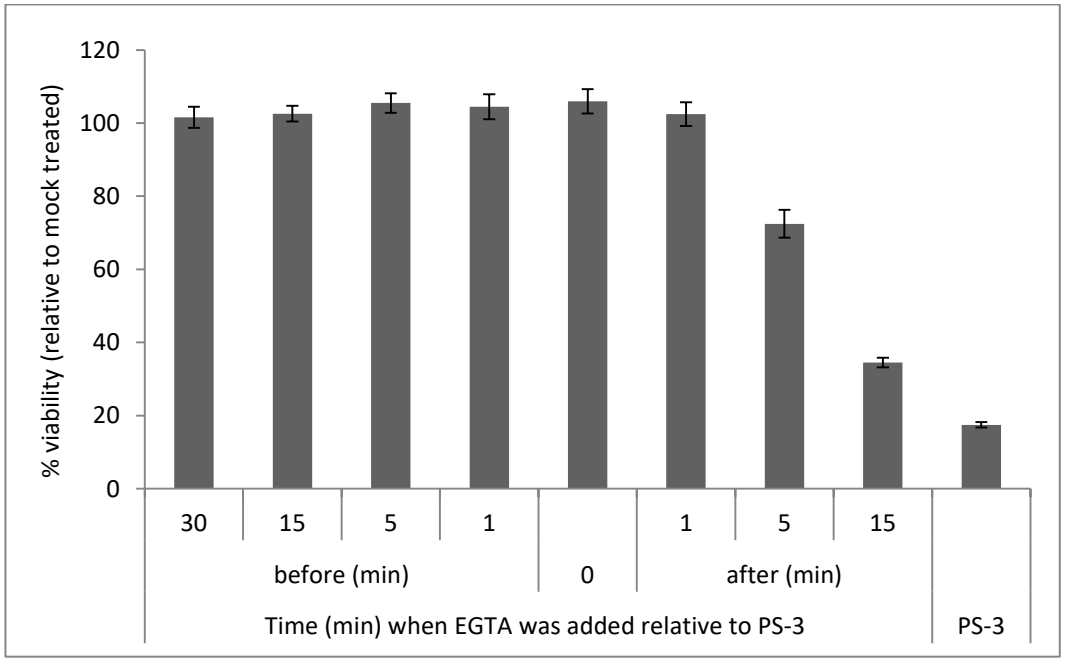

Figure 89 Administration time-dependent effect of EGTA on PS-3 treated cells.
HepG2 cells were seeded at the density of 25 x 10^4 cells/ml. The next day cells were treated with 2 mM EGTA at different time points: before, at the same time as, or after PS-3 (12 μg/ml). Viability was measured 6 hours after toxin addition using CellTiter-Blue. Control cells were treated with water and exposed to PS-3 (12 μg/ml) for 6 hours.

EGTA was less able to protect the cells when added more than a few minutes after the toxin.

5.3 Analysis of toxin - membrane interaction in the presence of EGTA

To elucidate whether EGTA acts prior or post membrane damage, membrane permeability in EGTA and PS-3 treated cells was assessed using CellTox-Green cytotoxicity cell assay (Figure 90) and the whole cell patch clamp technique (Figure 91).

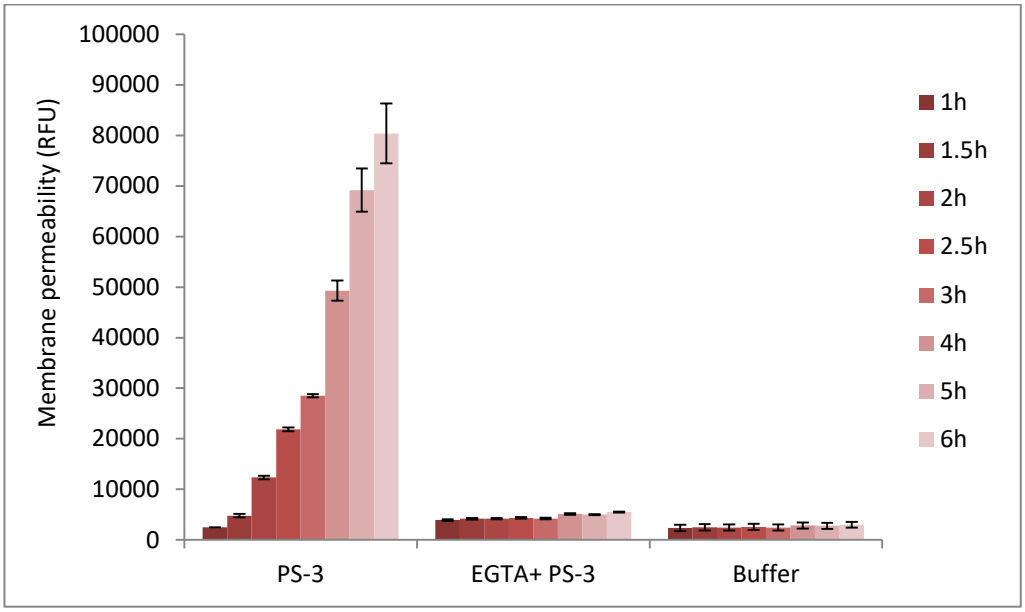

Figure 90 The effect of EGTA on HepG2 membrane permeability after PS-3 treatment.
HepG2 cells were seeded at the density of 25 x 10^4 cells/ml in the presence of CellTox-Green dye in a black 96-well plate. The next day cells were pre-treated with EGTA (5mM) 30 minutes before treatment with PS-3 (12 µg/ml). Membrane permeability was measured using CellTox-Green assay at different time points after toxin addition.

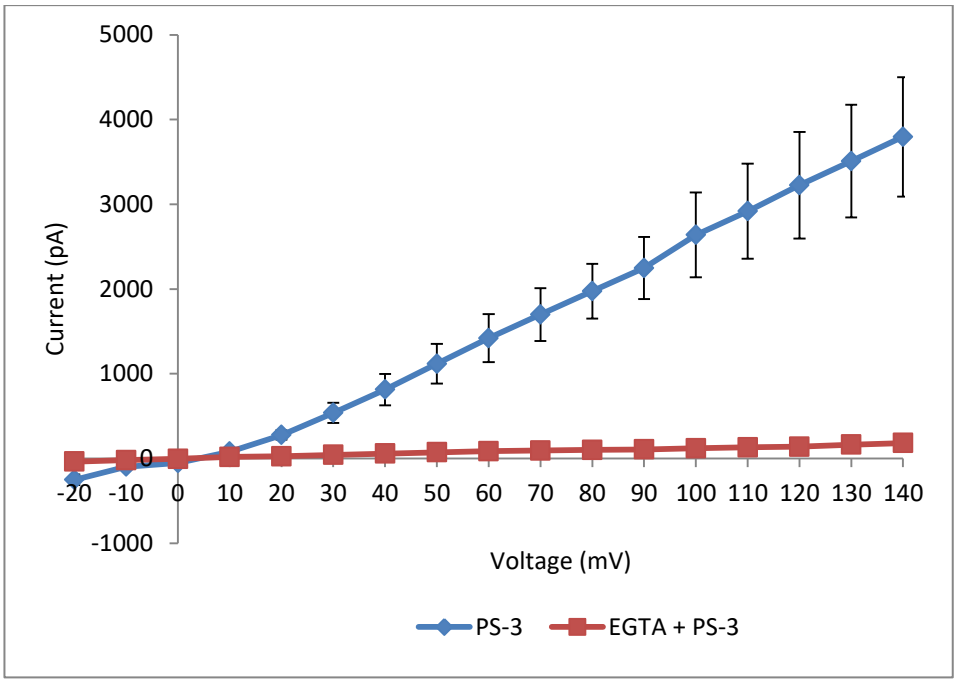

Figure 91 Whole cell patch clamp recordings from HepG2 cells exposed to PS-3 in the presence or absence of 2 mM EGTA.
HepG2 cells were seeded at the density of 5 x 10^4 cells/ml on the glass coverslip inside the 35 mm petri dish. The next day whole cell patch clamp recordings from a single cell were reported 20 minutes after the addition of PS-3 (12 µg/ml) to the bath in NaCl solution in the presence or absence of EGTA (2 mM). Currents were induced by a 1 second set of depolarizing potentials from −20 to 140 mV from a holding potential of −20 mV. Error bars indicate the standard error of the mean. The lines show the mean currents from three representative experiments from three different cells patched.

In EGTA and PS-3 treated cells membrane stayed impermeable to a small cytotoxic marker (<1 kDa) for 6 hours. Also, PS-3 was not able to induce large whole cell currents in the presence of EGTA within 20 minutes. Mean conductance levels were 12.5 and 266.9 nS for HepG2 cells treated with PS-3 in the presence and absence of EGTA respectively, as also shown in Table 4. Additionally, cells showed no signs of swelling in contrast to toxin treated cells in the absence of the chelator.

The effect of EGTA was tested on the ability of PS-3 to create channel openings in planar lipid bilayers. PLB KCl buffer containing 2 mM EGTA was placed in the cis chamber before the toxin was added and traces recorded (Figure 92).

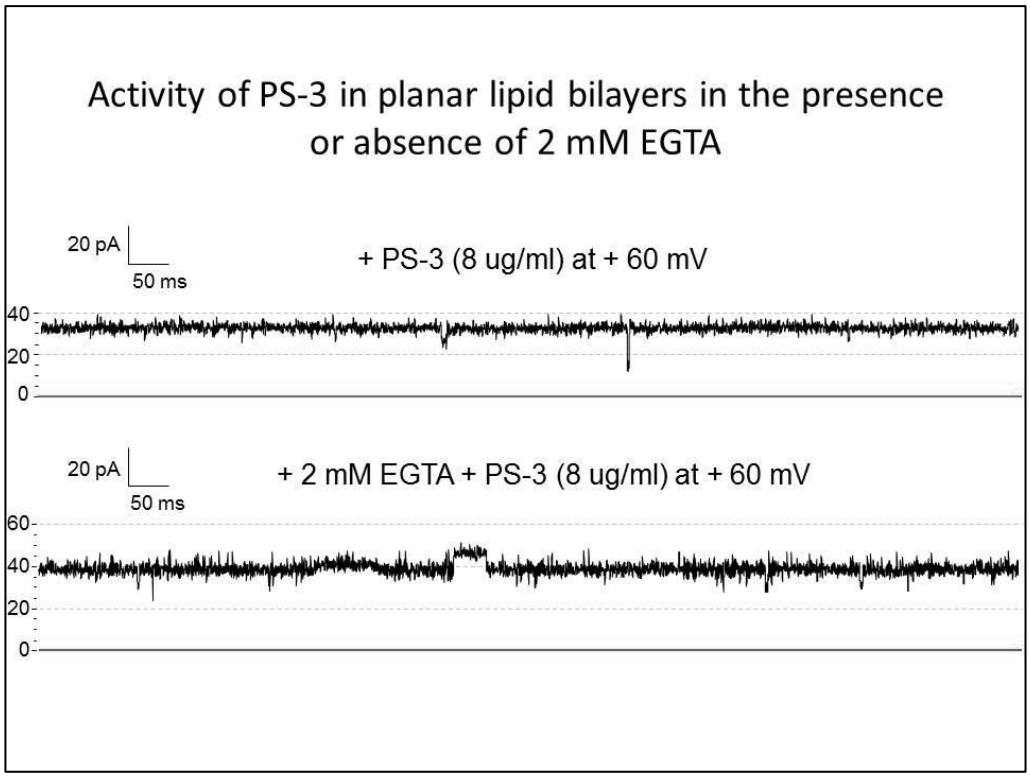

Figure 92 The effect of EGTA on PS-3 induced channel activity in planar lipid bilayers.
Formation of ion channels by PS-3 (8 µg/ml) was tested in planar lipid bilayers in the presence or absence of 2 mM EGTA. Representative current traces are shown at + 60 mV applied voltage in the absence (upper trace) and in the presence (lower trace) of 2 mM EGTA. Traces were filtered at 120 Hz.

EGTA did not prevent PS-3 induced pore formation in planar lipid bilayers.

For more clarification on the exact role of EGTA, i.e. whether it impedes the toxin binding or subsequent steps in the mode of action (e.g. oligomerization or pore formation), cell viability was assessed after transient EGTA and PS-3 treatment. A cell washing step after 20 minutes ensured that all non-bound toxin molecules and EGTA were removed as shown in experiment's outline in Figure 93.

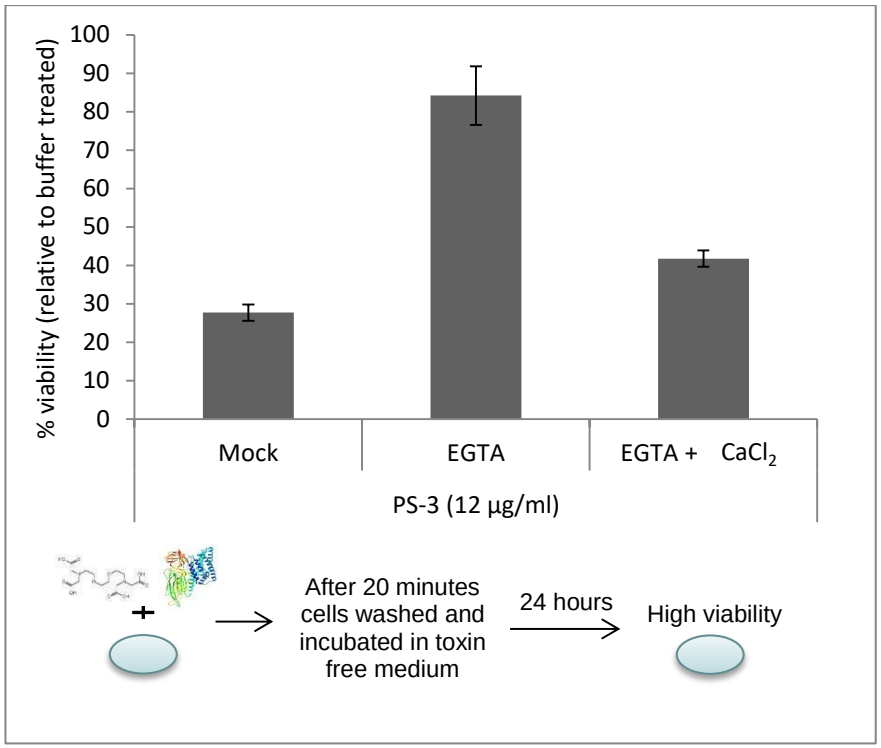

Figure 93 The effect of transient treatment with toxin and EGTA on HepG2 cell viability.
HepG2 cells were seeded at the density of 25 x 10^4 cells/ml. The next day cells were pre-incubated with either 5 mM EGTA or 5 mM EGTA and 5 mM $CaCl_2$ or water (mock). After 30 minutes PS-3 (12 µg/ml) or buffer was added and cells were incubated for further 20 minutes. Then all cells were washed twice with DPBS and re-suspended in complete culture medium. Viability was assessed using CellTiter-Blue 24 hours after toxin addition. Results are represented as % viability relative to cells washed after treatment with EGTA and buffer. Below results, experimental outline is presented graphically. Cells were exposed to toxin and EGTA for 20 minutes, followed by washes and addition of DMEM. High viability was recorded 24 hours later.

High viability in cells transiently treated with PS-3 and EGTA indicates that the chelator prevented toxin interaction with the membrane within the 20 minute incubation period – a time that was sufficient to initiate cytotoxic effect in cells transiently treated with PS-3 in the absence of EGTA. For confirmation this experiment was repeated three times using lower EGTA concentration (2 mM), each time yielding similar results (data not shown). Presence of Ca^{2+} counteracted EGTA effect and promoted efficient PS-3 toxicity within the 20 minute period. Cells were observed under the microscope after washing and re-suspending steps as well as after 20 hours. At each of these steps, cells treated with EGTA, Ca^{2+} and toxin as well as with toxin only showed significant

swelling (more than >90% of cells), whereas cells treated with EGTA and toxin presented little swelling (<10%).

It is shown in chapter 6 that PS-3 - as many other PFTs - induced p38 phosphorylation, a pathway activated by pore formation. It was speculated that if EGTA prevents PS-3 making pores, the chelator should also prevent phosphorylation of p38. Western blot was carried out to test this hypothesis. Cells were first pre-treated with EGTA, followed by toxin administration, cell lysis and detection of dually phosphorylated p38 (Figure 94).

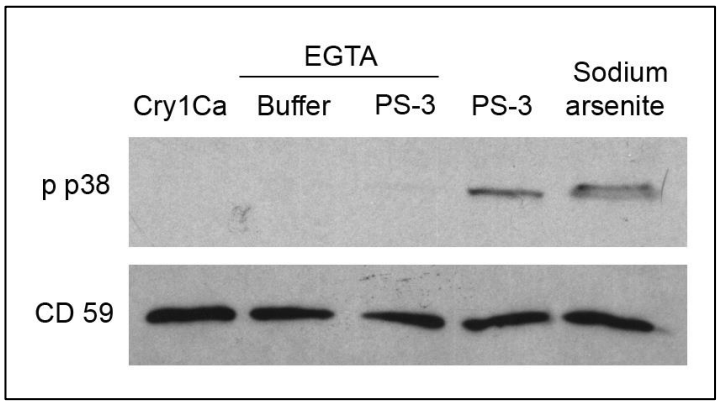

Figure 94 Analysis of p38 phosphorylation in EGTA pre-treated HepG2 cells exposed to PS-3.
HepG2 cells were pre-treated with EGTA (2 mM) or water only for 10 minutes. Next, Cry1Ca (15 μg/ml), sodium arsenite (0.5 mM), PS-3 (15 μg/ml) or buffer were added. Cells were lysed in NP-40 15 minutes after toxin treatment. 10 μg of proteins were loaded in each lane and after SDS-PAGE proteins were subject to western blot analysis for the presence of phosphorylated p38 (p p38) and CD59 (loading control).

Cell pre-incubation with EGTA significantly reduced p38 activation in PS-3 treated cells.

5.4 Assessment of possible indirect EGTA actions

Chelation of metal ions is considered here as a direct effect of EGTA, whereas any form of other interactions is considered as indirect. The following direct and indirect effects associated with EGTA administration may be resulting in toxicity abolition.

Direct:

- EGTA chelates metal ions present in extracellular medium,
- EGTA – in addition to extracellular ions - chelates metal ions bound to membrane proteins.

Indirect:

- EGTA binds or interacts with toxin,
- EGTA binds or affects cell membrane by means different from ion chelation,
- EGTA induces drop in pH due to H^+ release during chelation reaction.

To test if EGTA was causing the toxin to degrade or precipitate, PS-3 was incubated with or without EGTA followed by SDS - PAGE to assess toxin bands (Figure 95).

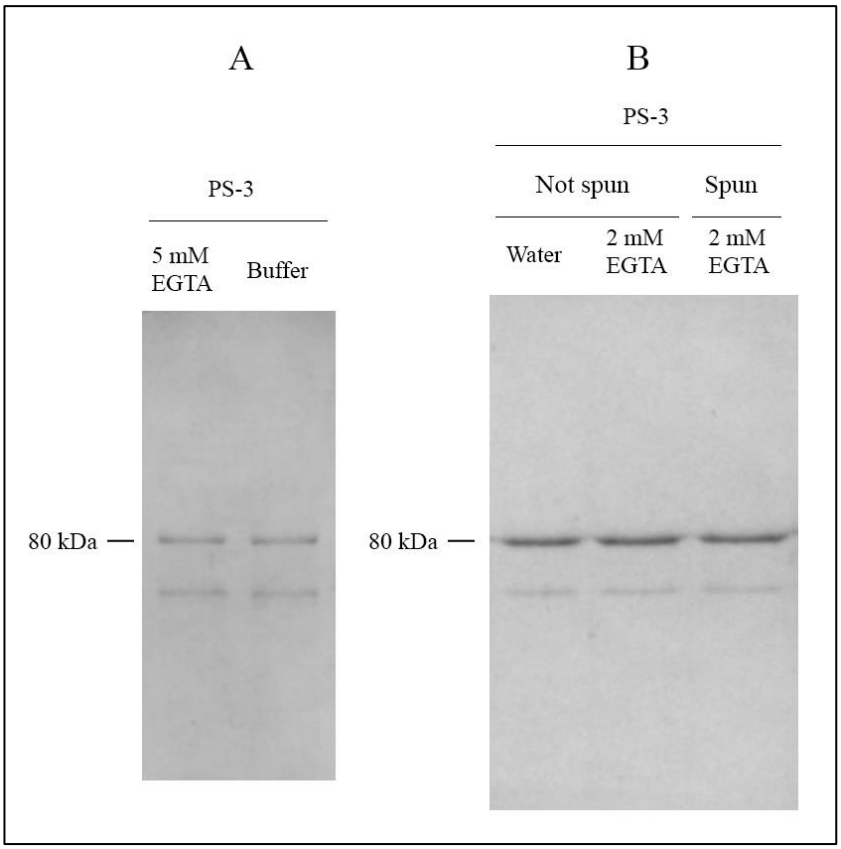

Figure 95 SDS-PAGE analysis of possible protein degradation and precipitation after incubation with EGTA.
A) 10 µl of activated PS-3 (120 µg/ml) was incubated with either 5 mM EGTA in PBS or appropriate volume of PBS for 1 hour at 37°C. After incubation samples were spun and run on a 7.5% SDS-PAGE gel. B) 10 µl of activated PS-3 (96 µg/ml) was incubated with either 2 mM EGTA in dH_2O or appropriate volume of dH_2O for 15 minutes at RT. After incubation samples were either spun or not and run on a 7.5% SDS-PAGE gel.

The size and quantity of toxin was unaffected by incubation with the chelator under different conditions. Also, soluble fraction after spinning did not look any different from the control bands indicating no toxin precipitation.

The possibility exists, although unlikely, that the toxin was bound by EGTA and this affected its toxicity. Only some proteins are able to bind EGTA and EDTA, but this occurs with very low affinity (Uversky, 2007). To test this possibility PS-3 was incubated with EGTA, dialysed and then tested on cells (Figure 96).

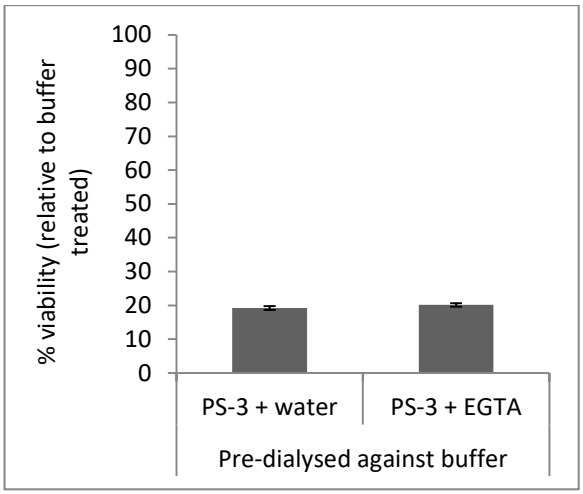

Figure 96 Assessment of PS-3 activity on HepG2 cells after toxin pre-incubation with EGTA and dialysis.
PS-3 (12 µg/ml) was incubated at RT for 30 minutes with either EGTA (2 mM) or water. Mixtures were transferred to Vivaspin500 desalting columns followed by 4 washes with DPBS buffer to remove unbound EGTA molecules. HepG2 cells were seeded at the density of 25 x 10^4 cells/ml. The next day cells were treated with dialysed retenates and viability was measured 5 hours after toxin administration using CellTiter-Blue.

Even though PS-3 had been in contact with EGTA, its toxicity was retained after dialysis, indicating that EGTA does not bind the toxin or does not affect its activity.

To test if EGTA physically affected cell membranes e.g. by binding, PS-3 toxicity was assessed in cells treated transiently with EGTA (Figure 97).

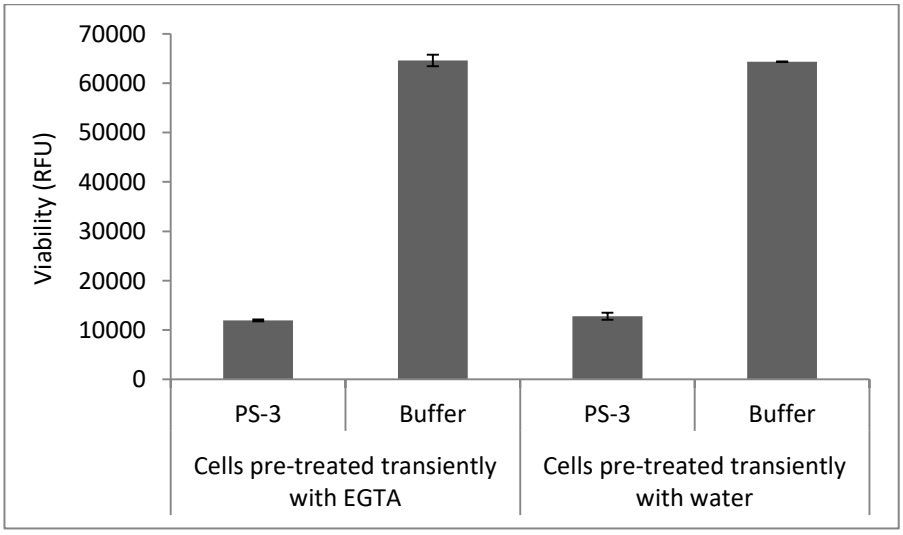

Figure 97 Assessment of PS-3 toxicity in HepG2 cells pre-treated transiently with EGTA.
HepG2 cells were seeded at the density of 25 x 10^4 cells/ml. The next day cells were pre-treated with either EGTA (2 mM) or water for 30 minutes followed by a cell wash and toxin (12 µg/ml) treatment in complete medium. Viability was measured 5 hours after toxin administration using CellTiter-Blue.

Cells transiently pre-treated with EGTA remained susceptible to PS-3. Cell washing removed EGTA suggesting it did not bind cell surfaces or that binding did not affect the activity of PS-3.

Soon after EGTA is added to the cells phenol red present in the culture medium changes colour from red to yellow, indicating a shift towards more acidic pH. It is because in distilled water chelators like EDTA or EGTA behave as weak acids. When a chelation reaction takes place protons in the chelation are displaced by metal cations resulting subsequently in a pH drop (Spencer, 1958). Moreover, pore formation activity by Cry1Aa in *M. sexta* BBMV in the presence of EGTA was shown previously to be affected by a pH change; EGTA was inhibitory at pH 10.5 but not 7.4 (Kirouac et al., 2006). Therefore, the pH of HepG2 cell suspension in complete DMEM was measured before and after the addition of 2 mM EGTA. Medium's pH dropped from 7.4 to 6.8. Activity of PS-3 was then assessed in the absence of EGTA in medium with lowered or increased pH values (Figure 98).

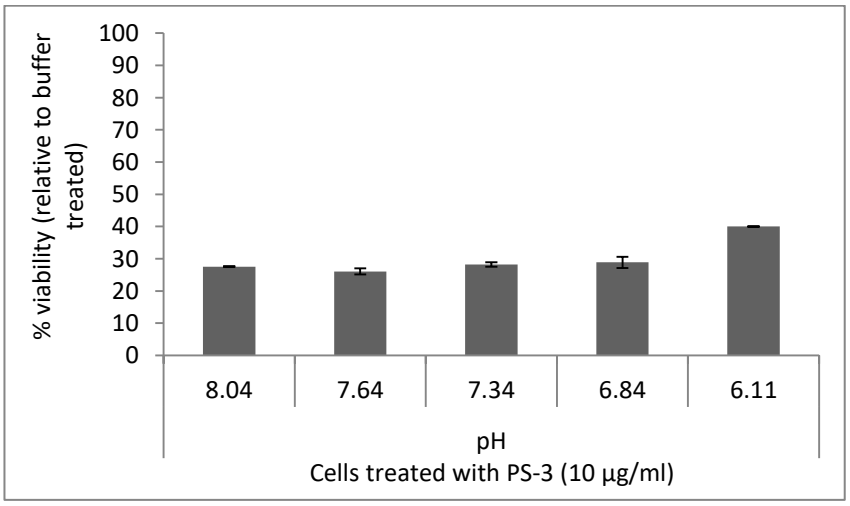

Figure 98 The effect of medium's pH on PS-3 activity against HepG2 cells.
HepG2 cells were seeded at the density of 25 x 10^4 cells/ml in complete DMEM. The next day cells were washed with DPBS and placed in medium with altered pH. pH of culture medium was adjusted in advance using either 10 mM NaOH or 1M HCl. PS-3 (10 µg/ml) was added 30 minutes later and cell viability was measured 5 hours after toxin addition using CellTiter-Blue.

A pH drop in the culture medium to 6.84, which mimicked EGTA induced pH change, did not influence PS-3 activity, suggesting that this cannot explain EGTA protective effect.

5.5 Effect of other chelators on PS-3 toxicity

Effects of chelators other than EGTA or EDTA were tested on PS-3 toxicity (Figure 99). DTPA is a membrane impermeable chelator often used in zinc depletion studies. Only zinc and to a lesser extent copper, but not calcium or magnesium ions, were able to counteract the cytotoxic effect of DTPA in breast cancer cell lines after 48 hour exposure (Hashemi et al., 2007), however DTPA has the capacity to bind other ions (Byegård et al., 1999). BAPTA is a derivative of EGTA, designed to be more selective for Ca^{2+} over Mg^{2+} than EGTA, however it forms lower affinity calcium chelates than EGTA: 6.71 versus 7.18 at pH 7.4 (Bolsover, 1994). Histidine is a chelator of many divalent ions including copper and iron but it presents negligible affinity for calcium. For this reason it has been used previously alongside EGTA to test the involvement of calcium in lymphocyte membrane permeability (Quastel et al., 1981, Segel et al., 1981). Contrary to previously mentioned chelators, which bind metals in a 1:1 molar ratio, histidine complexes metals in a ratio of 2:1.

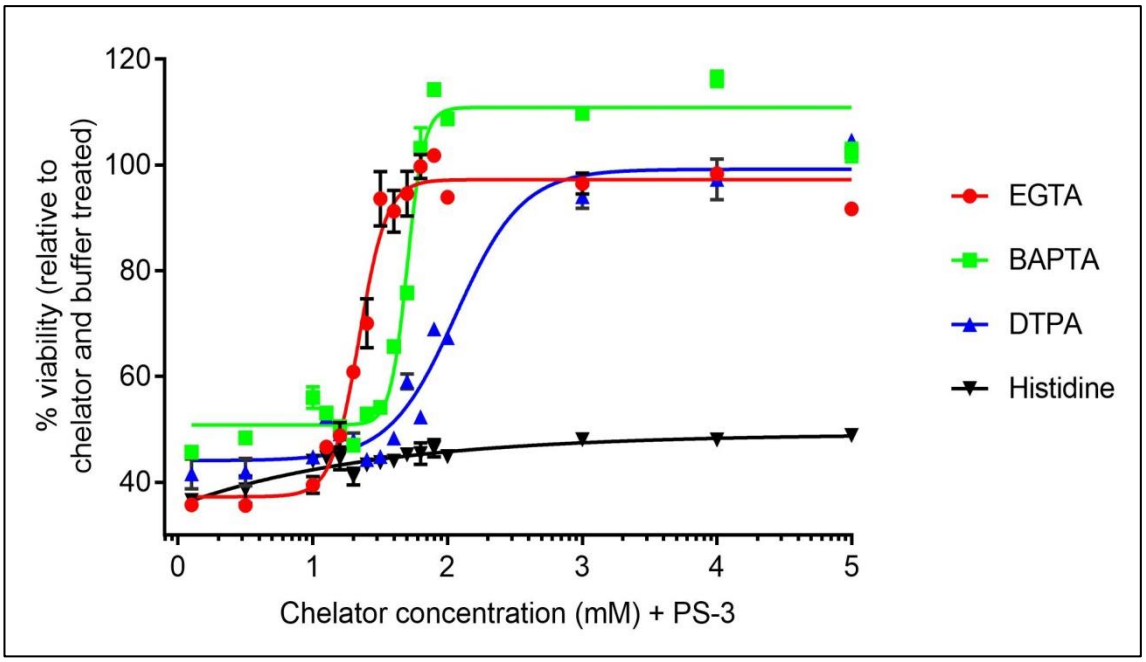

Figure 99 The effect of different metal chelators on PS-3 toxicity.
HepG2 cells were seeded at the density of 25 x 10^4 cells/ml in Advanced DMEM. The next day cells were incubated for 30 minutes with different concentrations of EGTA, BAPTA, DTPA or histidine before PS-3 (10 µg/ml) was added. Viability was measured 5 hours after toxin addition using CellTiter-Blue. Dose response curves were generated using Graphpad Prism.

Non-specific chelators like EGTA or BAPTA were most efficient at protecting cells from PS-3. It required higher concentration of DTPA to achieve this effect while histidine, even at high concentrations, had no significant impact.

5.6 Role of membrane bound ions in PS-3 toxicity

In order to better explain the role of extracellular calcium ions in PS-3 activity, titration of EGTA was performed in complete DMEM as well as in Ca^{2+} free DMEM with and without FCS - as supplementation with FCS additionally increases extracellular calcium pool (Figure 100). Experiments that involved Ca^{2+} free medium were carried out straight after cell seeding because lack of extracellular Ca^{2+} led to a detrimental fall in viability after 24 hours. Although the cells were not attached to the bottom of the 96-

well plate, the difference in morphology before and after toxin addition (swelling) was prominent.

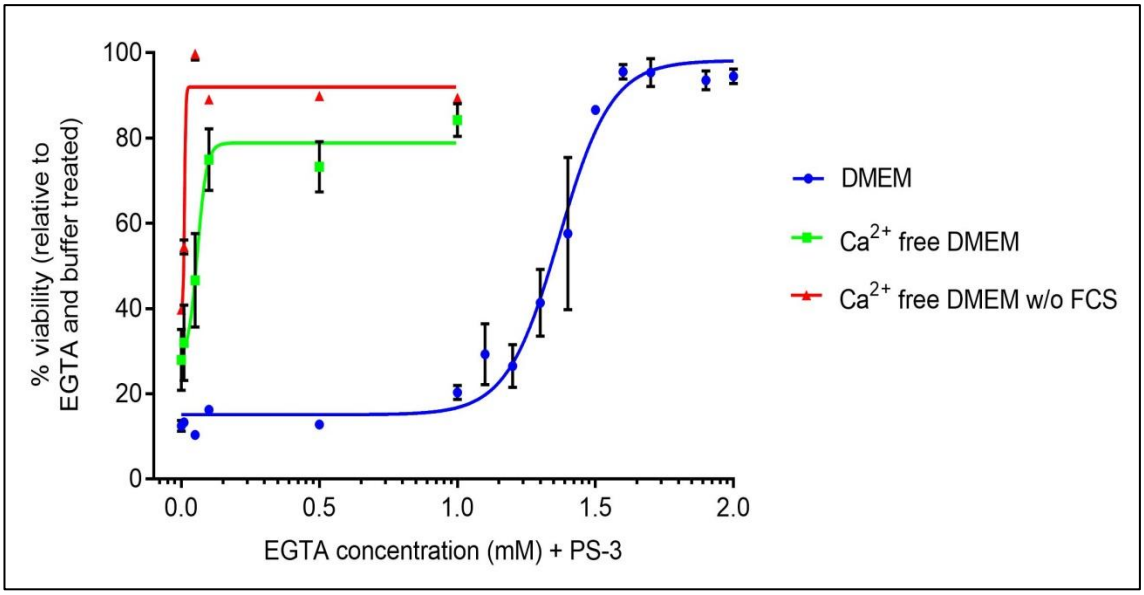

Figure 100 EGTA titration in culture media with different calcium levels and its effect on PS-3 activity.
HepG2 cells were seeded at the density of 25 x 10^4 cells/ml in complete DMEM, Ca^{2+} free DMEM with FCS, or Ca^{2+} free DMEM without FCS. Cells in complete DMEM were seeded 24 hours before the experiment and cells in Ca^{2+} free DMEM on the same day. Cells were treated with different concentrations of EGTA and 30 minutes later with PS-3 (12 µg/ml). CellTiter-Blue cell viability assay was used to measure viability 5 hours later. Dose response curves were generated using Graphpad Prism.

Cells in DMEM devoid of extracellular Ca^{2+} were able to resist PS-3 at much lower EGTA concentration compared to complete DMEM. When Ca^{2+} free DMEM was lacking FCS, cells resisted PS-3 at even lower chelator dose. Importantly, in the absence of EGTA toxin retained its activity in Ca^{2+} free DMEM (with or without FCS), suggesting that EGTA may be chelating extracellular metal ions other than calcium or ions bound to cellular membranes. To test this, a similar experiment was conducted measuring viability of PS-3 treated cells in DPBS in the presence of different BAPTA concentrations as shown in Figure 101 (BAPTA dose-response curve in Advanced DMEM from Figure 99 is included for comparison).

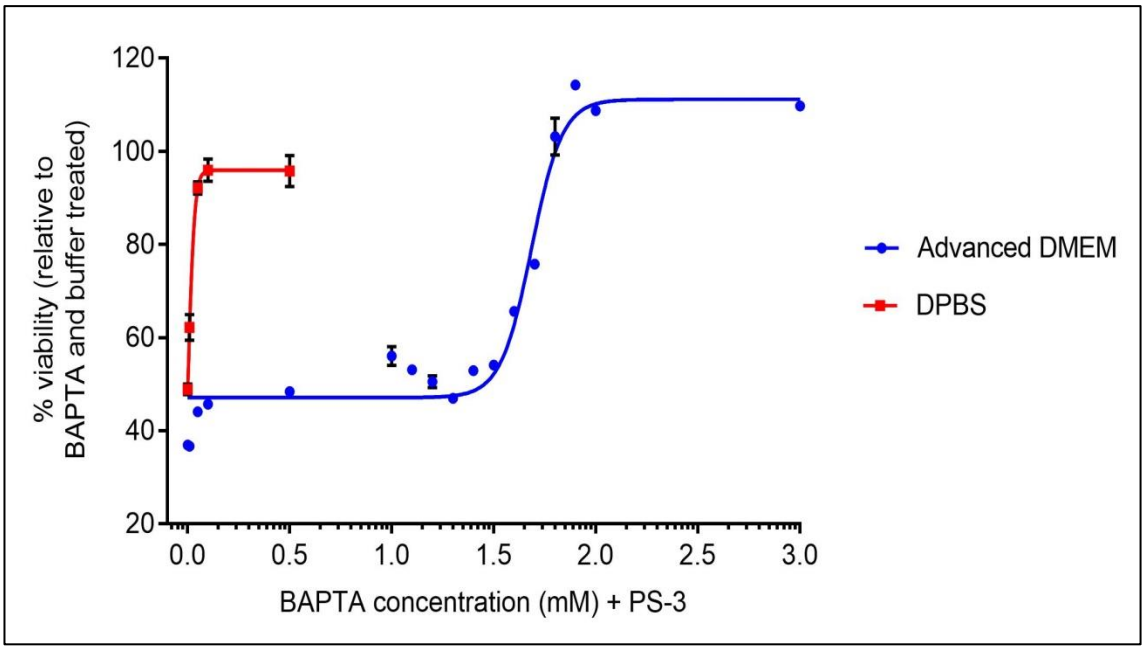

Figure 101 Titration of BAPTA in Advanced DMEM and DPBS and its effect on PS-3 activity.
HepG2 cells were seeded at the density of 25 x 10^4 cells/ml. BAPTA in DPBS treatment: cells were seeded in Advanced DMEM overnight. The next day cells were washed once with DPBS and fresh DPBS was placed in the wells. Different concentrations of BAPTA were added and 30 minutes later PS-3 was administered (10 µg/ml). Viability was measured 3 hours later using CellTiter-Blue. BAPTA in Advanced DMEM treatment: cells were seeded in Advanced DMEM. The next day cells were incubated with different concentrations of BAPTA. After 30 min PS-3 (10 µg/ml) was added and viability was measured 5 hours later using CellTiter-Blue. Dose response curves were generated using Graphpad Prism.

Much less BAPTA was required to abolish PS-3 toxicity in DPBS compared with Advanced DMEM. However, in DPBS in the absence of chelator, like previously observed in Ca^{2+} free DMEM, the toxin was still able to cause swelling and decrease cell viability, which suggests that cations bound to the membrane play a role in PS-3 toxicity.

5.7 Effect of metal ion supplementation on PS-3 toxicity

Considering that calcium ions counteracted the EGTA effect, it was tested whether increasing extracellular Ca^{2+} levels would increase PS-3 toxicity (Figure 102), like in the case of experiments with Cry1C and Sf9 cells (Monette et al., 1997).

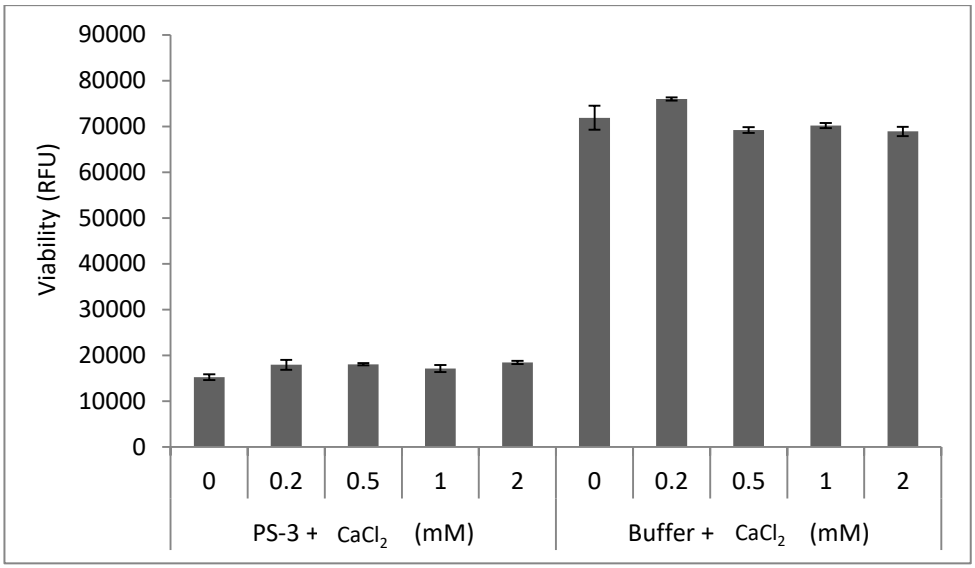

Figure 102 The effect of increased Ca^{2+} levels on PS-3 toxicity.
HepG2 cells were seeded at the density of 25 x 10^4 cells/ml in complete DMEM. The next day cells were supplemented with various concentrations of $CaCl_2$ for 10 minutes, followed by either toxin (12 μg/ml) or buffer administration. Viability was measured 5 hours after toxin treatment using CellTiter-Blue assay.

Adding extra calcium ions did not increase PS-3 toxicity. This is consistent with data presented in Figure 86, where the addition of as little as 1 mM $CaCl_2$ counteracted the 2 mM EGTA effect, whereas the addition of >1 mM $CaCl_2$ did not increase toxicity any further.

To test the effect of calcium and other metal ions on PS-3 activity in the absence of extracellular Ca^{2+}, salt supplementation was done in Ca^{2+} free medium. Low toxin dose was used to better visualise changes in toxicity (Figure 103).

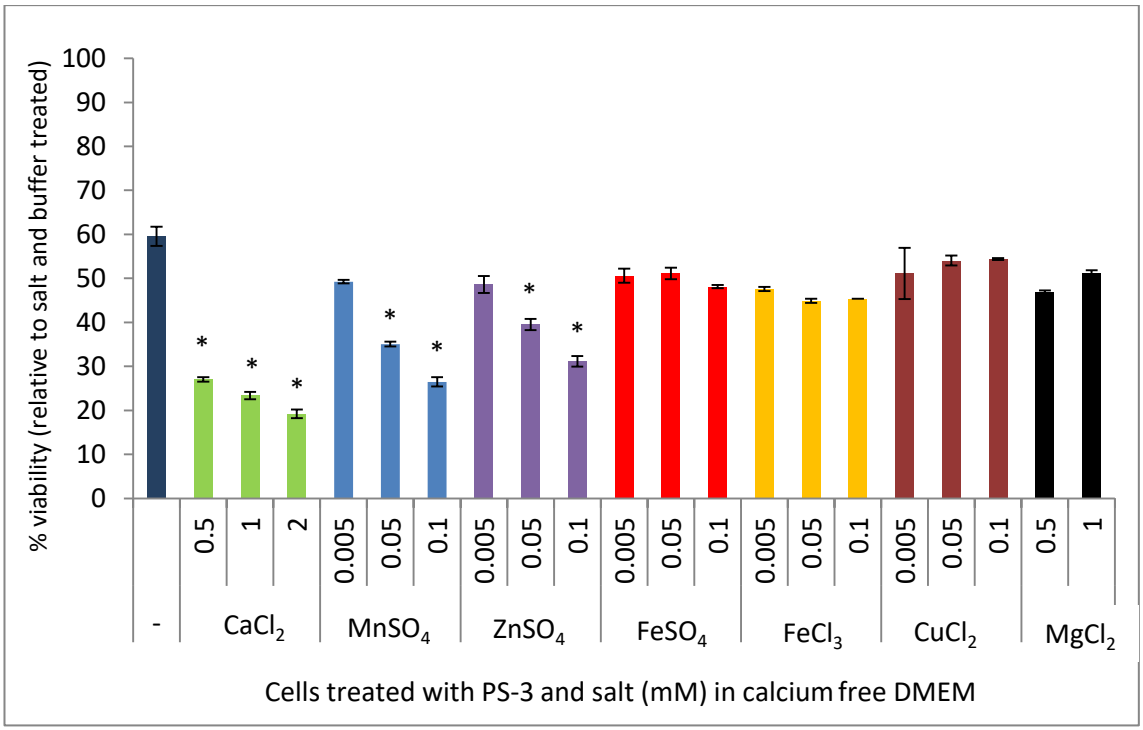

Figure 103 The effect of metal salts on residual PS-3 toxicity in Ca^{2+} free DMEM.
HepG2 cells were seeded at the density of 25 x 10^4 cells/ml in Ca^{2+} free DMEM. After 30 minutes cells were supplemented with various concentrations of metal salts: $CaCl_2$, $MnSO_4$, $ZnSO_4$, $FeSO_4$, $FeCl_3$, $CuCl_2$ or $MgCl_2$, followed by either PS-3 (5 µg/ml) or buffer treatment. Viability was measured 5 hours after toxin treatment using CellTiter-Blue assay. Bars with asterisks are significantly different from control cells exposed to PS-3 (5 µg/ml) in calcium free DMEM without supplementation (* $p < 0.005$, Post-Hoc comparison with Bonferroni correction).

In the absence of extracellular Ca^{2+}, low quantities of Mn^{2+} and Zn^{2+} enhanced PS-3 toxicity, as did Ca^{2+}. When similar experiments were conducted in complete and Advanced DMEM, so in the presence of normal Ca^{2+} concentrations, addition of low levels of Zn^{2+} or Mn^{2+} also enhanced PS-3 toxicity (data not shown).

5.8 Effect of metal ion supplementation on EGTA effect reversal

To further clarify which metal cations play a role in toxicity, EGTA and PS-3 treated cells were supplemented with different concentrations of metal ions to counteract the protective EGTA effect (Figure 104).

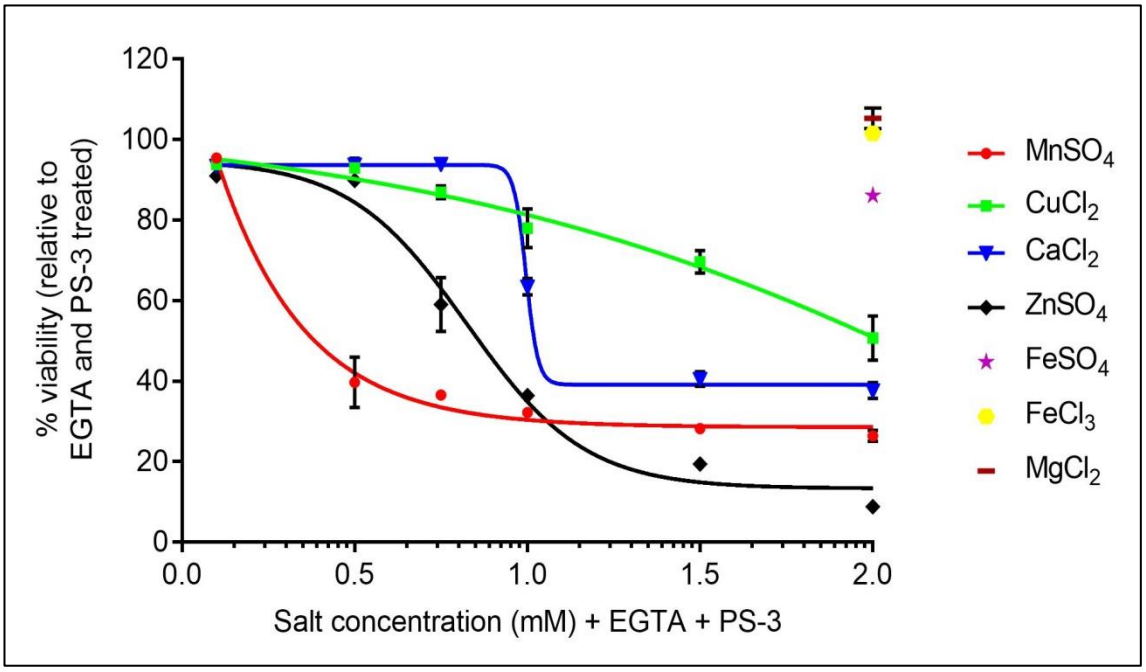

Figure 104 The effect of different salts on HepG2 cells exposed to EGTA and PS-3 in Ca^{2+} free DMEM.
HepG2 cells were seeded at the density of 25 x 10^4 cells/ml in Ca^{2+} free medium followed by treatment with 2 mM EGTA or water. 10 min later different concentrations of salts were added followed by either PS-3 (10 µg/ml) or buffer treatment. Viability was measured 5 hours later using CellTiter-Blue. Addition of high concentrations (>1 mM) of $ZnSO_4$ and $CuCl_2$ to cells resulted in decreased viability therefore normalisation was done for the effect of all salts. Normalized data was then plotted as a percentage of the EGTA and PS-3 treated cells. Dose response curves were generated using Graphpad Prism.

Ca^{2+}, Mn^{2+} and Zn^{2+} supplementation most strongly counteracted EGTA effect. It is worth noting that as little as 0.5 mM of Mn^{2+} was able to significantly reinstate toxicity. Cu^{2+} partially restored toxicity, however >1 mM concentrations of $ZnSO_4$ and $CuCl_2$ were toxic to cells (~35% viability drop in cells treated with 2 mM $CuCl_2$, 15% viability

drop in cells treated with 2 mM $ZnSO_4$; data not shown); data were normalized for this effect, but it could mask the real contribution of these ions in PS-3 action.

Unfortunately, addition of extra salts will affect the equilibria of existing EGTA chelates, e.g. addition of a large amount of Zn^{2+} could displace another metal cation from EGTA chelate making it available for the cells and facilitating toxicity . To avoid the problem of the unknown stoichiometry of each metal ion after supplementation in the presence of EGTA, similar experiment was performed where culture medium with EGTA was removed before salt and toxin addition in DPBS. Salt supplementation was done in DPBS for absolute control of buffer composition (Figure 105).

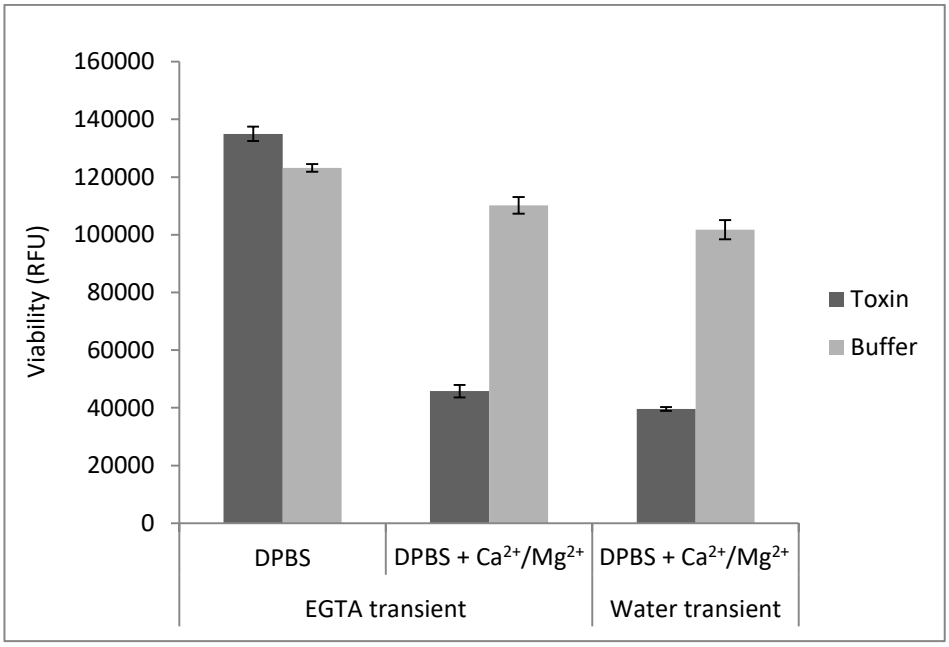

Figure 105 The effect of PS-3 on HepG2 cells in DPBS with or without Ca^{2+} and Mg^{2+} after transient EGTA treatment.
HepG2 cells were seeded at the density of 25 x 10^4 cells/ml in complete DMEM. The next day cells were treated with 2 mM EGTA or water for 10 minutes. After that medium was removed from wells and 90 µl of DPBS formulated either without or with Ca^{2+} (0.9 mM of $CaCl_2$) and Mg^{2+} (0.5 mM of $MgCl_2$) was added. 5 minutes later either PS-3 (10 µg/ml) or buffer was added. Viability was measured 4 hours later using CellTiter-Blue.

High viability in PS-3 treated cells in DPBS after EGTA removal suggests that together with removed medium all the metal cations needed for PS-3 toxicity have been also

removed due to EGTA chelation. When DPBS formulated to include Ca^{2+} and Mg^{2+} was used instead, swelling and drop in viability was present. These results and previous observations about Mg^{2+} insignificance (Figure 85, Figure 103 and Figure 104) suggest that Ca^{2+} alone is able to distinctly reinstate PS-3 activity. Analogous experiment was carried out in DPBS that included more metal salts (Figure 106).

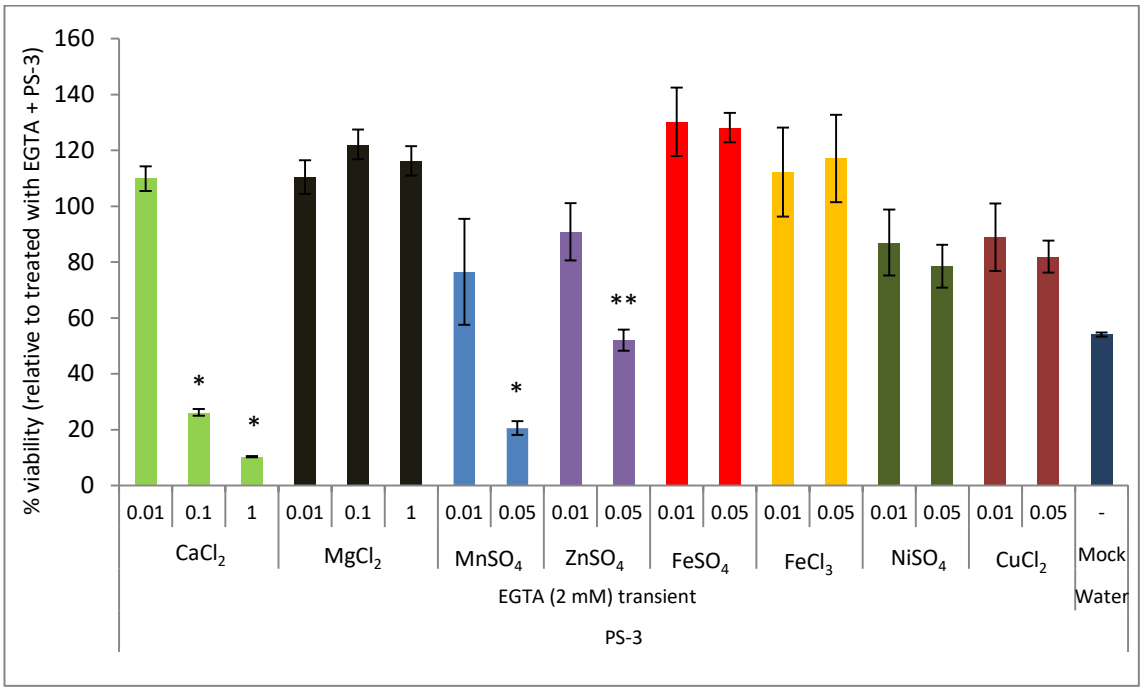

Figure 106 The effect of various salts on PS-3 treated cells in DPBS after EGTA removal.
HepG2 cells were seeded at the density of 25 x 10^4 cells/ml in complete DMEM. The next day cells were treated with 2 mM EGTA or water for 10 minutes. After that medium was removed from wells and DPBS was added. 5 minutes later different concentrations of salts were added followed by either PS-3 (10 µg/ml) or buffer treatment. Viability was measured 4 hours later using CellTiter-Blue. Addition of $NiSO_4$ and $CuCl_2$ to cells in DPBS resulted in decreased viability therefore normalisation was done for the effect of all salts. Normalized data was then plotted as a percentage of the EGTA and PS-3 treated cells. Bars with asterisks are significantly different from control cells exposed to PS-3 (10 µg/ml) in PBS without supplementation after transient treatment with 2 mM EGTA (* $p < 0.001$, ** $p < 0.05$, Post-Hoc comparison with Bonferroni correction).

The above results show that addition of $CaCl_2$, $MnSO_4$ and to a lesser extent $ZnSO_4$ not only restored but even elevated PS-3 toxicity compared to viability levels of PS-3 treated cells when water instead of EGTA was used for transient treatment.

It was noted that in the routinely used Nunclon surface treated 96-well plates, small percentage of adhered cells grow forming layers, with some of them probably being hidden from the treatment. Experiment was therefore repeated using a Poly-D-lysine coated 96 well-plate as it allows for even spreading out of cells, and ensures a more even exposure to EGTA (Figure 107).

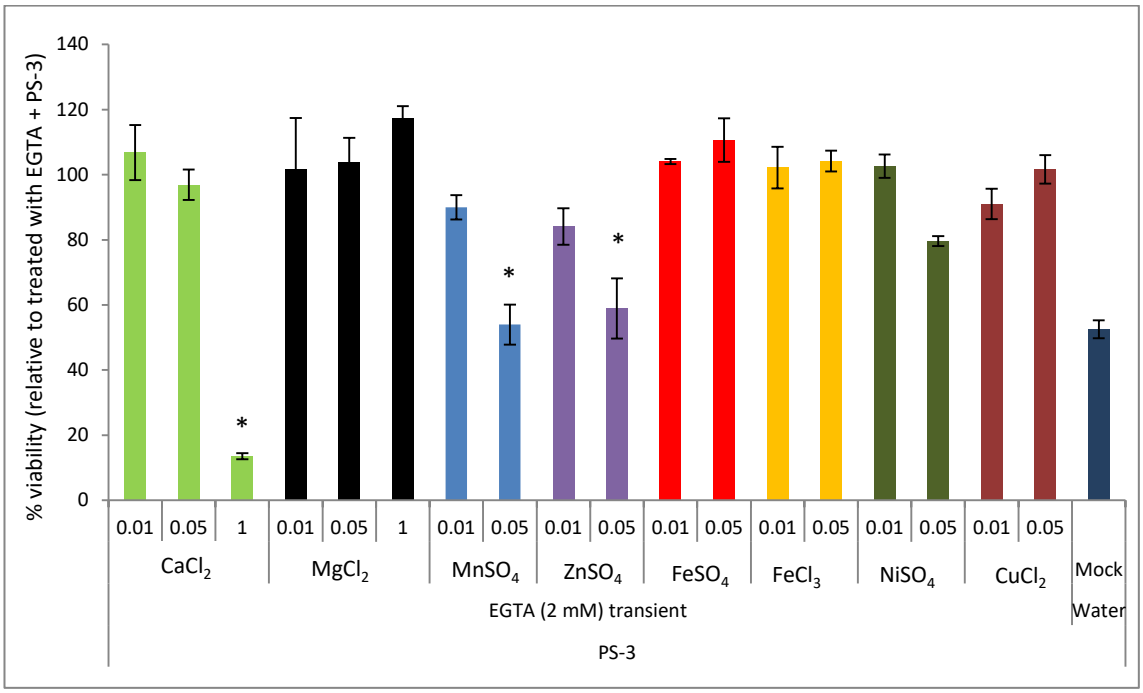

Figure 107 The effect of various salts on PS-3 treated cells in DPBS after EGTA removal (cells seeded on a Poly-D-lysine substrate).
HepG2 cells were seeded at the density of 25 x 10^4 cells/ml in complete DMEM in Poly-D-lysine coated 96-well plates. The next day cells were treated with 2 mM EGTA or water for 10 minutes. After that medium was removed from wells and DPBS was added. 5 minutes later different concentrations of salts were added followed by either PS-3 (10 µg/ml) or buffer treatment. Viability was measured 4 hours later using CellTiter-Blue. Addition of $NiSO_4$ and $CuCl_2$ to cells in DPBS resulted in decreased viability therefore normalisation was done for the effect of all salts. Normalized data was then plotted as a percentage of the EGTA and PS-3 treated cells. Bars with asterisks are significantly different from control cells exposed to PS-3 (10 µg/ml) in PBS without supplementation after transient treatment with 2 mM EGTA (* $p < 0.001$, Post-Hoc comparison with Bonferroni correction).

Results showed similar trend: trace levels of $MnSO_4$ and $ZnSO_4$ restored PS-3 toxicity. High levels of $CaCl_2$ (1mM), but less than present in DMEM formulation, not only restored but significantly enhanced toxicity of PS-3.

5.9 Discussion

EGTA is thought to be cell impermeant and not metabolised by cells. However, undoubtedly high dose and prolonged exposure will have an effect by the virtue of its metal-chelating property. Calcium is one of the most abundant metal ions present in extracellular fluids, and also in the DMEM formulation (Table 10). The literature has shown that removal of extracellular Ca^{2+} reversibly increases permeability of tight junctions, a multi-protein system that mediates cell to cell adhesion and transport in epithelial cells, leading to its disruption, cell contraction and reduction of cell-cell adhesion (Pitelka et al., 1983). Furthermore, mouse myoblast C2C12 cells treated with 1.75 mM EGTA for 24 hours showed significant changes in morphology resulting from changes in number and distribution of stress fibres and microtubules (Mermelstein et al., 2003). For these reasons all chelator experiments were carried out over a short time period of 5 hours. Results indicate that indirect interaction between the chelator and either cell membrane or the toxin was not responsible for alleviating PS-3 toxicity. Also, the EGTA induced fall in pH neither affected cell viability nor was responsible for toxicity inhibition. EGTA action appeared to result from the metal ion chelation activity.

Interestingly, high dose of PS-3 (>30 µg/ml) overcame 2 mM protective effect of EGTA, perhaps analogous to how other Cry toxins can spontaneously form pores in artificial lipid bilayers devoid of receptors when present at high dose (Schwartz et al., 1993, Slatin et al., 1990b). These results may suggest the capacity of PS-3 for spontaneous insertion and pore formation when the receptor is malfunctioned e.g. due to chelator action. This is supported by the fact that a high PS-3 dose also lowered

viability and initiated swelling in HeLa cells (section 4.10) and high conductance was observed in negative controls in single channel patch clamp experiments (section 4.7).

Experiments showed that the later EGTA was administered relative to toxin treatment, the more ineffective it was in cell protection. Gradual decrease in viability in wells where EGTA was added, 1, 5, and 15 minutes after PS-3, points to some sort of competition between the chelator and toxin. When a chelator like EGTA is added to a solution, equilibrium is reached relatively quickly within micro- to milliseconds, depending on rate constants and ionic strength. This may indicate that the initial few minutes are required for toxin interaction with the membrane. This would be the diffusion time it takes for the toxin to reach and bind membranes, but could also include oligomerisation. In HepG2 cells treated with PS-2, membrane associated oligomers were detected after 10 minute incubation with the signal reaching highest intensity after 60 minutes (Abe et al., 2008). Unfortunately, attempts to detect PS-3 oligomers embedded in HepG2 membranes were unsuccessful (section 7.5). It seems that as soon as EGTA is added (after PS-3), it prevents further toxin action but it cannot undo the damage already created. This is consistent with study by Kirouac et al. who showed that EDTA (and to some extent EGTA) inhibited the rate of pore formation by Cry1Aa but did not alter the pores that were already formed (Kirouac et al., 2006).

The membrane permeability assays showed that in EGTA and PS-3 treated cells membrane stayed impermeable to a small cytotoxic marker and a large current flow (whole cell patch clamp experiments) implying that EGTA protected cells from membrane damage. In agreement with this is the fact that EGTA also prevented p38 phosphorylation. It has been shown that non-lytic mutants of some PFTs like *E. coli*

Hemolysin A or *S. aureus* α-toxin failed to activate p38 (Husmann et al., 2006, Kloft et al., 2009). Moreover, a study by Ratner et al. demonstrated that EGTA abolished p38 activation in Pneumolysin treated A549 epithelial cells (Ratner et al., 2006). Lack of p38 activation in EGTA and PS-3 treated cells could then result either from the lack of binding or pore formation. Clarification came from the experiment in which removal of toxin and EGTA after transient treatment resulted in high cell viability opposed to low viability in control cells transiently treated with toxin only. These results indicate that EGTA prevented stable interaction between the toxin and cell membrane and not the subsequent steps. Interestingly, EGTA did not prevent pore formation by PS-3 in artificial membranes, indicating a biological context of this chelator effect. This may also be attributed to single channel recording being a highly sensitive method of channel detection. The latter may be true as high conductance values were also observed in EGTA and PS-3 treated cells in single channel patch clamp experiments, but not in the whole cell patch clamp experiments where macroscopic current from the whole cells was measured.

Chelator titration curves may support the idea of calcium being the cation of major importance in PS-3 mode of action. BAPTA which forms lower affinity calcium chelates compared to EGTA was somewhat less effective in preventing cell death than EGTA. The ability of high concentrations of DTPA to preserve cell viability was most likely caused by metal chelation other than zinc. 1.2 mM of DTPA was found to be the optimal concentration to chelate zinc in osteoblastic MC3T3-E1 cells (Cho et al., 2007), however much smaller concentrations of 0.1 mM were used successfully with MCF-7 and MDA-MB468 breast cancer cells (Hashemi et al., 2007). In experiments with PS-3, even 2 mM DTPA was not able to fully protect the cells from the toxin's damage.

Moreover histidine, which is a poor calcium chelator, did not inhibit PS-3 toxicity even at very high up to 10 mM concentration (data not shown).

PS-3 stayed active in Ca^{2+} free DMEM and DPBS, even in the absence of chelators. Formulation of DPBS contains only potassium and sodium salts in concentrations exceeding 2 mM. Moreover both EGTA and BAPTA have negligible affinities for K^+ or Na^+. These results imply that cations bound to the membrane proteins and not present in extracellular medium are important for PS-3 activity. If protein-metal affinity is weaker than chelator affinity for this metal, it may be pulled out of its binding protein partner.

Nonetheless, caution should be taken when analysing experiments with chelating agents like EGTA. Due to the fact that EGTA forms complexes with a large number of metallic cations, it is difficult to predict the levels of the un-chelated free metal ions available to cells after EGTA treatment in culture medium. EGTA-metal equilibria are calculated in a situation when EGTA is fully dissociated (alkaline pH) and only with one type of cation present. What is known is that both abundance of metal ions (if they are major constituents in DMEM like calcium or magnesium or minor like zinc or manganese ions) and their ability to form stable complexes with the chelator at experimental pH, highly influence the actual equilibria (Spencer, 1958). Table 10 presents quantities of major metal ions present in DMEM formulation and stability constants of complexes formed by EGTA and these ions.

Table 10 Levels of metal ions in complete DMEM and EGTA-metal stability constants.
Amounts of metal cations were obtained from supplier's website (Life Technologies). Stability constants were taken from Cheng, et al. (K. L.Cheng, 1982).

Ions	Presence in complete DMEM (mM)	EGTA-metal absolute stability constant
Ca^{2+}	1.8 (in DMEM)	11
Mg^{2+}	0.8 (in DMEM)	5.2
Fe^{3+}	0.0003 (in DMEM)	20.5
Fe^{2+}	Trace (in FCS)	11.9
Mn^{2+}	Trace (in FCS)	12.3
Zn^{2+}	Trace (in FCS)	14.5
Cu^{2+}	Trace (in FCS)	17.8

Considering then that the biological levels of Zn^{2+} and Mn^{2+} are in micromolar and nanomolar range respectively, the addition of large quantities (2 mM) of Zn^{2+} or Mn^{2+} to the cells most likely created variations in the equilibrium concentrations of all the strongly chelated as well as un-chelated ions releasing other ions that formed less stable complexes with EGTA. For example, added Zn^{2+} could displace Ca^{2+}, which when released could aid or affect PS-3 action.

However, despite the above, experiments where EGTA was present with cells throughout the experiment, displayed comparable results to experiments where ion supplementation was done without EGTA or after its removal, as graphically presented in Figure 108. In the absence of EGTA low quantities of Mn^{2+}, Zn^{2+} and Ca^{2+} enhanced PS-3 toxicity in Ca^{2+} free DMEM. When EGTA was present continuously with the cells, it was also supplementation with Ca^{2+}, Mn^{2+} and Zn^{2+} that most strongly counteracted EGTA effect. When the cells were only transiently treated with EGTA and cultured in DPBS, results showed similar trend: the addition of Ca^{2+}, Mn^{2+} and Zn^{2+} not only restored but in some cases increased PS-3 toxicity. Therefore Mn^{2+}, Zn^{2+} and Ca^{2+} seem to play an important role in PS-3 toxicity.

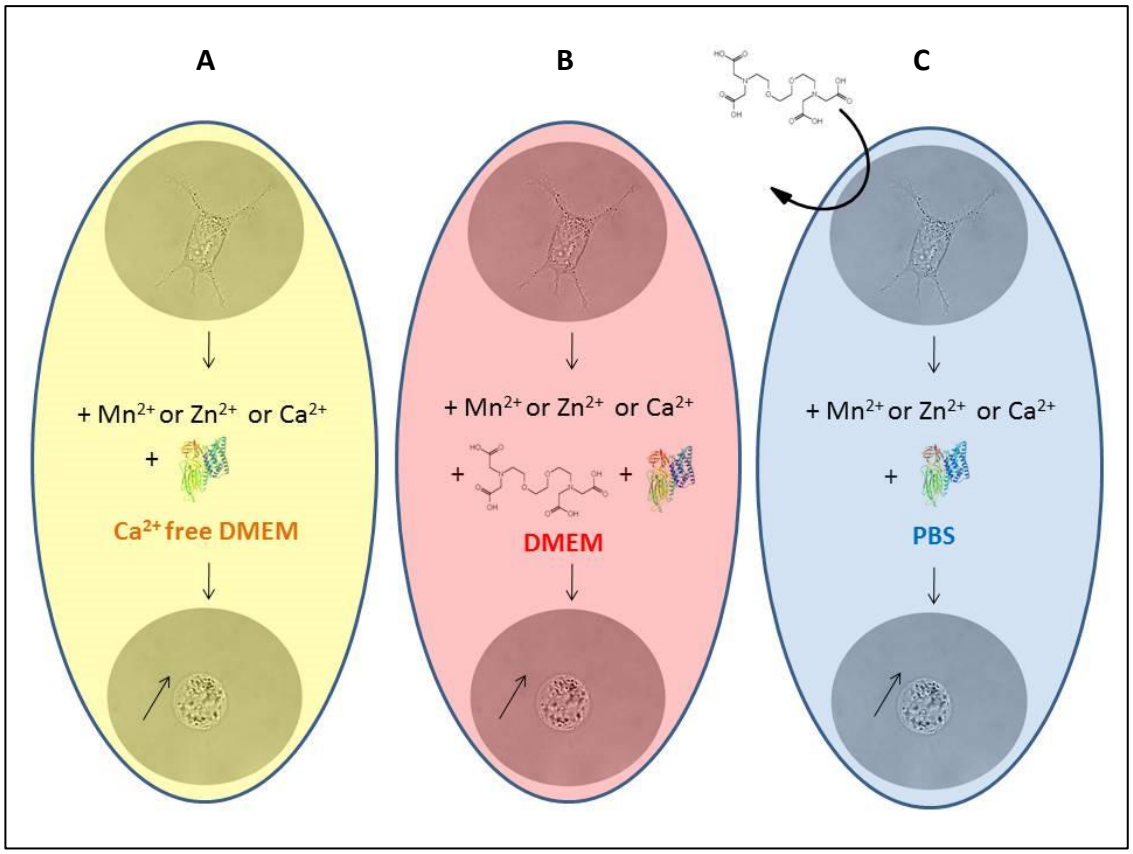

Figure 108 Experimental evidence for the role of Zn^{2+}, Ca^{2+} and Mn^{2+} in PS-3 toxicity.
Zn^{2+}, Ca^{2+} and Mn^{2+} enhanced PS-3 toxicity in Ca^{2+} free medium (A) and restored PS-3 toxicity after EGTA treatment in complete medium (B). Zn^{2+}, Ca^{2+} and Mn^{2+} also triggered PS-3 toxicity in DPBS after transient EGTA treatment (C).

There is no unified view on the role of divalent cations in Cry toxin mode of action. Some researchers claim they participate in signalling pathways. Zhang et al. showed that Cry1Ab toxicity can be abolished with EDTA, but not EGTA. This effect was interpreted as Mg^{2+} depletion based on the fact that EDTA binds Mg^{2+} more strongly than EGTA and because supplementation with magnesium salt restored toxicity (Zhang et al., 2005). Contrary to PS-3 experimental results, the chelator did not prevent Cry1Ab binding, as evidenced by the monomer and oligomer bands detected by western blots. The authors suggested the importance of Mg^{2+} in post-binding phase, specifically in cAMP synthesis and G protein stimulation (Zhang et al., 2005). PS-1 on the other hand seems to use changes in the cytosolic Ca^{2+} concentration as a

messenger system (Katayama et al., 2007). After cell injury, the levels of Ca^{2+} normally increase. This can be a rapid increase and may come from extracellular space, intracellular organelles that store Ca^{2+} or both of these (Thastrup et al., 1990). Experiments with PS-1 showed that the toxin induced Ca^{2+} influx from the extracellular environment triggering apoptosis. This influx was attributed to trimeric G-protein signalling, as suramin, which inhibits this pathway, suppressed both the Ca^{2+} influx and cytotoxicity in PS-1 treated HeLa cells (Katayama et al., 2007). In contrast to PS-1 and Cry1Ab, extracellular cations are not required for PS-3, as the toxin was still active in Ca^{2+} free medium or DPBS. Also, EGTA did not inhibit signal transduction pathways arising as a result of a post toxin-binding step. Instead it acted at an early stage by preventing a permanent toxin interaction with the membrane. However, based on experiment with chelators, the possibility of a signalling pathway playing a role in PS-3 mode of action cannot be excluded.

Another idea for the role of cations came from Fortier et al. who highlighted the importance of divalent cations, ionic strength and pH in the *Bt* mechanism of action (Fortier et al., 2005). It has been postulated that binding and pore formation could be influenced by electrostatic interactions between the toxin molecules and the membrane. Experiments using membrane potential measurements and osmotic swelling assays with BBMV showed that at higher pH values, both ionic strength and divalent cations generate a screening of the negative charges at the toxin and membrane surfaces increasing their interaction (Fortier et al., 2005). Also, data from Kirouac et al. study support the role of metal ions in processes other than signalling pathways. The authors showed that EDTA inhibited pore formation by Cry1Aa, Cry1Ac,

and Cry1Ea in isolated insect BBMV and so in a system devoid of cellular content (Kirouac et al., 2006).

The results of this study clearly indicate that PS-3 activity is abolished by means of chelating membrane bound metal ions. This could be explained by changes in conformation or functionality of a membrane receptor(s) as was proposed before to explain the EDTA effect on Cry1 toxins (Kirouac et al., 2006). Large conformational transition - from a rod-like to globular shape - in cadherin structure occurs upon the addition of EDTA (Pokutta et al., 1994). It has been further shown by Candas et al. that Ca^{2+} removal from the medium mediates cleavage of the ectodomain of cadherin BT-R1 – a target receptor for Cry1A toxin - leading to its destabilisation and proteolytic cleavage (Candas et al., 2002). A model is suggested that metal cations facilitate PS-3 toxicity by promoting receptor's structure and/or functionality as shown in Figure 109.

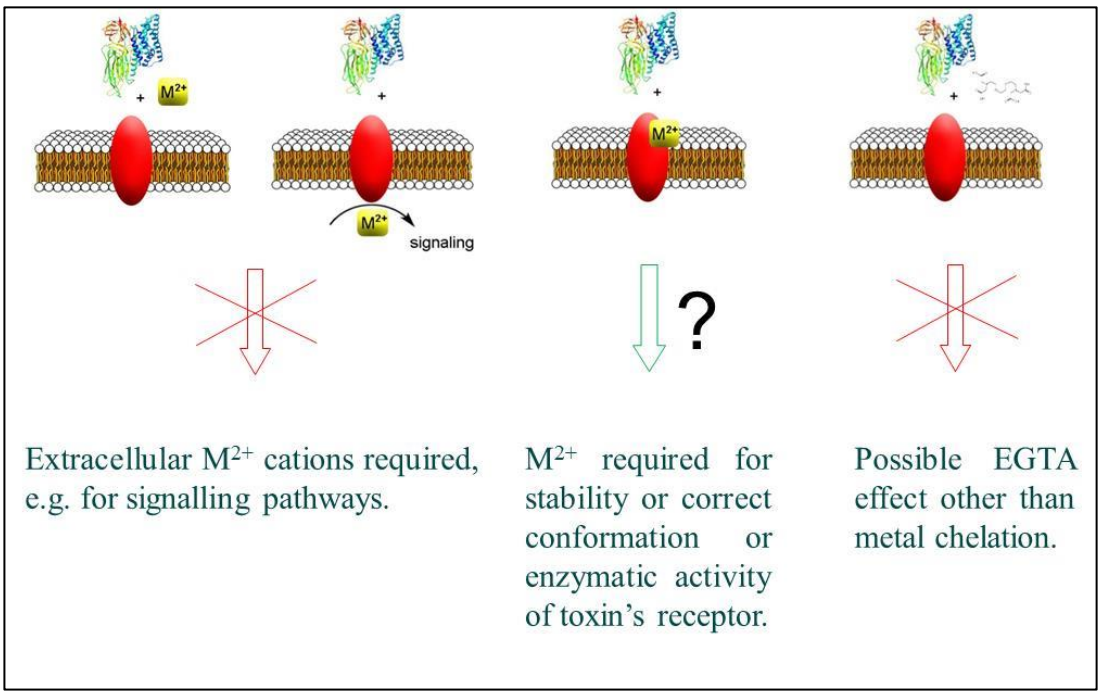

Figure 109 A proposed model for the role of divalent cations in PS-3 mode of action.
PS-3 remained toxic to HepG2 cells in DPBS, implying that extracellular metal cations are not required for toxin's activity. Also, experimental results excluded possible indirect effects of EGTA that could explain chelator's protective action. A model is proposed where metal cations (M^{2+}) facilitate PS-3 toxicity by either promoting receptor's functionality, appropriate conformation or its stability.

Ca^{2+}, Zn^{2+} and Mn^{2+} out of the metal ions tested most prominently restored or even enhanced PS-3 toxicity. Interestingly Zn^{2+} dependent metalloproteases (aminopeptidase N APN), Zn^{2+} binding proteins (alkaline phosphatase ALP) and Ca^{2+} stabilised proteins (cadherin-like proteins) have previously been identified as functional Cry toxin receptors in insects (Pigott and Ellar, 2007). The possibility that metal cations facilitate PS-3 toxicity in a cooperative fashion cannot be excluded. It may be that PS-3 requires two or more toxin receptors, each coordinating different metal. This would explain why non-specific chelators like EGTA protected cells better than e.g. DTPA. This is not a new idea; in a sequential binding model (mentioned in section 1.4) both APN and cadherin receptors have been proposed to be required for Cry1Ab toxicity towards *M. sexta* (Pacheco et al., 2009). Another possibility is that identified metals: Ca^{2+}, Zn^{2+} and Mn^{2+} show some functional redundancy. Proteins often adopt flexible metal binding sites, allowing non-specific interactions with many divalent metal cations depending on their bioavailability. However the results of salt supplementation experiments do not seem to follow the Irving-Williams rule: Mg^{2+} and $Ca^{2+} < Mn^{2+} < Fe^{2+} < Co^{2+} < Ni^{2+} < Cu^{2+} > Zn^{2+}$, with Mg^{2+} and Ca^{2+} being the weakest binding metals and Cu^{2+} and Zn^{2+} the strongest (Irving and Williams, 1953).

6. Cellular response to PS-3

6.1 Introduction

Investigating the mode of action of any toxin should not be limited to the analysis of its mechanistic behaviour but should also evaluate cellular response to this insult. Ultimately, both of these contribute to the final outcome, being either cell recovery or cell death. In this chapter five aspects of cellular response to PS-3 were examined and discussed:

- analysis of caspase 3/7 activation,
- analysis of ROS formation,
- analysis of damage permanency,
- analysis of p38 and ERK 1/2 activation,
- analysis of PKA activation.

In general, damaged cells undergo either apoptosis or necrosis. Apoptotic cell death is mediated by an intracellular program, with caspases being the main regulators. Morphologically apoptosis results in cell shrinkage, membrane blebbing, chromatin condensation and formation of apoptotic bodies. Numerous stimuli can trigger apoptosis, like intracellular signals when cells are stressed (intrinsic pathway) or extracellular ligands binding to the death receptors present in the cell membrane (extrinsic pathway). Intrinsic pathway leads to increased mitochondrial membrane permeability and extrinsic pathway results in formation of the death inducing signaling complex (DISC). In both pathways, regardless of the initial mechanisms, apoptosis is

driven by caspase activation. Initiator caspases (2, 8, 9, and 10) activate effector caspases (3, 6, and 7) which execute apoptosis by cleaving cellular proteins following aspartate amino acid residues (Li and Yuan, 2008). Common caspase targets include cytoskeletal proteins, nuclear lamins, DNases and caspases themselves. As mentioned in section 1.5, some PFTs are capable of inducing apoptotic pathway, like *S. aureus* α-toxin, listeriolysin O, and aerolysin (Guzmán et al., 1996, Imre et al., 2012, Jonas et al., 1994, Nelson et al., 1999). Cells may udergo apoptosis after exposure to low doses of toxin, even when high concentrations prompt necrosis. Activation of apoptosis was observed in HepG2 cells treated with PS-2 (from the A1547 strain), but only when a sub-lethal toxin dose was used (Ito et al., 2004). Interestingly PS-2 like protein from 4R2 strain (showing 100% sequence similarity to PS-2 from A1547 strain) induced apoptosis at a lethal dose in HepG2 and in various other cell lines (Brasseur et al., 2015b). Another parasporin - PS-1 - triggered apoptosis in HeLa cells mediated by the influx of calcium ions (Katayama et al., 2007). Apoptotic signalling was examined in PS-3 treated HepG2 cells by looking at caspase 3/7 activation.

Although, necrotic cell death is often considered accidental and uncontrolled (e.g. when caused by gross cell injury, like damage to the plasma membrane), there is more data emerging that necrosis can also be facilitated by regulated events, which is called programmed necrosis or necroptosis. Programmed necrosis is characterised by cell swelling, increase in intracellular Ca^{2+}, rapid ATP depletion, increase in ROS levels, inflammatory response and can be induced by a number of extracellular stimuli. The key signaling mediators include: receptor interacting protein (RIP) kinases, poly (ADP-ribose) polymerase-1 (PARP1), calpains and NADPH oxidases. Necrotic stimuli lead to RIP kinase activation facilitating excessive ROS production (Baines, 2010). High levels of

ROS - which can be NADPH oxidase derived or from a mitochondrial source - leads to irreversible damage to the intracellular molecules and cell death. An example of programmed necrosis in the context of exposure to PFTs comes from Kennedy et al. *Clostridium septicum* α-toxin induced a multifaceted necrotic cell death in murine myoblast cells, involving Ca^{2+} influx, calpain activation, disruption of mitochondrial activity, increased ROS levels, and a drastic drop of ATP levels (Kennedy et al., 2009). Some bacterial toxins specifically target mitochondria after entering into the host cells. They are predicted to form pores in mitochondrial membranes, ultimately affecting ROS levels and cell fate (Jiang et al., 2012). However, under physiological conditions, low levels of ROS activate various signaling pathways promoting cell growth and survival, such as tyrosine kinase, MAP kinase, NF-κB, Ras proteins, and hypoxia inducible factor α (Azad et al., 2009). Production of ROS has also been shown to exert antibacterial action (Fang, 2011). Interestingly, a number of pathogens have been demonstrated to inhibit ROS production by altering the activity of the NOX2 NADPH oxidase in order to increase survival in host cells. For example, listeriolysin O prevented NOX2 localization to the phagosomes in primary macrophages, decreasing as a consequence ROS production (Lam et al., 2011). Contribution of ROS formation to PS-3 cytotoxicity was evaluated by the analysis of H_2O_2 levels in toxin treated cells.

Cellular recovery after exposure to PFTs is dependent on many factors, among others: cell type, abundance and nature of toxin receptors, toxin concentration, and finally the toxin's mode of action and how it interacts with the membrane. For example, if a created pore is stable, cell recovery from such injury will be more challenging than if the pore is unstable. It has been demonstrated that heptamerized aerolysin is extremely stable (Lesieur et al., 1999) resulting in a slow 8 hour recovery of

membrane integrity, whereas SDS sensitive listeriolysin O oligomers generate lesions which can be restored within 1 hour (Gonzalez et al., 2011b). Cellular recovery after transient exposure to PS-3 was analysed looking at membrane integrity and cell viability in HepG2 cells.

PFTs can lead to the activation of various signalling pathways (section 1.5). p38 MAP kinase pathway has been well documented to be a conserved cellular response to different PFTs, like β-barrel and α-PFTs. A number of PFTs were shown to activate phosphorylation of p38 (listed in section 1.5), including Cry toxins. p38 pathway was activated in *C. elegans* treated with Cry5B toxin (Huffman et al., 2004) and *M. sexta* and *A. aegypti* treated with Cry1Ab and Cry11Aa respectively (Cancino-Rodezno et al., 2010). In addition to p38 pathway, it was shown that some PFTs like proaerolysin and listeriolysin O (Gonzalez et al., 2011b), *Mycobacterium tuberculosis* secretory protein ESAT-6 (Ganguly et al., 2007) and Parasporin-2 Aa1 (Brasseur et al., 2015a) also triggered activation of ERK pathway. This chapter covers the assessment of PS-3 induced activation of p38 and ERK 1/2.

The role of the PKA pathway in the *Bt* mode of action (section 1.4), although it does not have many supporters, and its work was strongly confronted (Kirouac et al., 2006), continues to be cited and has become one of the models for *Bt* Cry toxin action. Mainly for this reason, stimulation of this pathway was analysed in PS-3 treated cells, which is also presented in this chapter.

6.2 Analysis of caspase 3/7 activation

To find out if PS-3 induces the apoptotic signalling pathway in HepG2 cells, caspase 3/7 levels were measured 2, 4, 6 and 8 hours after treatment with a lethal toxin dose by measuring the luminescent signal produced by caspase cleavage of the substrate (Figure 110). Etoposide was used as a positive control, as this drug induces apoptosis in HepG2 cells by inhibiting DNA synthesis (Hande, 1998).

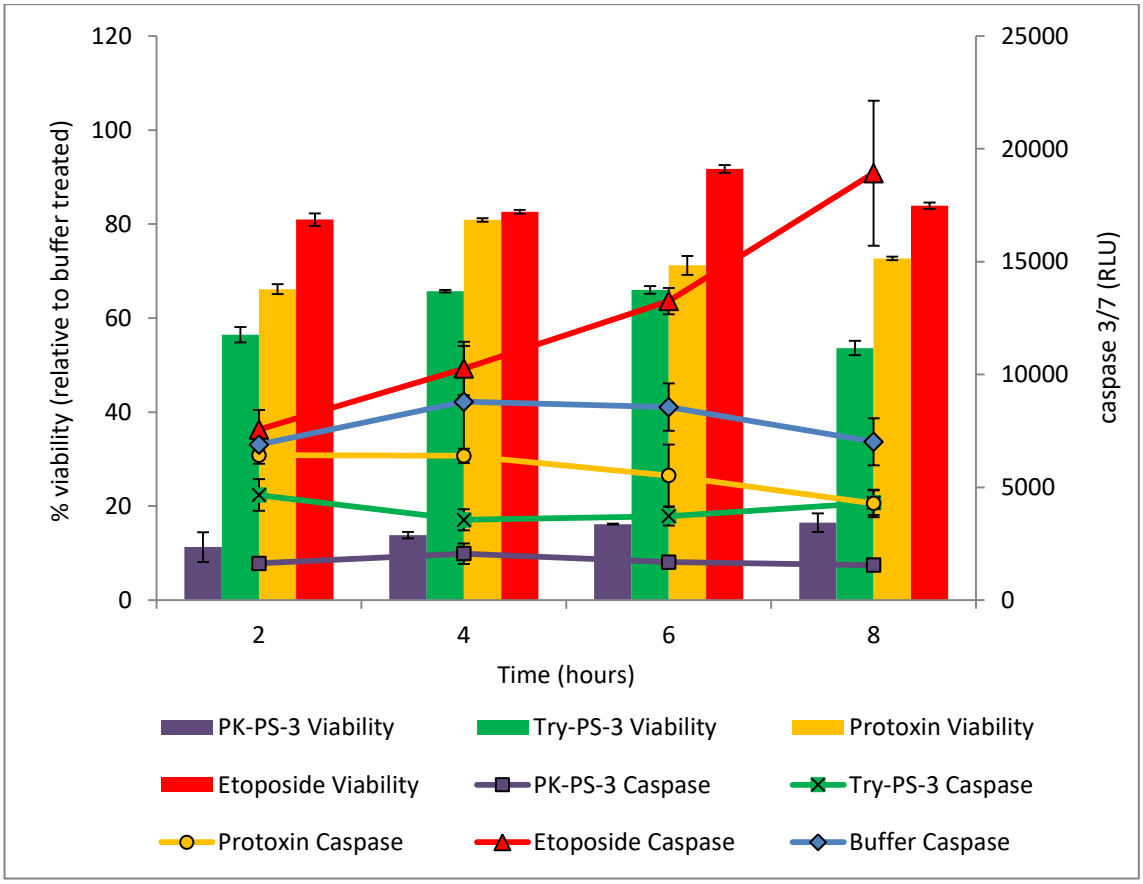

Figure 110 Assessment of caspase 3/7 activation and viability levels in PS-3 treated cells over 8 hours.
HepG2 cells were seeded at the density of 5.5 x 10^4 cells/ml in a black 96-well plate. The next day cells were treated with non-purified, dialysed toxins: protoxin (100 µg/ml), trypsin treated PS-3 (100 µg/ml), proteinase K treated PS-3 (50 µg/ml), etoposide (100 µg/ml) or buffer. Caspase and viability levels were measured at different time points over a period of 8 hours using the ApoTox-Glo Triplex Assay.

Caspase 3/7 levels were not elevated in PS-3 treated cells over the period of 8 hours. Etoposide induced caspase 3/7 activation over time.

To examine the effects of purified toxins and sub-lethal PS-3 concentrations on caspase 3/7 activation, HepG2 cells were treated with various toxin dilutions, followed by viability and caspase assessment in a multiplexed experiment (Figure 111).

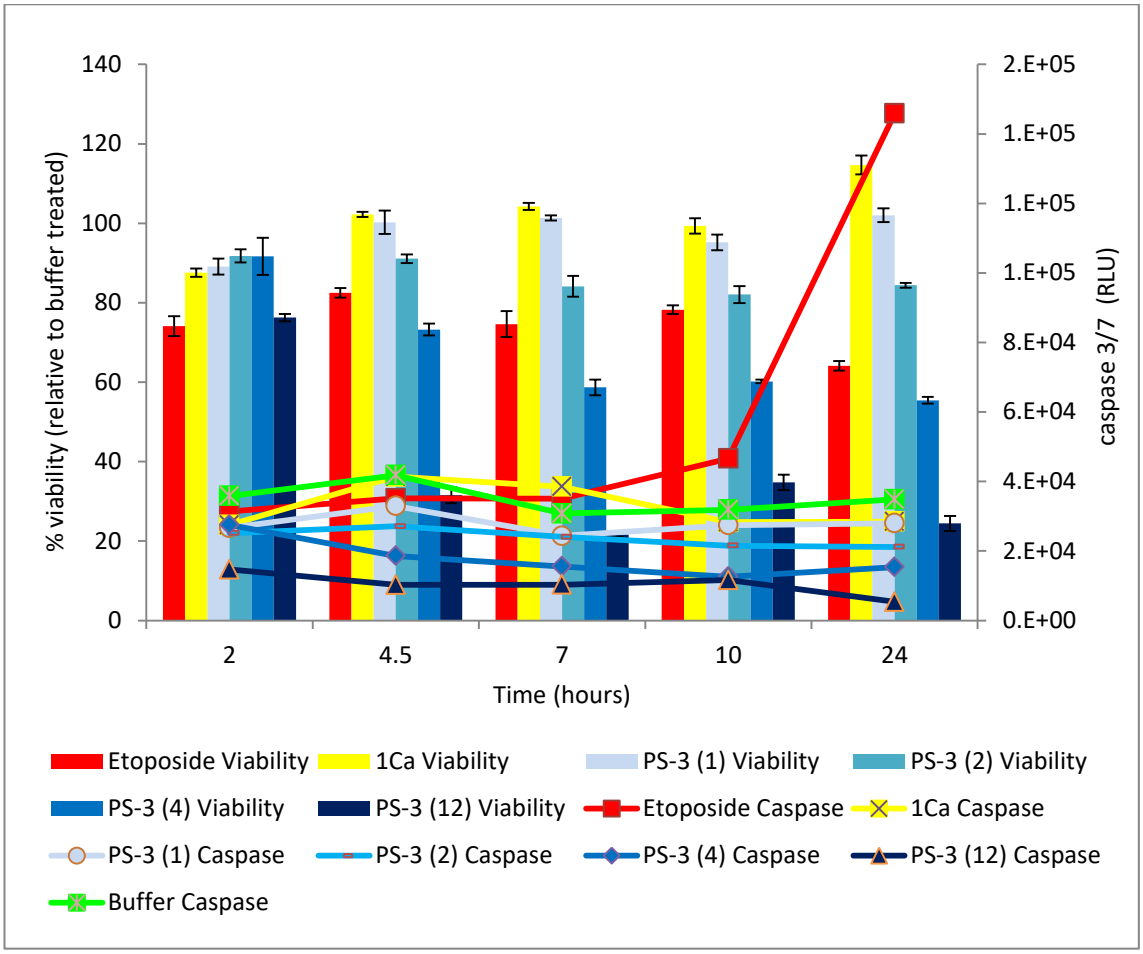

Figure 111 Assessment of caspase 3/7 activation and viability levels in PS-3 treated cells over 24 hours.
HepG2 cells were seeded at the density of 25 x 10^4 cells/ml in a black 96-well plate. The next day cells were treated with trypsin activated purified toxins: PS-3 (1, 2, 4, or 12 µg/ml), Cry1Ca (12 µg/ml), etoposide (100 µg/ml) or buffer. Caspase 3/7 levels were measured at different time points over a period of 24 hours using Caspase-Glo 3/7 assay. This was multiplexed with viability assessment using CellTiter-Blue assay as described in the methods section.

Low doses of PS-3, as well as Cry1Ca, did not result in elevation of caspase 3/7 levels in susceptible cells within 24 hours. The overall results indicate that PS-3 does not induce apoptosis at either lethal or sub-lethal doses.

6.3 Estimation of ROS levels

Hydrogen peroxide (H_2O_2) is a widely used indicator to measure ROS levels. Produced from another reactive species – the superoxide anion (O_2^-) - it is a convenient marker due to its stability and a high diffusion rate across plasma membrane (Lee et al., 2004). Some culture media may contain H_2O_2 - called abiotic ROS - that arises from spontaneous oxidation of medium components, (which can be eliminated by cells' intracellular catalase activity during culture). On the other hand pyruvic acid eliminates H_2O_2 abiotically, reacting directly with hydrogen peroxide and reducing any background signal. Due to the fact that the ROS-Glo H_2O_2 assay detects H_2O_2 regardless of its source, assessment of ROS levels in PS-3 treated cells was conducted in medium without (Figure 112) and with (Figure 113) sodium pyruvate supplementation. Menadione, a drug that causes oxidative stress was used as a positive control.

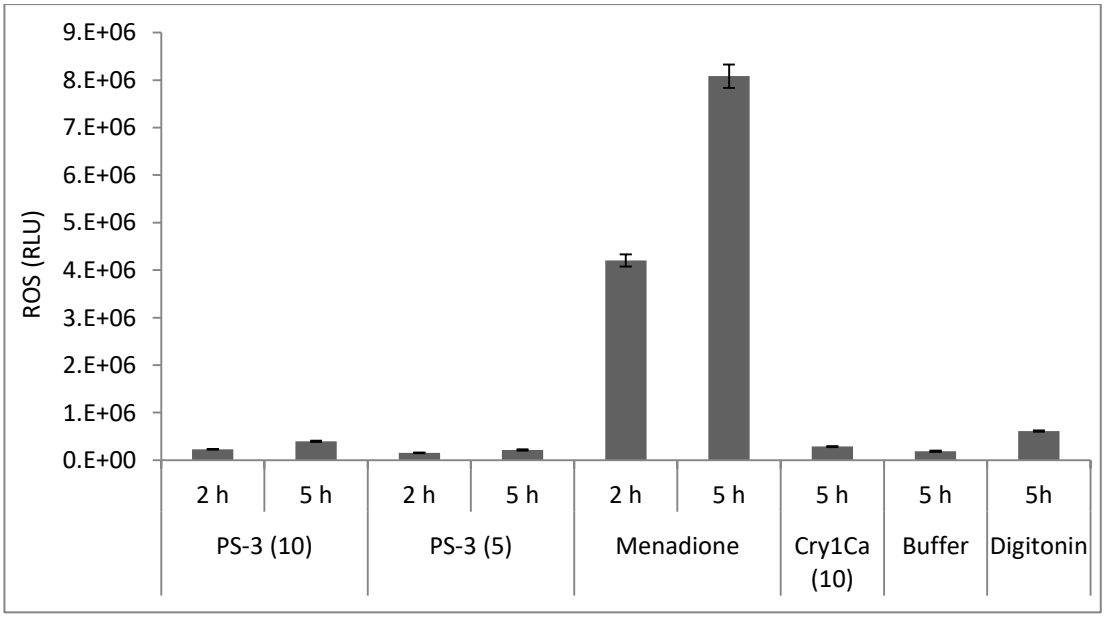

Figure 112 Estimation of H_2O_2 levels in PS-3 treated HepG2 cells in the absence of sodium pyruvate.
HepG2 cells were seeded at the density of 25 x 10^4 cells/ml in a white 96-well plate in DMEM without phenol red and without sodium pyruvate. The next day cells were dosed with H_2O_2 substrate and incubated with PS-3 (10 or 5 µg/ml), menadione (50 µM), Cry1Ca (10 µg/ml), digitonin (13 µg/ml) or buffer for indicated amount of time. Luminescent signal was measured using ROS-Glo H_2O_2 Assay.

PS-3 at a concentration of 5 or 10 µg/ml did not induce oxidative stress in HepG2 cells within 5 hours. In the absence of sodium pyruvate abiotic ROS production was very high in all no cell controls (data not shown) with values similar to that obtained for cells treated with menadione for 2 hours.

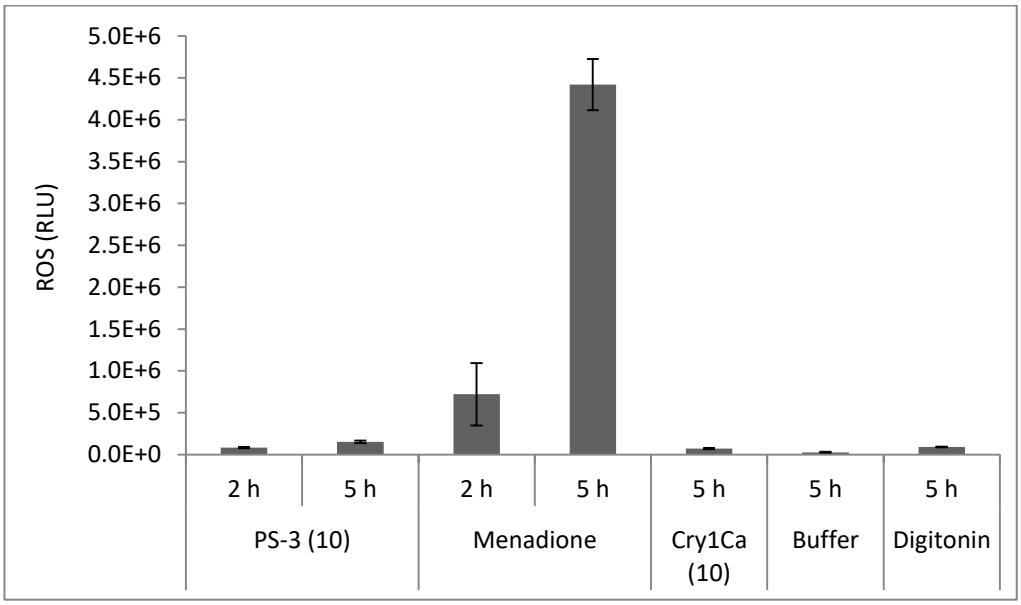

Figure 113 Estimation of H_2O_2 levels in PS-3 treated HepG2 cells in the presence of sodium pyruvate.
HepG2 cells were seeded at the density of 25 x 10^4 cells/ml in a white 96-well plate in complete DMEM (with sodium pyruvate). The next day cells were dosed with H_2O_2 substrate and incubated with PS-3 (10 µg/ml), menadione (50 µM), Cry1Ca (10 µg/ml), digitonin (13 µg/ml) or buffer for indicated amount of time. Luminescent signal was measured using ROS-Glo H_2O_2 Assay.

In the presence of sodium pyruvate abiotic ROS production was low and close to the levels observed in the presence of buffer treated cells (data not shown). Results in the presence of the cells were similar to the ones obtained in the first experiment; ROS formation in toxin treated cells was still minimal.

6.4 Evaluation of cellular recovery after transient exposure to PS-3

It was assessed whether membrane damage and decrease in viability after brief toxin treatment was transient or permanent. This could shed some light on pore stability and cells' ability to recover from the damage. HepG2 cells were pulse treated with PS-3, washed and cultured in a toxin free medium. Another group of cells were incubated continuously with the toxin. Membrane damage was detected using a cytotoxic assay measuring membrane permeability to a big protease marker. Viability and membrane permeability readings were taken at different time points (Figure 114).

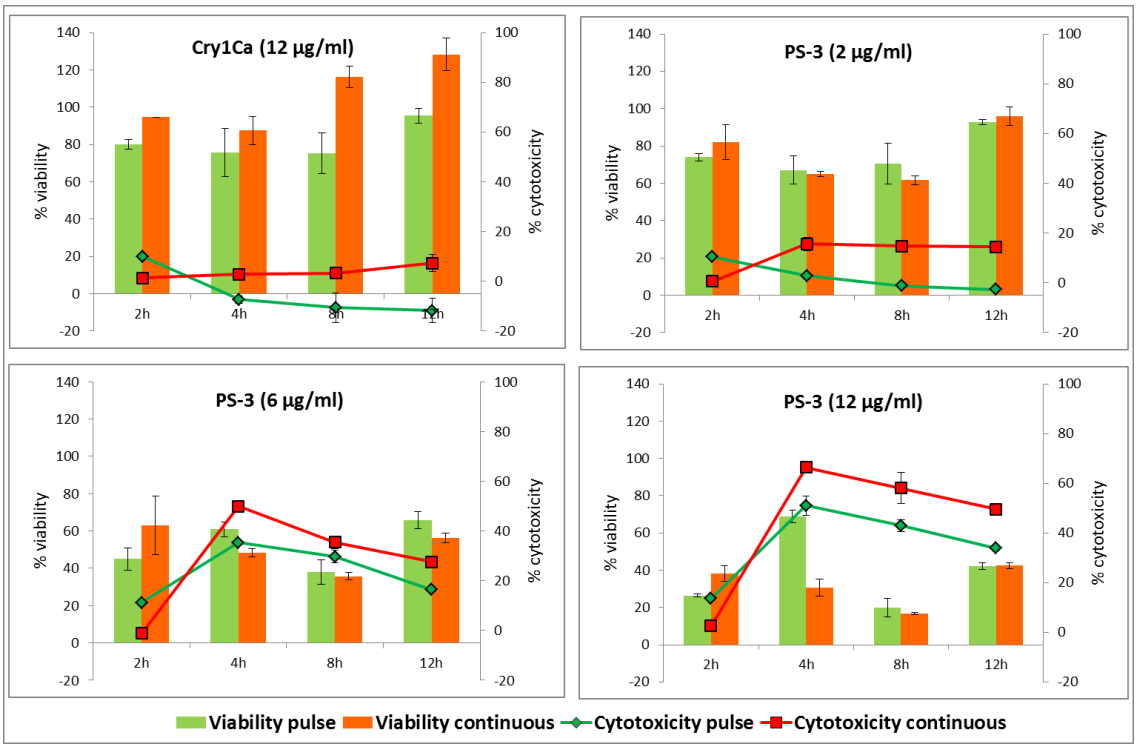

Figure 114 HepG2 cell viability and cytotoxicity after transient or continuous exposure to PS-3.
HepG2 cells were seeded at the density of 25 x 10^4 cells/ml in a white 96 well-plate. The next day cells were treated with PS-3 (2, 6, 12 µg/ml), Cry1Ca (12 µg/ml) or buffer for 20 minutes, washed twice with DPBS and cultured in a toxin free medium (pulse treatment) or continuously in the presence of toxin for 24 hours (continuous treatment). Viability was measured using CellTiter-Blue. The reagent was added to all cells at the same time and kept for the final two hours of incubation, before the reading. Viability data were DMEM subtracted and plotted as a percentage of the buffer treated cells at appropriate time point. Membrane damage was assessed using CytoTox-Glo assay. Cytotoxicity data were buffer signal subtracted and plotted as a percentage of the digitonin treated cells (43.7 µg/ml) at appropriate time point.

Viability levels were reduced in cells treated with high doses of PS-3, but there was no significant difference between pulse and continuous treatments except 4 hour time point at 12 μg/ml toxin dose. The cytotoxic assay results showed dose-dependent changes in membrane permeability. In cells treated with high doses of PS-3 (6 and 12 μg/ml) values increased in the first four hours. After that they slightly declined, regardless of the toxin exposure type. Comparing pulse with continuous exposure, cells treated with PS-3 continuously showed somewhat greater membrane damage (up to 20% difference). However, this occurred due to the relatively high cytotoxic signal in cells treated transiently with buffer and a low signal in cells treated continuously with buffer, that were subtracted from appropriate data, leading to these differences. Cell washing step (present in the pulse but not continuous treatment) most likely contributed to damage in pulse treated cells. This difference in cytotoxicity seems to result from experimental procedure rather than the toxin's activity. Overall, these results suggest that little cellular recovery occurred after transient exposure to toxin.

6.5 Activation of ERK 1/2 and p38 MAP kinase pathways

To analyse the involvement of the p38 MAPK pathway, HepG2 cell extracts after treatment with PS-3 were examined by western blotting with antibodies specific for the dually phosphorylated and non-phosphorylated forms of p38 (Figure 115). Cells were lysed in non-ionic NP-40 buffer and NP-40 containing SDS (0.5%). As mentioned in section 1.5, following p38 activation, it is translocated to the nucleus. Therefore, to make sure all phosphorylated p38 is available for detection, SDS was included to break open nuclei. Sodium arsenite, a potent p38 inducer, was used as a positive control.

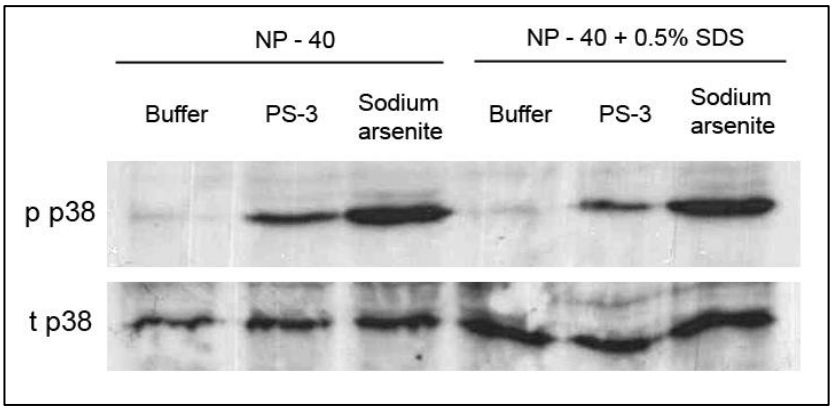

Figure 115 Analysis of p38 activation in PS-3 treated HepG2 cells extracted in NP-40 buffer with or without SDS.
HepG2 cells were treated with buffer, PS-3 (2 µg/ml), or sodium arsenite (0.5 mM) for 30 minutes. Then cells were lysed in NP-40 buffer with or without 0.5% SDS. 15 µg of protein from each sample were loaded in each lane and analysed by western blot for the presence of total (t p38) or phosphorylated (p p38) p38.

p38 phosphorylation was elevated in cells treated with an EC_{50} PS-3 dose (2 µg/ml), as well as in the positive control. Cell lysis in the presence of SDS did not yield more p p38 signal compared to cells lysed in NP-40 only. For this reason and because >0.1% SDS interferes with the Bio-Rad Protein Assay used for protein concentration measurement, further experiments involved cell lysis in just NP-40. Next, phosphorylation of p38 was assessed in cells treated with higher PS-3 concentrations (Figure 116).

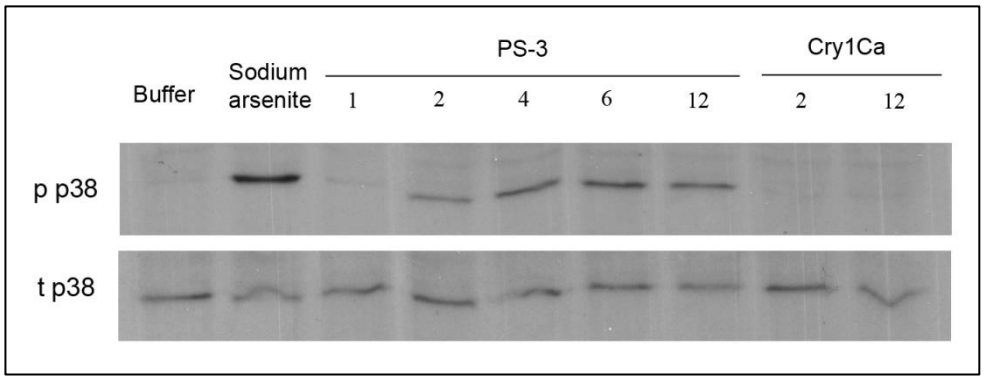

Figure 116 Analysis of p38 activation in HepG2 cells treated with various PS-3 doses.
HepG2 cells were treated with buffer, sodium arsenite (0.5 mM), PS-3 (1, 2, 4, 6, 12 µg/ml), or Cry1Ca (2, 12 µg/ml) for 15 minutes. Then cells were lysed in NP-40 buffer. 15 µg of protein from each sample were loaded in each lane and analysed by western blot for the presence of total or phosphorylated p38.

Low doses of PS-3 (1-4 μg/ml) caused p38 phosphorylation in a dose-dependent manner. The signal in cells treated with higher doses of PS-3 (4-12 μg/ml) reached a plateau. Conversely, neither low nor high doses of activated Cry1Ca produced a signal.

To characterize the temporality of PS-3 induced p38 phosphorylation, a time course from 1-15 min was investigated (Figure 117).

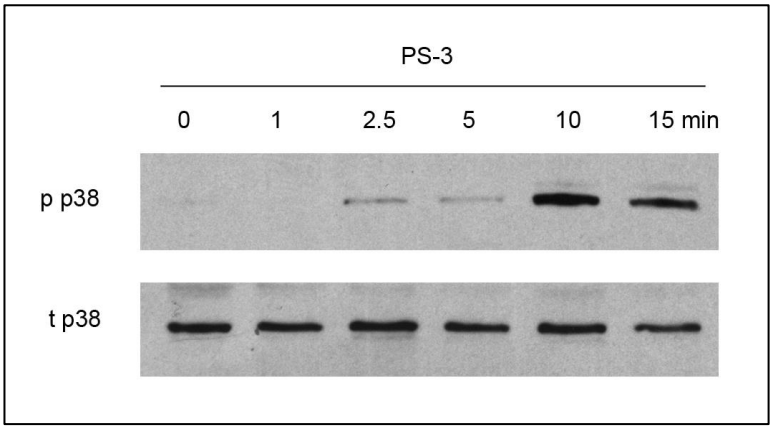

Figure 117 A time course of p38 phosphorylation in PS-3 treated HepG2 cells.
HepG2 cells were treated with PS-3 (12 μg/ml) for different amounts of time before they were lysed in NP-40 buffer. 13 μg of protein from each sample were loaded in each lane and analysed by western blot for the presence of total or phosphorylated p38.

p38 phosphorylation reached its maximum level at 10 minutes after toxin treatment. Assessment of exposures longer than 15 min was not possible with high PS-3 doses due to the cells' swelling and fragility (cell content was lost due to cells breaking open during washes).

SB202190 is a highly selective inhibitor of p38 MAP kinase, with a specificity similar to that of the widely used SB203580 (Davies et al., 2000). It selectively inhibits the α and β isoforms by binding within the ATP pocket of the active kinase and was successfully used before to inhibit p38 activity in HepG2 cells (Wu et al., 2006). Cell

viability was determined after treatment with SB202190 alone or in combination with different doses of PS-3 or sodium arsenite as shown (Figure 118).

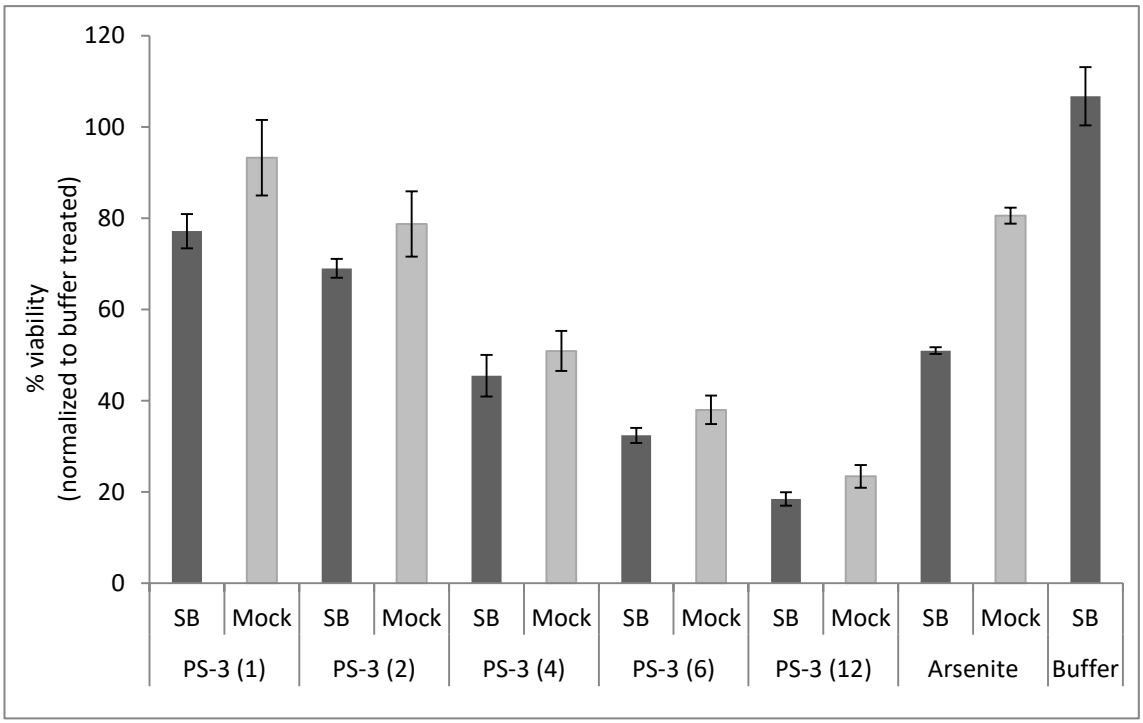

Figure 118 The effect of p38 inhibitor on HepG2 cell survival after treatment with PS-3.
HepG2 cells were seeded at the density of 25 x 10^4 cells/ml. The next day cells were incubated with SB202190 inhibitor (25 μM) or dH_2O (mock) for 30 minutes before treatment with either PS-3 (1, 2, 4, 6, 12 μg/ml), sodium arsenite (50 μM) or buffer. Cell viability was measured 24 hours after toxin treatment using CellTiter-Blue. A paired t-test (2 - tailed) indicated a statistically significant difference ($p < 0.05$) between mean viability of mock and inhibitor treated cells for each treatment with PS-3.

SB202190 moderately reduced the viability of cells treated with low or high doses of toxin after 24 hours compared to cells treated with toxin only (the inhibitor showed only slight effect after 4 hour incubation with the toxin, data not shown). SB202190 showed more acute effect on arsenic toxicity. These data suggest that activation of p38 may be part of cellular protective responses to the toxin but it cannot efficiently lead to cell recovery.

It was hypothesized that the activation of p38 MAP kinase pathway after toxin exposure would vary in different cell lines that possess different degree of

susceptibility to PS-3. To test that, p38 phosphorylation was analysed in PS-3 treated HeLa (Figure 119) and HL-60 (Figure 120) cells.

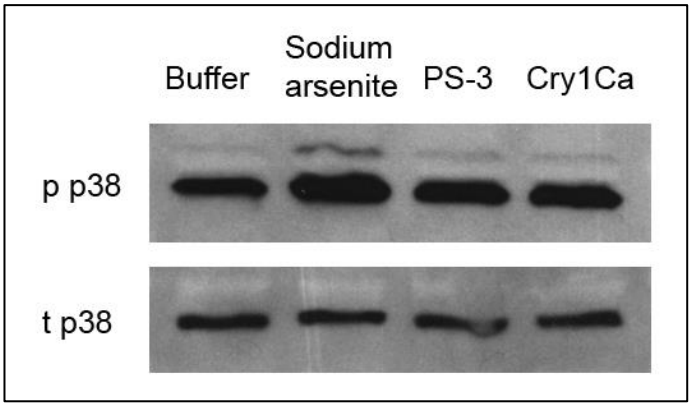

Figure 119 Assessment of p38 activation in PS-3 treated HeLa cells.
HeLa cells were treated with PS-3 (12 µg/ml), buffer, sodium arsenite (0.5 mM), or Cry1Ca (12 µg/ml) for 30 minutes. Next, cells were lysed in NP-40 buffer. 17 µg of protein from each sample were loaded in each lane and analysed by western blot for the presence of total or phosphorylated p38.

Results showed high levels of activated p38 in HeLa cells regardless of toxin exposure. The experiment was repeated with the same outcome (data not shown).

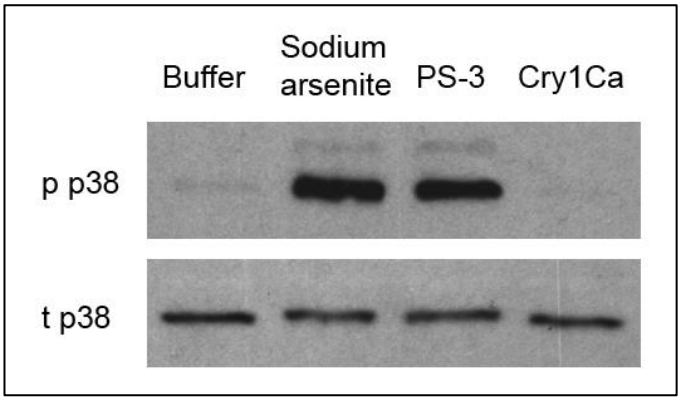

Figure 120 Assessment of p38 activation in PS-3 treated HL-60 cells.
HL-60 cells were treated with trypsin activated PS-3 (12 µg/ml), buffer, sodium arsenite (0.5 mM), or Cry1Ca (12 µg/ml) for 30 minutes. Next, cells were lysed in NP-40 buffer. 5 µg of protein from each sample were loaded in each lane and analysed by western blot for the presence of total or phosphorylated p38.

PS-3 strongly activated p38 in HL-60 cells. The experiment was repeated producing the same results (data not shown).

High levels of phosphorylated p38 in HeLa cells seem endogenous and did not differ between treatments. Activation of p38 in HL-60 was substantial in PS-3 treated cells and insignificant in the negative controls. Even though HL-60 cells showed little susceptibility to trypsin activated PS-3 (section 4.10), they were profoundly affected by PS-3 activated with proteinase K (Souissi et al. unpublished). Therefore, activation of p38 in HL-60 cells may be toxin specific.

ERK activation was assessed after treatment with PS-3 by western blotting with antibodies detecting individually-, dually- or non-phosphorylated forms of ERK 1 and ERK 2 (Figure 121).

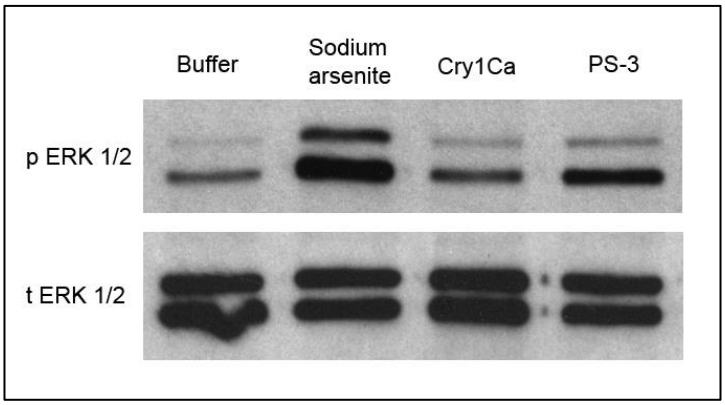

Figure 121 Analysis of ERK 1/2 phosphorylation in HepG2 cells exposed to PS-3.
HepG2 cells were treated with PS-3 (12 µg/ml), buffer, sodium arsenite (0.5 mM), or Cry1Ca (12 µg/ml) for 15 minutes. Next, cells were lysed in NP-40. 10 µg of protein from each sample were loaded in each lane and analysed by western blot for the presence of total (t ERK) or phosphorylated (p ERK) ERK 1/2.

Signal of ERK 1/2 activation in PS-3 treated cells was slightly elevated compared to cells treated with buffer or Cry1Ca. The experiment was repeated and included more PS-3 concentrations (Figure 122). Loaded samples came from the same source as samples loaded in the experiment presented in Figure 116.

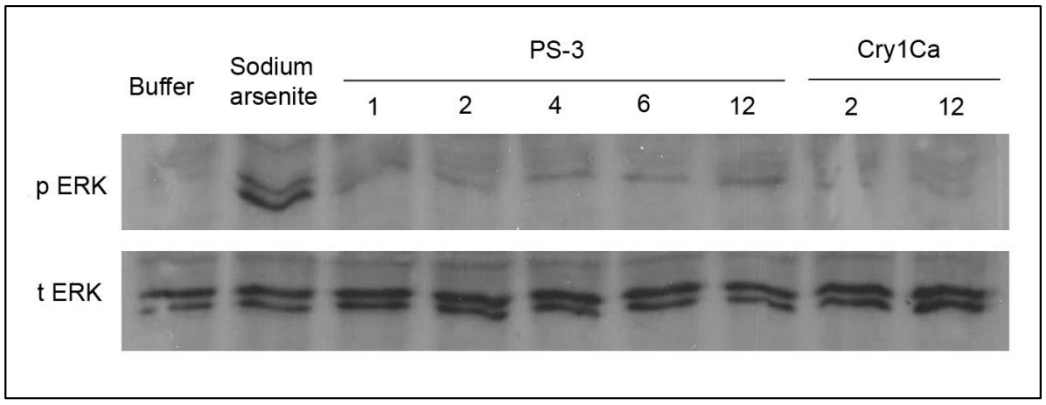

Figure 122 Analysis of ERK 1/2 activation in HepG2 cells treated with various PS-3 concentrations.
HepG2 cells were treated with buffer, sodium arsenite (0.5 mM), PS-3 (1, 2, 4, 6, 12 µg/ml) or Cry1Ca (2, 12 µg/ml) for 15 minutes. Then cells were lysed in NP-40 buffer. 15 µg of protein from each sample were loaded in each lane and analysed by western blot for the presence of total or phosphorylated ERK 1/2.

Results confirmed that 15 minute cell exposure to PS-3 induced only slight activation of ERK 1/2. Similarly to p38, a time course or ERK 1/2 activation was analysed from 1-15 minutes (Figure 123). Loaded samples came from the same source as samples loaded in the experiment presented in Figure 117.

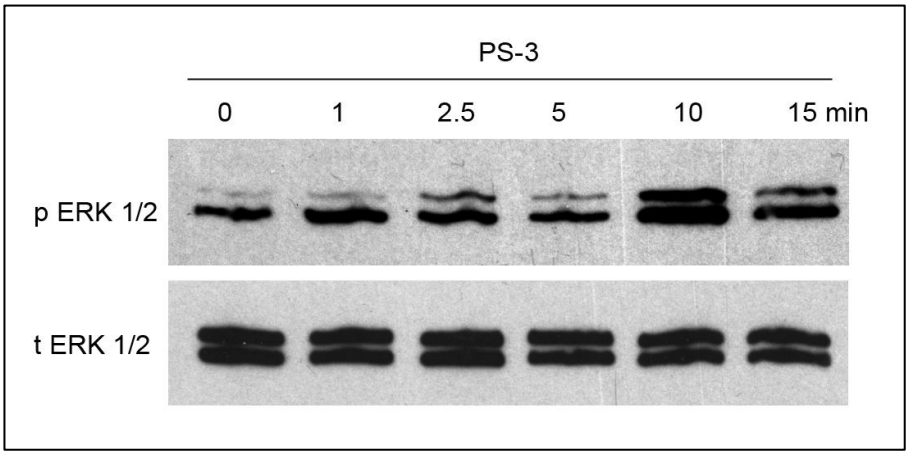

Figure 123 A time course of ERK1/2 phosphorylation in HepG2 cells treated with PS-3.
HepG2 cells were treated with PS-3 (12 µg/ml) for different amounts of time before they were lysed in NP-40 buffer. 13 µg of protein from each sample were loaded in each lane and analysed by western blot for the presence of total or phosphorylated ERK 1/2.

Similarly to p38, ERK 1/2 phosphorylation reached its maximum level at 10 minutes after exposure. Activation of ERK1/2 pathway by PS-3 was evident, however without testing specific inhibitors little can be concluded about its role in cellular protection.

6.6 Analysis of PKA activation

The effect of PKA inhibitors was tested on PS-3 activity in a viability assay (Figure 124).

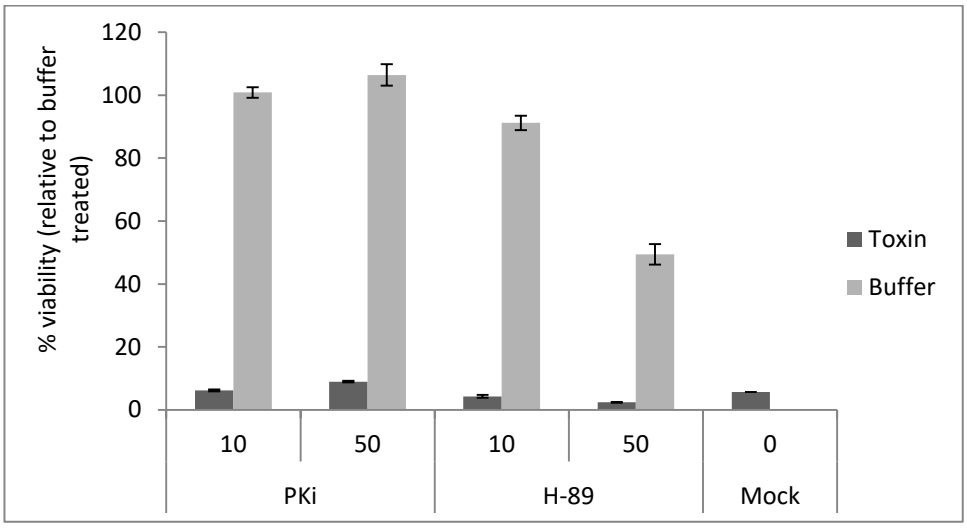

Figure 124 The effect of PKA inhibitors on PS-3 toxicity.
HepG2 cells were seeded at the density of 25 x 10^4 cells/ml in Advanced DMEM. The next day cells were pre-treated with H-89 (10 or 50 µM) or PKi (10 or 50 µM) for 30 minutes. Next, PS-3 was added (12 µg/ml) and viability was measured 6 hours later using CellTiter-Blue.

Neither H-89 nor PKi prevented toxin activity. Cell viability was still reduced and neither inhibitor rescued cells from PS-3 induced swelling. At 50 µM H-89 significantly decreased HepG2 viability in control cells.

To validate these results, another approach was adopted. After activation, catalytic PKA domains diffuse from cytoplasm into the nucleus where they phosphorylate many nuclear factors, CREB being the major one (Lodish, 2008). PKA activity in PS-3 treated cells was therefore investigated by western blot analysis of CREB phosphorylation (p CREB). 8-bromo-cAMP (8-br-cAMP), a cAMP analogue and activator of PKA, was used as a positive control and functionality of previously used PKA inhibitors was also assessed (Figure 125).

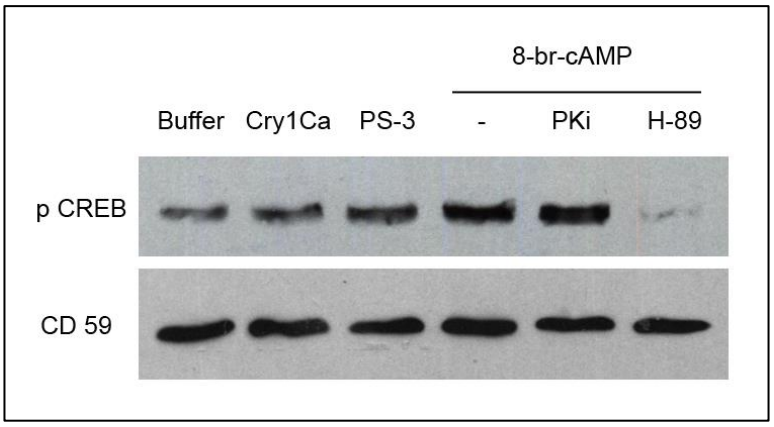

Figure 125 Analysis of CREB activation in PS-3 treated cells and analysis of PKA inhibition efficiency.
HepG2 cells were seeded in complete DMEM. 24 hours before the experiment medium was changed to Advanced DMEM. Cells were treated with either PKi (50 µM), H-89 (100 µM) or water for 30 minutes. Next, 8-br-cAMP (0.5 mM) was added and cells were incubated for another 30 minutes, before cell lysis in NP-40. Another set of cells were treated with either PS-3 (15 µg/ml), Cry1Ca (20 µg/ml) or buffer for 15 minutes, before cell lysis in NP-40. 20 µg of protein from each sample were loaded in each lane and analysed by western blot for the presence of phosphorylated CREB (p CREB) or CD59 (loading control).

Control cells showed high endogenous levels of p CREB. There was no significant increase in CREB phosphorylation in cells exposed to PS-3. 8-br-cAMP slightly elevated p CREB levels, which was evidently inhibited by H-89 but not PKi. To confirm this result experiment was repeated using SDS containing RIPA buffer for harsher cell lysis, nuclear membrane disruption as well as increased dose of 8-br-cAMP (Figure 126).

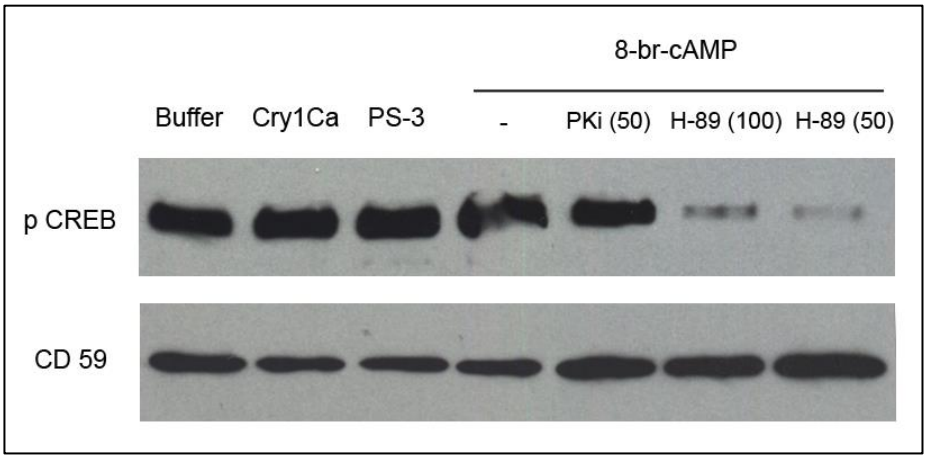

Figure 126 Analysis of CREB activation in PS-3 treated cells and analysis of PKA inhibition in RIPA lysed cells.
HepG2 cells were seeded in complete DMEM. 24 hours before experiment medium was changed to Advanced DMEM. Cells were treated with either PKi (50 µM), H-89 (50 or 100 µM) or water for 30 minutes. Next, 8-br-cAMP (1 mM) was added and cells were incubated for another 30 minutes, before cell lysis in RIPA. Another set of cells were treated with either PS-3 (15 µg/ml), Cry1Ca (15 µg/ml) or buffer for 15 minutes, before cell lysis in RIPA. 10 µg of protein from each sample were loaded in each lane and analysed by western blot for the presence of p CREB and CD59.

In general, p CREB signal was stronger when cells were lysed in RIPA (despite lower protein amount loaded per lane), which additionally lysed nuclear proteins. However, results showed similar information: p CREB was equally present in cells exposed to PS-3 or buffer only, and H-89 - but not PKi - inhibited CREB activation.

6.7 Discussion

Several methods have been developed to detect apoptosis. Activation of caspase 3/7 is widely accepted as a reliable apoptotic indicator since this protease is an important effector caspase associated with the initiation of apoptosis. PS-3 did not induce caspase 3/7 activation. Even 24 hour exposure to a low toxin dose did not elevate their levels. These results indicate that the PS-3 mediated cell death is primarily non-apoptotic.

Analysis of ROS results points to a suggestion that formation of reactive oxygen species is not part of PS-3 induced cytotoxicity, viewed whether as a marker of programmed necrosis or one of cellular protective responses. However, ROS-independent programmed necrosis cannot be excluded as some cells like macrophages, HT-29, and Jurkat cells undergo programmed necrosis independent of ROS formation (Moquin and Chan, 2010).

Formation of oligomeric structures and pore forming activity have been demonstrated for some of Cry toxins, reviewed in Bravo et al. (Bravo et al., 2007), but stability of created pores was often not assessed in a biological context. For example, experiments with ionic currents in artificial lipid bilayers revealed formation of stable

channels by oligomeric Cry1Ab (Rausell et al., 2004), but these experiments disregard cellular mechanisms leading to membrane resealing. Some of the pioneer research work on innate immunity against Cry toxin was done by the Aroian group. Among other cellular responses, rapid and efficient membrane resealing was demonstrated in vivo in *C. elegans* after Cry5B exposure via endocytic and exocytic vesicle trafficking pathways (Los et al., 2011).

In an attempt to understand the stability of lesions created by PS-3, viability and membrane damage were estimated after transient and continuous treatment with PS-3. Viability results were quite erratic over time regardless of the treatment, similar to the 24 hour viability time-course experiment (Figure 40), indicating that this type of assay may be unsuitable for over time cell viability monitoring. The decline in cytotoxic signal after 4 hours in cells treated with high PS-3 concentrations was most likely due to the decreased activity of the protease marker released from dead cells. According to the manufacturer its half-life is estimated to be around 10 hours (Niles et al., 2007). In this situation, where cell death occurred rapidly and the incubation time was greater than 10 hours, the degree of cytotoxicity at 12 hours was probably underestimated. As mentioned earlier, the differences in the degree of membrane damage in pulse and continuous treatments resulted most likely from experimental procedure and should not be attributed to the toxin's action. After the initial 4 hours the cytotoxic curves representing pulse and continuous treatments were quite similar with no significantly descending trend, suggesting that little recovery of damaged membrane occurred over time in pulse or continuous treated cells. It has been suggested that when cells are exposed to a high dose of PFT, they die quickly as a result of rapid and irreversible membrane damage; and when the dose is sub-lethal, or exposure brief, cells have the

ability to respond to the insult and produce signals promoting protection mechanisms, like restoring membrane integrity (Gonzalez et al., 2011b). HepG2 cells had no ability to repair the membrane within 12 hours even though toxin exposure lasted only 20 minutes, which indicates permanent membrane damage and implies formation of stable pores. This is consistent with experimental results presented in Figure 42, Figure 43 and Figure 93, where transient exposure to PS-3 resulted in low cell viability. Also, formation of stable pores was demonstrated for PS-3 in PLB experiments, and inhibition of p38 activity, discussed later, was almost indifferent to cell fate. However, alternative methods are needed to assess cellular recovery as cell assays used here seem unsuitable. For example, continuous real-time monitoring of viability and cytotoxicity using non-toxic reagents would solve the problem of erratic data and time constraints due to short half-life of the marker enzyme.

It is thought that PFTs induce the p38 MAPK pathway via osmotic stress following pore formation (Porta et al., 2011, Ratner et al., 2006); however, other studies had demonstrated that the p38 activation was not caused directly by osmotic stress but by ionic imbalance, specifically loss of intracellular potassium (Gonzalez et al., 2011b, Kloft et al., 2009). Despite these differences, the authors of these studies agree that membrane damage is a prerequisite for p38 phosphorylation, as defective in pore formation mutants did not cause activation of p38 (Kloft et al., 2009, Ratner et al., 2006), which was mentioned in section 5.3. In HepG2 cells p38 was phosphorylated after exposure to lethal or sub-lethal toxin doses and the maximum signal was reached at 10 minutes post-treatment. HepG2 cells did not show any swelling or other morphological changes after 10 minute incubation with the toxin (even at the time of cell lysis at 15 minutes), indicating that swelling was not the direct cause of p38

activation. Rather, it may depend on the degree of cell susceptibility and membrane damage as PS-3 induced p38 activation in HepG2 and HL-60, but not so in HeLa cells. This is consistent with the viability results of HL-60 being partially affected and HeLa not being affected by 12 μg/ml PS-3 treatment (Figure 81 and Figure 79 respectively).

Published data suggest a differential role of p38 after attack by PFTs. Neural cells exposed to pneumolysin underwent p38 dependent apoptosis (Stringaris et al., 2002). Inhibition of p38 had a detrimental effect on the ATP recovery in keratinocyte cells treated with Staphylococcal α toxin, but had no effect when cells were treated with streptolysin O (Husmann et al., 2006). Finally, p38 MAP kinase pathway was shown play a pivotal role in *C. elegans* defence against Cry5B. Two downstream transcriptional targets were identified, one of them interestingly being a homolog of a human cation efflux transporter (Huffman et al., 2004). Additionally, experiments using p38 inhibitor caused hypersensitivity to aerolysin in hamster kidney cells (Huffman et al., 2004). The authors speculate that despite a conserved mechanism of p38 activation, cells have evolved to cope with membrane damage using different strategies; depending on pore size and/or its stability. For example, cells would initiate exo- and endo-cytosis based repair to deal with large channels but may rely on various signalling pathways, p38 being one of them, in response to small pores (Aroian and van der Goot, 2007, Husmann et al., 2006).

p38 MAP kinase pathway, although activated in PS-3 treated cells, does not seem to be greatly beneficial as SB202190 only moderately reduced cell viability even in cells exposed to sub-lethal toxin doses. Presumably the inhibitor suppressed, to some degree, cellular recovery making cells less able to withstand the injury but

further studies involving the identification of downstream p38 MAPK targets are a prerequisite for better understanding. SB202190 showed a more profound effect on arsenite toxicity. Sodium arsenite was demonstrated to induce p38 dependent apoptosis in neural cells (Namgung and Xia, 2000). However the mechanism of action in HepG2 seems to be different as the inhibitor did not rescue cell viability. This is in agreement with a previous study by Qi et al. who showed that SB202190 also enhanced cytotoxicity of arsenic species in HepG2 (Qi et al., 2012). Unfortunately, the inhibitor's functionality was not assessed in a western blot as SB202190 prevents p38 activity but not its activation. Antibodies against downstream p38 targets should be used to achieve that.

Depending on cell type and stimulus ERK 1/2 MAP kinase pathway has been shown to control cell survival by regulating the activity of pro- and anti - apoptotic transcription factors (Cagnol and Chambard, 2010, Lu and Xu, 2006). PS-2 Aa1 activated both apoptosis and ERK 1/2 phosphorylation in PC-3 cells (prostate cancer cell line) and role of this MAPK pathway in apoptosis was postulated. However, a specific ERK 1/2 inhibitor did not protect the cells from toxin induced apoptosis (Brasseur et al., 2015a). Another role for the ERK pathway after PFT injury was suggested by Gonzalez et al. They suggested that both p38 and ERK pathways play a role in the recovery of ion homeostasis as inhibition of either of these significantly diminished restoration of intracellular K^+ in intestinal human cell line after listeriolysin O or aerolysin exposure (Gonzalez et al., 2011b). PS-3 induced ERK 1/2 activation was slight but clearly evident at 10 minutes after treatment. Yet, without examining signalling events linked to the activation of this pathway and experiments with ERK inhibitors, little can be concluded about its role in the cellular response to PS-3.

To test whether PKA has a specific role in PS-3 toxicity, the effect of PKA specific (PKi) and non-specific (H-89) inhibitors was assessed on the toxin's action. Neither H-89 nor PKi prevented PS-3 activity. Additionally, phosphorylation of CREB - one of PKA targets - was analysed. CREB has been shown to be activated by various kinases, like: PKA, PKC, CaM KI, CaM K II, CaM KIV and others (Bito et al., 1996). PKi specifically inhibits PKA, whereas H-89 inhibits PKA and other kinases like PKC, Casein Kinase I, MLCK, CaM KII, Rho Kinase II (Lochner and Moolman, 2006). Western blot results clearly indicate that endogenous levels of p CREB arise in HepG2 cells due to kinase activity that is inhibited by H-89, but other than PKA, as H-89 but not PKi inhibited the signal. These and cell viability results signify that neither PKA nor any other kinase mentioned earlier and inhibited by H-89 play a role in the PS-3 mode of action.

7. In search for the receptor

7.1 Introduction

Detailed information about Cry toxin receptors was given in section 1.6. This chapter presents experiments based on different strategies used to identify PS-3 receptor; they are graphically presented in Figure 127.

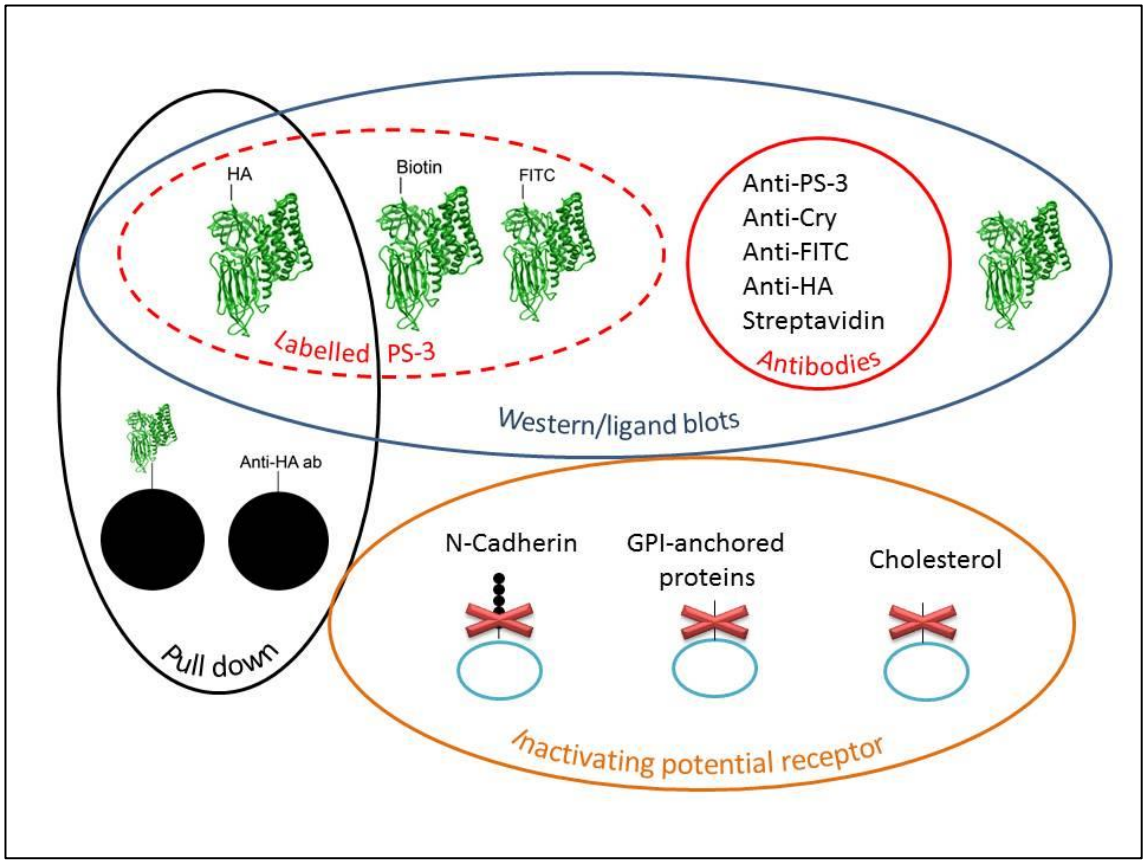

Figure 127 Different strategies used in an attempt to identify PS-3 receptor.
Strategies for the PS-3 receptor identification involved three main types of assays: pull down with directly and indirectly (via HA tag) immobilized toxin, ligand and western blots with labelled and non-labelled PS-3 and viability cell assays where cells were depleted of a certain membrane component.

Ligand blotting constituted a big portion of experiments aimed at receptor recognition. This method has been successfully used before for the detection of Cry toxin receptors

as well as to study interactions between receptors and Cry toxins (Budatha et al., 2007, Contreras et al., 2013, Hayakawa et al., 2004, Krishnan et al., 2010, Shitomi et al., 2006). In principle, membrane proteins are separated using SDS-PAGE. The gel is then blotted onto a nitrocellulose membrane. This is followed by membrane incubation with the toxin, which is often labelled. Providing that the toxin binds to the receptor, the complex can be then detected by antibody against the toxin or the tag attached to it. PS-3 was labelled with different labels: FITC, biotin, HA tag. Additionally genetic engineering was done on the HA-labelled PS-3 to improve its function as a probe. Two buffers used for cell lysis included harsh denaturing ionic RIPA and mild non-ionic NP-40. In later experiments N-octyl glucoside (NOG), a non-ionic detergent frequently used for the solubilisation of membrane proteins, was used.

Pull down is another technique for the identification of protein-protein interactions. The advantage of this approach is that both toxin and cellular proteins are in their native state (providing that non-denaturing lysis buffer like NP-40 or NOG was used for cell lysis). In pull down experiments PS-3 was either directly immobilised to the beads via sulfhydryl groups or indirectly via the HA tag. Beads were then exposed to the HepG2 cell extract, washed, spun and different fractions were analysed on a gel.

The nature of the receptor was investigated by manipulating the membrane of susceptible cells and observing how it affected PS-3 activity. Lipid rafts are detergent resistant domains of the plasma membrane that contain high levels of cholesterol, sphingolipids and glycosylphosphatidylinositol (GPI-) anchored proteins, which are involved in signal transduction and protein sorting (Simons and Toomre, 2000). Lipid rafts are the targets for many bacterial PFTs, including insecticidal Cry toxins (Diep et

al., 1998, Giddings et al., 2004, Gordon et al., 1999, Zhuang et al., 2002) and some parasporins (Abe et al., 2008). Consequently, cholesterol and GPI-anchored proteins are plausible candidates for PS-3 receptors. Especially that they have been identified as receptors for PFTs before (Diep et al., 1998, Gordon et al., 1999, Heuck et al., 2010). The effect of depletion of these two biological molecules was tested on PS-3 toxicity. To study the role of GPI-anchored proteins in cytotoxicity, phosphatidylinositol-specific phospholipase C (PI-PLC) was used to enzymatically remove GPI-anchored proteins from the cell membrane. In order to reduce membrane cholesterol, cells were pre-treated with methyl-β-cyclodextrin - MβCD, which increases the solubility of membrane lipids. Also, blocking of N-cadherin was attempted with the antibodies against that protein.

7.2 Different anti-Cry antibodies

Initial attempts to detect PS-3 in western blot experiments involved the use of antibodies against other Cry toxins (Figure 128). The probability of PS-3 being recognised by any of them was high as antibodies were polyclonal and had been raised against three-domain class of Cry toxins.

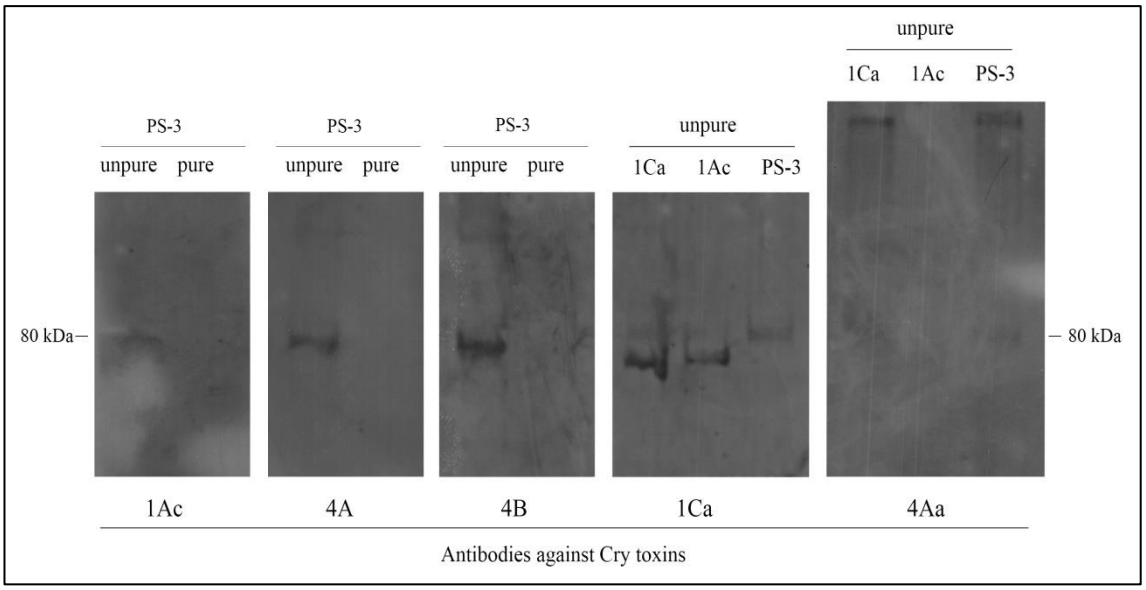

Figure 128 Detection of purified and non-purified PS-3 using antibodies against other three domain Cry toxins. Toxin samples were run on 7.5% SDS-PAGE gels: non-purified (580 µg/ml) or ÄKTA purified trypsin activated PS-3 (50 µg/ml), Cry1Ca (266 µg/ml), Cry1Ac (220 µg/ml). After transfer membranes were cut and incubated overnight with appropriate primary antibody diluted 1:2000 v/v. The next day the membranes were incubated with secondary antibody and detected with ECL.

Most antibodies were able to detect the non-purified form of PS-3, except the antibody raised against Cry3Aa (data not shown). None of the antibodies bound to purified PS-3, which may indicate that antibodies were binding to some impurity in the non-purified form of the toxin and that there is no specific binding to the toxin itself, especially that these antibodies were raised against not highly purified proteins that had been cut out of SDS gel. Bands detected in PS-3 and Cry1Ca lanes exposed to anti-Cry1Ca or anti-Cry4Aa antibodies were almost identical. Explanation may come from the fact that both recombinant Cry1Ca and PS-3 were produced in the same *Bt* strain. Due to the fact that only one of two PS-3 bands was detected and only in non-purified form, the above mentioned antibodies were not used in further experiments.

7.3 Anti-PS-3 antibody and its purification

Preparation of immunogen

Trypsin activated PS-3 with ricin domain deleted (ricin Δ PS-3) was purified by size exclusion chromatography and concentrated to be used as immunogen (Figure 129). Ricin Δ PS-3 was chosen - and not PS-3 - to obtain one band after protease cleavage. More importantly, presence of the ricin B lectin domain was found in many other carbohydrate binding proteins (Hazes, 1996), and so antibodies raised against the non-truncated PS-3 could bind directly to the cell extract increasing non-specific background.

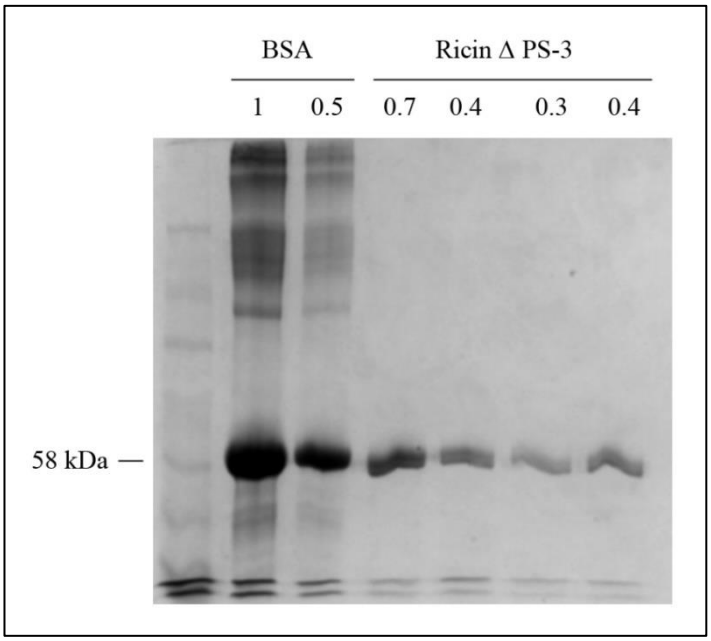

Figure 129 Purification of ricin Δ PS-3.
Trypsin activated ricin Δ PS-3 was purified and concentrated into four stock samples. Protein concentration was measured and samples were run on a 7.5% SDS-PAGE gel: 0.7, 0.4, 0.3 and 0.4 mg/ml. 1 and 0.5 mg/ml BSA samples are included for intensity comparison.

Purified samples were sent to Dundee Cell Products for delivering rabbit polyclonal affinity purified antibodies against ricin Δ PS-3.

Western and ligand blots using anti-PS-3 antibody

Affinity purified anti-PS-3 antibody was obtained at a concentration of 5 mg/ml. Its cross-reactivity with cell extract proteins was analysed in a western blot (Figure 130).

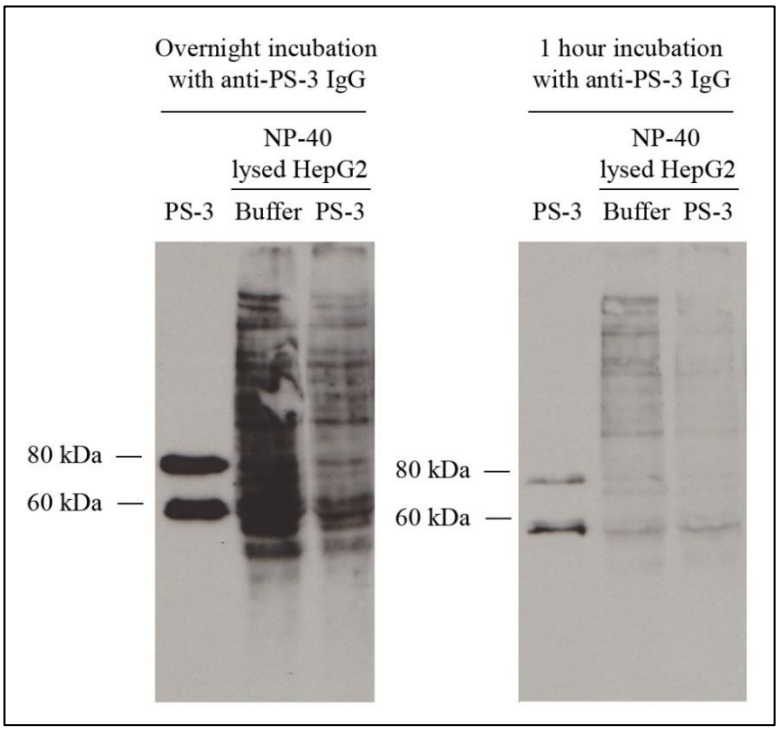

Figure 130 Western blot analysis of the cross-reactivity of anti-PS-3 antibody with cellular proteins.
HepG2 cells were treated with either non-purified trypsin activated PS-3 (81.7 µg) or buffer for 20 minutes before being lysed with NP-40. Samples were run on 7.5% SDS-PAGE gels followed by western blot with anti-PS-3 antibody (PS-3 IgG). Purified trypsin activated PS-3 was included as a control. 11 µg of protein per well were loaded in lanes with cell extracts; 0.3 µg of purified toxin. Membrane on the left was incubated with anti-PS-3 antibody (0.7 µg/ml) overnight at 4°C, whereas membrane on the right for 1.5 hours at RT.

Both upper and lower toxin bands of trypsin activated PS-3 were detected by the antibody. No additional bands were spotted in the lanes with cell extract treated previously with toxin compared to cells treated with buffer. Finally, there was a high non-specific binding in the lanes with cell extract and various conditions were investigated to decrease it:

- Blocking solution: milk or BSA (various concentrations: 3-7%),
- Blocking time (1 hour at RT – overnight at 4°C),

- Concentration of PS-3 in ligand blot experiments (2.4 – 12 µg/ml),
- Incubation time with PS-3 (1 hour at RT – overnight at RT),
- Concentration of anti-PS-3 antibody (0.5- 2.5 µg/ml),
- Incubation time with anti-PS-3 antibody (1 hour at RT– overnight at 4°C),
- Concentration of secondary antibody (0.25 – 0.5 µg/ml),
- Washing buffer: PBST or TBST (Tween-20: 0.02 - 0.1%).

However despite changing the above, the non-specific background signal remained visible. Cross-reactivity was independent of the lysis buffer used (RIPA, NP-40 or NOG) and was also high for HeLa cell extracts (data not shown).

To ensure total protein analysis, debris pellets formed after centrifugation of the lysates were resolved on a gel alongside soluble protein fractions in a ligand blot experiment with PS-3 and anti-PS-3 antibody (Figure 131).

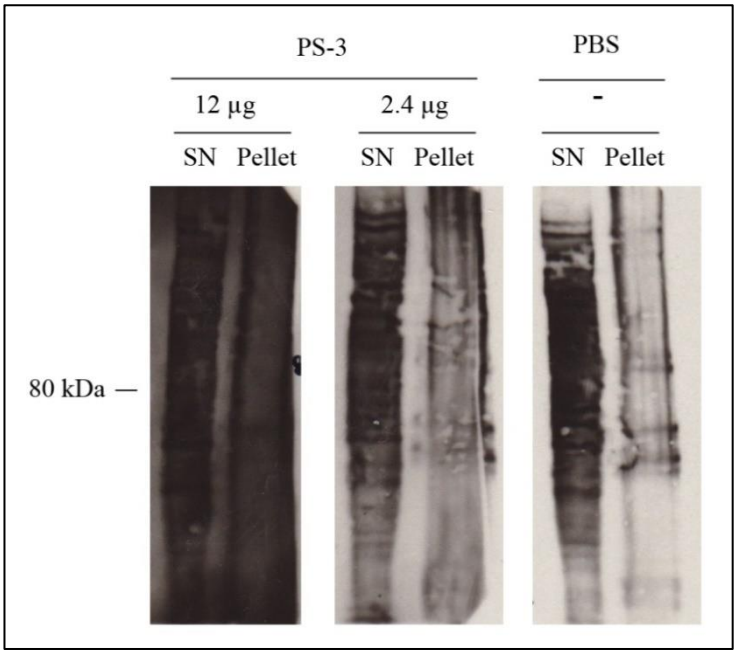

Figure 131 Ligand blot analysis of pellet and soluble HepG2 protein fractions with PS-3 and anti-PS-3 antibody. HepG2 cells were lysed with RIPA. Soluble fractions (SN) and pellets after lysis were run on a 7.5% SDS-PAGE gel. 11 µg of protein per well were loaded in lanes with cell extracts. After transfer membrane was cut and pieces were incubated with 12, 2.4 or 0 µg of purified PS-3 in PBS followed by incubation with anti-PS-3 antibody (1 µg/ml) and ECL detection.

Proteins present in the pellet, similarly to soluble fractions, did not specifically associate with the toxin. Cross-reactivity with anti-PS-3 antibody was high. Increasing the amount of PS-3 during membrane-toxin incubation step increased membrane darkening without exposing new bands.

Purification of anti-PS-3 antibody using HA-PS-3

To reduce cross-reactivity, additional purification of anti-PS-3 antibody was attempted using HA-protoxin and anti-HA resin (Figure 132). HA-protoxin was used instead of activated PS-3 due to instability of the tag after processing, explained in section 7.5.

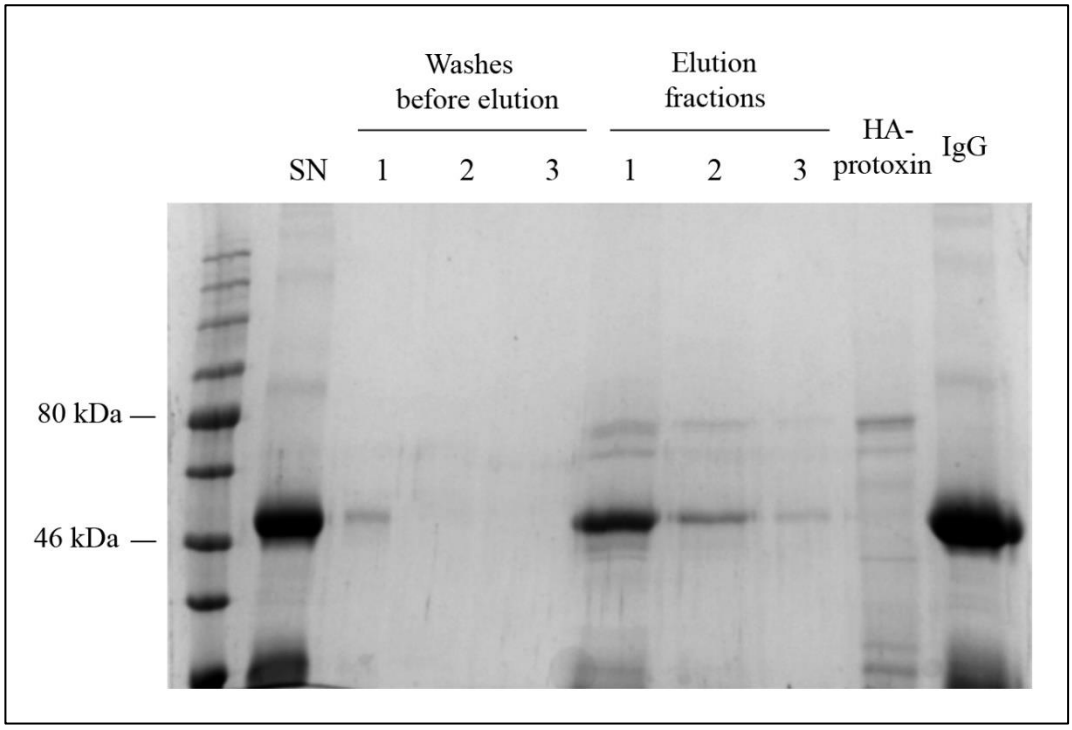

Figure 132 Purification of anti-PS-3 antibody using HA-PS-3 and anti-HA resin.
Pull down assay was performed using anti-HA resin. 50 µl of pelleted washed resin was incubated with purified HA-tagged protoxin (73 µg). Samples were incubated for 1 hour at RT rotating. Next, 150 µl of anti-PS-3 antibody was added and mixture was incubated for another hour at RT rotating. Antibody-HA-PS-3 complex was eluted with glycine and samples were run on a 7.5% SDS-PAGE gel: SN – supernatant collected after incubation with antibody, samples of three washes before and after elution; HA-protoxin and anti-PS-3 antibody (IgG) were run for comparison.

A portion of anti-PS-3 antibody was successfully eluted with the HA tagged protoxin. Purified antibody was then used in a western blot experiment (Figure 133). Even though the eluted antibody was complexed with HA-protoxin, the experiment was performed mainly to assess whether or not purification would solve the high cross-reactivity problem.

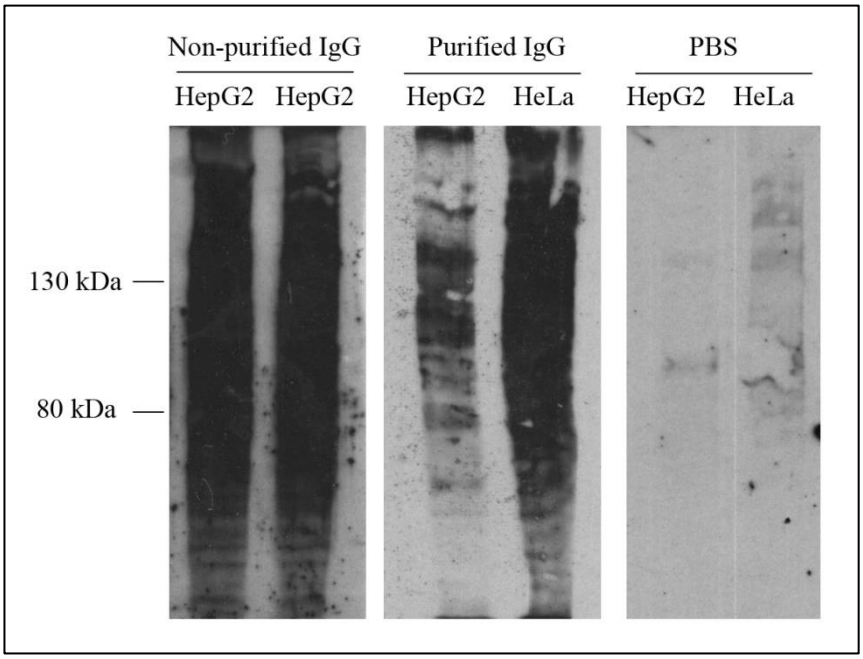

Figure 133 Western blot analysis of cross-reactivity of resin purified anti-PS-3 antibody.
NOG lysed HepG2 and HeLa cells were run on a 7.5% SDS-PAGE gel. 25 and 31 µg of protein per well were loaded in lanes with HepG2 and HeLa cell extracts respectively. After transfer membrane was cut and incubated with non-purified (1 µg/ml), resin purified (2 µg/ml) anti-PS-3 antibody (IgG) or PBS only. Membranes were incubated with secondary antibody and ECL detection reagent.

Purification of anti-PS-3 antibody lessened to a certain degree the cross-reactivity problems, but not sufficiently enough.

7.4 Biotin labelled PS-3

Characterisation of biotin-PS-3

Biotinylation is the process of covalently attaching biotin (244.3 Da) to a protein of interest, which then can be detected with a labelled avidin or streptavidin. Trypsin treated PS-3 was biotinylated as described in the method section. Western blot was performed to confirm biotin attachment (Figure 134).

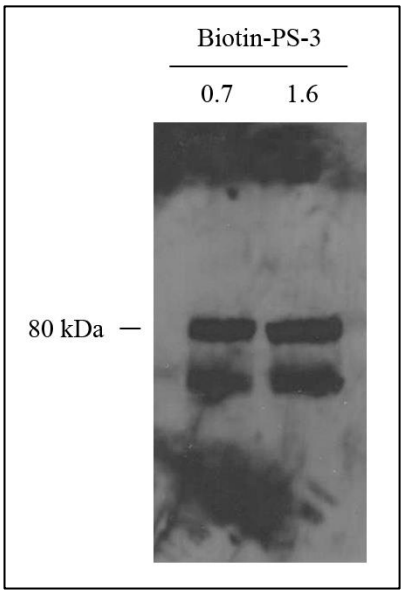

Figure 134 Western blot analysis of the efficiency of PS-3 biotinylation.
Non-purified, dialysed, trypsin activated PS-3 was biotinylated according to manufacturer's instruction. Biotinylated toxin fractions were run on a 7.5% SDS-PAGE gel: 0.7 µg and 1.6 µg of protein were loaded in respective lanes. Proteins were detected with streptavidin conjugated to HRP and ECL detection.

Western blot confirmed successful toxin labelling. Next, labelled PS-3 was purified and its toxicity assessed on HepG2 cells (Figure 135).

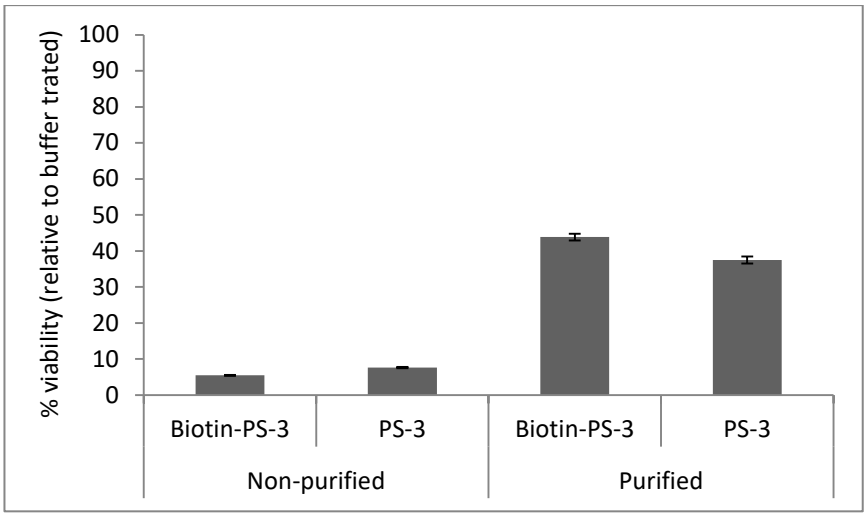

Figure 135 Analysis of the effect of biotinylated PS-3 on HepG2 cell viability.
HepG2 cells were seeded at the density of 25 x 10^4 cells/ml. Next day cells were treated with non-purified PS-3 before biotinylation (32 µg/ml), or after biotin attachment (28 µg/ml), purified biotinylated toxin (3.4 µg/ml), or purified PS-3 (2.5 µg). Cell viability was measured 24 hours later using CellTiter-Blue.

Biotinylation hardly affected PS-3 toxicity e.g. by sterically blocking binding.

Ligand blots using biotin-PS-3

Next, biotin-PS-3 was used in ligand blot experiments (Figure 136).

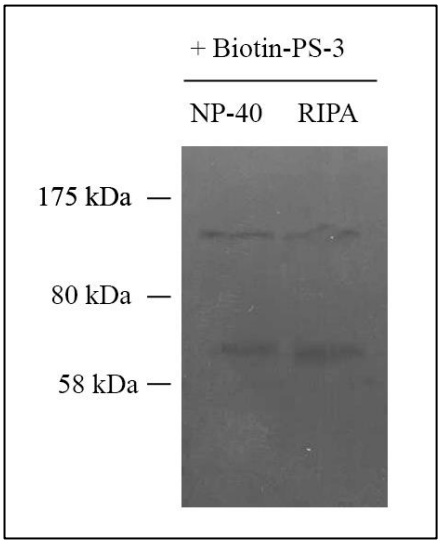

Figure 136 Ligand blot analysis of HepG2 cell extracts using biotinylated PS-3 as a probe.
HepG2 cells lysed with NP-40 or RIPA were resolved on a 7.5% SDS-PAGE gel. 15 µg or proteins were loaded in each lane. After transfer membrane was incubated with biotinylated, purified PS-3 (0.5 µg in PBS-T) and detected by streptavidin-HRP and ECL detection.

Two bands were detected in each lane, with 66 and 126 kDa calculated band sizes. To test if the signal was due to non-specific binding the experiment was repeated with appropriate controls (Figure 137).

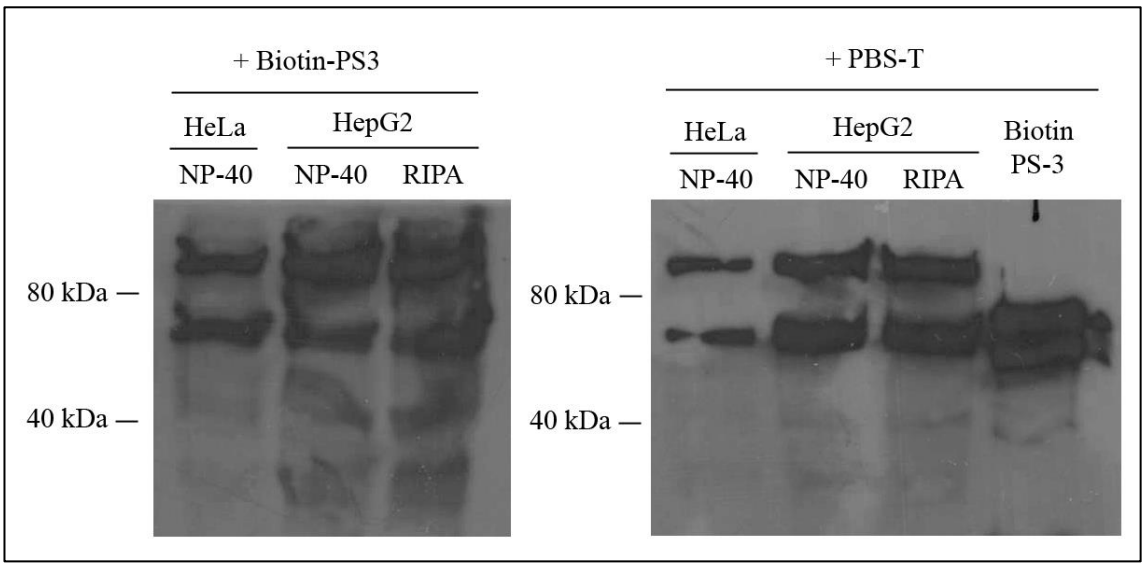

Figure 137 Ligand blot analysis of HepG2 and HeLa cell extracts using biotinylated PS-3 or buffer as a probe. HepG2 and HeLa cell extracts lysed with NP-40 or RIPA (20 µg of protein loaded per lane) and biotinylated purified toxin (34 µg/ml) were resolved by 12% SDS-PAGE gels. After transfer and blocking membrane was cut. One piece was incubated with biotinylated purified PS-3 (0.5 µg in PBS-T) and the second one in with buffer only (PBS-T). This was followed by incubation with streptavidin-HRP and ECL detection.

The same two bands were detected whether or not the membrane was probed with biotinylated PS-3, indicating that streptavidin bound non-specifically to some proteins both in HeLa and HepG2 cell extracts. No other bands, unless masked by the present bands, were visible on the membrane exposed to the toxin probe that could potentially point to a specific interaction. Western blot was repeated with proteins resolved on a 7.5% SDS-PAGE gel. The same non-specific bands were obtained (data not shown). For this reason, further experiments did not involve biotinylated toxin and alternative ways of PS-3 tagging were sought.

7.5 HA tagged PS-3

HA (human influenza hemagglutinin) is a surface glycoprotein of the human virus involved in infectivity. The HA tag has been developed from its epitope (amino acids 98-106) and since then it has been widely used as a general tag in expression vectors (Wilson et al., 1984).

HA tag (amino acid sequence: YPYDVPDYA) was chosen for PS-3 labelling as it does not contain Arg or Lys residues, that could otherwise be cleaved off during trypsin activation. Its localisation was designed to be within the core protein sequence that would not undergo enzymatic processing, but at the same time exposed and easily accessible for detection by antibodies. For these reasons HA tag was integrated into the *cry41Aa* gene after the DNA sequence coding for the domain III in ORF2 but before the ricin domain. By specifically designed PCR primers, HA tag was attached and ricin domain deleted at the same time (Etherington et al., unpublished). A sequence alignment of PS-3, HA tagged PS-3 and ricin Δ PS-3 was performed using Clustal Omega software (Sievers et al., 2011), which is presented in Figure 138.

```
DelR-HA      GGPIWIDKIEFIPLSPIPELPVYPGTYQIVTALNNSSVVTSEEFCMGIGLTTYPYDVPDYA
FL           GGPIWIDKIEFIPLSPIPELPVYPGTYQIVTALNNSSVVTSEEFCMGIGLTTRCGVNLWSN
DelR         GGPIWIDKIEFIPLSPIPELPVYPGTYQIVTALNNSSVVTSEEFCMGIGLTTRS------
             **************************************************

DelR-HA      ------------------------------------------------------------
FL           NGNTLQKWRFVYNGDQNAFQIKSTPNEDLVLSGSNSGTSVTAETNQNRPNQYWLIEEAGN
DelR         ------------------------------------------------------------


DelR-HA      -------------------------------------------
FL           GYVYLRSKGNPNLVLDVAGTSTANGTNIILWNYNGSTNQKFKLS
DelR         -------------------------------------------
```

Figure 138 Clustal Omega sequence alignment of PS-3, HA-PS-3 and ricin Δ PS-3.
The following C-terminal sequences were aligned in Clustal Omega: PS-3 full length (FL), ricin Δ PS-3 (DelR) and HA tagged ricin Δ PS-3 (DelR-HA). Ricin domain is highlighted in green, HA tag in yellow.

Characterisation of HA-PS-3

Western blot was performed to detect the presence of the HA tag attached to PS-3 using anti-HA antibody (Figure 139).

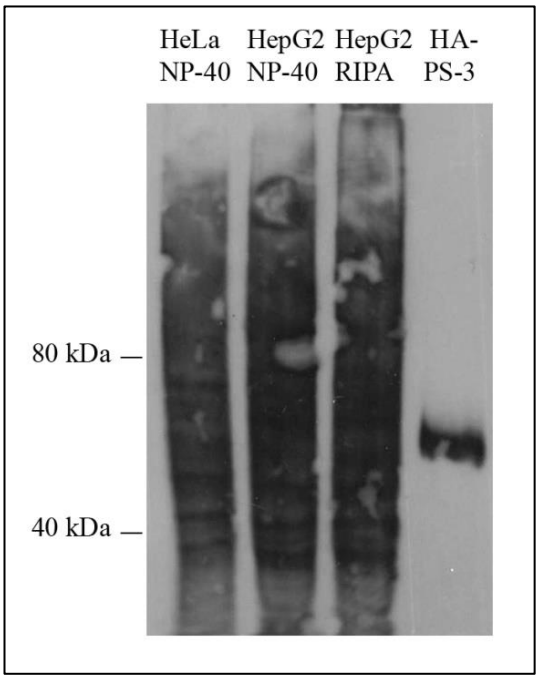

Figure 139 Western blot analysis of the HA tag attachment to PS-3.
HepG2 and HeLa cells were lysed with either RIPA or NP-40. Cell extracts and purified trypsin treated HA-PS-3 were resolved on a 7.5% SDS-PAGE gel. 8 µg of protein were loaded in lanes with cell extract and 1.28 µg of protein in the toxin lane. Membrane was incubated with anti-HA antibody and appropriate HRP-conjugated antibody followed by ECL detection.

HA tagged toxin was successfully detected as a single band of around 60 kDa (due to lack of the ricin domain). Although anti-HA antibody showed high non-specific signal in the lanes with cell extracts, background noise was significantly improved by using 5% skimmed milk in PBS-T at blocking and antibody incubation steps (data not shown).

Next, the toxicity of purified HA-PS-3 was assessed on HepG2 cells. Results presented in Figure 140 showed that HA-tagging slightly affected PS-3 toxicity.

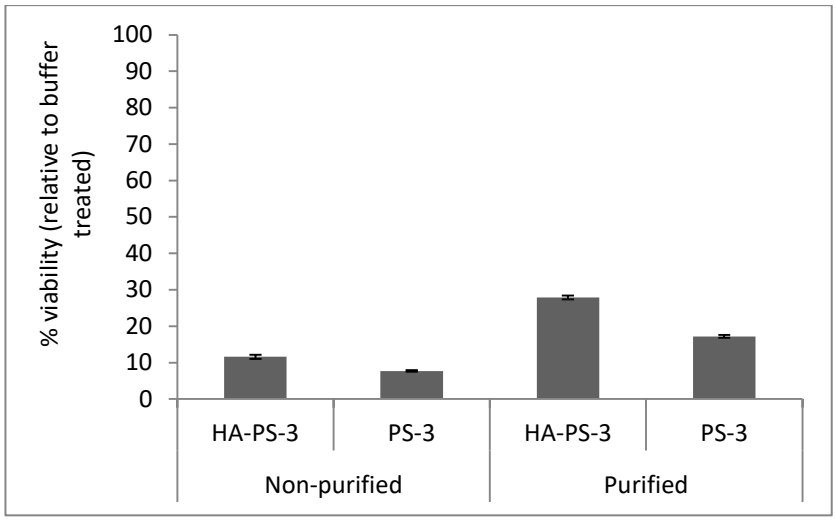

Figure 140 Analysis of the effect of HA tagged PS-3 on HepG2 cell viability.
HepG2 cells were seeded at the density of 25 x 10^4 cells/ml. The next day cells were treated with trypsin activated HA-PS-3 before (53 µg/ml), or after (12.8 µg/ml) purification. Non-purified (33 µg/ml) and purified PS-3 (12 µg/ml) were tested for comparison.

Western and ligand blots using HA-PS-3

Figure 141 and Figure 142 show results of ligand blot experiments with HA-PS-3, where HepG2 protein samples were resolved using SDS-PAGE or a native gel respectively.

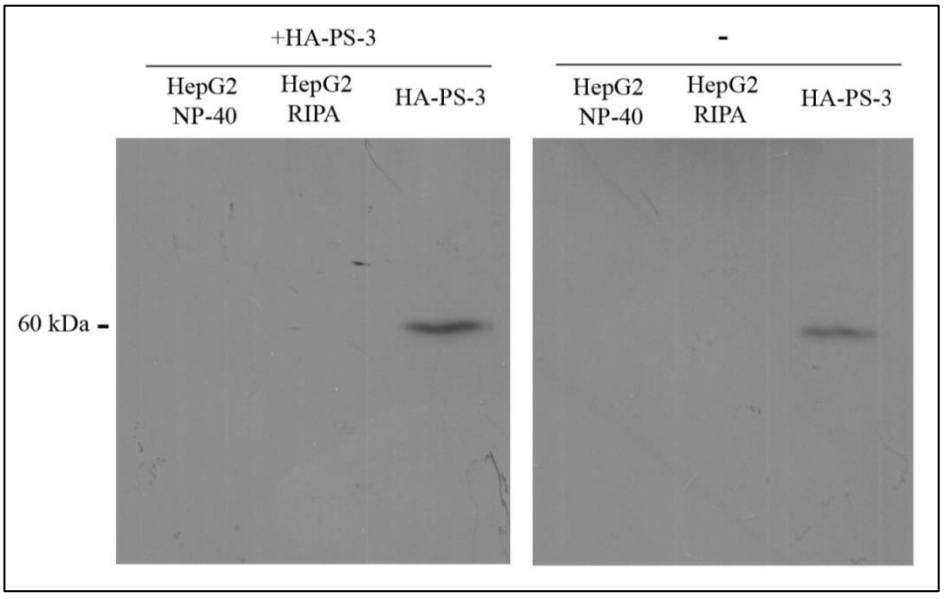

Figure 141 Ligand blot analysis of HepG2 cell extracts run on an SDS-PAGE gel using HA-PS-3 as a probe.
HepG2 cells were lysed with either NP-40 or RIPA. Samples were run on a 12% SDS-PAGE gel. After transfer membrane was cut and incubated with either HA-PS-3 in PBS-T (5.3 µg/ml) or PBS-T. In lanes with cell extract: 7.5 µg of protein were loaded and in the toxin lane: 2.6 µg of trypsin activated HA-PS-3. Both membranes were then incubated with HRP conjugated anti-HA antibody followed by the ECL detection.

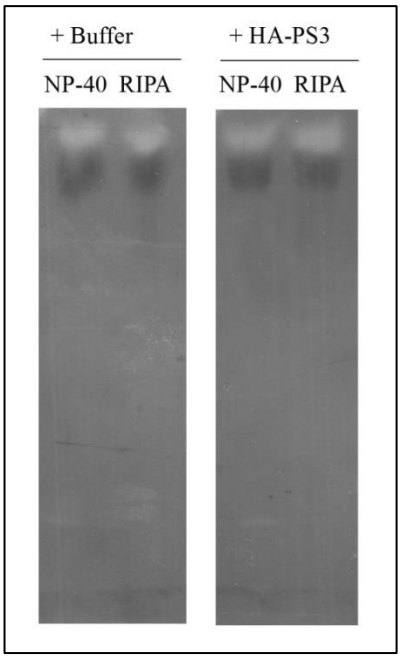

Figure 142 Ligand blot analysis of HepG2 cell extracts run on a native PAGE gel using HA-PS-3 as a probe.
HepG2 cells were lysed with either NP-40 or RIPA. Samples were run on a native 7.5% PAGE gel. 11 µg of protein were loaded in each lane. After transfer and blocking the membrane was cut into two pieces, one incubated with HA-PS-3 in PBS-T (2.5 µg/ml), second with PBS-T. Both membranes were then incubated with HRP conjugated anti-HA antibody followed by the ECL detection.

No bands were detected that would suggest any kind of interaction with the labelled toxin. The same results were obtained when different percentage gel or higher HA-PS-3 concentration was used (data not shown). Exposing membrane to a very high toxin dose resulted in excessively dark background, even when film exposure was shortened to a minimum (data not shown). Diluting HA-PS-3 in other buffers like: PBS without Tween-20, 5% milk in PBS-T, 3% BSA in PBS-T, or a binding buffer (0.01% BSA, 0.1% Tween-20 in PBS) successfully used for Cry1Ab in toxin-receptor binding assays (Pacheco et al., 2009), did not improve the results (data not shown). The same was true about shortening or lengthening incubation time that membrane was in contact with HA-PS-3 (data not shown).

The next set of western blot experiments involved HepG2 cells that had been exposed to HA-PS-3 for 20 minutes before being lysed. Since the interaction between

the cells and the toxin most definitely had occurred and because of denaturing conditions of SDS-PAGE, a band of molecular weight close to HA-PS-3 or higher (toxin oligomers) was expected in lanes with toxin treated-cell extracts as a result of toxin dissociation from the receptor (Figure 143). The same cell extract samples were also tested in a native PAGE western blot experiment (Figure 144).

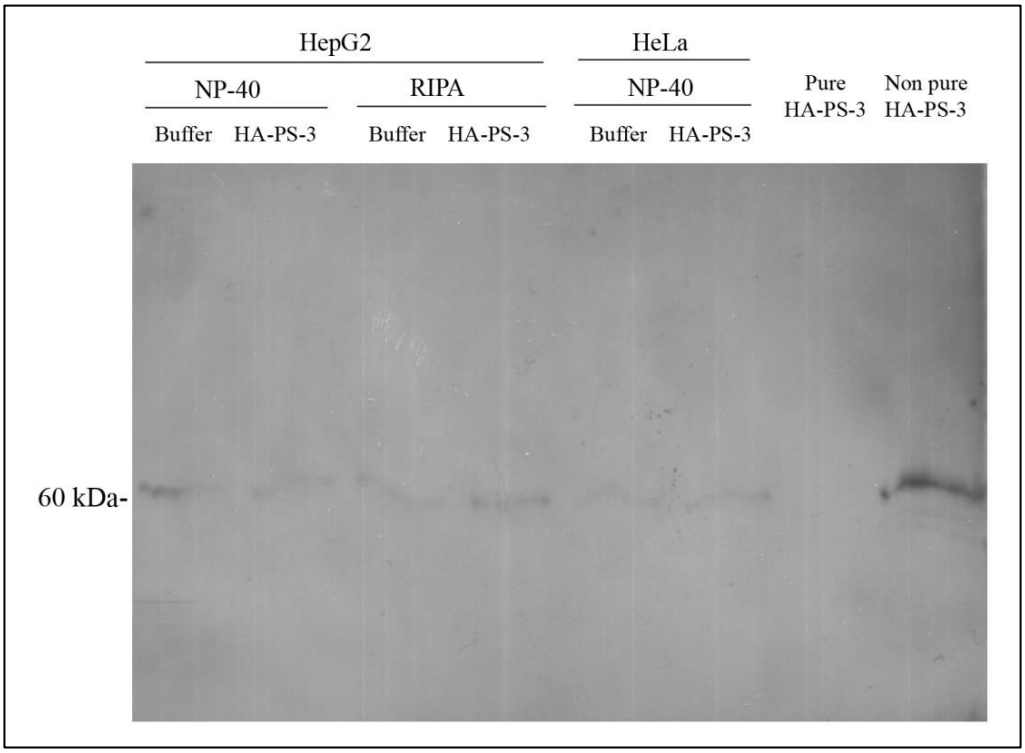

Figure 143 Western blot analysis of extracts from HepG2 cells treated with or without HA-PS-3.
HepG2 cells were treated with either purified HA-PS-3 (10 µg/ml) or buffer for 20 minutes before being lysed with either NP-40 or RIPA. Samples were run on a 7.5% SDS-PAGE gel. After transfer the membrane was incubated with anti-HA antibody. Non-purified and purified HA-PS-3 was included as a control. 15 µg of protein per well were loaded in lanes with cell extracts; 1.2 µg of purified and 5.3 µg of non-purified trypsin activated toxin.

If the toxin did not form stable oligomers after 20 minutes of treatment, the band around 60 kDa representing the monomer units should be expected as boiling and SDS treatment should detach the toxin from the receptor and produce a signal. If the toxin produced SDS-resistant oligomers within this time, these should be represented as high molecular weight bands, similarly to experiments done with Parasporin-2 (Abe et al., 2008). However, there was no difference between extracts from cells previously

treated with or without HA-PS-3. It could be that the toxin concentration in protein samples was too small for detection. Non-specific signal was observed around 60 kDa in all lanes containing cell extract. The lack of signal in lane with purified HA-PS-3 was probably due to its low concentration or - discussed later – HA tag cleavage.

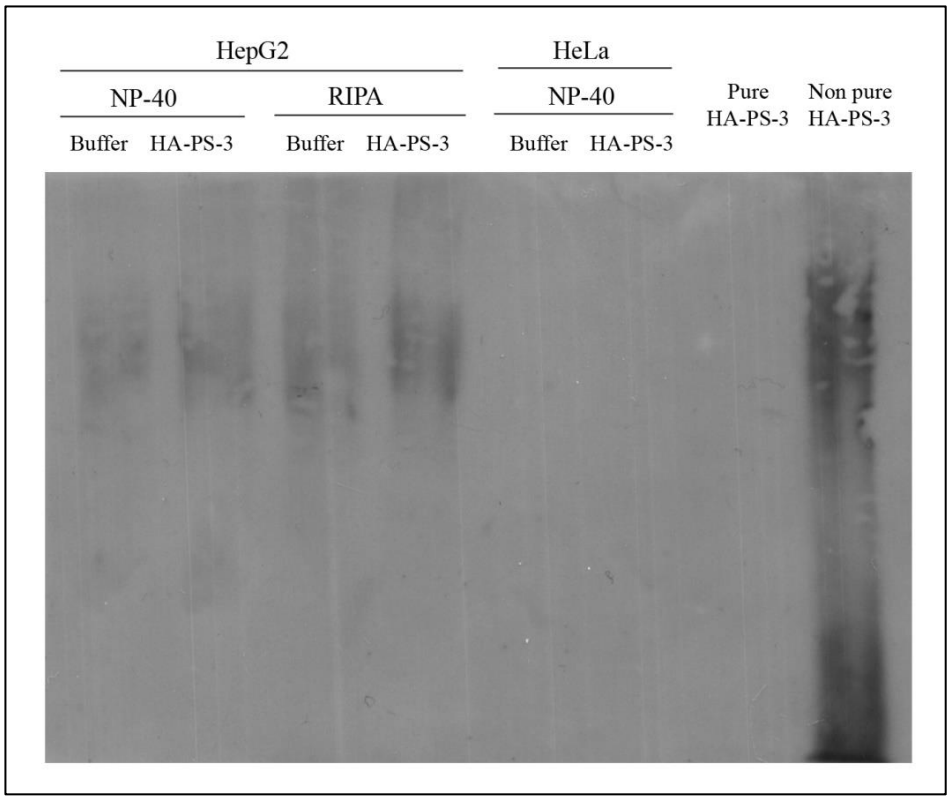

Figure 144 A native PAGE western blot analysis of extracts from HepG2 cells treated with or without HA-PS-3. HepG2 cells were treated with either purified HA-PS-3 (10 µg/ml) or buffer for 20 minutes before being lysed with either NP-40 or RIPA. Samples were run on a 7.5% native PAGE gel. After transfer the membrane was incubated with anti-HA antibody. Non-purified and purified HA-PS-3 was included as a control. 15 µg of protein per well were loaded in lanes with cell extracts; 1.2 µg of purified toxin and 5.3 µg of non-purified trypsin activated toxin.

HepG2 cells exposed to either buffer or HA-PS-3 before lysis showed the same non-specific signal on the native gel. HA-PS-3 could not be detected in lanes with the cell extract using native conditions, probably due to small amounts or tag cleavage.

Experiments with Parasporin-2 showed that oligomerization is time and temperature dependent, occurring efficiently at 37°C but not at 4°C. As the signal for the monomeric PS-2 decreased with time, the oligomeric band appeared stronger,

starting from 30 minutes after cell exposure to toxin (Abe et al., 2008). Oligomerization may also increase the chemiluminescent signal as the stability of oligomeric toxin complexes in the membrane is thought to be greatly enhanced compared with monomeric protein binding, as was demonstrated clearly for aerolysin (Lesieur et al., 1999). Since 20 minute treatment with HA-PS-3 may not have been enough to promote oligomerization, cells were pulse treated with HA-PS-3 for 20 minutes, washed and then incubated for another 40 minutes at 37°C, followed by protein extraction. In addition, to ensure saturation at binding sites on the cell surface, cells were exposed to increased toxin dose (60 µg/ml). Since Cry1Ab oligomers were temperature sensitive at 100° C (Gómez et al., 2014), boiled and non-boiled samples were compared using the western blot technique (Figure 145).

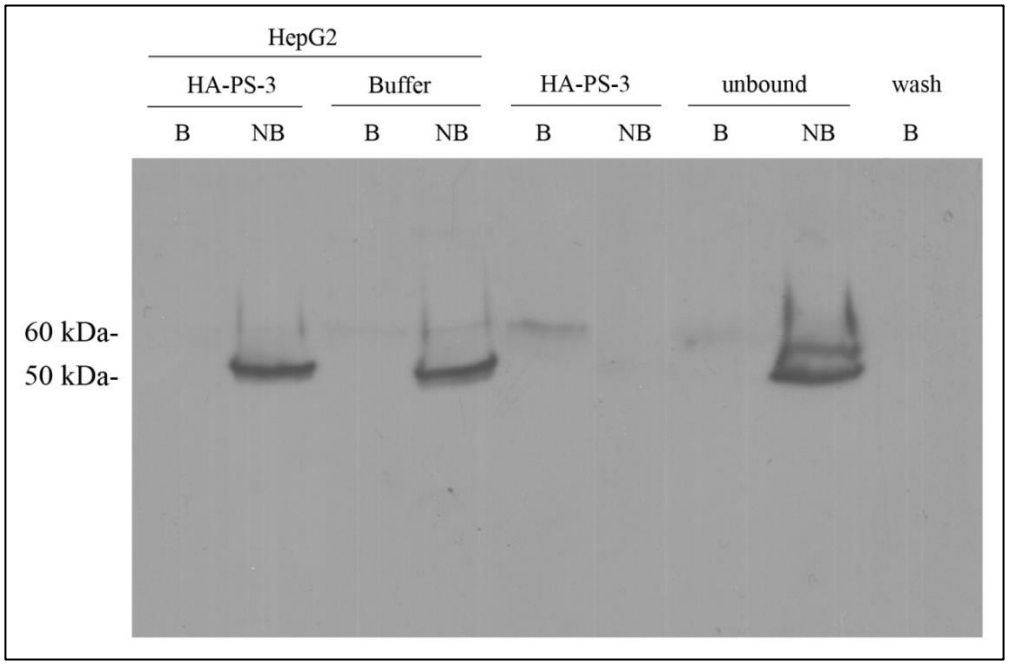

Figure 145 Western blot of heat-denatured and non-denatured extracts from cells exposed to high HA-PS-3 dose. HepG2 cells were treated with non-purified, concentrated trypsin activated HA-PS-3 (60 µg/ml) or with buffer for 20 minutes before being washed 3 times with PBS. DMEM collected after 20 minutes containing unbound toxin (unbound) and PBS collected after the first cell wash (wash) were also run. Then fresh cell medium was added and cells were incubated at 37°C for additional 40 minutes. After that time most of the medium was gently removed and cells were lysed with NP-40. Samples were run on a 12% SDS-PAGE gel followed by membrane incubation with anti-HA antibody. Samples were boiled (B) or not boiled (NB) with sample loading buffer prior to loading. HA-PS-3 diluted in NP-40 was included as a control. 9 µg of protein per well were loaded in lanes with cell extracts and 4.8 µg of HA-PS-3 in toxin lanes.

The expected 60 kDa toxin band in the lane with denatured cells pre-exposed to HA-PS-3 was absent. The 50 kDa band strongly present in non-boiled samples most likely represents non-specific binding since it originated from the culture medium (present in unbound fraction), not the cells. Signal in the toxin control lane was low. Similar bands were obtained when experiment was repeated with toxin and buffer treated cells lysed in RIPA (data not shown).

The low signal observed for HA-PS-3 indicated that HA tag may have been lost during proteolysis. To test that, the HA-protoxin was digested with different proteases. Digested toxins were analysed by western blotting using anti-HA antibody (Figure 146) and additionally visualized on an SDS-PAGE gel (Figure 147).

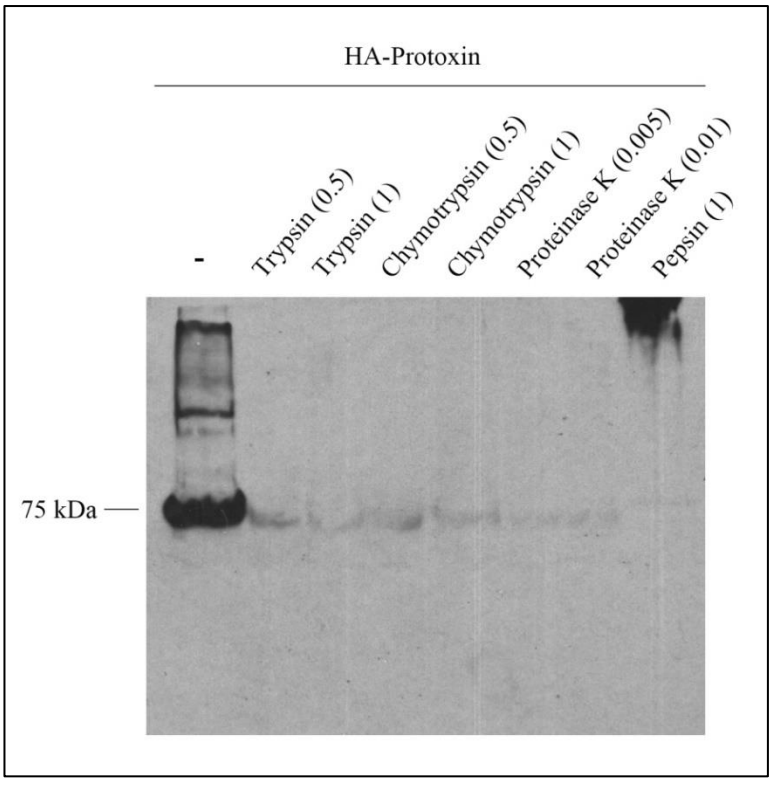

Figure 146 Western blot assessment of proteolytic cleavage of the HA tagged protoxin.
HA tagged protoxin was digested with different proteases: trypsin (0.5 or 1 mg/ml), chymotrypsin (0.5 or 1 mg/ml), proteinase K (0.005 or 0.01 mg/ml) or pepsin (1 mg/ml). Samples were run on a 7.5% SDS-PAGE gel (as shown in Figure 147) and western blotted using anti-HA antibody.

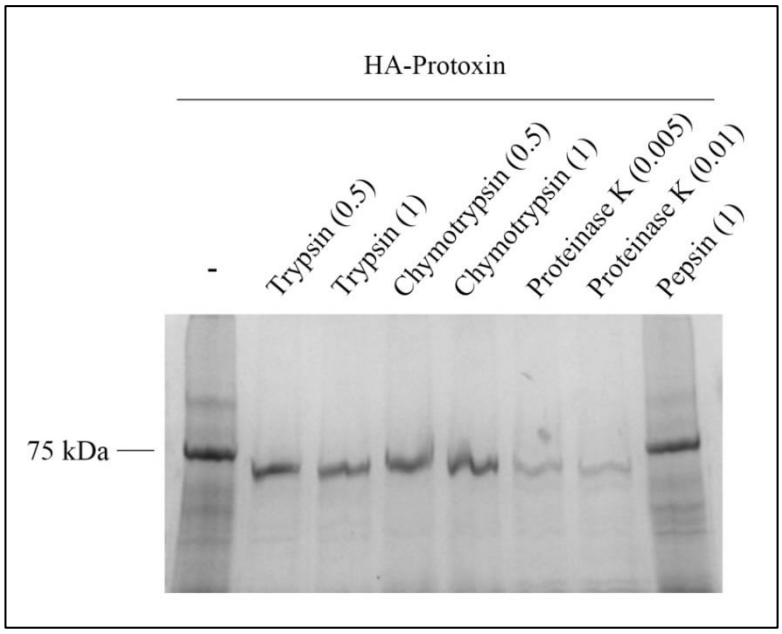

Figure 147 SDS-PAGE analysis of proteolytic cleavage of the HA tagged protoxin.
HA tagged protoxin was digested with different proteases: trypsin (0.5 or 1 mg/ml), chymotrypsin (0.5 or 1 mg/ml), proteinase K (0.005 or 0.01 mg/ml) or pepsin (1 mg/ml). Samples were run on a 7.5% SDS-PAGE gel.

Regardless of the protease used, signal of activated HA-protoxin was weak compared to the protein yield observed by SDS-PAGE, indicating loss of the tag. Since activated HA-PS-3 was immunodetected before (Figure 139, Figure 142), various HA-PS-3 samples were tested in a dot blot experiment to investigate this issue (Figure 148).

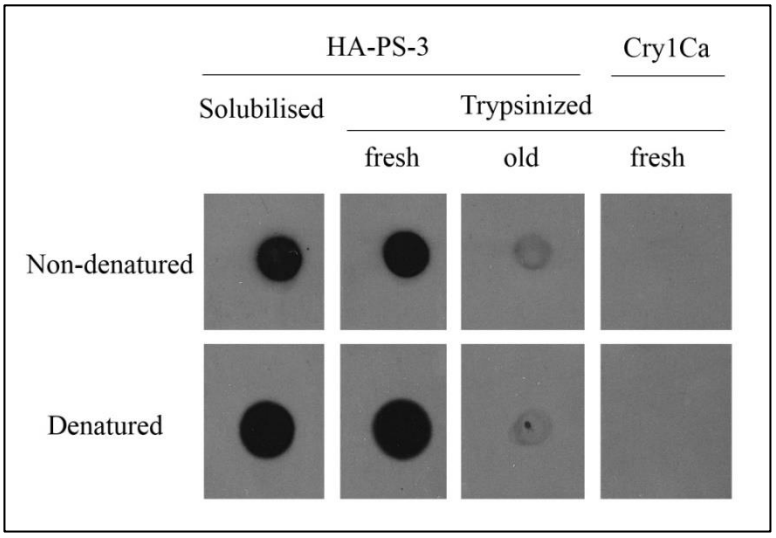

Figure 148 Dot blot analysis of HA tag cleavage in activated HA-PS-3 samples.
Denatured and non-denatured samples of HA-PS-3 trypsinized previously (old) and on the same day (fresh) were spotted on a nitrocellulose membrane (5 µg of protein spotted). HA tagged protoxin and activated Cry1Ca were spotted for comparison. This was followed by membrane incubation with anti HA antibody and ECL detection.

The dot blot and previous results suggest that proteolytic cleavage and the length of sample storage increase instability of the tag. For this reason HA tagged protoxin was used in subsequent experiments.

To increase the efficiency of membrane protein extraction, NOG buffer was used for cell lysis. It is a non-denaturing, mild detergent frequently used for the solubilisation and isolation of membrane proteins. Figure 149 shows a ligand blot experiment with HepG2 cells lysed with NOG and HA-protoxin used as a probe at membrane incubation step (to ensure the presence of the tag).

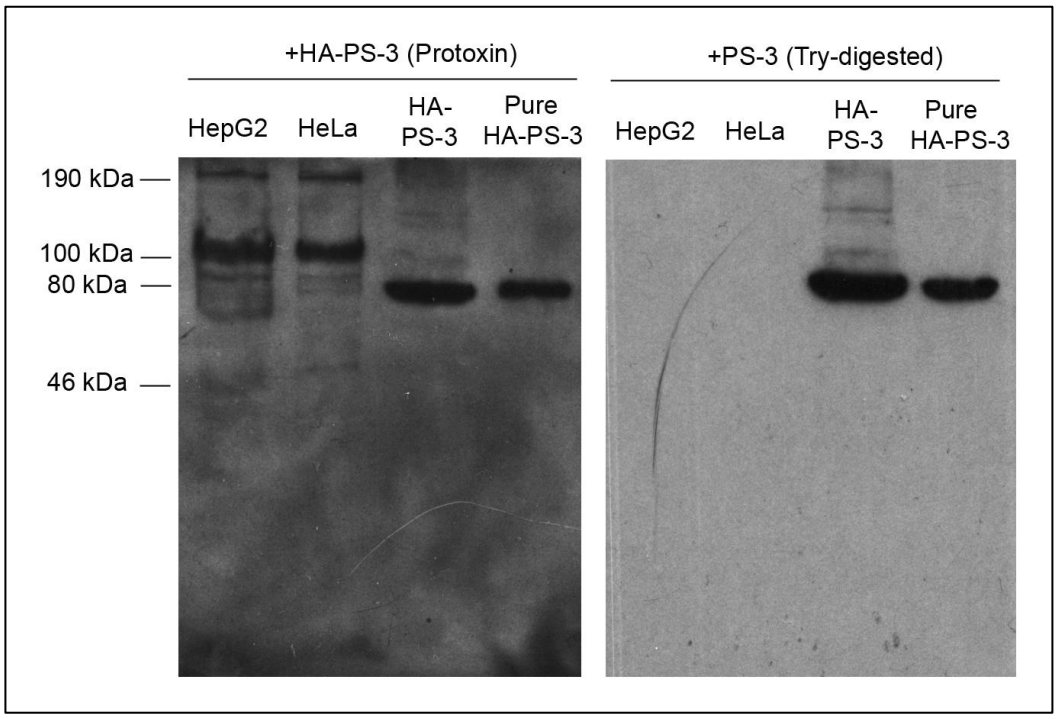

Figure 149 Ligand blot analysis of HepG2 and HeLa cell extracts using HA-protoxin as a probe.
HepG2 and HeLa cells were lysed in NOG buffer. Cell extracts were run on 12% SDS-PAGE gels (32 µg of protein were loaded in HepG2 lanes and 31 µg in HeLa lanes). Non-purified and purified HA-protoxin (2.9 and 0.5 µg of protein respectively) was run as a control. After transfer membrane was blocked and cut vertically. One piece was incubated with HA-protoxin in PBS (17 µg/ml) and the second one with trypsin activated PS-3 in PBS (18 µg/ml) for 1 hour at RT. Membranes were washed, incubated with anti HA antibody and signal was detected with ECL.

Interestingly, prominent high MW bands were observed in HepG2 and HeLa lanes incubated with HA-protoxin. Purified HA-PS-3 protoxin resulted in a strong band as

expected. Experiment was repeated resulting in similar bands although less intensive (data not shown).

To investigate the possibility of the HA tag being the binding component in the HA-PS-3 protein, the following experiment was performed. Cell extracts from three different cell lines were run on an SDS-PAGE gel. After blocking the membrane was cut into two, with one piece incubated with HA-protoxin and the other with HA peptide at the concentration matching that of a toxin (Figure 150).

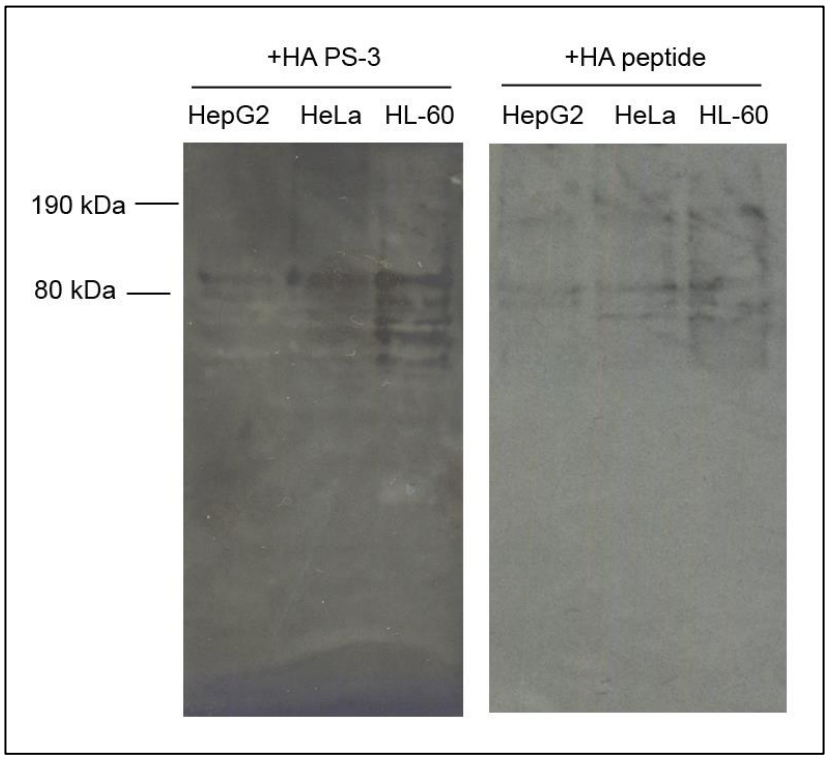

Figure 150 Ligand blot analysis of false positive bands using an HA peptide as a probe.
HepG2, HL-60 and HeLa cells were lysed in NOG buffer. Cell extracts were run on a 10% SDS-PAGE gel (25.7 µg of protein were loaded in HepG2 lanes, 23.7 µg in HL-60 and 31 µg in HeLa lanes). After transfer membrane was blocked, washed and cut vertically. One piece was incubated with HA peptide in PBS (0.037 µM) and the second one with ÄKTA purified HA-protoxin in PBS (0.0375 µM - equivalent roughly to 3 µg/ml) for 1 hour at RT. Membranes were washed, incubated with anti HA antibody and detected with ECL.

Similar bands present in both membranes indicate that the previously observed signal is due to the HA tag reactivity rather than specific toxin binding.

Pull downs using HA-PS-3

The next method used to identify the receptor was a co-immunoprecipitation assay. HA tagged PS-3 (the bait protein) was captured by anti-HA antibody coupled to resin. This complex was then incubated with a cell lysate to identify binding partners. The proteins of interest were eluted from the beads with appropriate buffers and the samples were analysed using SDS-PAGE. Since the verification of proteolytic HA tag cleavage, HA tagged protoxin was used in the majority of pull down experiments. Initial experiments tested the binding efficiency of the resin (Figure 151).

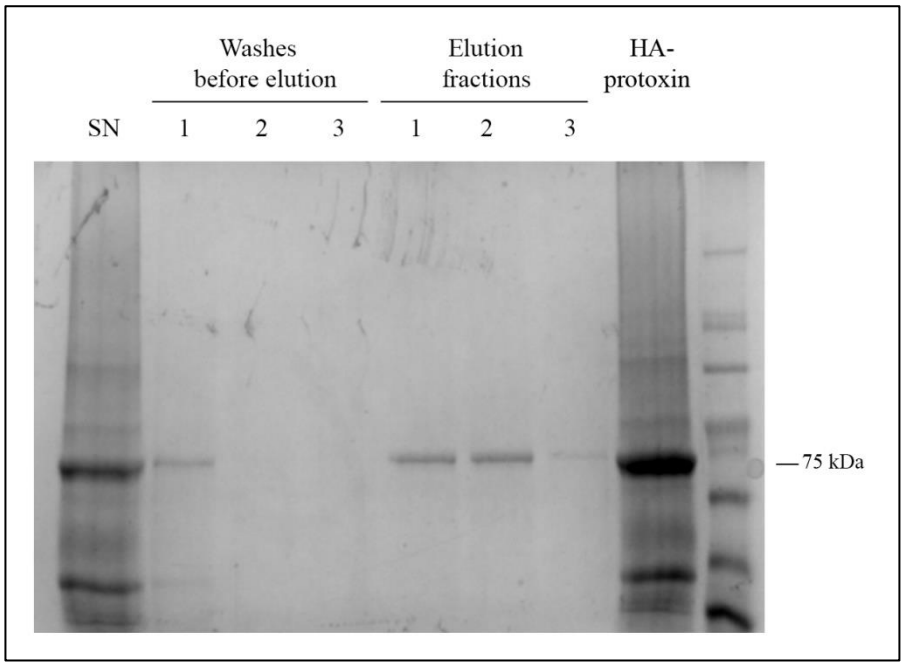

Figure 151 Analysis of elution efficiency in a pull down using HA-tagged protoxin.
Pull down assay was performed using anti-HA resin. 50 µl of pelleted washed resin was incubated with HA-tagged protoxin (145 µg). Samples were incubated overnight at 4°C, eluted with glycine and run on a 7.5% SDS-PAGE gel: SN–supernatant collected after overnight incubation (for estimation of binding efficiency), samples of three washes before and after elution, HA-protoxin – toxin used in the experiment.

Toxin band was successfully detected in the fractions eluted with glycine. The same result was achieved when HA-protoxin was eluted with 3 M NaSCN (data not shown). Pull down with trypsin activated HA tagged PS-3 did not produce the toxin band in the

elution fractions consistent with the tag being cleaved during proteolysis (data not shown). The amount of eluted toxin was very similar whether incubation was carried out at 4°C or at RT (data not shown).

Next, presence of the HA tag in eluted samples was confirmed in a western blot experiment (Figure 152).

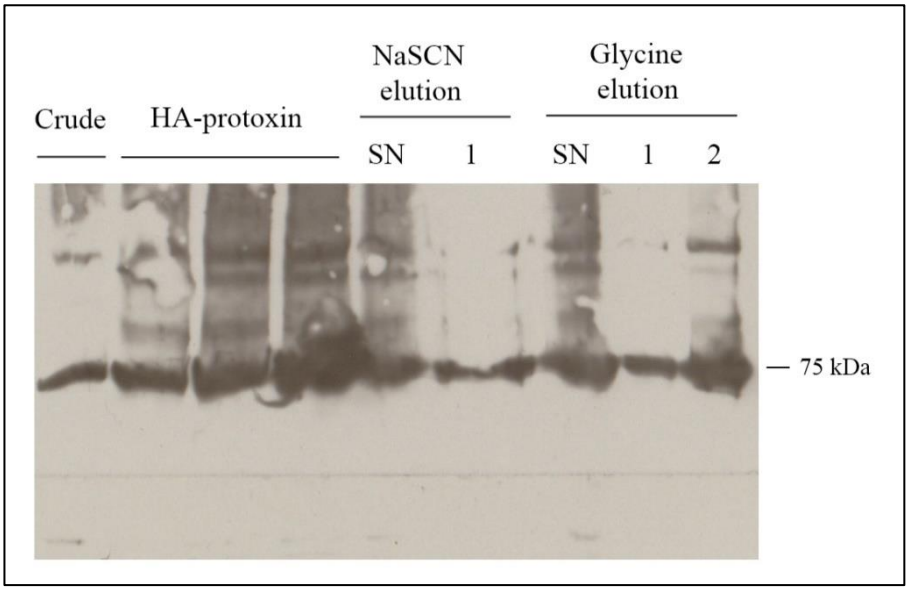

Figure 152 Western blot analysis of the presence of the HA tag in eluted fractions.
HA-tagged PS-3 crude (crude), HA-protoxin, supernatant collected after incubation with toxin (SN) and fractions eluted with either NaSCN (1) or glycine (1 and 2) were resolved on a 7.5% SDS-PAGE gel. Membrane was blocked and incubated with anti-HA HRP-conjugated antibody followed by ECL detection.

Western blot confirmed the presence of the tag in eluted fractions. The subsequent experiments involved incubating resin first with HA-protoxin, and then with a cell lysate. Figure 153 presents experiment with RIPA lysed cell extract; Figure 154 NOG lysed cells. Analysis of false positive pulldown interactions involved: no toxin (Figure 153) and no HA tag (Figure 154) controls.

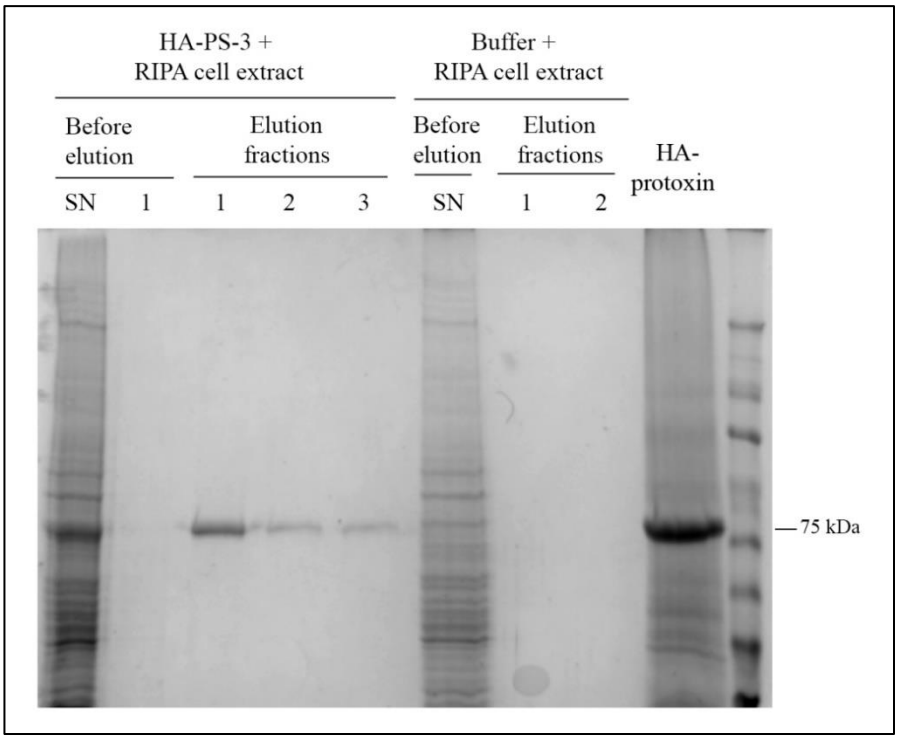

Figure 153 SDS-PAGE analysis of a pull down experiment with HA-PS-3 protoxin and RIPA lysed cell extract.
50 µl of pelleted washed anti-HA resin was incubated with HA-protoxin (87 µg). Samples were incubated for 1 hour at RT. After that RIPA lysed cell extract was added (164 µg) and mixture incubated for another hour rotating at RT. Resin was washed three times. Protein was eluted with glycine and samples run on a 7.5% SDS-PAGE gel: SN- supernatant collected after incubation with cell extract, first wash before and three washes after elution, HA-protoxin – toxin used in this experiment. Pull down was also performed in the absence of toxin (lanes on the right).

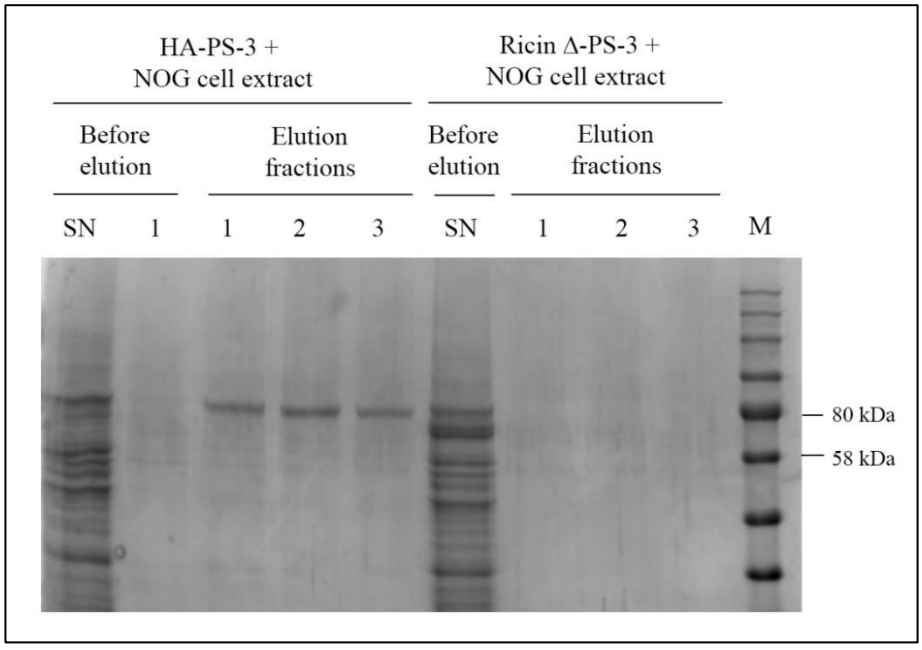

Figure 154 SDS-PAGE analysis of a pull down experiment with HA-PS-3 protoxin and NOG lysed cell extract.
50 µl of pelleted washed anti-HA resin was incubated with HA-protoxin (58 µg). Samples were incubated for 1 hour at RT. After that NOG lysed cell extract was added (322 µg) and mixture incubated for another hour rotating at RT. Resin was washed three times. Protein was eluted with glycine and samples run on a 7.5% SDS-PAGE gel: SN – supernatant collected after incubation with cell extract, first wash before and three washes after elution, HA-protoxin – toxin used in this experiment. Pull down was also performed in the presence of non-labelled ricin Δ PS-3.

Unfortunately no direct protein-protein interactions were demonstrated using the pull down method. No non-specific interactions occurred either. Pull down experiments with incubation at 4° C or using NP-40 lysed cells resulted in similar data. Running elution samples on a 12% SDS-PAGE gel resulted in very faint low MW bands, but these results were inconsistent (data not shown).

7.6 HA tagged PS-3 (K688A)

Previous results showed that HA tag was cleaved after protease treatment. It was suspected that trypsin cleaves PS-3 at the C-terminus not as previously thought at arginine (R) at position 713 but at lysine (K) at position 668 (Souissi et al., unpublished). For these reasons a mutagenesis experiment was designed to create a substitution at position 668 changing lysine into alanine (K668A) in HA tagged ricin Δ PS-3 (PS-3-ΔR-HA). In this way the HA tag could be available for detection in western blotting or pull down assay after trypsin treatment. The PS-3-ΔR-HA ORF2 protein sequence with the mutation site is presented below.

MNQNCNNNGYEVLNSGKGYCQPRYPFAQAPGSELQNMGYKEWMNMCTSGDPTVLGEGYSADVRDAVI
TSINIASYLLSVPFPPAGVAAGILGALLGLLWPTNTQAVWEAFMNTVEALINQKLDEYARSKAISELNGLKNV
LELYQDAADDWNENPGDLRNKNRVLTEFRNVNGHFENSMPSFAVRNFEVNLLPVYAEAANLHLLLLRDAV
KFGEGWGMSTDPGAERDDMYRRLRSRTEIYTDHCVNTYNQGLQQAKSLQANVSDYSRYPWTQYNQSGG
FSYREAKGEYRGTENWNLYNAFRRDMTILVLDIIAQFPTYDPGLYSRPVKSELTREVYTDIRGTTWRSDANLN
TIDAIENRMVGSRQLQLFTWLTEMKFYIRNTGSITSYTHGDLMVGLEKKIRKTNDNDQWLPLEGQNTSYTRI
DRPGIELGKNYWYYARTQQWFETRLLQLWANTDVLSLNAGTVGNEFWVRDVPDYRNIYARSTRNHFIEN
HRLSWIKFEPVRDNCPFAWPGYKQLSALLFGWTHNSVDLNNIISQYRITQIPAVKAYWNRGAFSVIRGPGST
GGNLVQLGTGGEVSVKVRPEQTGSDWYRVRIRYAAGSRGRLNVKKYVSSIHASVTYDYNMTMSSSTQGTY
NSFQYLDVYNFRLAEPEFEVWLTNESGGPIWIDKIEFIPLSPIPELPVYPGTYQIVTALNNSSVVTSEEFCMGIG
LTTYPYDVPDYA

Blue – conserved block number 5 Yellow – HA tag Red – amino acid changed

DNA mutagenesis

DNA from *Bt* pSVP2741Aa-ΔR-HA strain was purified and PCR was set up overnight as described in the methods section. The PCR product was run on a gel (Figure 155).

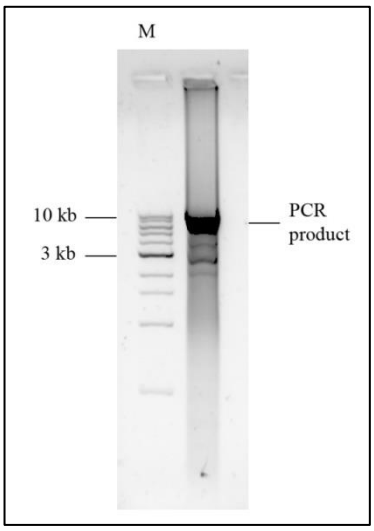

Figure 155 Site-directed mutagenesis of Cry41Aa-ΔR-HA.
DNA from Cry41Aa-ΔR-HA strain was purified using QIAprep kit and PCR was set up overnight with primers to substitute lysine at position 668 into alanine. PCR product containing the substitution was run on 1% agarose gel next to a 1 kb ladder (M).

PCR product was digested with *Dpn*I to remove methylated template DNA. DNA after digestion was purified and run on a gel (Figure 156).

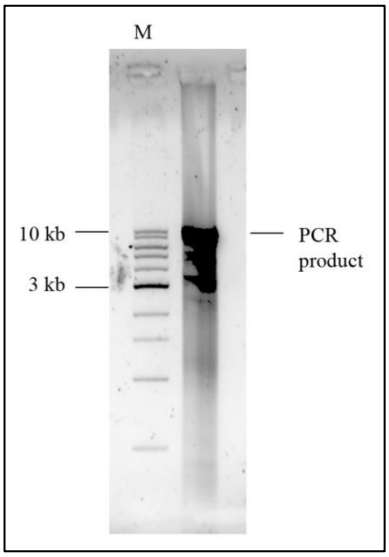

Figure 156. PCR product after digestion with *Dpn*I and purification.
After mutagenesis PCR product was digested with *Dpn*I and purified using QIAquick kit and run on 1% agarose gel next to a 1kb ladder (M).

After digestion with *Dpn*I, purified DNA was ligated overnight. This DNA was used in a transformation into *E. coli* DH5α. Four colonies after transformation named: 1, 2, 3, and 4 were picked and grown. Plasmids were extracted by DNA purification and digested with *Hae*III to confirm the right constructs. *Hae*III digested DNAs were run on a gel (Figure 157).

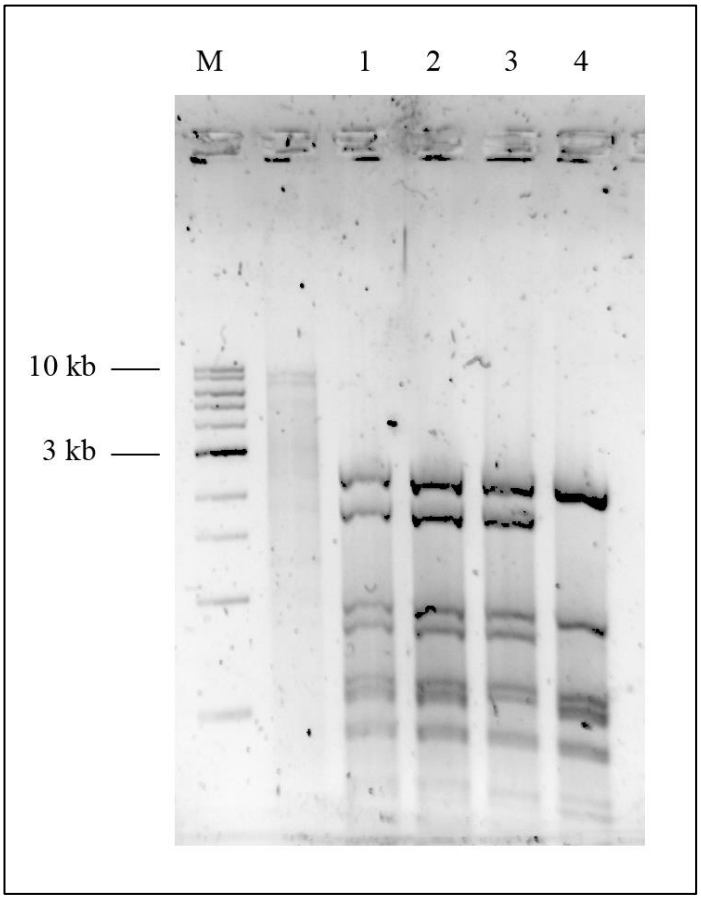

Figure 157 *Hae*III DNA digest after transformation into *E. coli* DH5α.
Purified DNAs after 1st transformation into *E. coli* DH5α named 1, 2, 3, and 4 were digested with *Hae*III and run on a 1% agarose gel.

Banding patterns of digested DNAs were compared to a predicted digest performed using NEBcutter (Figure 158). This provides information about the presence or absence of restriction sites at the expected position within the plasmid and initially confirms correct insert sequence.

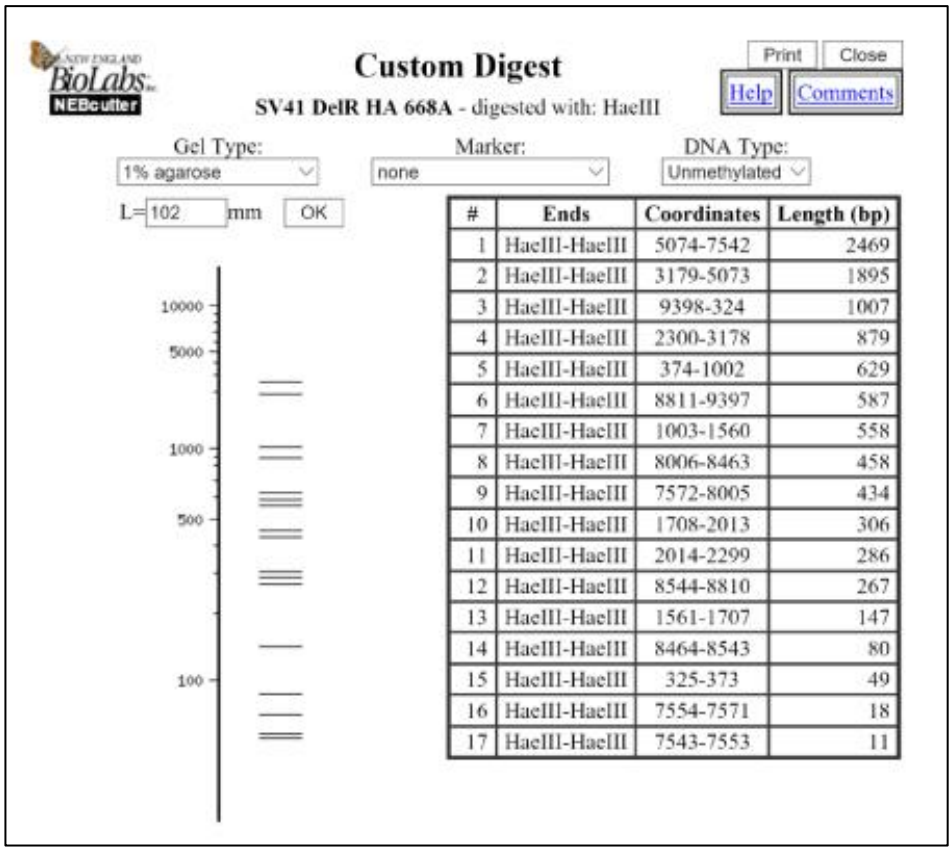

#	Ends	Coordinates	Length (bp)
1	HaeIII-HaeIII	5074-7542	2469
2	HaeIII-HaeIII	3179-5073	1895
3	HaeIII-HaeIII	9398-324	1007
4	HaeIII-HaeIII	2300-3178	879
5	HaeIII-HaeIII	374-1002	629
6	HaeIII-HaeIII	8811-9397	587
7	HaeIII-HaeIII	1003-1560	558
8	HaeIII-HaeIII	8006-8463	458
9	HaeIII-HaeIII	7572-8005	434
10	HaeIII-HaeIII	1708-2013	306
11	HaeIII-HaeIII	2014-2299	286
12	HaeIII-HaeIII	8544-8810	267
13	HaeIII-HaeIII	1561-1707	147
14	HaeIII-HaeIII	8464-8543	80
15	HaeIII-HaeIII	325-373	49
16	HaeIII-HaeIII	7554-7571	18
17	HaeIII-HaeIII	7543-7553	11

Figure 158 Predicted DNA banding pattern of *Hae*III digested mutated plasmid sequence.
Virtual *Hae*III digest was performed on the plasmid sequence: Cry41Aa ΔR-HA containing the K668A mutation using NEBcutter.

Comparing banding patterns it is clear that sample 3 is missing 558 bp band and sample 4: 1895 and 879 bp bands. Therefore next steps were done with samples 1 and 2. DNAs 1 and 2 were transformed into *E.coli* GM216 strain to produce non-methylated DNA. After transformation, colonies were scraped from ampicillin plates, purified and digested with *Hae*III. DNAs were run on a gel (Figure 159).

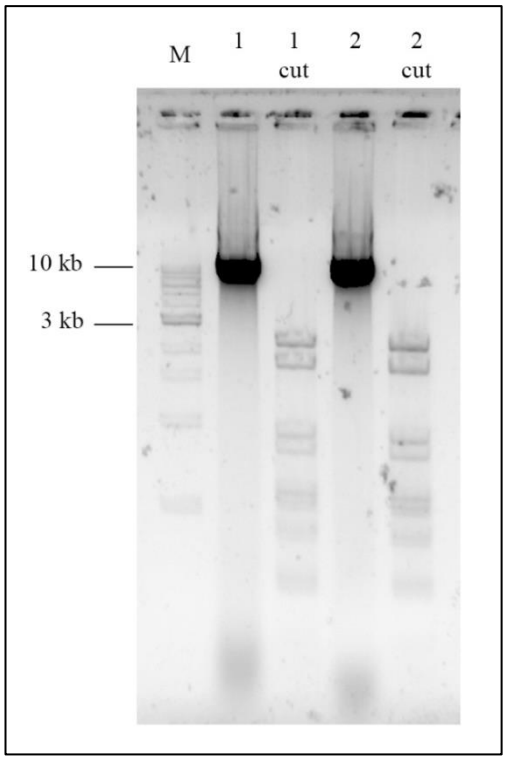

Figure 159 *Hae*III digest of DNAs 1 and 2 obtained after transformation into *E.coli* GM2163.
DNAs 1 and 2 after transformation into *E.coli* GM2163 were purified using QIAprep kit, digested with *Hae*III and run on a 1% agarose gel.

Banding pattern after *Hae*III digest initially verified correct DNA. DNAs 1 and 2 were sequenced to confirm the mutations. Sequencing results were aligned with the non-mutated template (Cry41Aa-ΔR-HA) and presented in Figure 160 and Figure 161.

```
1          TTTGAAGTATGGCTTACTAATGAAAGTGGCGGGCCTATTTGGATTGACGCAATTGAATTC
DelR-HA    TTTGAAGTATGGCTTACTAATGAAAGTGGCGGGCCTATTTGGATTGACAAAATTGAATTC
           ***********************************************..**********

1          ATTCCGCTAAGTCCGATTCCGGAACTACCAGTATATCCTGGTACCTATCAAATCGTGACA
DelR-HA    ATTCCGCTAAGTCCGATTCCGGAACTACCAGTATATCCTGGTACCTATCAAATCGTGACA
           ************************************************************

1          GCTTTAAATAATAGTAGTGTTGTAACTAGCGAGGAGTTTTGTATGGGTATTGGCTTAACC
DelR-HA    GCTTTAAATAATAGTAGTGTTGTAACTAGCGAGGAGTTTTGTATGGGTATTGGCTTAACC
           ************************************************************

1          ACTTATCCAACATGACAATGTCAAGTTCTACACA---GGGGACTTATAATTCGTTTCAGT
DelR-HA    ACTTATCCATATGATGT--TCCAGATTATGCTTAAaggtgtgcaacta-tccctgactaa
           *********:.: .: :    **..**.*.*: *   * * .*::.** * * * :*:.:
```

Figure 160 Sequence alignment of non-mutated Cry41Aa-ΔR-HA and DNA 1 after transformation into *E.coli* GM216.
DNA 1, obtained after transformation into *E.coli* GM216, and Cry41Aa-ΔR-HA (DelR-HA) non-mutated sequence were aligned in Clustal Omega. Mutation site is depicted in red and partial HA tag sequence in yellow. Figure shows C-terminal sequence fragments.

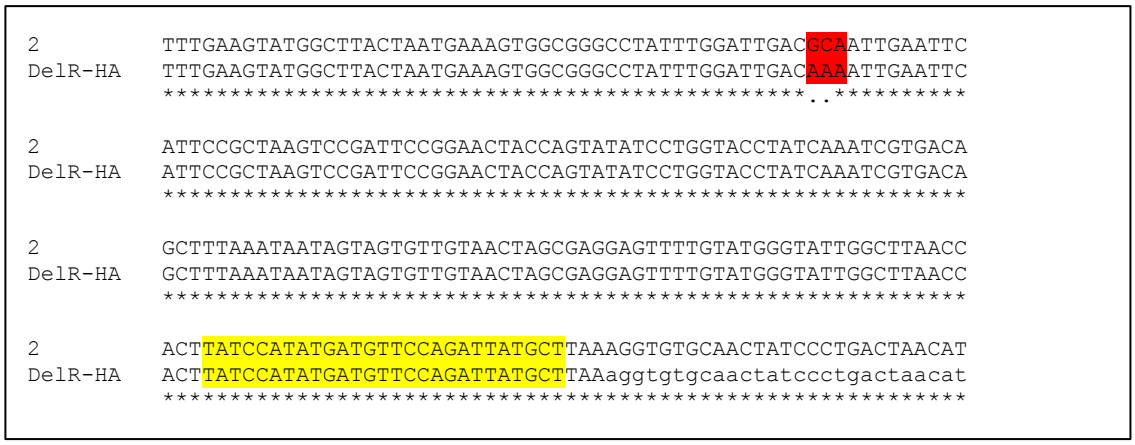

Figure 161 Sequence alignment of non-mutated Cry41Aa-ΔR-HA and DNA 2 after transformation into *E.coli* GM216.
DNA 2, obtained after transformation into *E.coli* GM216, and Cry41Aa-ΔR-HA (DelR-HA) non-mutated sequence were aligned in Clustal Omega. Mutation site is depicted in red and full HA tag sequence in yellow. Figure shows C-terminal sequence fragments.

Both DNAs contained the desired mutation, but DNA 1 did not contain an intact HA tag sequence; therefore DNA 2 was used in the next step. DNA 2 was transformed into *Bt* 4D7. After transformation cells were picked from two separate *Bt* colonies (labelled α and β) and DNA was purified. DNAs α and β were transformed back into *E.coli* DH5α. After transformation colonies were prepped, DNA extracted and sent for sequencing. Sequences α and β were compared with non-mutated Cry41Aa ΔR-HA (Figure 162 and Figure 163). Both constructs contained the mutation and the intact HA tag sequence.

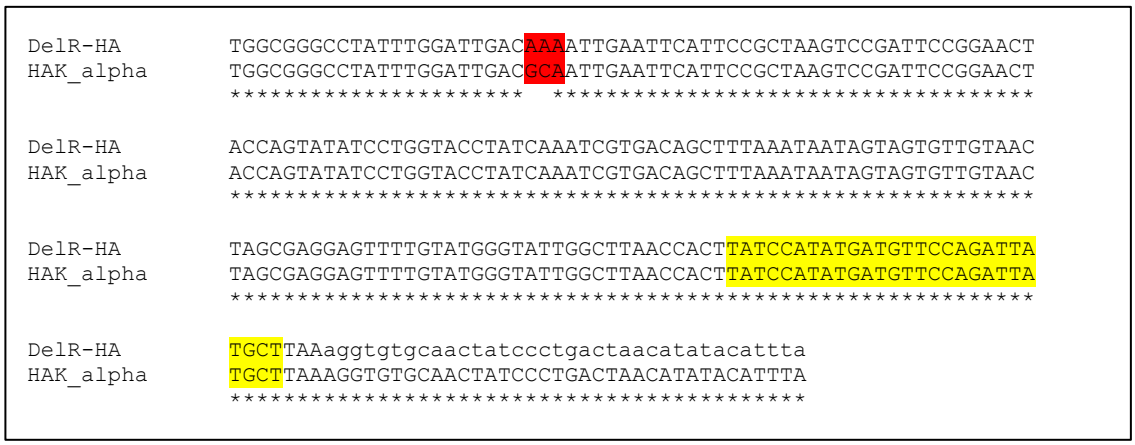

Figure 162 Sequence alignment of non-mutated Cry41Aa-ΔR-HA and DNA α after transformation into *E.coli* DH5α.
DNA α, obtained after transformation into *E.coli* DH5α (HAK_alpha), and Cry41Aa-ΔR-HA (DelR-HA) non-mutated sequence were aligned in Clustal Omega. Mutation site is depicted in red and full HA tag sequence in yellow. The figure shows C-terminal sequence fragments.

```
DelR-HA         GGCGGGCCTATTTGGATTGACAAAATTGAATTCATTCCGCTAAGTCCGATTCCGGAACTA
HAK_beta        GGCGGGCCTATTTGGATTGACGCAATTGAATTCATTCCGCTAAGTCCGATTCCGGAACTA
                ********************  ************************************

DelR-HA         CCAGTATATCCTGGTACCTATCAAATCGTGACAGCTTTAAATAATAGTAGTGTTGTAACT
HAK_beta        CCAGTATATCCTGGTACCTATCAAATCGTGACAGCTTTAAATAATAGTAGTGTTGTAACT
                ************************************************************

DelR-HA         AGCGAGGAGTTTTGTATGGGTATTGGCTTAACCACTTATCCATATGATGTTCCAGATTAT
HAK_beta        AGCGAGGAGTTTTGTATGGGTATTGGCTTAACCACTTATCCATATGATGTTCCAGATTAT
                ************************************************************


DelR-HA         GCTTAAaggtgtgcaactatccctgactaacatatacattta
HAK_beta        GCTTAAAGGTGTGCAACTATCCCTGACTAACATATACATTTA
                ****************************************
```

Figure 163 Sequence alignment of non-mutated Cry41Aa-ΔR-HA and DNA β after transformation into *E.coli* DH5α. DNA β, obtained after transformation into E.coli DH5α (HAK_beta), and Cry41Aa-ΔR-HA (DelR-HA) non-mutated sequence were aligned in Clustal Omega. Mutation site is depicted in red and full HA tag sequence in yellow. The figure shows C-terminal sequence fragments.

Characterisation of HA-PS-3 (K668A)

HA-PS-3 (K668A) α was grown and harvested. Protein sizes and levels were compared with the full length PS-3 before and after activation (Figure 164).

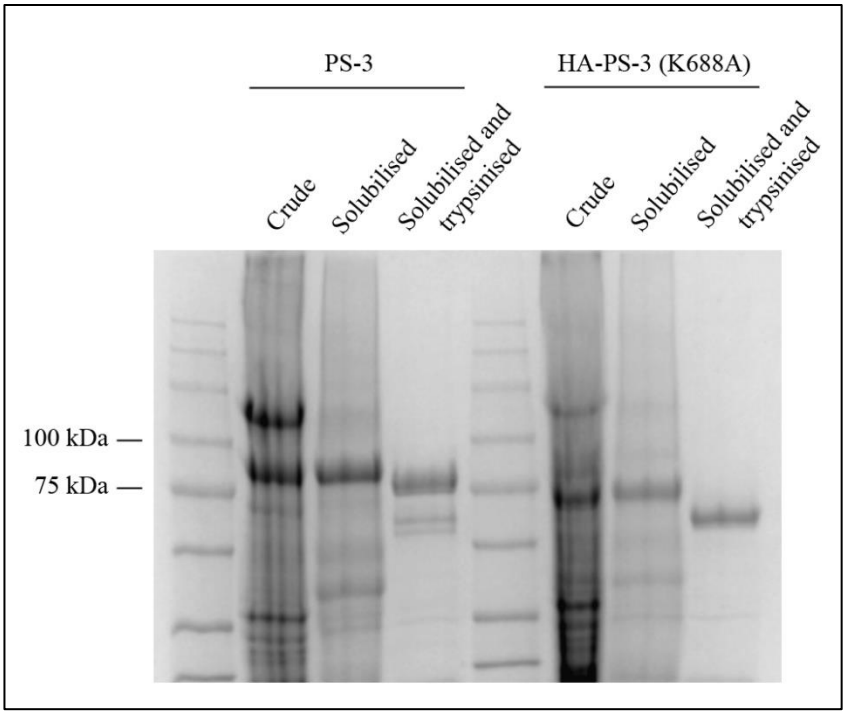

Figure 164 SDS-PAGE analysis of HA-PS-3 (K688A) protein levels and sizes compared to PS-3.
Equal amounts of crude PS-3 and mutant HA-PS-3 (K688A) were solubilised for 1 hour at 37°C in 50 mM sodium carbonate (pH 10.5) in the presence of 5 mM DTT and activated with trypsin (1 mg/ml) for 1 hour at 37°C. Samples at different stages of activation were run on a 7.5% SDS-PAGE gel.

SDS-PAGE showed successful expression and confirmed predicted MW differences in size between the full length PS-3 and the mutant protein. Solubilised mutant migrated around 75 kDa and its trypsin activated form - around 60 kDa, similar to sizes observed before for HA tagged PS-3 (Figure 147 and Figure 141). Mutant protein was stable after trypsin proteolysis indicating that mutation had no major structural impact.

A dot blot was performed to confirm the presence of the tag in solubilised and trypsin activated HA-PS-3 (K688A) (Figure 165).

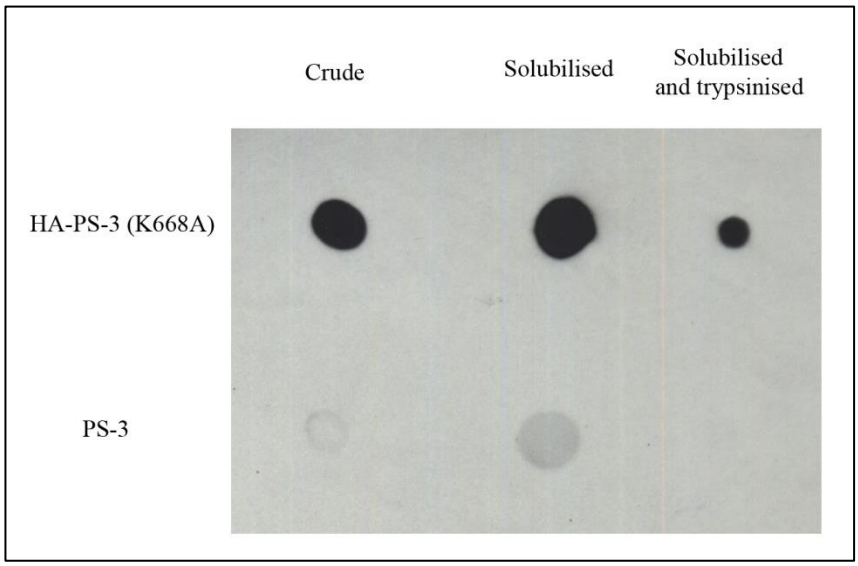

Figure 165 Dot blot analysis of the presence of the HA tag in HA-PS-3 (K688A).
HA-PS-3 (K688A) and PS-3 crude solutions were solubilised and digested with trypsin similar to samples presented in Figure 164. Samples at each stage were spotted on a nitrocellulose membrane, blotted with anti-HA antibody, followed by ECL detection.

Signal from the HA tag was detected in all mutant samples.

Next, toxicity of trypsin activated HA-PS-3 (K688A) was established. When tested at high concentration, the mutant retained cytotoxic activity (Figure 166).

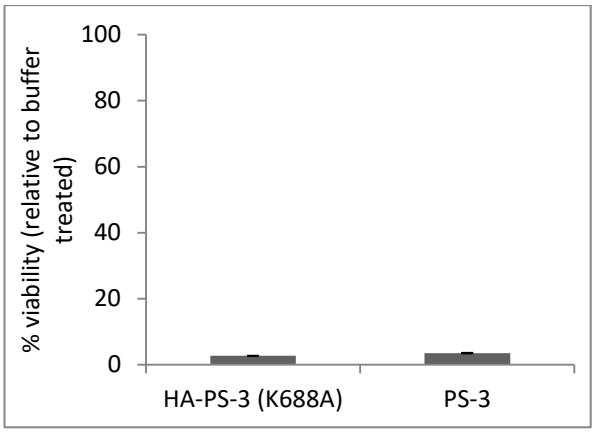

Figure 166 Analysis of the effect of HA-PS-3 (K688A) on HepG2 cell viability.
HepG2 cells were seeded at the density of 25 x 10^4 cells/ml. The next day cells were treated with non-purified trypsin activated toxins: PS-3 (46 µg/ml), or HA-PS-3 (K688A) (46 µg/ml). Viability was measured 24 hours later using CellTiter-Blue.

Ligand blot using HA-PS-3 (K688A)

Trypsin activated HA-PS-3 (K688A) was used in a ligand blot experiment (Figure 167).

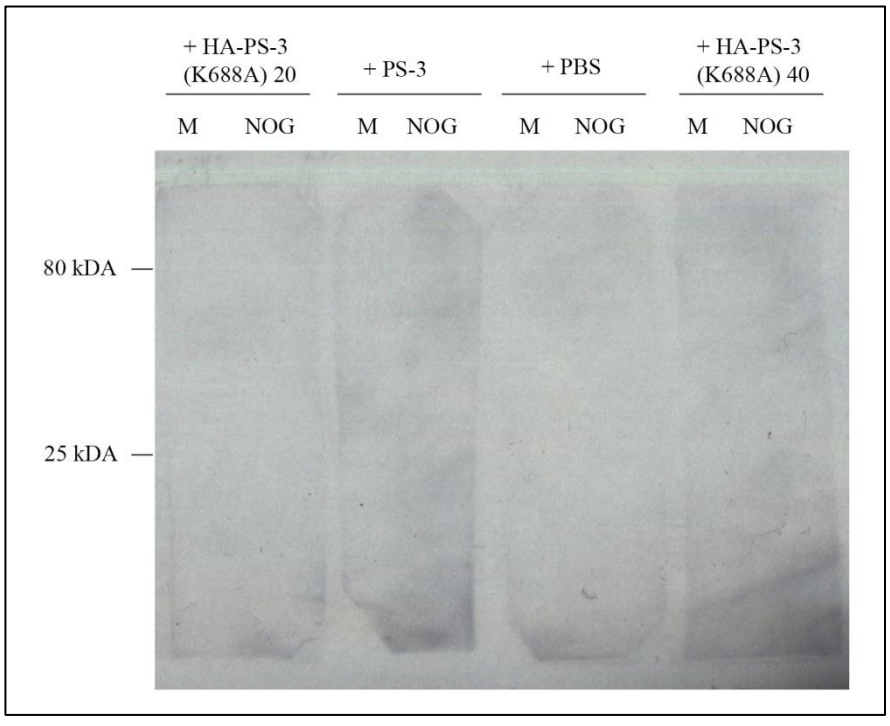

Figure 167 Ligand blot analysis of HepG2 cell extracts using HA-PS-3 (K688A) as a probe.
HepG2 cells were lysed with NOG. Samples were run next to the protein marker on a 12% SDS-PAGE gel (15.6 µg of protein were loaded). After transfer membrane was blocked, washed and cut vertically into four pieces. Membranes were incubated for 1 hour at RT with non-purified trypsin activated toxins in PBS: HA-PS-3 (K688A) (either 20 or 40 µg/ml), PS-3 (18.4 µg/ml) or PBS only. Membranes were washed, incubated with anti-HA antibody and signal detected with ECL.

HA-PS-3 (K688A) used as a probe produced no detectable signal in this experiment.

Pull down using HA-PS-3 (K688A)

Pull down assays were performed using trypsin activated HA-PS-3 (K688A) in the presence or absence of NOG lysed HepG2 cells (Figure 168).

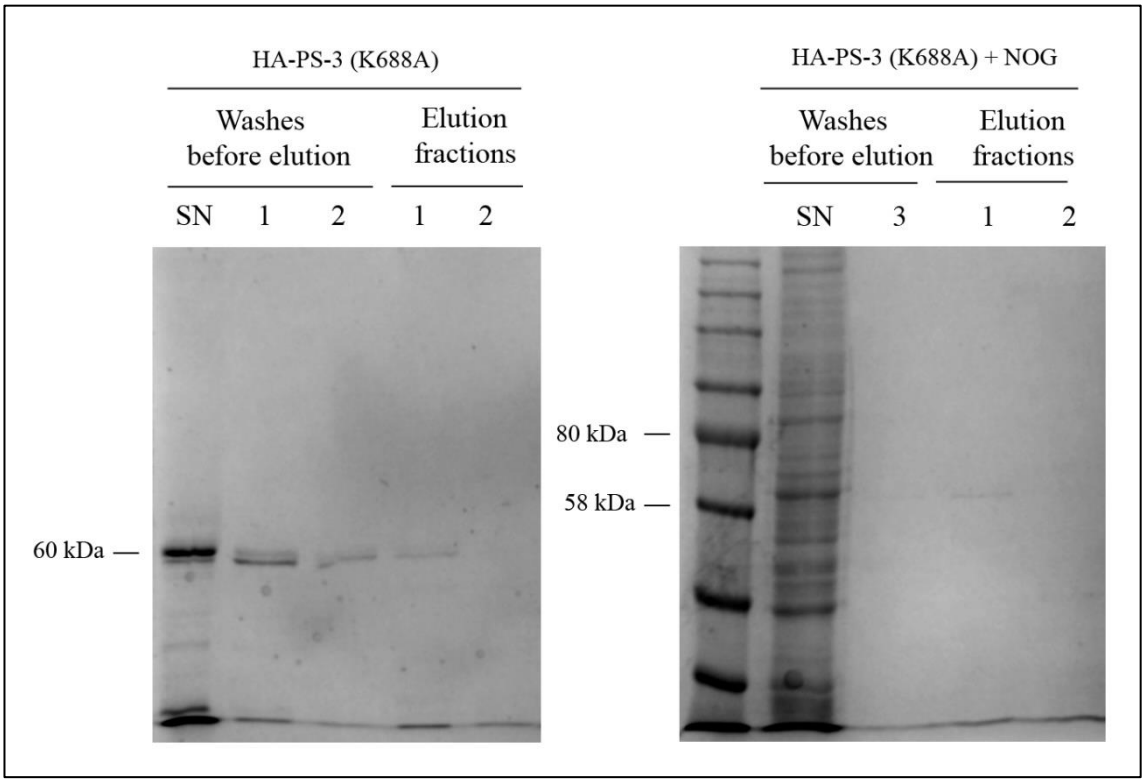

Figure 168 SDS-PAGE analysis of a pull down experiment with activated HA-PS-3 (K688A) in the presence or absence of NOG lysed HepG2 cell extract.
50 µl of pelleted washed anti-HA resin was incubated with trypsin activated HA-PS-3 (K688A) (52 µg) in a doublet. Samples were incubated for 1 hour at RT rotating. After that, to one of the tubes, NOG lysed cell extract was added (257 µg) and the mixture was incubated for another hour rotating at RT. Proteins were eluted with glycine and run on a 7.5% (pull down with HA-PS-3 K688A on the left) and a 12% (pull down with HA-PS-3 K688A and NOG cell extract on the right) SDS-PAGE gel: SN – supernatant collected after resin incubation with toxin (gel on the left) or cell extract (gel on the right), samples from washes before and after elution.

The binding efficiency of trypsin activated HA-PS-3 (K688A) to anti-HA resin was poor compared with pull downs with HA-protoxin (Figure 151). No specific binding between the mutant toxin and the proteins present in the NOG cell extract was observed.

7.7 FITC labelled PS-3

Characterisation of FITC-PS-3

Trypsin activated PS-3 was labelled with FITC as described in the methods section. The labelling was confirmed by measuring fluorescence of labelled toxin and control samples at different stages of labelling (Figure 169).

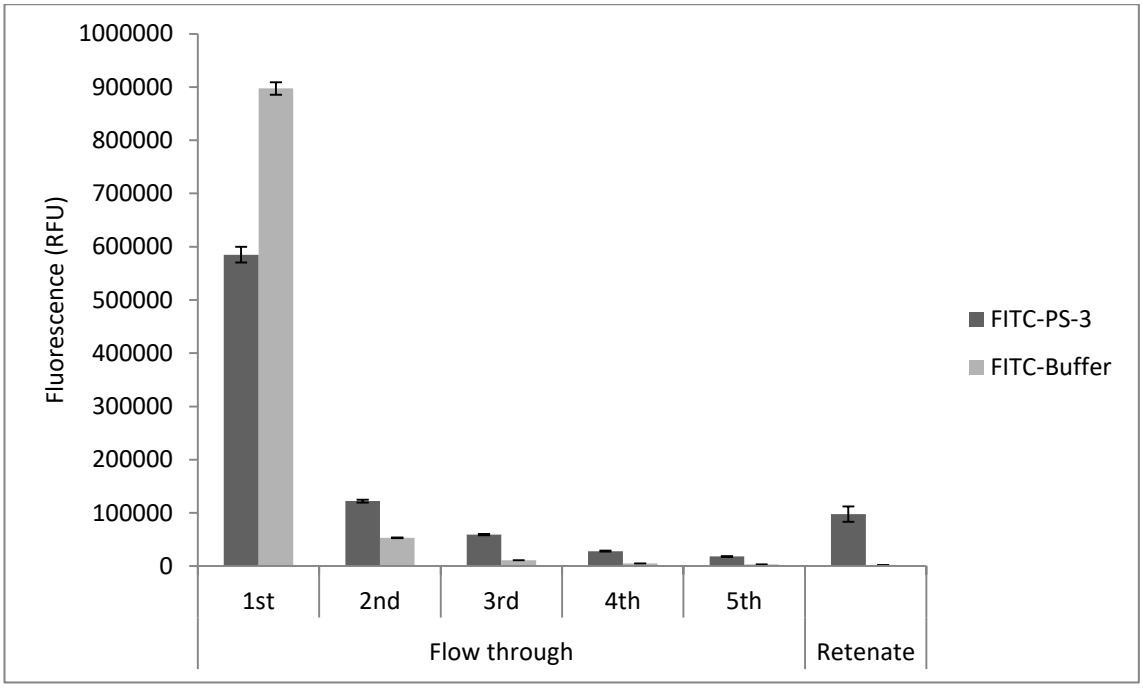

Figure 169 Analysis of FITC labelling efficiency.
Trypsin activated, purified and concentrated PS-3 (1.15 mg/ml) and sodium carbonate (pH 8.5) were labelled with FITC as described in the methods section. Fluorescent properties of flow-through (1-5) and retenate samples were assessed by spotting 10 µl of each sample in a 96-well plate and measuring fluorescent signal 15 minutes later using blue optical filter Ex 490 nm/Em 510-570 nm (FITC Ex/Em wavelength: 494/518 nm).

PS-3 retained fluorescent properties after labelling and excess dye removal.

Labelled toxin was then used in a live cell imagining experiment. Cells were exposed briefly to FITC labelled PS-3 for 10 minutes, followed by two washes with DPBS. Fresh DMEM was added and cells were observed using FITC and bright-field

channels in a wide-field configuration using Zeiss Axiovert 200M microscope. However, despite observing clear cytotoxic effects, fluorescence was very week. Signal appeared more as faint spots rather than the cell outline and did not differ from non-labelled PS-3 or no toxin controls (data not shown).

Next, FITC-labelled toxin was used in a cell assay, where the cells were exposed continuously or briefly to dialysed samples: FITC-PS-3 or FITC-buffer (Figure 170).

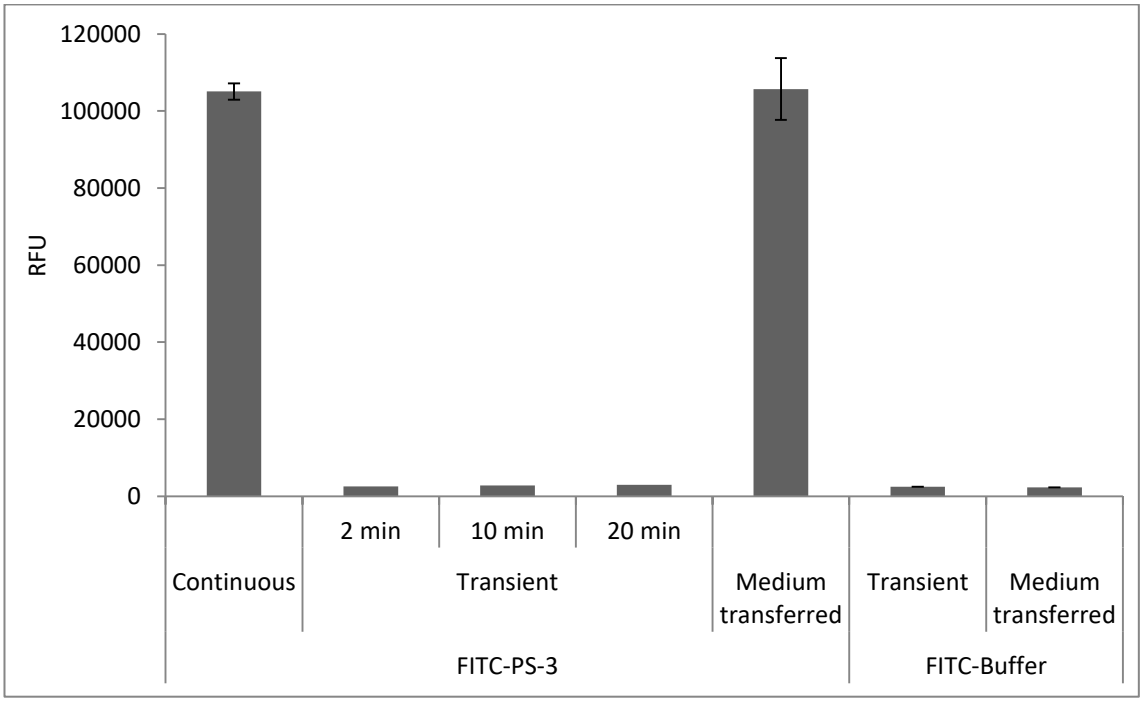

Figure 170 Analysis of fluorescent signal from cells treated transiently or continuously with FITC-PS-3.
HepG2 cells were seeded at the density of 25 x 10^4 cells/ml. The next day cells were treated with either dialysed FITC-PS-3 (115.2 µg/ml) or dialysed FITC-buffer (sodium carbonated pH 8.5). Toxin was applied either permanently (continuous), transiently (for 2, 10 or 20 minutes followed by cell wash and fresh medium addition) or continuously with medium transferred from the well treated transiently for 20 minutes (Medium transferred). Cells treated with FITC-buffer after transient and continuous (medium transferred) exposure are included as a control. Fluorescent signal was measured 1 hour after toxin addition using blue optical filter Ex 490 nm/Em 510-570 nm.

Similarly to live imaging experiment, the cells treated transiently with FITC-PS-3 did not retain fluorescence although all of them showed extensive swelling. Cells treated continuously with FITC-PS-3 presented high fluorescence and showed extensive swelling. Interestingly, medium with FITC-PS-3 transferred after 20 minutes to a new

set of cells contained very well conserved fluorescein, similarly to the results obtained in a viability assay where one toxin dose transferred nine times retained its full activity (Figure 43). FITC-labelled Cry1Ca or FITC alone (concentration matched to FITC bound to PS-3) did not induce swelling (data not shown).

The ability of anti-FITC antibody for immunodetection of the labelled toxin was tested in a dot blot experiment (Figure 171).

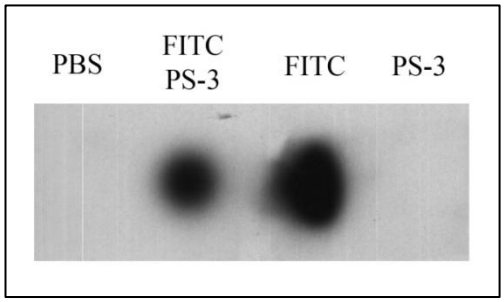

Figure 171 Dot blot analysis of FITC-PS-3 labelling.
5 µl of trypsin activated PS-3 prior and post FITC labelling (5.7 µg of protein); PBS and FITC (appropriately diluted to match FITC concentration bound to PS-3) were spotted on a nitrocellulose membrane, blotted with anti-FITC antibody followed by ECL detection.

FITC was successfully detected in FITC-PS-3. To sum up, despite successful toxin labelling, no significant binding to HepG2 cells was detected using cell culture assays.

Ligand blot using FITC-PS-3

Next, FITC-labelled toxin was used as a probe in a ligand blot experiment (Figure 172).

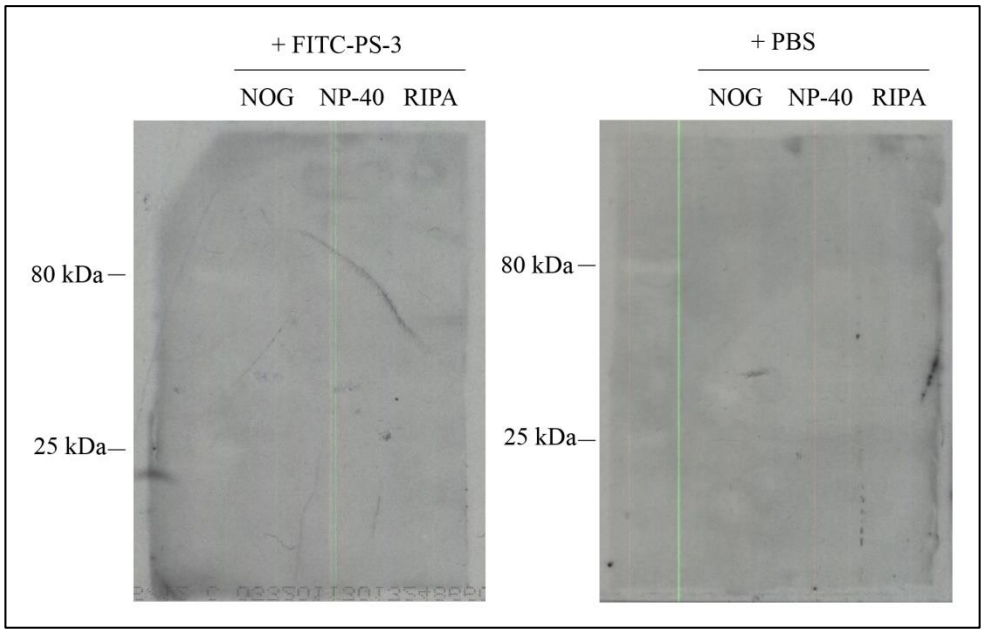

Figure 172 Ligand blot analysis of HepG2 cell extracts using FITC-PS-3 as a probe.
Cells were lysed with NOG, RIPA or NP-40. Samples were run on a 12% SDS-PAGE gel (20 µg of protein were loaded). After transfer membrane was blocked, washed and cut. One piece was incubated with FITC-PS-3 (17.2 µg/ml) and the other one with PBS. Membranes were washed, incubated with anti-FITC antibody and detected with ECL.

FITC-PS-3 did not associate with any of the proteins.

7.8 PS-3 immobilization via sulfhydryl groups

SulfoLink Coupling Resin was used to allow covalent attachment of toxin to beaded agarose via sulfhydryl (-SH) groups. Iodoacetyl groups present on the resin interact with a protein that contains reduced cysteine residues forming covalent thioether bonds that permanently attach protein to the resin. Cysteine linkage was chosen for a reason. The -SH group, being less common than e.g. $-NH_2$, would ensure that labelling occurs at a specific amino acid position limiting the possibility of the linkage blocking or adversely affecting toxin's structure and function. Distribution of cysteines in the structure of PS-3 protoxin was examined (Figure 173) using a model generated by

Phyre[2] (Kelley et al., 2015) and viewed using UCSF Chimera 1.10.1 (Pettersen et al., 2004).

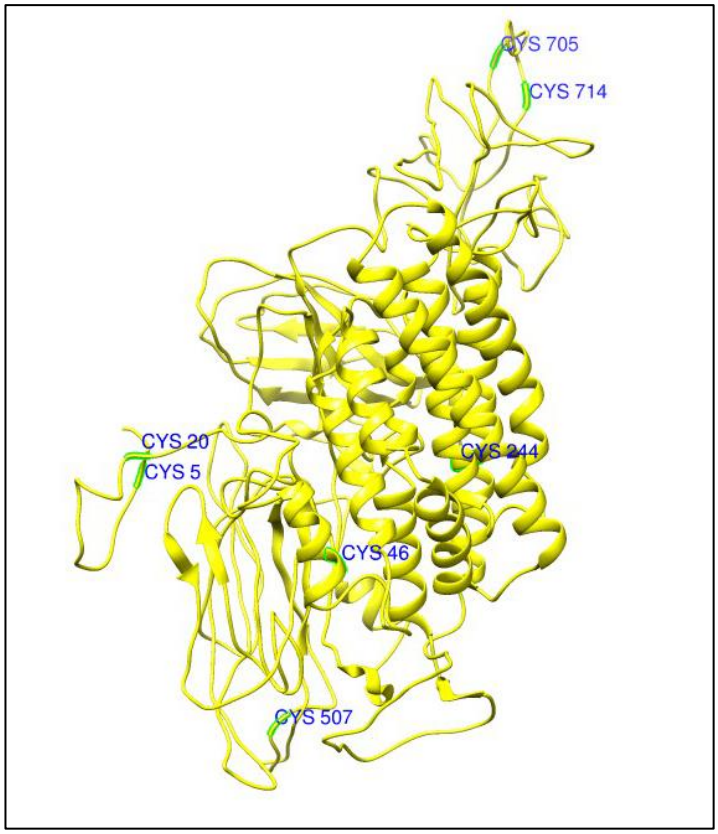

Figure 173 Distribution of cysteines in PS-3 protoxin sequence.
A model of PS-3 protoxin was generated by Phyre[2] and viewed using UCSF Chimera 1.10.1. PS-3 protoxin structure is in yellow, positions of cysteines are marked in green with blue labels.

Cysteines at position 5 and 20 are cleaved off during N-terminal activation by trypsin. Cysteines at position 705 and 714 lie within the C-terminus and are also most likely cleaved during proteolysis, while Cys244 and Cys507 are probably not exposed. Cys46 is exposed and appeared to be a good candidate residue for coupling.

Characterisation of PS-3 coupled resin

Trypsin activated PS-3 was coupled to SulfoLink resin as described in the methods section. Coupling efficiency was analysed using SDS-PAGE (Figure 174).

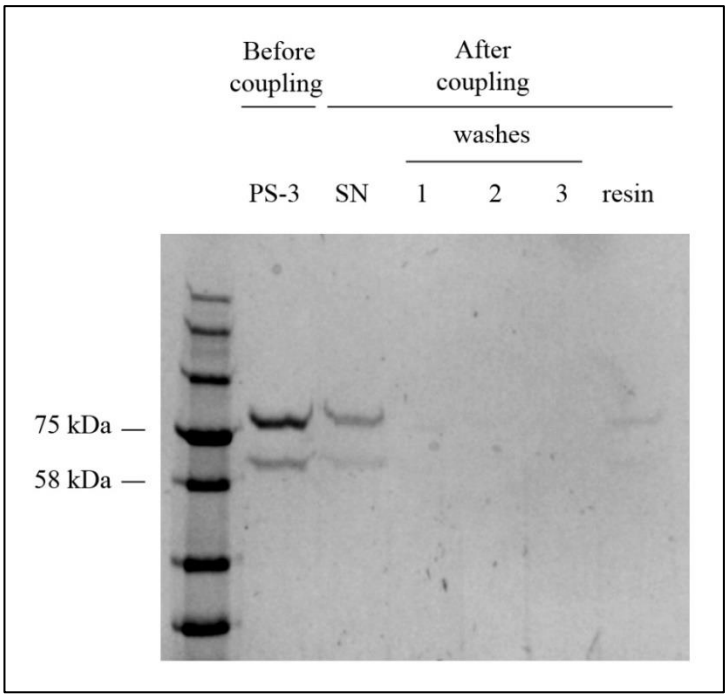

Figure 174 SDS-PAGE analysis of PS-3 immobilization to resin via sulfhydryl groups.
Purified trypsin activated PS-3 was coupled to SulfoLink resin. Samples at different stages of this process were run on a 7.5% SDS-PAGE gel: ÄKTA purified and concentrated PS-3 used for coupling (168 µg/ml), SN – supernatant collected after coupling (for estimation of binding efficiency), three washes after coupling, and coupled resin.

The weak toxin band in the resin lane may indicate that coupling efficiency was poor. However the crosslinking acts by covalently immobilizing sulfhydryl-containing proteins; hence the coupled toxin may have not entered the gel, despite boiling and SDS treatment, due to a large size of resin beads. Next, toxin coupled resin was tested in a dot blot experiment for PS-3 detection using anti-PS-3 antibody (Figure 175).

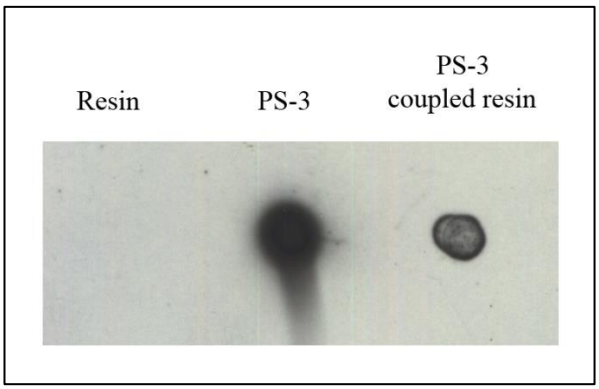

Figure 175 Dot blot analysis of PS-3 coupled resin.
5 µl of trypsin activated PS-3 prior and post coupling (0.84 µg of protein) as well as non-coupled resin were spotted on a nitrocellulose membrane, blotted with anti-PS-3 antibody, followed by ECL detection.

PS-3 coupled resin produced a signal confirming successful attachment of the toxin. Coupled resin was incubated with adhered HepG2 and HepG2 cells in suspension (after cell trypsinization) to establish cell swelling, however even when the cells were in suspension they did not stay in contact with relatively larger resin beads. Swelling was not observed most likely due to insufficient physical contact between the immobilized toxin and the cells (data not shown).

Pull down using PS-3 coupled resin

Figure 176 presents results of a pull down experiment performed with PS-3 coupled resin and NOG lysed HepG2 cells.

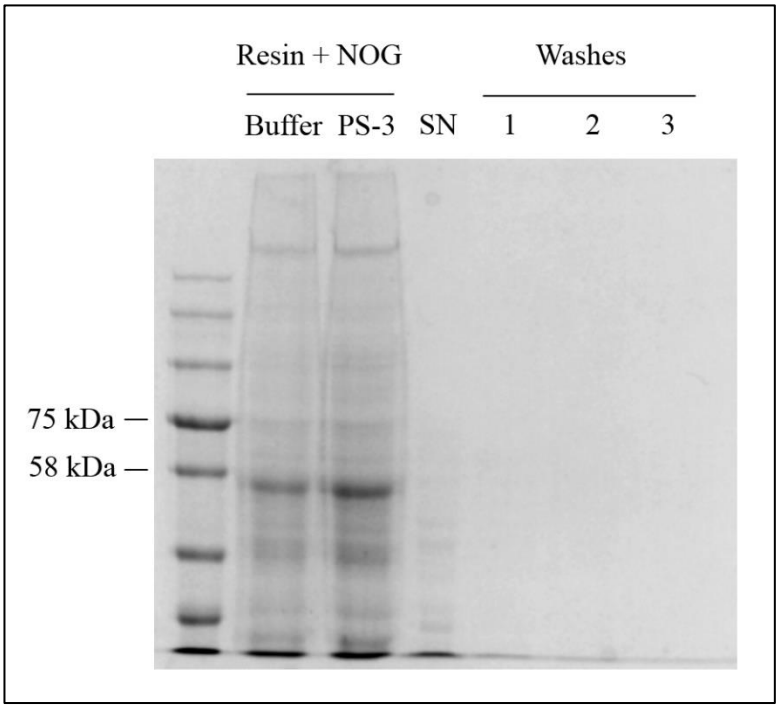

Figure 176 SDS-PAGE analysis of a pull down experiment using PS-3 coupled resin and NOG lysed cell extract.
50 µl of pelleted washed SulfoLink resin was incubated with ÄKTA purified trypsin activated PS-3 (74 µg) or buffer only as described in the methods section. After incubation non-specific binding sites were blocked with L-cysteine-HCl buffer in both samples. Resins were washed and incubated with NOG lysed HepG2 cell extracts (260 µg). Samples were analysed on a 7.5% SDS-PAGE gel: washed resin after incubation with toxin or buffer and NOG cell extract, SN – supernatant collected after resin incubation with toxin and NOG cell extract, samples from three resin washes after incubation with toxin and NOG cell extract.

Despite covalent bond between resin and the toxin, this experiment was performed in hope that denaturing conditions of SDS-PAGE would release any proteins bound to PS-3. The presence of the same bands in lanes with resin incubated with or without the toxin indicates non-specific binding of cell extract proteins to the resin. Strong intensity of the bands in resin lanes compared with the supernatant lane indicates high affinity of the HepG2 proteins for the beads despite resin blocking with L-cysteine-HCl. PS-3 band could not be detected, which may be due to its covalent immobilization to resin. Due to time constraints this method was not optimised further.

7.9 Analysis of N-cadherin blocking on PS-3 activity

Antibodies may be utilized to block a surface protein in the cell culture. Through administering a specific antibody that binds to the protein of interest, physical interactions of that protein with other proteins can be inhibited. Expression levels of different cadherins were analysed in HepG2 cells using the Human Protein Atlas representing human proteome database (Uhlén et al., 2015). One, identified at both the mRNA and protein level, was N-cadherin or cadherin-2 (CDH2). Its sequence was analysed and in the membrane proximal extracellular domain, a sequence ^{694}SILRVKV^{700} was identified, similar to ^{1336}SILTVTV^{1342} present in cadherin repeat 11 in *M. sexta* BT-R1 and identified as Cry1A binding site (Gómez et al., 2003). A rabbit polyclonal anti N-cadherin antibody was purchased (synthetic peptide used as an immunogen corresponded to 701-714 amino acid sequence of the extracellular domain in the human N-cadherin). Functionality of antibody was assessed in a western

blot. Expression levels of N-cadherin were analysed in HepG2, HeLa and HL-60 cells (Figure 177).

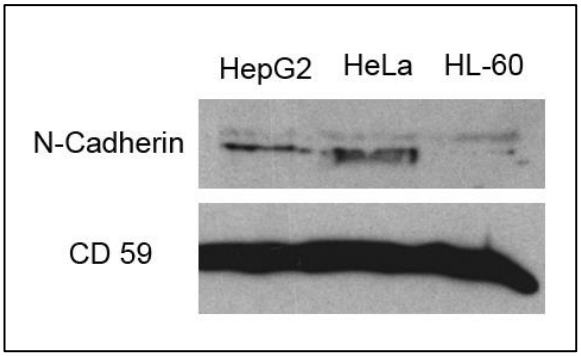

Figure 177 Expression levels of N-cadherin in different cell lines.
HepG2, HeLa and HL-60 cells were lysed in NOG buffer. Cell extracts were run on a 10% SDS-PAGE gel. 25 µg of protein were loaded in each lane. Samples were analysed by western blot for the presence of N-cadherin or CD59.

The antibody successfully detected N-cadherin in HepG2 cells and the levels of expression for the three cell lines correlated well with the data deposited online in the Human Protein Atlas for each of the cell line (data not shown).

Next, PS-3 toxicity was examined in HepG2 cells pre-incubated with anti N-cadherin antibody (Figure 178).

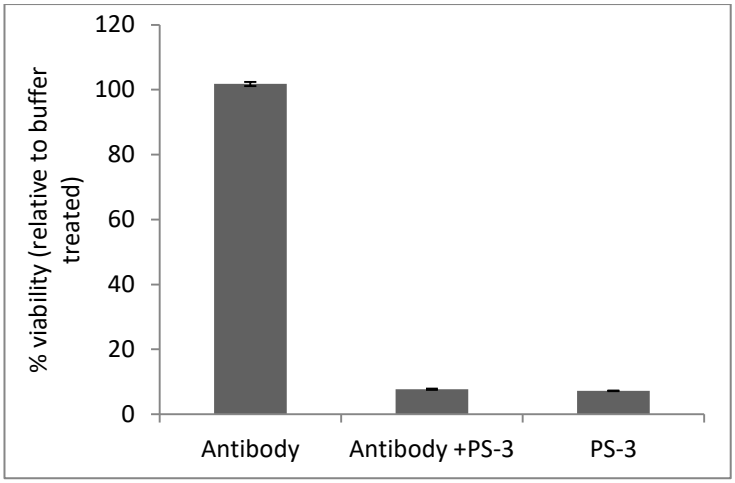

Figure 178 The effect of HepG2 cell pre-incubation with anti N-cadherin antibody on PS-3 activity.
HepG2 cells were seeded at the density of 25 x 10^4 cells/ml in complete DMEM. The next day medium was changed to Advanced DMEM without FCS and antibiotics and cells were treated with anti N-cadherin antibody (23.8 µg/ml) or 50:50 glycerol: DPBS (v/v). 24 hours later either PS-3 (12 µg/ml) or buffer was administered. Viability was measured 24 hours after toxin addition using CellTiter-Blue.

Activity of PS-3 was unaffected by pre-incubation with the anti N-cadherin antibody, however the binding between the antibody and N-cadherin was not analysed.

7.10 Assessment of cholesterol depletion and GPI-linked protein cleavage on PS-3 toxicity

HepG2 cells were sequentially adapted to medium containing 0% serum by passaging cells in decreasing amount of FCS. This was done because serum components may interfere with enzyme activity through binding or even degrading molecules added to the medium. FCS was decreased in four passages from 10%, 7.5%, 5%, 2.5% to 0%. The change from 2.5% to 0% FCS was too stressful for cells as they did not attach to the flask. PI-PLC experiment was attempted using cells cultured in 2.5% FCS as these cells stayed connected to the flask and showed similar morphology to HepG2 cultured in 10% FCS. However, when cells were washed with DPBS prior to PI-PLC addition, the majority of the cells detached from the plate. Moreover, cell viability assayed by Trypan Blue was only 50% (data not shown). Because of these obstacles, PI-PLC and MβCD assays were performed using cells cultured in 10% FCS, with medium changed to Advanced DMEM (without FCS supplementation) prior to enzyme treatment.

Cholesterol or GPI-anchored proteins were depleted from the membrane with MβCD and PI-PLC enzyme respectively. After a wash with DPBS, the cells were incubated with or without PI-PLC or MβCD in the culture medium without serum, followed by PS-3 treatment. Cytotoxicity of PS-3 against these cells was then evaluated in a viability assay (Figure 179) and by a visual inspection of cell morphology.

Prolonged incubation with 5 mM MβCD or PI-PLC caused some cell detachment and death therefore viability was measured after 2 hours. Removal of PI-PLC or MβCD before PS-3 addition resulted in cell detachment, hence was aborted (data not shown).

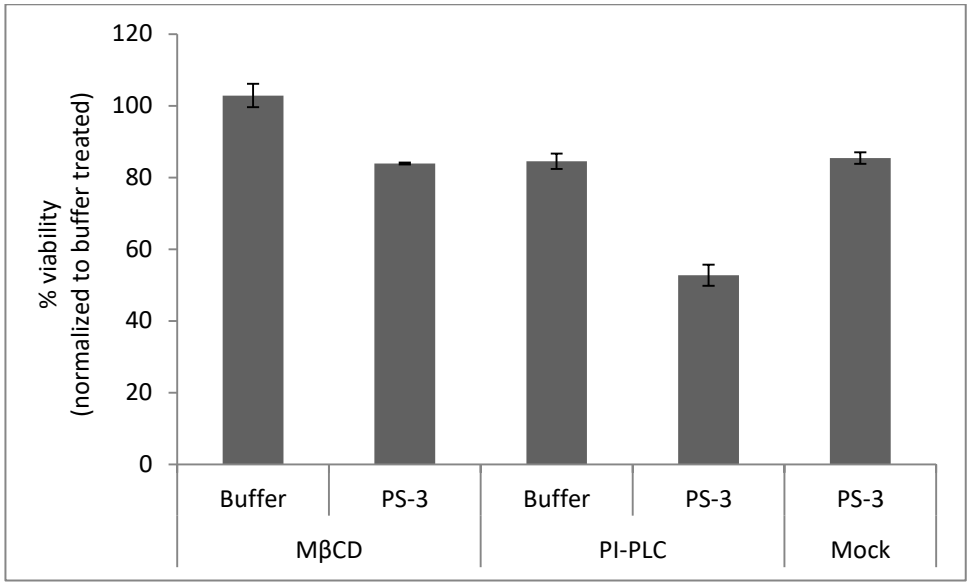

Figure 179 Analysis of PS-3 activity in HepG2 cells pre-treated with PI-PLC or MβCD.
HepG2 cells were seeded at the density of 25 x 10^4 cells/ml in complete DMEM. The next day cells were washed with DPBS and medium changed to Advanced DMEM without FCS and antibiotics. Next, cells were pre-incubated with 5mM of MβCD for 30 minutes or PI-PLC (250 mU per 2.25 x 10^4 cells) for 1 hour at 37°C. After that PS-3 (12 µg/ml) or buffer was added. CellTiter-Blue reagent was added 20 minutes later and the readings were taken 2 hours after toxin addition.

The results showed that 5 mM MβCD and a high dose of PI-PLC were not able to reduce PS-3 activity with PI-PLC somewhat affecting cell viability. No difference was noted in the degree of cell swelling in the toxin treated wells with or without enzyme pre-treatment as observed 20 minutes after PS-3 addition.

To confirm the effectiveness of the PI-PLC treatment, the amount of GPI-anchored CD59 - a membrane glycoprotein present on the cell membrane - was studied by immunoblotting with anti-CD59 antibody. The cells were incubated in the absence or presence of PI-PLC, then washed and lysed. Cell extracts were analysed by western blotting (Figure 180).

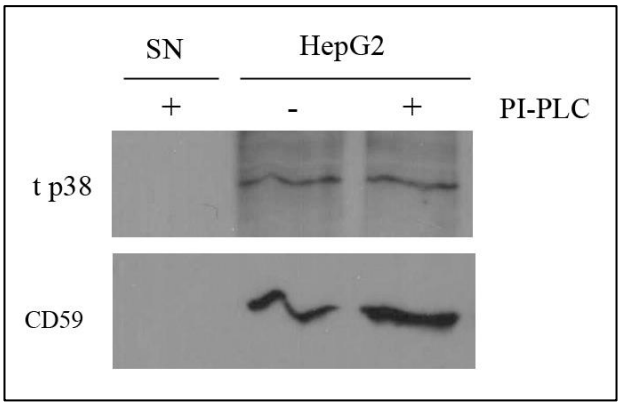

Figure 180 Western blot analysis of CD59 cleavage from the cell membrane after PI-PLC treatment.
HepG2 cells were seeded in a 6-well plate. The next day cells were washed with DPBS and culture medium changed to Advanced DMEM. 25 x 10^4 cells were treated with PI-PLC (500 mU) or buffer for 1 hour at 37°C, followed by cell lysis with RIPA. 15 µg of protein were loaded in each lane. Samples were analysed by western blotting with antibodies against CD59 or total p38 (t p38 - loading control) including supernatant (SN) collected after PI-PLC treatment and before cell lysis.

The presence of CD59 band in the pellet fraction of the cells pre-treated with PI-PLC indicates that the cleavage of the phosphodiester bond in the GPI-anchored proteins was ineffective. Experiment was repeated with enzyme treatment performed in a different buffer called PI-PLC buffer (Figure 181), which consisted of: 10 mM tris-HCl, 144 mM NaCl, 0.05% BSA, pH 7.4.

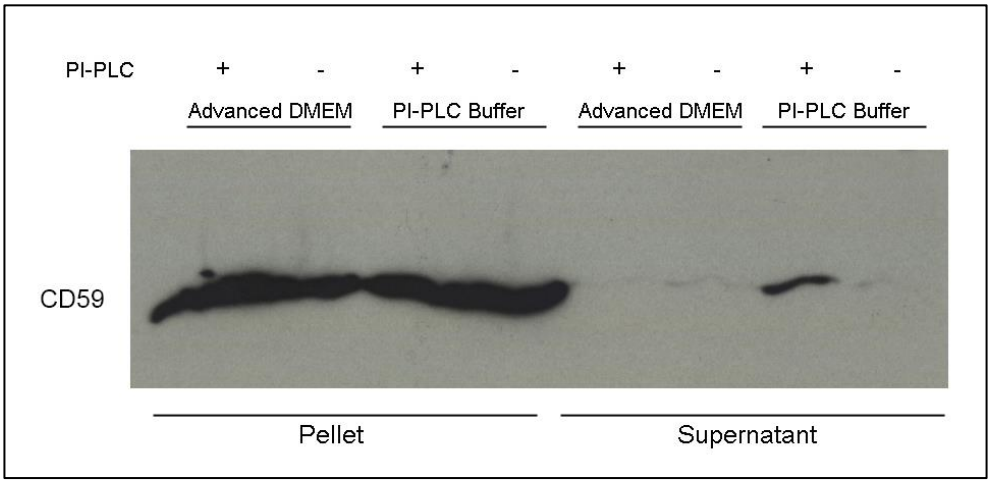

Figure 181 Western blot analysis of CD59 cleavage in the supernatant and pellet fractions using PI-PLC buffer.
HepG2 cells were washed with DPBS twice and trypsinized. 25 x 10^4 cells were re-suspended in either Advanced DMEM or PI-PLC buffer +/- 116 mU of PI-PLC. Cells were incubated at 37°C for 1 hour with occasional gentle shaking. After that cells were spun. Supernatant and RIPA lysed pellets were analysed by a western blot using anti CD59 antibody. 15 µg of protein were loaded in each lane.

Performing the digest in PI-PLC buffer allowed the enzyme to cleave some of CD59. The strong CD59 signal in the lysed cellular pellet suggests that the cleavage was only partial or that it represents an intracellular pool of CD59.

The effect of GPI-anchored protein cleavage and cholesterol depletion on PS-3 toxicity was re-assessed using the PI-PLC buffer and a kinetic viability cell assay (Figure 182 and Figure 183 for PI-PLC and MβCD assay respectively).

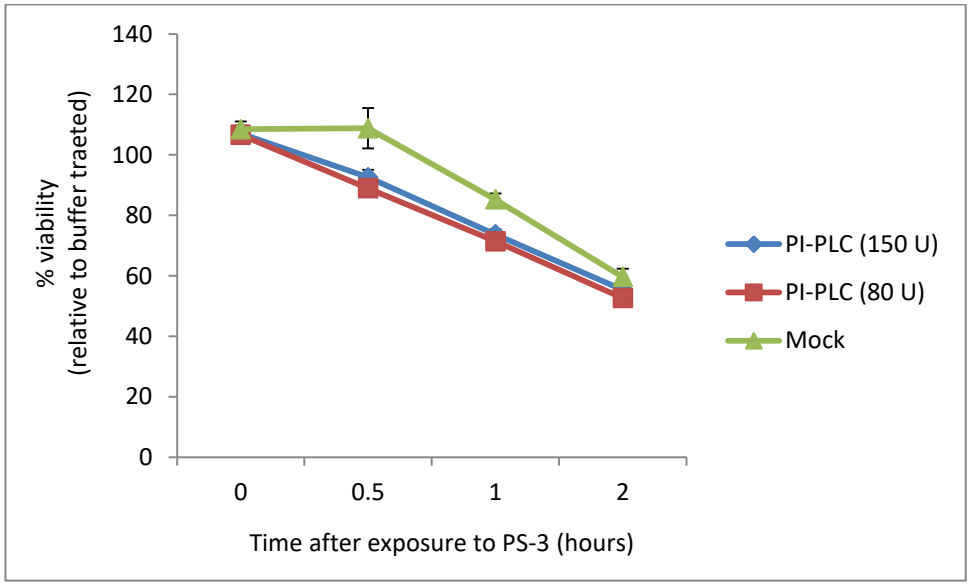

Figure 182 Analysis of PS-3 activity in HepG2 cells pre-treated with PI-PLC in PI-PLC buffer.
HepG2 cells were seeded at the density of 25 x 10^4 cells/ml in a white 96-well plate in PI-PLC buffer in the presence of viability reagents. Next, cells were incubated with various amounts of PI-PLC (U) for 60 minutes, before the toxin (10 µg/ml) was added. Luminescent readings were recorded at different time-points after toxin addition using RealTime-Glo cell viability assay.

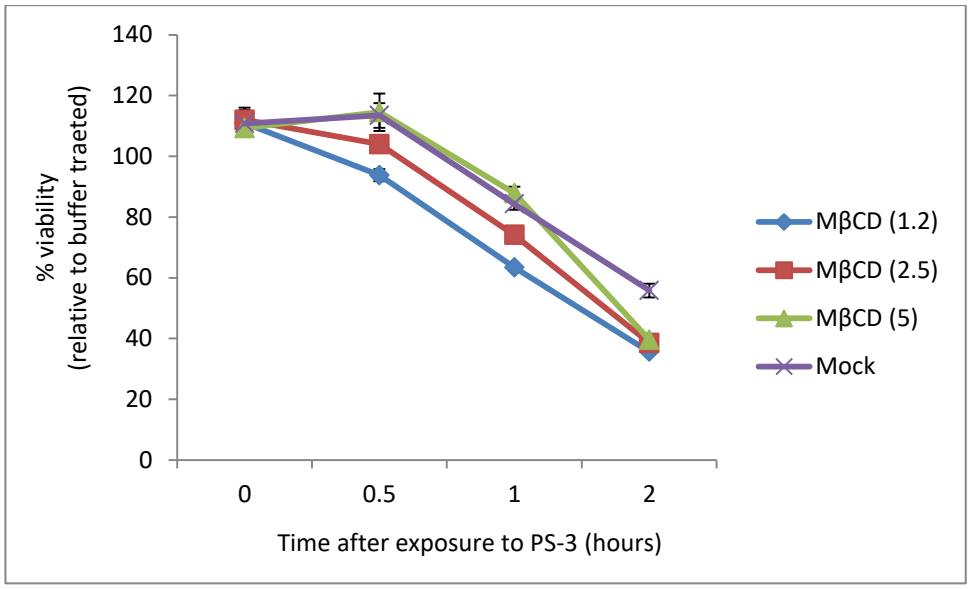

Figure 183 Analysis of PS-3 activity in HepG2 cells pre-treated with MβCD in PI-PLC buffer.
HepG2 cells were seeded at the density of 25 x 10^4 cells/ml in a white 96-well plate in PI-PLC buffer in the presence of viability reagents. Next, cells were incubated with various concentrations of MβCD (mM) for 30 minutes, before the toxin (10 µg/ml) was added. Luminescent readings were recorded at different time-points after toxin addition using RealTime-Glo cell viability assay.

Cell pre-treatment with PI-PLC and MβCD in the simple buffer had no significant effect on PS-3 toxicity, correspondingly to previous viability assay results (Figure 179). The above results may indicate that GPI-linked proteins and cholesterol do not play a significant role in toxin's mode of action.

7.11 Discussion

Ligand blot experiments did not identify any proteins that PS-3, used as a probe, would bind to specifically. Lanes with HepG2 cells - supposedly containing molecules critical for high susceptibility to the toxin - did not present a band profile different from resistant HeLa cells. The reasons why receptor was not identified may be many. The simplest being, that it may not be a protein. PS-3 receptor could have a lipid nature. Glycolipids have been identified as binding partners for Cry14A and Cry5B in *C.*

elegance before (Griffitts et al., 2005). Even if it is proteinous, denaturing conditions of SDS-PAGE used in the majority of western blot experiments may have destroyed discontinuous epitopes that the toxin may require for binding. PS-3 may have not been able to recognize continuous epitopes even if they represent the receptor. Another possibility is that the non-specific bands could have masked specific signal due to low resolution of the SDS-PAGE. However, with so many methods of detection used and different MW sizes of non-specific bands depending on the method used, it is very improbable. Results presented in Figure 43 and Figure 170 suggest that PS-3 interaction with the membrane is weak and/or involves a small amount of toxin molecules and may be beyond detection using a western blot system. Yet another possibility, although unlikely, is that there is no receptor and the mode of action is in this respect different from other Cry toxins.

Strong cross-reactivity of cellular proteins with either labelled toxin or antibodies was evident. Anti-PS-3 antibody resulted in a high degree of non-specific binding with the resolved proteins that could not be improved despite laborious method optimization. Epitope mapping, where immuno-reactive regions of the antigen are recognized to improve protein-protein interaction could be highly beneficial. However, the polyclonal character of this antibody may be the issue. It is thought that only 0.5 – 5% of the antibodies in a polyclonal mixture recognize the target antigen (Bradbury and Pluckthun, 2015). Additional purification of anti-PS-3 antibody using anti-HA resin and HA-PS-3 did not improve the background signal. Antibodies against other Cry toxins also bound non-specifically, but only to the non-purified form of PS-3 and could not detect the purified toxin.

Streptavidin too produced non-specific binding interactions. Biotin is a vitamin derived from diet and intestinal bacteria, important for fatty acid metabolism. It functions as a cofactor facilitating transfer of carbon dioxide during the action of certain carboxylases and decarboxylases (Wood and Warnke, 1981). Liver, among a few other tissues, is relatively abundant in biotin-containing enzymes (Dakshinamurti and Mistry, 1963, Wood and Barden, 1977). Experiments of intracellular distribution of biotin in liver cells showed that about 50% of biotin bound enzymes are present in a cytosolic fraction, especially in mitochondria and nuclei (Dakshinamurti and Mistry, 1963). Furthermore, streptavidin itself contains a tripeptidyl sequence that shows high resemblance to the binding sequence of fibronectin and other adhesion molecules, increasing the non-specific binding of streptavidin to cell surface (Alon et al., 1990, Alon et al., 1993). High auto fluorescent background observed in experiments with biotin labelled PS-3 may be due to these reasons.

The HA-PS-3 did not display a significant cross-reactivity with resolved proteins, except for when HepG2 cells were lysed with NOG buffer. This non-specific binding was through the HA tag and not anti-HA antibody or PS-3. Instability of the HA tag after trypsin digest was problematic to detect as freshly activated toxin contained the tag. The HA tag degraded along with the increasing length of sample storage. HA tagged protoxin was detected better by the antibody, but did not contribute to protein receptor identification. Protoxin binding to the receptor may have been impaired due to the lack of the N-terminal processing. HA-PS-3 (K688A) mutant, engineered to solve this problem, offered the presence of a stable tag, but did not facilitate any specific binding.

There are many possibilities to explain the lack of fluorescence in FITC-PS-3 treated cells. Toxin may have not been labelled efficiently or fluorescence quenched after interaction with the membrane. More likely, only a minute amount of toxin is required to trigger toxicity, which was also concluded from results of another viability assay (Figure 43). Moreover, this could explain why HA-PS-3 was not detected by anti-HA antibody in cells exposed to the high toxin dose prior to cell lysis, even when exposure time was extended to increase the chances of presumable oligomerisation.

Pull down assays were performed using either HA tagged toxin or toxin immobilised on beads. Efficiency of toxin-resin binding varied. Satisfactory binding was obtained for HA-protoxin. Surprisingly, HA-PS-3 (K688A) showed reduced binding compared to HA-protoxin. Binding efficiency of PS-3 coupled to resin via sulfhydryl groups was difficult to assess due to its covalent immobilization and lack of a proper elution buffer. In all cases, pull downs did not identify any proteins binding specifically. Due to the negative results and time constraints these methods were not optimised further.

Cadherin-like proteins have been identified as functional Cry toxin receptors in insects with toxin binding regions located near the membrane proximal extracellular domain and adjacent cadherin repeats (Pigott and Ellar, 2007). Cadherin functional blockage with antibodies was successfully performed in vivo (Gänzler-Odenthal and Redies, 1998) and in vitro (Qian et al., 2004). Based on the information about human N-cadherin mentioned earlier, a blocking assay was performed to evaluate the role of N-cadherin as a potential PS-3 receptor. Cell pre-incubation with anti- N-cadherin antibody did not affect the activity of PS-3, however the binding between the antibody

and N-cadherin was not analysed. Providing that the binding took place and association with other molecules - like PS-3 - was impaired, it can be assumed that N-cadherin does not facilitate PS-3 binding to the cell membrane.

Western blot analysis after PI-PLC treatment indicated a strong influence of the buffer on the activity of this enzyme. PI-PLC was capable of releasing some of CD59 in the presence of a basic physiological buffer, but not in the serum free medium. After PI-PLC treatment, CD59 was detected also in the pellet, which may represent an intracellular pool of CD59. In fact, Amet et al. already demonstrated that human hepatocytes expressed high levels of intracellular CD59 (Amet et al., 2012), which makes CD59 not an ideal marker for PI-PLC cleavage in these experiments. MβCD is frequently used to efficiently deplete cells of cholesterol. The amount of the membrane cholesterol after treatment with MβCD was not quantified, however 5 mM MβCD was documented previously to cause ∼40% reduction of total cholesterol pool in HepG2 cells (Guo et al., 2011). Viability assays showed that a high dose of neither MβCD nor PI-PLC were able to prevent reduced viability and swelling after toxin application. Although the protein and the lipid levels after depletion were not assessed in details, the results may indicate that GPI-linked proteins and cholesterol do not play a significant role in the toxin’s mode of action.

8. General discussion

Bt based pesticides have been widely used for over 50 years with no harmful effects on humans (Koch et al., 2015). Parasporins represent a group of *Bt* toxins that can specifically kill certain human tumour cells in vitro and their application in anti-cancer therapy was suggested. Some parasporins, like PS-3, are closely related in structure to *Bt* toxins commercially used as bio-pesticides, however at the moment parasporin activity cannot be predicted based on a toxin's sequence. This research was conducted to elucidate the mode of action of PS-3.

Results of the experiments performed in this study are consistent with PS-3 being a pore forming toxin. Similar to insecticidal Cry toxins, proteolytic activation of PS-3 was necessary for toxicity. Two different size fragments resulting from proteolytic activation showed after chromatographic separation cytotoxicity towards HepG2 cells, indicating partial cleavage sites most likely at the C-terminus. Rapid swelling was microscopically observed in susceptible cells, analogous to insect cells losing the ability to regulate osmotic pressure after exposure to Cry toxins (Knowles and Ellar, 1987). PS-3 significantly and rapidly decreased cell viability and ATP levels, and did not induce activation of caspases or oxidative stress, consistent with ROS-independent necrotic cell death. The EC_{50} of PS-3 was 2.17 µg/ml, similar to the previous calculation (Yamashita et al., 2005). Cell exposure to PS-3 resulted in membrane rapidly becoming permeable, allowing the detection of both a small and a large size cytotoxic marker. This effect was both time and dose dependent. The size of primary lesions was estimated <1 nm. In the absence of intracellular content and membrane proteins PS-3

induced channel formation in PLBs as well as in biological membrane patches of various origins. PLB experiments ultimately confirmed the pore forming nature of PS-3.

Pre-treatment of HepG2 cells with EGTA inhibited PS-3 toxicity by means of metal ion chelation. Further investigation indicated that EGTA acts early in the toxin's mechanism of action by preventing stable interaction with the membrane and the subsequent steps of membrane damage and p38 phosphorylation. More clarification came from the experiments involving different chelators, ionic buffer composition, ion supplementation and PLBs. EGTA exerted its protective effect by chelating cations bound to plasma membrane components, most likely candidates being: Ca^{2+}, Mn^{2+} and Zn^{2+}, which may work in a co-operative fashion. The exact function of these cations is unknown. Ca^{2+} and Zn^{2+} dependent proteins represent some well-known, functional receptors of Cry toxins in insects (Pigott and Ellar, 2007). Therefore a role of cations in facilitating a receptor's structure or enzymatic activity may provide a plausible explanation (Kirouac et al., 2006).

Another aspect of the PS-3 mode of action was analysed from the viewpoint of cellular responses to the toxin, although the investigation was limited to a few signalling pathways. Activation of p38 MAPK is a conserved cellular response to PFTs (Porta et al., 2011). Consistently with PS-3 being a PFT, activation of p38 MAPK was clearly evident in susceptible cells and reached its maximum before cell swelling ensued. Inhibition of p38 activity did not rescue cell viability, agreeing with the belief that this pathway is not universally protective following PFT attack (Husmann et al., 2006, Stringaris et al., 2002, Aroian and van der Goot, 2007). It is also consistent with little membrane recovery observed in cells transiently treated with PS-3. Moreover,

PS-3 also activated ERK 1/2 MAPK but its role was not assessed. One model of Cry toxin's action invokes the involvement of adenylyl cyclase and PKA signalling pathway (Zhang et al., 2006), which was addressed in this study. Western blot results and experiments with PKA inhibitors clearly indicated that PKA and various other kinases do not play a role in the PS-3 mode of action.

PS-3 is active against a very narrow cell type range. Five cell lines not examined before (2 lymphoblastoid, 2 Burkitt's lymphoma and CHOK1 cells) did not show susceptibility towards a high toxin dose; however it seems that cells' resistance can be overcome by increasing toxin concentration, e.g. HeLa cells (Yamashita et al., 2000). Why PS-3 targets some cancer cells remains unknown. Similar to insecticidal Cry toxins, specificity and selectivity of parasporins indicate the involvement of a specific receptor in toxicity. Also, an increasing number of membrane bound proteins that are specific for cancer cells are being discovered (Grimm et al., 2011). Many attempts were made aimed to identify a PS-3 receptor. Experiments, based on the assumption that the receptor is proteinaceous in nature, proved unsuccessful for various reasons described in chapter 7. Additional experiments with membrane depletion of certain components excluded for the moment cholesterol and GPI-linked proteins from being significant players in the PS-3 mode of action. Results also suggest that the toxin-membrane interaction is weak or involves a small amount of toxin. Nevertheless, the presence of a receptor in the membranes of susceptible cells is still anticipated and will undoubtedly be the subject of future analyses.

The application of parasporins in the medical field was suggested based on their preferential activities against cancer cells (Ohba et al., 2009). The concept of drug

targeting is not new (Fahmy et al., 2005). Nanoparticle drug delivery system is a well-known component of that, but not exclusive. There are other efficient systems of targeted therapy like oncolytic viruses, which are modified not to target non-dividing and differentiated cells resulting in selective infection and lysis of cancer cells (Kaufman et al., 2015). Recently, the utilization of CRISPR/Cas9 - a genome editing method – for targeted gene therapy is underway (Sachdeva et al., 2015). The high specificity of PS-3 is definitely an advantage. However, despite many other drawbacks and pharmacological concerns, a big protein size poses a risk of immunogenicity, especially if the region required for toxicity cannot be narrowed down to a drug size molecule, which is the case for the three domain Cry toxins, where each structural domain is required for action. Also, the health risks that parasporins pose on humans are unknown. In this study, PS-3 was demonstrated to act like a PFT in vitro.

Future research will focus on receptor identification to gain a deeper understanding about PS-3 specificity and to evaluate a potential application of this knowledge in the medical field. Methods like thin layer chromatography, photo-reactive crosslinking or carbohydrate blocking may prove useful in achieving that. Also, comparative transcriptome analysis of susceptible and resistant HepG2 cells is already underway (Souissi et al., unpublished). More patch clamp experiments using smaller toxin dose would help to establish if channel activity is affected by the side of exposed membrane and its origin. It would be also interesting to test if EGTA blocks toxicity of PS-3 activated with proteinase K in HL-60 cells and if the same cations restore its activity, which would suggest the presence of similar receptors in HepG2 and HL-60 cells. High throughput analysis of kinase phosphorylation profiles could be used to simultaneously detect other proteins/pathways involved in cellular response.

9. References:

ABDULLAH, M. A. F., VALAITIS, A. P. & DEAN, D. H. 2006. Identification of a Bacillus thuringiensis Cry11Ba toxin-binding aminopeptidase from the mosquito, Anopheles quadrimaculatus. *BMC Biochemistry,* 7**,** 16-16.

ABE, Y., SHIMADA, H. & KITADA, S. 2008. Raft-targeting and oligomerization of parasporin-2, a Bacillus thuringiensis crystal protein with anti-tumour activity. *Journal of Biochemistry,* 143**,** 269-275.

ABRAMI, L., FIVAZ, M., GLAUSER, P.-E., PARTON, R. G. & VAN DER GOOT, F. 1998. A Pore-forming Toxin Interacts with a GPI-anchored Protein and Causes Vacuolation of the Endoplasmic Reticulum. *The Journal of Cell Biology,* 140**,** 525-540.

ADANG, M. J., CRICKMORE, N. & JURAT-FUENTES, J. L. 2014. Chapter Two - Diversity of Bacillus thuringiensis Crystal Toxins and Mechanism of Action. *In:* TARLOCHAN, S. D. & SARJEET, S. G. (eds.) *Advances in Insect Physiology.* Academic Press.

AGAISSE, H. & LERECLUS, D. 1995. How does Bacillus thuringiensis produce so much insecticidal crystal protein? *Journal of Bacteriology,* 177**,** 6027-32.

AGRAWAL, N., MALHOTRA, P. & BHATNAGAR, R. K. 2002. Interaction of Gene-Cloned and Insect Cell-Expressed Aminopeptidase N of Spodoptera litura with Insecticidal Crystal Protein Cry1C. *Applied and environmental microbiology,* 68**,** 4583-4592.

AKIBA, T., ABE, Y., KITADA, S., KUSAKA, Y., ITO, A., ICHIMATSU, T., KATAYAMA, H., AKAO, T., HIGUCHI, K., MIZUKI, E., OHBA, M., KANAI, R. & HARATA, K. 2009a. Crystal structure of the parasporin-2 Bacillus thuringiensis toxin that recognizes cancer cells. *J Mol Biol,* 386**,** 121-33.

AKIBA, T., ABE, Y., KITADA, S., KUSAKA, Y., ITO, A., ICHIMATSU, T., KATAYAMA, H., AKAO, T., HIGUCHI, K., MIZUKI, E., OHBA, M., KANAI, R. & HARATA, K. 2009b. Crystal Structure of the Parasporin-2 Bacillus thuringiensis Toxin That Recognizes Cancer Cells. *Journal of Molecular Biology,* 386**,** 121-133.

AKIBA, T., ICHIMATSU, T., KATAYAMA, H., AKAO, T., NAKAMURA, O., MIZUKI, E., OHBA, M. & HARATA, K. 2005. Structure of parasporin-1, a novel bacterial cytotoxin against human cancer cells. *Acta Crystallographica Section A,* 61**,** c250.

AKIBA, T. & OKUMURA, S. 2016. Parasporins 1 and 2: Their structure and activity. *Journal of Invertebrate Pathology*.

ALON, R., BAYER, E. A. & WILCHEK, M. 1990. Streptavidin contains an RYD sequence which mimics the RGD receptor domain of fibronectin. *Biochemical and Biophysical Research Communications,* 170**,** 1236-1241.

ALON, R., BAYER, E. A. & WILCHEK, M. 1993. Cell adhesion to streptavidin via RGD-dependent integrins. *Eur J Cell Biol,* 60**,** 1-11.

AMET, T., GHABRIL, M., CHALASANI, N., BYRD, D., HU, N., GRANTHAM, A., LIU, Z., QIN, X., HE, J. J. & YU, Q. 2012. CD59 incorporation protects hepatitis C virus against complement-mediated destruction. *Hepatology,* 55**,** 354-363.

AROIAN, R. & VAN DER GOOT, F. G. 2007. Pore-forming toxins and cellular non-immune defenses (CNIDs). *Current Opinion in Microbiology,* 10**,** 57-61.

ARONSON, A. I., TYRELL, D. J., FITZ-JAMES, P. C. & BULLA, L. A., JR. 1982. Relationship of the syntheses of spore coat protein and parasporal crystal protein in Bacillus thuringiensis. *J Bacteriol,* 151**,** 399-410.

ATSUMI, S., MIYAMOTO, K., YAMAMOTO, K., NARUKAWA, J., KAWAI, S., SEZUTSU, H., KOBAYASHI, I., UCHINO, K., TAMURA, T., MITA, K., KADONO-OKUDA, K., WADA, S., KANDA, K., GOLDSMITH, M. R. & NODA, H. 2012a. Single amino acid mutation in an ATP-binding cassette transporter gene causes resistance to Bt toxin Cry1Ab in the

silkworm, Bombyx mori. *Proceedings of the National Academy of Sciences,* 109**,** E1591–E1598.

ATSUMI, S., MIYAMOTO, K., YAMAMOTO, K., NARUKAWA, J., KAWAI, S., SEZUTSU, H., KOBAYASHI, I., UCHINO, K., TAMURA, T., MITA, K., KADONO-OKUDA, K., WADA, S., KANDA, K., GOLDSMITH, M. R. & NODA, H. 2012b. Single amino acid mutation in an ATP-binding cassette transporter gene causes resistance to Bt toxin Cry1Ab in the silkworm, Bombyx mori. *Proc Natl Acad Sci U S A,* 109.

AYRA-PARDO, C., RAYMOND, B., GULZAR, A., RODRÍGUEZ-CABRERA, L., MORÁN-BERTOT, I., CRICKMORE, N. & WRIGHT, D. J. 2015. Novel genetic factors involved in resistance to Bacillus thuringiensis in Plutella xylostella. *Insect Molecular Biology,* 24**,** 589-600.

AZAD, M. B., CHEN, Y. & GIBSON, S. B. 2009. Regulation of autophagy by reactive oxygen species (ROS): implications for cancer progression and treatment. *Antioxid Redox Signal,* 11**,** 777-90.

BAINES, C. 2010. Role of the mitochondrion in programmed necrosis. *Frontiers in Physiology,* 1.

BANKS, D. J., JURAT-FUENTES, J. L., DEAN, D. H. & ADANG, M. J. 2001. Bacillus thuringiensis Cry1Ac and Cry1Fa δ-endotoxin binding to a novel 110 kDa aminopeptidase in Heliothis virescens is not N-acetylgalactosamine mediated. *Insect Biochemistry and Molecular Biology,* 31**,** 909-918.

BAXTER, S. W., BADENES-PÉREZ, F. R., MORRISON, A., VOGEL, H., CRICKMORE, N., KAIN, W., WANG, P., HECKEL, D. G. & JIGGINS, C. D. 2011. Parallel Evolution of Bacillus thuringiensis Toxin Resistance in Lepidoptera. *Genetics,* 189**,** 675-679.

BEAR, C. E. 1990. A nonselective cation channel in rat liver cells is activated by membrane stretch. *American Journal of Physiology - Cell Physiology,* 258**,** C421-C428.

BELLIER, A., CHEN, C.-S., KAO, C.-Y., CINAR, H. N. & AROIAN, R. V. 2009. Hypoxia and the Hypoxic Response Pathway Protect against Pore-Forming Toxins in <italic>C. elegans</italic>. *PLoS Pathog,* 5**,** e1000689.

BENZ, R., MAIER, E., LADANT, D., ULLMANN, A. & SEBO, P. 1994. Adenylate cyclase toxin (CyaA) of Bordetella pertussis. Evidence for the formation of small ion-permeable channels and comparison with HlyA of Escherichia coli. *Journal of Biological Chemistry,* 269**,** 27231-27239.

BERRY, C. 2012. The bacterium, Lysinibacillus sphaericus, as an insect pathogen. *Journal of Invertebrate Pathology,* 109**,** 1-10.

BERRY, C. & CRICKMORE, N. in press. Structural classification of insecticidal proteins – towards an in silico characterization of novel toxins. *Journal of Invertebrate Pathology*

BIETLOT, H. P., VISHNUBHATLA, I., CAREY, P. R., POZSGAY, M. & KAPLAN, H. 1990. Characterization of the cysteine residues and disulphide linkages in the protein crystal of Bacillus thuringiensis. *Biochem J,* 267**,** 309-15.

BIOTECH, P. 2010. Gel filtration Principles and Methods. *Handbooks from GE Healthcare.* Pharmacia Biotech.

BISCHOF, L. J., KAO, C.-Y., LOS, F. C. O., GONZALEZ, M. R., SHEN, Z., BRIGGS, S. P., VAN DER GOOT, F. G. & AROIAN, R. V. 2008. Activation of the Unfolded Protein Response Is Required for Defenses against Bacterial Pore-Forming Toxin In Vivo. *PLoS Pathogens,* 4**,** e1000176.

BITO, H., DEISSEROTH, K. & TSIEN, R. W. 1996. CREB phosphorylation and dephosphorylation: a Ca(2+)- and stimulus duration-dependent switch for hippocampal gene expression. *Cell,* 87**,** 1203-14.

BOLSOVER, S. 1994. A practical guide to the study of calcium in living cells: edited by Richard Nuccitelli, Academic Press, 1994. £34.50 (368 pages) ISBN 0 12 522810 4. *Trends in Cell Biology,* 4**,** 443.

BOONSERM, P., DAVIS, P., ELLAR, D. J. & LI, J. 2005. Crystal Structure of the Mosquito-larvicidal Toxin Cry4Ba and Its Biological Implications. *Journal of Molecular Biology,* 348**,** 363-382.

BOONSERM, P., MO, M., ANGSUTHANASOMBAT, C. & LESCAR, J. 2006. Structure of the Functional Form of the Mosquito Larvicidal Cry4Aa Toxin from Bacillus thuringiensis at a 2.8-Angstrom Resolution. *Journal of Bacteriology,* 188**,** 3391-3401.

BOUMA, M. E., ROGIER, E., VERTHIER, N., LABARRE, C. & FELDMANN, G. 1989. Further cellular investigation of the human hepatoblastoma-derived cell line HepG2: morphology and immunocytochemical studies of hepatic-secreted proteins. *In Vitro Cell Dev Biol,* 25**,** 267-75.

BRADBURY, A. & PLUCKTHUN, A. 2015. Reproducibility: Standardize antibodies used in research. *Nature,* 518**,** 27-9.

BRADFORD, M. M. 1976. A rapid and sensitive method for the quantitation of microgram quantities of protein utilizing the principle of protein-dye binding. *Anal Biochem,* 72**,** 248-54.

BRASSEUR, K., AUGER, P., ASSELIN, E., PARENT, S., COTE, J. C. & SIROIS, M. 2015a. Parasporin-2 from a New Bacillus thuringiensis 4R2 Strain Induces Caspases Activation and Apoptosis in Human Cancer Cells. *PLoS One,* 10.

BRASSEUR, K., AUGER, P., ASSELIN, E., PARENT, S., COTE, J. C. & SIROIS, M. 2015b. Parasporin-2 from a New Bacillus thuringiensis 4R2 Strain Induces Caspases Activation and Apoptosis in Human Cancer Cells. *PLoS One,* 10**,** e0135106.

BRAVO, A., GILL, S. & SOBERON, M. 2007. Mode of action of Bacillus thuringiensis Cry and Cyt toxins and their potential for insect control. *Toxicon,* 49**,** 423 - 435.

BRAVO, A., GÓMEZ, I., CONDE, J., MUÑOZ-GARAY, C., SÁNCHEZ, J., MIRANDA, R., ZHUANG, M., GILL, S. S. & SOBERÓN, M. 2004. Oligomerization triggers binding of a Bacillus thuringiensis Cry1Ab pore-forming toxin to aminopeptidase N receptor leading to insertion into membrane microdomains. *Biochimica et Biophysica Acta (BBA) - Biomembranes,* 1667**,** 38-46.

BRAVO, A., LIKITVIVATANAVONG, S., GILL, S. S. & SOBERÓN, M. 2011. Bacillus thuringiensis: A story of a successful bioinsecticide. *Insect Biochemistry and Molecular Biology,* 41**,** 423-431.

BRAVO, A. & SOBERÓN, M. 2008. How to cope with insect resistance to Bt toxins? *Trends in Biotechnology,* 26**,** 573-579.

BREIT, S., KOLB, H.-A., APFEL, H., HABERLAND, C., SCHMITT, M., HÄUSSINGER, D., GRAF, J. & LANG, F. 1997. Regulation of ion channels in rat hepatocytes. *Pflügers Archiv,* 435**,** 203-210.

BRETSCHNEIDER, A., HECKEL, D. G. & PAUCHET, Y. 2016. Three toxins, two receptors, one mechanism: Mode of action of Cry1A toxins from Bacillus thuringiensis in Heliothis virescens. *Insect Biochem Mol Biol,* 76**,** 109-17.

BUDATHA, M., MEUR, G. & DUTTA-GUPTA, A. 2007. A novel aminopeptidase in the fat body of the moth Achaea janata as a receptor for Bacillus thuringiensis Cry toxins and its comparison with midgut aminopeptidase. *Biochemical Journal,* 405**,** 287-297.

BUZDIN, A. A., REVINA, L. P., KOSTINA, L. I., ZALUNIN, I. A. & CHESTUKHINA, G. G. 2002. Interaction of 65- and 62-kD proteins from the apical membranes of the Aedes aegypti larvae midgut epithelium with Cry4B and Cry11A endotoxins of Bacillus thuringiensis. *Biochemistry (Mosc),* 67**,** 540-6.

BYEGÅRD, J., SKARNEMARK, G. & SKÅLBERG, M. 1999. The stability of some metal EDTA, DTPA and DOTA complexes: Application as tracers in groundwater studies. *Journal of Radioanalytical and Nuclear Chemistry,* 241**,** 281-290.

CAGNOL, S. & CHAMBARD, J. C. 2010. ERK and cell death: mechanisms of ERK-induced cell death--apoptosis, autophagy and senescence. *FEBS J,* 277**,** 2-21.

CANCINO-RODEZNO, A., ALEXANDER, C., VILLASEÑOR, R., PACHECO, S., PORTA, H., PAUCHET, Y., SOBERÓN, M., GILL, S. S. & BRAVO, A. 2010. The mitogen-activated protein kinase p38 is involved in insect defense against Cry toxins from Bacillus thuringiensis. *Insect Biochemistry and Molecular Biology,* 40**,** 58-63.

CANDAS, M., FRANCIS, B. R., GRIKO, N. B., MIDBOE, E. G. & BULLA, L. A. 2002. Proteolytic Cleavage of the Developmentally Important Cadherin BT-R1 in the Midgut Epithelium of Manduca sexta†. *Biochemistry,* 41**,** 13717-13724.

CAPIOD, T. & OGDEN, D. C. 1989. The properties of calcium-activated potassium ion channels in guinea-pig isolated hepatocytes. *The Journal of Physiology,* 409**,** 285-295.

CARROLL, J. & ELLAR, D. J. 1997. Analysis of the large aqueous pores produced by a Bacillus thuringiensis protein insecticide in Manduca sexta midgut-brush-border-membrane vesicles. *Eur J Biochem,* 245**,** 797-804.

CHAKROUN, M., BANYULS, N., BEL, Y., ESCRICHE, B. & FERRÉ, J. 2016. Bacterial Vegetative Insecticidal Proteins (Vip) from Entomopathogenic Bacteria. *Microbiology and Molecular Biology Reviews,* 80**,** 329-350.

CHEN, J., AIMANOVA, K. G., FERNANDEZ, L. E., BRAVO, A., SOBERON, M. & GILL, S. S. 2009. Aedes aegypti cadherin serves as a putative receptor of the Cry11Aa toxin from Bacillus thuringiensis subsp. israelensis. *The Biochemical journal,* 424**,** 191-200.

CHEN, R. R., REN, X. L., HAN, Z. J., MU, L. L., LI, G. Q., MA, Y. & CUI, J. J. 2014. A cadherin-like protein from the beet armyworm Spodoptera exigua (Lepidoptera: Noctuidae) is a putative Cry1Ac receptor. *Arch Insect Biochem Physiol,* 86**,** 58-71.

CHEN, W. H., YEH, T. H., TSAI, M. C., CHEN, D. S. & WANG, T. H. 1997. Characterization of Ca(2+)- and voltage-dependent nonselective cation channels in human HepG2 cells. *J Formos Med Assoc,* 96**,** 503-10.

CHO, Y.-E., LOMEDA, R.-A. R., RYU, S.-H., LEE, J.-H., BEATTIE, J. H. & KWUN, I.-S. 2007. Cellular Zn depletion by metal ion chelators (TPEN, DTPA and chelex resin) and its application to osteoblastic MC3T3-E1 cells. *Nutrition Research and Practice,* 1**,** 29-35.

COHEN, S., ALBECK, S., BEN-DOV, E., CAHAN, R., FIRER, M., ZARITSKY, A. & DYM, O. 2011. Cyt1Aa toxin: Crystal structure reveals implications for its membrane-perforating function. *Journal of Molecular Biology,* 413**,** 804-814.

COHEN, S., DYM, O., ALBECK, S., BEN-DOV, E., CAHAN, R., FIRER, M. & ZARITSKY, A. 2008. High-Resolution Crystal Structure of Activated Cyt2Ba Monomer from Bacillus thuringiensis subsp. israelensis. *Journal of Molecular Biology,* 380**,** 820-827.

CONTRERAS, E., SCHOPPMEIER, M., REAL, M. D. & RAUSELL, C. 2013. Sodium Solute Symporter and Cadherin Proteins Act as Bacillus thuringiensis Cry3Ba Toxin Functional Receptors in Tribolium castaneum. *Journal of Biological Chemistry,* 288**,** 18013-18021.

CRICKMORE, N., BAUM, J., BRAVO, A., LERECLUS, D., NARVA, K., SAMPSON, K., SCHNEPF, E., SUN, M. AND ZEIGLER, D.R. 2016. Bacillus thuringiensis toxin nomenclature

CRICKMORE, N., BONE, E. J., WILLIAMS, J. A. & ELLAR, D. J. 1995. Contribution of the individual components of the δ-endotoxin crystal to the mosquitocidal activity of Bacillus thuringiensis subsp. israelensis. *FEMS Microbiology Letters,* 131**,** 249-254.

CRICKMORE, N. & ELLAR, D. J. 1992. Involvement of a possible chaperonin in the efficient expression of a cloned CryIIA δ-endotoxin gene in Bacillus thuringiensis. *Molecular Microbiology,* 6**,** 1533-1537.

CRICKMORE, N., WHEELER, V. C. & ELLAR, D. J. 1994. Use of an operon fusion to induce expression and crystallisation of a *Bacillus thuringiensis* δ-endotoxin encoded by a cryptic gene. *Molecular and General Genetics MGG,* 242**,** 365-368.

CRICKMORE, N., ZEIGLER, D. R., FEITELSON, J., SCHNEPF, E., VAN RIE, J., LERECLUS, D., BAUM, J. & DEAN, D. H. 1998. Revision of the Nomenclature for the Bacillus thuringiensis Pesticidal Crystal Proteins. *Microbiology and Molecular Biology Reviews,* 62**,** 807-813.

DAKSHINAMURTI, K. & MISTRY, S. P. 1963. Tissue and Intracellular Distribution of Biotin-C14OOH in Rats and Chicks. *Journal of Biological Chemistry,* 238**,** 294-296.

DAVIES, S. P., REDDY, H., CAIVANO, M. & COHEN, P. 2000. Specificity and mechanism of action of some commonly used protein kinase inhibitors. *Biochemical Journal,* 351**,** 95-105.

DE MAAGD, R. A., BRAVO, A., BERRY, C., CRICKMORE, N. & SCHNEPF, H. E. 2003. Structure, diversity, and evolution of protein toxins from spore-forming entomopathogenic bacteria. *Annu Rev Genet,* 37**,** 409-33.

DENOLF, P., HENDRICKX, K., VAN DAMME, J., JANSENS, S., PEFEROEN, M., DEGHEELE, D. & VAN RIE, J. 1997. Cloning and Characterization of Manduca Sexta and Plutella Xylostella Midgut Aminopeptidase N Enzymes Related to Bacillus Thuringiensis Toxin-Binding Proteins. *European Journal of Biochemistry,* 248**,** 748-761.

DERBYSHIRE, D. J., ELLAR, D. J. & LI, J. 2001. Crystallization of the Bacillus thuringiensis toxin Cry1Ac and its complex with the receptor ligand N-acetyl-d-galactosamine. *Acta Crystallographica Section D,* 57**,** 1938-1944.

DIEP, D. B., NELSON, K. L., RAJA, S. M., PLESHAK, E. N. & BUCKLEY, J. T. 1998. Glycosylphosphatidylinositol Anchors of Membrane Glycoproteins Are Binding Determinants for the Channel-forming Toxin Aerolysin. *Journal of Biological Chemistry,* 273**,** 2355-2360.

DONOVAN, W. P., ENGLEMAN, J. T., DONOVAN, J. C., BAUM, J. A., BUNKERS, G. J., CHI, D. J., CLINTON, W. P., ENGLISH, L., HECK, G. R., ILAGAN, O. M., KRASOMIL-OSTERFELD, K. C., PITKIN, J. W., ROBERTS, J. K. & WALTERS, M. R. 2006. Discovery and characterization of Sip1A: A novel secreted protein from Bacillus thuringiensis with activity against coleopteran larvae. *Appl Microbiol Biotechnol,* 72**,** 713-9.

DORSCH, J. A., CANDAS, M., GRIKO, N. B., MAATY, W. S. A., MIDBOE, E. G., VADLAMUDI, R. K. & BULLA JR, L. A. 2002. Cry1A toxins of Bacillus thuringiensis bind specifically to a region adjacent to the membrane-proximal extracellular domain of BT-R1 in Manduca sexta:: involvement of a cadherin in the entomopathogenicity of Bacillus thuringiensis. *Insect Biochemistry and Molecular Biology,* 32**,** 1025-1036.

DU, C., MARTIN, P. A. & NICKERSON, K. W. 1994. Comparison of Disulfide Contents and Solubility at Alkaline pH of Insecticidal and Noninsecticidal Bacillus thuringiensis Protein Crystals. *Appl Environ Microbiol,* 60**,** 3847-53.

EBELING, W., HENNRICH, N., KLOCKOW, M., METZ, H., ORTH, H. D. & LANG, H. 1974. Proteinase K from Tritirachium album Limber. *European Journal of Biochemistry,* 47**,** 91-97.

EKINO, K., OKUMURA, S., ISHIKAWA, T., KITADA, S., SAITOH, H., AKAO, T., OKA, T., NOMURA, Y., OHBA, M., SHIN, T. & MIZUKI, E. 2014. Cloning and characterization of a unique cytotoxic protein parasporin-5 produced by Bacillus thuringiensis A1100 strain. *Toxins (Basel),* 6**,** 1882-95.

ELISABETH GASTEIGER, C. H., ALEXANDRE GATTIKER, SÉVERINE DUVAUD, MARC R. WILKINS, RON D. APPEL, AND AMOS BAIROCH 2005. Protein Identification and Analysis Tools on the ExPASy Server. *The Proteomics Protocols Handbook.*

ELLIS, R. T., STOCKHOFF, B. A., STAMP, L., SCHNEPF, H. E., SCHWAB, G. E., KNUTH, M., RUSSELL, J., CARDINEAU, G. A. & NARVA, K. E. 2002. Novel Bacillus thuringiensis Binary Insecticidal Crystal Proteins Active on Western Corn Rootworm, Diabrotica virgifera virgifera LeConte. *Applied and environmental microbiology,* 68**,** 1137-1145.

FAHMY, T. M., FONG, P. M., GOYAL, A. & SALTZMAN, W. M. 2005. Targeted for drug delivery. *Materials Today,* 8**,** 18-26.

FANG, F. C. 2011. Antimicrobial Actions of Reactive Oxygen Species. *mBio,* 2.

FERNANDEZ, LUISA E., AIMANOVA, KARLYGASH G., GILL, SARJEET S., BRAVO, A. & SOBERÓN, M. 2006. A GPI-anchored alkaline phosphatase is a functional midgut receptor of Cry11Aa toxin in Aedes aegypti larvae. *Biochemical Journal,* 394**,** 77-84.

FICKL, H., COCKERAN, R., STEEL, H. C., FELDMAN, C., COWAN, G., MITCHELL, T. J. & ANDERSON, R. 2005. Pneumolysin-mediated activation of NFκB in human neutrophils is antagonized by docosahexaenoic acid. *Clinical & Experimental Immunology,* 140**,** 274-281.

FLANNAGAN, R. D., YU, C.-G., MATHIS, J. P., MEYER, T. E., SHI, X., SIQUEIRA, H. A. A. & SIEGFRIED, B. D. 2005. Identification, cloning and expression of a Cry1Ab cadherin receptor from European corn borer, Ostrinia nubilalis (Hübner) (Lepidoptera: Crambidae). *Insect Biochemistry and Molecular Biology,* 35**,** 33-40.

FORTIER, M., VACHON, V., KIROUAC, M., SCHWARTZ, J. L. & LAPRADE, R. 2005. Differential effects of ionic strength, divalent cations and pH on the pore-forming activity of Bacillus thuringiensis insecticidal toxins. *J Membr Biol,* 208**,** 77-87.

GABRIEL NARVAEZ, V. V., DONG XU, JEAN-CHARLES CÔTÉ, JEAN-LOUIS SCHWARTZ 2014. PS1Aa2 induces ionic channels in lipid bilayer membranes and calcium oscillations in sensitive cells *Paper presented at: 47th Annual Meeting of the Society for Invertebrate Pathology; 2014 Aug 3-7; Mainz, Germany*

GAHAN, L. J., GOULD, F. & HECKEL, D. G. 2001. Identification of a Gene Associated with Bt Resistance in Heliothis virescens. *Science,* 293**,** 857-860.

GAHAN, L. J., PAUCHET, Y., VOGEL, H. & HECKEL, D. G. 2010. An ABC transporter mutation is correlated with insect resistance to Bacillus thuringiensis Cry1Ac toxin. *PLoS Genet,* 6.

GALITSKY, N., CODY, V., WOJTCZAK, A., GHOSH, D., LUFT, J. R., PANGBORN, W. & ENGLISH, L. 2001. Structure of the insecticidal bacterial [delta]-endotoxin Cry3Bb1 of Bacillus thuringiensis. *Acta Crystallographica Section D,* 57**,** 1101-1109.

GANGULY, N., GIANG, P. H., BASU, S. K., MIR, F. A., SIDDIQUI, I. & SHARMA, P. 2007. Mycobacterium tuberculosis 6-kDa Early Secreted Antigenic Target (ESAT-6) protein downregulates Lipopolysaccharide induced c-myc expression by modulating the Extracellular Signal Regulated Kinases 1/2. *BMC Immunology,* 8**,** 24-24.

GÄNZLER-ODENTHAL, S. I. I. & REDIES, C. 1998. Blocking N-Cadherin Function Disrupts the Epithelial Structure of Differentiating Neural Tissue in the Embryonic Chicken Brain. *The Journal of Neuroscience,* 18**,** 5415-5425.

GARCZYNSKI, S. F., CRIM, J. W. & ADANG, M. J. 1991. Identification of putative insect brush border membrane-binding molecules specific to Bacillus thuringiensis delta-endotoxin by protein blot analysis. *Applied and environmental microbiology,* 57**,** 2816-2820.

GELBER, S. E., AGUILAR, J. L., LEWIS, K. L. T. & RATNER, A. J. 2008. Functional and Phylogenetic Characterization of Vaginolysin, the Human-Specific Cytolysin from Gardnerella vaginalis. *Journal of Bacteriology,* 190**,** 3896-3903.

GERHARDT, P. 1994. *Methods for General and Molecular Bacteriology*, American Society for Microbiology.

GIDDINGS, K. S., ZHAO, J., SIMS, P. J. & TWETEN, R. K. 2004. Human CD59 is a receptor for the cholesterol-dependent cytolysin intermedilysin. *Nature structural & molecular biology,* 11**,** 1173-1178.

GILL, M. & ELLAR, D. 2002. Transgenic Drosophila reveals a functional in vivo receptor for the Bacillus thuringiensis toxin Cry1Ac1. *Insect Molecular Biology,* 11**,** 619-625.

GILL, S. S., COWLES, E. A. & FRANCIS, V. 1995. Identification, Isolation, and Cloning of a Bacillus thuringiensis CryIAc Toxin-binding Protein from the Midgut of the Lepidopteran Insect Heliothis virescens. *Journal of Biological Chemistry,* 270**,** 27277-27282.

GONG, X., MING, X., DENG, P. & JIANG, Y. 2010. Mechanisms regulating the nuclear translocation of p38 MAP kinase. *Journal of Cellular Biochemistry,* 110**,** 1420-1429.

GONZALEZ, E., GRANADOS, J., SHORT, J., AMMONS, D. & RAMPERSAD, J. 2011a. Parasporins from a Caribbean Island: Evidence for a Globally Dispersed Bacillus thuringiensis Strain. *Current Microbiology,* 62**,** 1643-1648.

GONZALEZ, J. M., JR., DULMAGE, H. T. & CARLTON, B. C. 1981. Correlation between specific plasmids and delta-endotoxin production in Bacillus thuringiensis. *Plasmid,* 5**,** 352-65.

GONZALEZ, M. R., BISCHOFBERGER, M., FRECHE, B., HO, S., PARTON, R. G. & VAN DER GOOT, F. G. 2011b. Pore-forming toxins induce multiple cellular responses promoting survival. *Cell Microbiol,* 13**,** 1026-43.

GORDON, V. M., NELSON, K. L., BUCKLEY, J. T., STEVENS, V. L., TWETEN, R. K., ELWOOD, P. C. & LEPPLA, S. H. 1999. Clostridium septicum Alpha Toxin Uses Glycosylphosphatidylinositol-anchored Protein Receptors. *Journal of Biological Chemistry,* 274**,** 27274-27280.

GÓMEZ, I., DEAN, D. H., BRAVO, A. & SOBERÓN, M. 2003. Molecular Basis for Bacillus thuringiensis Cry1Ab Toxin Specificity: Two Structural Determinants in the Manduca sexta Bt-R1 Receptor Interact with Loops α-8 and 2 in Domain II of Cy1Ab Toxin. *Biochemistry,* 42**,** 10482-10489.

GÓMEZ, I., SÁNCHEZ, J., MIRANDA, R., BRAVO, A. & SOBERÓN, M. 2002. Cadherin-like receptor binding facilitates proteolytic cleavage of helix α-1 in domain I and oligomer pre-pore formation of Bacillus thuringiensis Cry1Ab toxin. *FEBS Letters,* 513**,** 242-246.

GÓMEZ, I., SÁNCHEZ, J., MUÑOZ-GARAY, C., MATUS, V., GILL, SARJEET S., SOBERÓN, M. & BRAVO, A. 2014. Bacillus thuringiensis Cry1A toxins are versatile proteins with multiple modes of action: two distinct pre-pores are involved in toxicity. *Biochemical Journal,* 459**,** 383-396.

GRAF, J., HENDERSON, R. M., KRUMPHOLZ, B. & BOYER, J. L. 1987. Cell membrane and transepithelial voltages and resistances in isolated rat hepatocyte couplets. *The Journal of Membrane Biology,* 95**,** 241-254.

GRIFFITTS, J. S., HASLAM, S. M., YANG, T., GARCZYNSKI, S. F., MULLOY, B., MORRIS, H., CREMER, P. S., DELL, A., ADANG, M. J. & AROIAN, R. V. 2005. Glycolipids as Receptors for Bacillus thuringiensis Crystal Toxin. *Science,* 307**,** 922-925.

GRIFFITTS, J. S., HUFFMAN, D. L., WHITACRE, J. L., BARROWS, B. D., MARROQUIN, L. D., MÜLLER, R., BROWN, J. R., HENNET, T., ESKO, J. D. & AROIAN, R. V. 2003. Resistance to a Bacterial Toxin Is Mediated by Removal of a Conserved Glycosylation Pathway Required for Toxin-Host Interactions. *Journal of Biological Chemistry,* 278**,** 45594-45602.

GRIFFITTS, J. S., WHITACRE, J. L., STEVENS, D. E. & AROIAN, R. V. 2001. Bt Toxin Resistance from Loss of a Putative Carbohydrate-Modifying Enzyme. *Science,* 293**,** 860-864.

GRIMM, D., BAUER, J., PIETSCH, J., INFANGER, M., EUCKER, J., EILLES, C. & SCHOENBERGER, J. 2011. Diagnostic and therapeutic use of membrane proteins in cancer cells. *Curr Med Chem,* 18**,** 176-90.

GROCHULSKI, P., MASSON, L., BORISOVA, S., PUSZTAI-CAREY, M., SCHWARTZ, J.-L., BROUSSEAU, R. & CYGLER, M. 1995. Bacillus thuringiensisCrylA(a) Insecticidal Toxin: Crystal Structure and Channel Formation. *Journal of Molecular Biology,* 254**,** 447-464.

GROULX, N., MCGUIRE, H., LAPRADE, R., SCHWARTZ, J.-L. & BLUNCK, R. 2011. Single Molecule Fluorescence Study of the Bacillus thuringiensis Toxin Cry1Aa Reveals Tetramerization. *The Journal of Biological Chemistry,* 286**,** 42274-42282.

GÜERECA, L. & BRAVO, A. 1999. The oligomeric state of Bacillus thuringiensis Cry toxins in solution. *Biochimica et Biophysica Acta (BBA) - Protein Structure and Molecular Enzymology,* 1429**,** 342-350.

GUO, C.-J., LIU, D., WU, Y.-Y., YANG, X.-B., YANG, L.-S., MI, S., HUANG, Y.-X., LUO, Y.-W., JIA, K.-T., LIU, Z.-Y., CHEN, W.-J., WENG, S.-P., YU, X.-Q. & HE, J.-G. 2011. Entry of Tiger Frog Virus (an Iridovirus) into HepG2 Cells via a pH-Dependent, Atypical, Caveola-Mediated Endocytosis Pathway. *Journal of Virology,* 85**,** 6416-6426.

GUO, S., YE, S., LIU, Y., WEI, L., XUE, J., WU, H., SONG, F., ZHANG, J., WU, X., HUANG, D. & RAO, Z. 2009. Crystal structure of Bacillus thuringiensis Cry8Ea1: An insecticidal toxin toxic to underground pests, the larvae of Holotrichia parallela. *Journal of Structural Biology,* 168**,** 259-266.

GUO, Z., KANG, S., CHEN, D., WU, Q., WANG, S., XIE, W., ZHU, X., BAXTER, S. W., ZHOU, X., JURAT-FUENTES, J. L. & ZHANG, Y. 2015. MAPK Signaling Pathway Alters Expression of Midgut ALP and ABCC Genes and Causes Resistance to Bacillus thuringiensis Cry1Ac Toxin in Diamondback Moth. *PLoS Genetics,* 11**,** e1005124.

GURCEL, L., ABRAMI, L., GIRARDIN, S., TSCHOPP, J. & VAN DER GOOT, F. G. 2006. Caspase-1 Activation of Lipid Metabolic Pathways in Response to Bacterial Pore-Forming Toxins Promotes Cell Survival. *Cell,* 126**,** 1135-1145.

GUZMÁN, C. A., DOMANN, E., RONDE, M., BRUDER, D., DARJI, A., WEISS, S., WEHLAND, J., CHAKRABORTY, T. & TIMMIS, K. N. 1996. Apoptosis of mouse dendritic cells is triggered by listeriolysin, the major virulence determinant of Listeria monocytogenes. *Molecular Microbiology,* 20**,** 119-126.

HANDE, K. R. 1998. Etoposide: four decades of development of a topoisomerase II inhibitor. *European Journal of Cancer,* 34**,** 1514-1521.

HASHEMI, M., GHAVAMI, S., ESHRAGHI, M., BOOY, E. P. & LOS, M. 2007. Cytotoxic effects of intra and extracellular zinc chelation on human breast cancer cells. *European Journal of Pharmacology,* 557**,** 9-19.

HAYAKAWA, T., SHITOMI, Y., MIYAMOTO, K. & HORI, H. 2004. GalNAc pretreatment inhibits trapping of Bacillus thuringiensis Cry1Ac on the peritrophic membrane of Bombyx mori. *FEBS Letters,* 576**,** 331-335.

HAZES, B. 1996. The (QxW)3 domain: a flexible lectin scaffold. *Protein science : a publication of the Protein Society,* 5**,** 1490-1501.

HECKEL, D. G. 2012. Learning the ABCs of Bt: ABC transporters and insect resistance to Bacillus thuringiensis provide clues to a crucial step in toxin mode of action. *Pestic Biochem Physiol,* 104.

HERRERO, S., BEL, Y., HERNANDEZ-MARTINEZ, P. & FERRE, J. 2016. Susceptibility, mechanisms of response and resistance to Bacillus thuringiensis toxins in Spodoptera spp. *Curr Opin Insect Sci,* 15**,** 89-96.

HERTLE, R., HILGER, M., WEINGARDT-KOCHER, S. & WALEV, I. 1999. Cytotoxic action of Serratia marcescens hemolysin on human epithelial cells. *Infection and Immunity,* 67**,** 817-825.

HEUCK, A., MOE, P. & JOHNSON, B. 2010. The Cholesterol-Dependent Cytolysin Family of Gram-Positive Bacterial Toxins. *In:* HARRIS, J. R. (ed.) *Cholesterol Binding and Cholesterol Transport Proteins:.* Springer Netherlands.

HODGKIN, A. L. & HOROWICZ, P. 1959. The influence of potassium and chloride ions on the membrane potential of single muscle fibres. *The Journal of Physiology,* 148**,** 127-160.

HOFMANN, C., VANDERBRUGGEN, H., HÖFTE, H., VAN RIE, J., JANSENS, S. & VAN MELLAERT, H. 1988. Specificity of Bacillus thuringiensis delta-endotoxins is correlated with the presence of high-affinity binding sites in the brush border membrane of target insect midguts. *Proceedings of the National Academy of Sciences of the United States of America,* 85**,** 7844-7848.

HOFTE, H. & WHITELEY, H. 1989. Insecticidal crystal proteins of Bacillus thuringiensis. *Microbiol Mol Biol Rev,* 53**,** 242 - 255.

HÖFTE, H. & WHITELEY, H. R. 1989. Insecticidal crystal proteins of Bacillus thuringiensis. *Microbiological Reviews,* 53**,** 242-255.

HUA, G., JURAT-FUENTES, J. L. & ADANG, M. J. 2004. Fluorescent-based assays establish Manduca sexta Bt-R1a cadherin as a receptor for multiple Bacillus thuringiensis Cry1A toxins in Drosophila S2 cells. *Insect Biochemistry and Molecular Biology,* 34**,** 193-202.

HUA, G., ZHANG, R., ABDULLAH, M. A. F. & ADANG, M. J. 2008. Anopheles gambiae Cadherin AgCad1 Binds the Cry4Ba Toxin of Bacillus thuringiensis israelensis and a Fragment of AgCad1 Synergizes Toxicity. *Biochemistry,* 47**,** 5101-5110.

HUA, G., ZHANG, R., BAYYAREDDY, K. & ADANG, M. J. 2009. Anopheles gambiae Alkaline Phosphatase Is a Functional Receptor of Bacillus thuringiensis jegathesan Cry11Ba Toxin. *Biochemistry,* 48**,** 9785-9793.

HUFFMAN, D. L., ABRAMI, L., SASIK, R., CORBEIL, J., VAN DER GOOT, F. G. & AROIAN, R. V. 2004. Mitogen-activated protein kinase pathways defend against bacterial pore-forming toxins. *Proceedings of the National Academy of Sciences of the United States of America,* 101**,** 10995-11000.

HUI, F., SCHEIB, U., HU, Y., SOMMER, R. J., AROIAN, R. V. & GHOSH, P. 2012. Structure and glycolipid binding properties of the nematicidal protein Cry5B. *Biochemistry,* 51**,** 9911-21.

HUSMANN, M., DERSCH, K., BOBKIEWICZ, W., BECKMANN, E., VEERACHATO, G. & BHAKDI, S. 2006. Differential role of p38 mitogen activated protein kinase for cellular recovery from attack by pore-forming S. aureus alpha-toxin or streptolysin O. *Biochem Biophys Res Commun,* 344**,** 1128-34.

IBM 2013. SPSS Statistics for Windows. Version 22.0 ed. NY: IBM Corp. .

IDONE, V., TAM, C., GOSS, J. W., TOOMRE, D., PYPAERT, M. & ANDREWS, N. W. 2008. Repair of injured plasma membrane by rapid Ca2+-dependent endocytosis. *J Cell Biol,* 180**,** 905-14.

IKAWA, S., TSUDA, Y., FUKADA, T., SUGIMOTO, K. & HIMENO, M. 2000. cDNA Cloning of the Cry1Aa Receptor Variants from Bombyx mori and Their Expression in Mammalian Cells. *Bioscience, Biotechnology, and Biochemistry,* 64**,** 2682-2685.

IMRE, G., HEERING, J., TAKEDA, A.-N., HUSMANN, M., THIEDE, B., ZU HERINGDORF, D. M., GREEN, D. R., VAN DER GOOT, F. G., SINHA, B., DÖTSCH, V. & RAJALINGAM, K. 2012. Caspase-2 is an initiator caspase responsible for pore-forming toxin-mediated apoptosis. *The EMBO Journal,* 31**,** 2615-2628.

IRVING, H. & WILLIAMS, R. J. P. 1953. 637. The stability of transition-metal complexes. *Journal of the Chemical Society (Resumed)***,** 3192-3210.

ITO, A., SASAGURI, Y., KITADA, S., KUSAKA, Y., KUWANO, K., MASUTOMI, K., MIZUKI, E., AKAO, T. & OHBA, M. 2004. A Bacillus thuringiensis Crystal Protein with Selective Cytocidal Action to Human Cells. *Journal of Biological Chemistry,* 279**,** 21282-21286.

JIANG, J.-H., TONG, J. & GABRIEL, K. 2012. Hijacking Mitochondria: Bacterial Toxins that Modulate Mitochondrial Function. *IUBMB Life,* 64**,** 397-401.

JONAS, D., WALEV, I., BERGER, T., LIEBETRAU, M., PALMER, M. & BHAKDI, S. 1994. Novel path to apoptosis: Small transmembrane pores created by staphylococcal alpha-toxin in T lymphocytes evoke internucleosomal DNA degradation. *Infection and Immunity,* 62**,** 1304-1312.

JURAT-FUENTES, J. L. & ADANG, M. J. 2004. Characterization of a Cry1Ac-receptor alkaline phosphatase in susceptible and resistant Heliothis virescens larvae. *European Journal of Biochemistry,* 271**,** 3127-3135.

JURAT-FUENTES, J. L. & ADANG, M. J. 2006a. Cry toxin mode of action in susceptible and resistant Heliothis virescens larvae. *Journal of Invertebrate Pathology,* 92**,** 166-171.

JURAT-FUENTES, J. L. & ADANG, M. J. 2006b. The Heliothis virescens Cadherin Protein Expressed in Drosophila S2 Cells Functions as a Receptor for Bacillus thuringiensis Cry1A but Not Cry1Fa Toxins. *Biochemistry,* 45**,** 9688-9695.

JURAT-FUENTES, J. L., GAHAN, L. J., GOULD, F. L., HECKEL, D. G. & ADANG, M. J. 2004. The HevCaLP Protein Mediates Binding Specificity of the Cry1A Class of Bacillus thuringiensis Toxins in Heliothis virescens. *Biochemistry,* 43**,** 14299-14305.

K. L.CHENG, K. U., T. LMAMURA EBS. 1982. CRC Handbook of Organic Analytical Reagents.

KAO, C.-Y., LOS, F. C. O., HUFFMAN, D. L., WACHI, S., KLOFT, N., HUSMANN, M., KARABRAHIMI, V., SCHWARTZ, J.-L., BELLIER, A., HA, C., SAGONG, Y., FAN, H., GHOSH, P., HSIEH, M., HSU, C.-S., CHEN, L. & AROIAN, R. V. 2011. Global Functional Analyses of Cellular Responses to Pore-Forming Toxins. *PLoS Pathog,* 7**,** e1001314.

KATAYAMA, H., KUSAKA, Y. & MIZUKI, E. 2011. Parasporin-1 receptor and use thereof. Google Patents.

KATAYAMA, H., KUSAKA, Y., YOKOTA, H., AKAO, T., KOJIMA, M., NAKAMURA, O., MEKADA, E. & MIZUKI, E. 2007. Parasporin-1, a Novel Cytotoxic Protein from Bacillus thuringiensis, Induces Ca2+ Influx and a Sustained Elevation of the Cytoplasmic Ca2+ Concentration in Toxin-sensitive Cells. *Journal of Biological Chemistry,* 282**,** 7742-7752.

KATAYAMA, H., YOKOTA, H., AKAO, T., NAKAMURA, O., OHBA, M., MEKADA, E. & MIZUKI, E. 2005a. Parasporin-1, a Novel Cytotoxic Protein to Human Cells from Non-Insecticidal Parasporal Inclusions of Bacillus thuringiensis. *Journal of Biochemistry,* 137**,** 17-25.

KATAYAMA, H., YOKOTA, H., AKAO, T., NAKAMURA, O., OHBA, M., MEKADA, E. & MIZUKI, E. 2005b. Parasporin-1, a Novel Cytotoxic Protein to Human Cells from Non-Insecticidal Parasporal Inclusions of Bacillus thuringiensis. *J Biochem,* 137**,** 17 - 25.

KAUFMAN, H. L., KOHLHAPP, F. J. & ZLOZA, A. 2015. Oncolytic viruses: a new class of immunotherapy drugs. *Nat Rev Drug Discov,* 14**,** 642-662.

KEETON, T. P. & BULLA, L. A. 1997. Ligand specificity and affinity of BT-R1, the Bacillus thuringiensis Cry1A toxin receptor from Manduca sexta, expressed in mammalian and insect cell cultures. *Applied and environmental microbiology,* 63**,** 3419-3425.

KELLEY, L. A., MEZULIS, S., YATES, C. M., WASS, M. N. & STERNBERG, M. J. E. 2015. The Phyre2 web portal for protein modeling, prediction and analysis. *Nat. Protocols,* 10**,** 845-858.

KENNEDY, C. L., SMITH, D. J., LYRAS, D., CHAKRAVORTY, A. & ROOD, J. I. 2009. Programmed Cellular Necrosis Mediated by the Pore-Forming α-Toxin from Clostridium septicum. *PLoS Pathogens,* 5**,** e1000516.

KIM, H. S., YAMASHITA, S., AKAO, T., SAITOH, H., HIGUCHI, K., PARK, Y. S., MIZUKI, E. & OHBA, M. 2000. In vitro cytotoxicity of non-Cyt inclusion proteins of a Bacillus thuringiensis isolate against human cells, including cancer cells. *Journal of Applied Microbiology,* 89**,** 16-23.

KIROUAC, M., VACHON, V., NOËL, J.-F., GIRARD, F., SCHWARTZ, J.-L. & LAPRADE, R. 2002. Amino acid and divalent ion permeability of the pores formed by the Bacillus thuringiensis toxins Cry1Aa and Cry1Ac in insect midgut brush border membrane vesicles. *Biochimica et Biophysica Acta (BBA) - Biomembranes,* 1561**,** 171-179.

KIROUAC, M., VACHON, V., QUIEVY, D., SCHWARTZ, J.-L. & LAPRADE, R. 2006. Protease Inhibitors Fail To Prevent Pore Formation by the Activated Bacillus thuringiensis Toxin Cry1Aa in Insect Brush Border Membrane Vesicles. *Applied and environmental microbiology,* 72**,** 506-515.

KITADA, S., ABE, Y., MAEDA, T. & SHIMADA, H. 2009. Parasporin-2 requires GPI-anchored proteins for the efficient cytocidal action to human hepatoma cells. *Toxicology,* 264**,** 80-88.

KITADA, S., ABE, Y., SHIMADA, H., KUSAKA, Y., MATSUO, Y., KATAYAMA, H., OKUMURA, S., AKAO, T., MIZUKI, E., KUGE, O., SASAGURI, Y., OHBA, M. & ITO, A. 2006. Cytocidal Actions of Parasporin-2, an Anti-tumor Crystal Toxin from Bacillus thuringiensis. *Journal of Biological Chemistry,* 281**,** 26350-26360.

KLOFT, N., BUSCH, T., NEUKIRCH, C., WEIS, S., BOUKHALLOUK, F., BOBKIEWICZ, W., CIBIS, I., BHAKDI, S. & HUSMANN, M. 2009. Pore-forming toxins activate MAPK p38 by causing loss of cellular potassium. *Biochemical and Biophysical Research Communications,* 385**,** 503-506.

KLOFT, N., NEUKIRCH, C., BOBKIEWICZ, W., VEERACHATO, G., BUSCH, T., VON HOVEN, G., BOLLER, K. & HUSMANN, M. 2010. Pro-autophagic signal induction by bacterial pore-forming toxins. *Medical Microbiology and Immunology,* 199**,** 299-309.

KNAPP, O. S., BRADLEY; POPOFF MICHEL R. 2010. The Aerolysin-Like Toxin Family of Cytolytic, Pore-Forming Toxins. *The Open Toxinology Journal,* 3: 53-68.

KNIGHT, P. J. K., CRICKMORE, N. & ELLAR, D. J. 1994. The receptor for Bacillus thuringiensis CrylA(c) delta-endotoxin in the brush border membrane of the lepidopteran Manduca sexta is aminopeptidase N. *Molecular Microbiology,* 11**,** 429-436.

KNOWLES, B. H. & DOW, J. A. T. 1993. The crystal δ-endotoxins of Bacillus thuringiensis: Models for their mechanism of action on the insect gut. *BioEssays,* 15**,** 469-476.

KNOWLES, B. H. & ELLAR, D. J. 1987. Colloid-osmotic lysis is a general feature of the mechanism of action of Bacillus thuringiensis δ-endotoxins with different insect specificity. *Biochimica et Biophysica Acta (BBA) - General Subjects,* 924**,** 509-518.

KOCH, M. S., WARD, J. M., LEVINE, S. L., BAUM, J. A., VICINI, J. L. & HAMMOND, B. G. 2015. The food and environmental safety of Bt crops. *Frontiers in Plant Science,* 6**,** 283.

KOLLER, C. N., BAUER, L. S. & HOLLINGWORTH, R. M. 1992. Characterization of the pH-mediated solubility of Bacillus thuringiensis var. san diego native δ-endotoxin crystals. *Biochemical and Biophysical Research Communications,* 184**,** 692-699.

KOUMI S, S. R., ARAMAKI T. 1994. Characterization of the calcium-activated chloride channel in isolated guinea-pig hepatocytes. *The Journal of General Physiology,* 104**,** 357-373.

KRISHNAMOORTHY, M., JURAT-FUENTES, J. L., MCNALL, R. J., ANDACHT, T. & ADANG, M. J. 2007. Identification of novel Cry1Ac binding proteins in midgut membranes from Heliothis virescens using proteomic analyses. *Insect Biochemistry and Molecular Biology,* 37**,** 189-201.

KRISHNAN, K., KER, J., MOHAMMED, S. & NADARAJAH, V. 2010. Identification of Glyceraldehyde-3-phosphate dehydrogenase (GAPDH) as a binding protein for a 68-kDa Bacillus thuringiensis parasporal protein cytotoxic against leukaemic cells. *Journal of Biomedical Science,* 17**,** 86.

KRISHNAN, V. 2013. *Investigation of Parasporins, the cytotoxic proteins from the bacterium Bacillus thuringiensis* The degree of Doctor of Philosophy, University of Sussex.

LAEMMLI, U. K. 1970. Cleavage of structural proteins during the assembly of the head of bacteriophage T4. *Nature,* 227**,** 680-5.

LAM, GRACE Y., FATTOUH, R., MUISE, ALEIXO M., GRINSTEIN, S., HIGGINS, DARREN E. & BRUMELL, JOHN H. 2011. Listeriolysin O Suppresses Phospholipase C-Mediated Activation of the Microbicidal NADPH Oxidase to Promote Listeria monocytogenes Infection. *Cell host & microbe,* 10**,** 627-634.

LECADET, M. M., FRACHON, E., DUMANOIR, V. C., RIPOUTEAU, H., HAMON, S., LAURENT, P. & THIÉRY, I. 1999. Updating the H-antigen classification of Bacillus thuringiensis. *Journal of Applied Microbiology,* 86**,** 660-672.

LECKBAND, D. & PRAKASAM, A. 2006. MECHANISM AND DYNAMICS OF CADHERIN ADHESION. *Annual Review of Biomedical Engineering,* 8**,** 259-287.

LEE, D., KATAYAMA, H., AKAO, T., MAEDA, M., TANAKA, R., YAMASHITA, S., SAITOH, H., MIZUKI, E. & OHBA, M. 2001. A 28 kDa protein of the Bacillus thuringiensis serovar shandongiensis isolate 89-T-34-22 induces a human leukemic cell-specific cytotoxicity. *Biochim Biophys Acta,* 1547**,** 57-63.

LEE, J., KOO, N. & MIN, D. B. 2004. Reactive Oxygen Species, Aging, and Antioxidative Nutraceuticals. *Comprehensive Reviews in Food Science and Food Safety,* 3**,** 21-33.

LEE, M. K., WALTERS, F. S., HART, H., PALEKAR, N. & CHEN, J.-S. 2003. The Mode of Action of the Bacillus thuringiensis Vegetative Insecticidal Protein Vip3A Differs from That of Cry1Ab δ-Endotoxin. *Applied and environmental microbiology,* 69**,** 4648-4657.

LESIEUR, C., FRUTIGER, S., HUGHES, G., KELLNER, R., PATTUS, F. & VAN DER GOOT, F. G. 1999. Increased Stability upon Heptamerization of the Pore-forming Toxin Aerolysin. *Journal of Biological Chemistry,* 274**,** 36722-36728.

LI, J., KONI, P. A. & ELLAR, D. J. 1996. Structure of the mosquitocidal δ-endotoxin CytB from Bacillus thuringiensis sp. kyushuensis and implications for membrane pore formation. *Journal of Molecular Biology,* 257**,** 129-152.

LI, J. & YUAN, J. 2008. Caspases in apoptosis and beyond. *Oncogene,* 27**,** 6194-206.

LI, J. D., CARROLL, J. & ELLAR, D. J. 1991. Crystal structure of insecticidal delta-endotoxin from Bacillus thuringiensis at 2.5 A resolution. *Nature,* 353**,** 815-21.

LIANG, Y., PATEL, S. S. & DEAN, D. H. 1995. Irreversible Binding Kinetics of Bacillus thuringiensis CryIA δ-Endotoxins to Gypsy Moth Brush Border Membrane Vesicles Is Directly Correlated to Toxicity. *Journal of Biological Chemistry,* 270**,** 24719-24724.

LILIEN, J. & BALSAMO, J. 2005. The regulation of cadherin-mediated adhesion by tyrosine phosphorylation/dephosphorylation of β-catenin. *Current Opinion in Cell Biology,* 17**,** 459-465.

LIU, G. J., SIMPSON, A. M., SWAN, M. A., TAO, C., TUCH, B. E., CRAWFORD, R. M., JOVANOVIC, A. & MARTIN, D. K. 2003. ATP-sensitive potassium channels induced in liver cells after transfection with insulin cDNA and the GLUT2 transporter regulate glucose-stimulated insulin secretion. *The FASEB journal : official publication of the Federation of American Societies for Experimental Biology,* 17**,** 1682-1684.

LIU, Y.-B. & TABASHNIK, B. E. 1997. Synergism of Bacillus thuringiensis by Ethylenediamine Tetraacetate in Susceptible and Resistant Larvae of Diamondback Moth (Lepidoptera: Plutellidae). *Journal of Economic Entomology,* 90**,** 287-292.

LOCHNER, A. & MOOLMAN, J. A. 2006. The Many Faces of H89: A Review. *Cardiovascular Drug Reviews,* 24**,** 261-274.

LODISH, H. 2008. *Molecular Cell Biology*, W. H. Freeman.

LONI, L., TACCA, M. D. & DANESI, R. 2001. Pharmacogenetics of anticancer drugs in non-Hodgkin lymphomas. *British Journal of Cancer,* 85**,** 1425-1431.

LORENCE, A. 1995. δ-Endotoxins induce cation channels in Spodoptera frugiperda brush border membranes in suspension and in planar lipid bilayers. *FEBS Letters,* 360**,** 217-222.

LOS, F. C., RANDIS, T. M., AROIAN, R. V. & RATNER, A. J. 2013. Role of pore-forming toxins in bacterial infectious diseases. *Microbiol Mol Biol Rev,* 77**,** 173-207.

LOS, F. C. O., KAO, C.-Y., SMITHAM, J., MCDONALD, K. L., HA, C., PEIXOTO, C. A. & AROIAN, R. V. 2011. RAB-5 and RAB-11-dependent vesicle-trafficking pathways are required for plasma membrane repair after attack by bacterial pore-forming toxin. *Cell host & microbe,* 9**,** 147-157.

LU, Z. & XU, S. 2006. ERK1/2 MAP kinases in cell survival and apoptosis. *IUBMB Life,* 58**,** 621-31.

LUO, K., SANGADALA, S., MASSON, L., MAZZA, A., BROUSSEAU, R. & ADANG, M. J. 1997. The Heliothis virescens 170 kDa aminopeptidase functions as "Receptor A" by mediating specific Bacillus thuringiensis Cry1A δ-endotoxin binding and pore formation. *Insect Biochemistry and Molecular Biology,* 27**,** 735-743.

MALHI, H., IRANI, A. N., RAJVANSHI, P., SUADICANI, S. O., SPRAY, D. C., MCDONALD, T. V. & GUPTA, S. 2000. KATP Channels Regulate Mitogenically Induced Proliferation in Primary Rat Hepatocytes and Human Liver Cell Lines: IMPLICATIONS FOR LIVER GROWTH CONTROL AND POTENTIAL THERAPEUTIC TARGETING. *Journal of Biological Chemistry,* 275**,** 26050-26057.

MARTIN, P. A. & TRAVERS, R. S. 1989. Worldwide Abundance and Distribution of Bacillus thuringiensis Isolates. *Applied and environmental microbiology,* 55**,** 2437-2442.

MASSON, L., LU, Y.-J., MAZZA, A., BROUSSEAU, R. & ADANG, M. J. 1995. The CryIA(c) Receptor Purified from Manduca sexta Displays Multiple Specificities. *Journal of Biological Chemistry,* 270**,** 20309-20315.

MCNALL, R. J. & ADANG, M. J. 2003. Identification of novel Bacillus thuringiensis Cry1Ac binding proteins in Manduca sexta midgut through proteomic analysis. *Insect Biochemistry and Molecular Biology,* 33**,** 999-1010.

MEHDIZADEH, S. 1991. Understanding cell toxicology: Principles and practice. E. Walum, K. Stenberg and D. Jenssen. Series in Biochemistry and Biotechnology. Ellis Horwood Ltd.: Chichester, England, 206 pages, £45. (1990). *Cell Biochemistry and Function,* 9**,** 295-295.

MENG, X. J. & WEINMAN, S. A. 1996. cAMP- and swelling-activated chloride conductance in rat hepatocytes. *American Journal of Physiology - Cell Physiology,* 271**,** C112-C120.

MERMELSTEIN, C. S., REBELLO, M. I. L., AMARAL, L. M. & COSTA, M. L. 2003. Changes in cell shape, cytoskeletal proteins and adhesion sites of cultured cells after extracellular Ca2+ chelation. *Brazilian Journal of Medical and Biological Research,* 36**,** 1111-1116.

MIDBOE, E. G., CANDAS, M. & BULLA, J. L. A. 2003. Expression of a midgut-specific cadherin BT-R1 during the development of Manduca sexta larva. *Comparative Biochemistry and Physiology Part B: Biochemistry and Molecular Biology,* 135**,** 125-137.

MILLIKAN, R. A., BISHOP, E. S. & SOCIETY, A. T. 1917. *Elements of Electricity: A Practical Discussion of the Fundamental Laws and Phenomena of Electricity and Their Practical Applications in the Business and Industrial World*, American Technical Society.

MIZUKI, E., OHBA, M., AKAO, T., YAMASHITA, S., SAITOH, H. & PARK, Y. 1999a. Unique activity associated with non-insecticidal Bacillus thuringiensis parasporal inclusions in vitro cell-killing action on human cancer cells. *J Appl Microbiol,* 86**,** 477 - 486.

MIZUKI, E., OHBA, M., AKAO, T., YAMASHITA, S., SAITOH, H. & PARK, Y. S. 1999b. Unique activity associated with non-insecticidal Bacillus thuringiensis parasporal inclusions: in vitro cell-killing action on human cancer cells. *J Appl Microbiol,* 86**,** 477-86.

MIZUKI, E., PARK, Y., SAITOH, H., YAMASHITA, S., AKAO, T., HIGUCHI, K. & OHBA, M. 2000. Parasporin, a human leukaemic cell-recognising parasporal protein of Bacillus thuringiensis. *Clin Diagn Lab Immunol,* 7**,** 625 - 634.

MONETTE, R., POTVIN, L., BAINES, D., LAPRADE, R. & SCHWARTZ, J. L. 1997. Interaction between Calcium Ions and Bacillus thuringiensis Toxin Activity against Sf9 Cells (Spodoptera frugiperda, Lepidoptera). *Applied and environmental microbiology,* 63**,** 440-7.

MOQUIN, D. & CHAN, F. K.-M. 2010. The molecular regulation of programmed necrotic cell injury. *Trends in Biochemical Sciences,* 35**,** 434-441.

MORSE, R. J., YAMAMOTO, T. & STROUD, R. M. 2001. Structure of Cry2Aa Suggests an Unexpected Receptor Binding Epitope. *Structure,* 9**,** 409-417.

MOULE, S. K. & MCGIVAN, J. D. 1990. Regulation of the plasma membrane potential in hepatocytes--mechanism and physiological significance. *Biochim Biophys Acta,* 1031**,** 383-97.

MUELLER, P., RUDIN, D. O., TIEN, H. T. & WESCOTT, W. C. 1963. METHODS FOR THE FORMATION OF SINGLE BIMOLECULAR LIPID MEMBRANES IN AQUEOUS SOLUTION. *The Journal of Physical Chemistry,* 67**,** 534-535.

NADARAJAH, V. D., TING, D., CHAN, K. K., MOHAMED, S. M., KANAKESWARY, K. & LEE, H. L. 2008. Selective cytotoxic activity against leukemic cell lines from mosquitocidal Bacillus thuringiensis parasporal inclusions. *Southeast Asian J Trop Med Public Health,* 39**,** 235-45.

NAGAMATSU, Y., KOIKE, T., SASAKI, K., YOSHIMOTO, A. & FURUKAWA, Y. 1999. The cadherin-like protein is essential to specificity determination and cytotoxic action of the Bacillus thuringiensis insecticidal CryIAa toxin. *FEBS Letters,* 460**,** 385-390.

NAGAMATSU, Y., OKAMURA, S., SAITOU, H., AKAO, T. & MIZUKI, E. 2010. Three Cry Toxins in Two Types from <I>Bacillus thuringiensis</I> Strain M019 Preferentially Kill Human Hepatocyte Cancer and Uterus Cervix Cancer Cells. *Bioscience, Biotechnology, and Biochemistry,* 74**,** 494-498.

NAGAMATSU, Y., TODA, S., YAMAGUCHI, F., OGO, M., KOGURE, M., NAKAMURA, M., SHIBATA, Y. & KATSUMOTO, T. 1998. Identification of Bombyx mori midgut receptor for Bacillus thuringiensis insecticidal CryIA(a) toxin. *Biosci Biotechnol Biochem,* 62**,** 718-26.

NAMGUNG, U. & XIA, Z. 2000. Arsenite-Induced Apoptosis in Cortical Neurons Is Mediated by c-Jun N-Terminal Protein Kinase 3 and p38 Mitogen-Activated Protein Kinase. *The Journal of Neuroscience,* 20**,** 6442-6451.

NEHER, E. & SAKMANN, B. 1976. Single-channel currents recorded from membrane of denervated frog muscle fibres. *Nature,* 260**,** 799-802.

NELSON, K. L., BRODSKY, R. A. & BUCKLEY, J. T. 1999. Channels formed by subnanomolar concentrations of the toxin aerolysin trigger apoptosis of T lymphomas. *Cellular Microbiology,* 1**,** 69-74.

NILES, A. L., MORAVEC, R. A., ERIC HESSELBERTH, P., SCURRIA, M. A., DAILY, W. J. & RISS, T. L. 2007. A homogeneous assay to measure live and dead cells in the same sample by detecting different protease markers. *Analytical Biochemistry,* 366**,** 197-206.

O'BRIEN, J., WILSON, I., ORTON, T. & POGNAN, F. 2000. Investigation of the Alamar Blue (resazurin) fluorescent dye for the assessment of mammalian cell cytotoxicity. *European Journal of Biochemistry,* 267**,** 5421-5426.

OCHOA-CAMPUZANO, C., REAL, M. D., MARTÍNEZ-RAMÍREZ, A. C., BRAVO, A. & RAUSELL, C. 2007. An ADAM metalloprotease is a Cry3Aa Bacillus thuringiensis toxin receptor. *Biochemical and Biophysical Research Communications,* 362**,** 437-442.

OHBA, M., MIZUKI, E. & UEMORI, A. 2009. Parasporin, a new anticancer protein group from Bacillus thuringiensis. *Anticancer Research,* 29**,** 427 - 434.

OKUMURA, S., ISHIKAWA, T., SAITOH, H., AKAO, T. & MIZUKI, E. 2013. Identification of a second cytotoxic protein produced by Bacillus thuringiensis A1470. *Biotechnol Lett,* 35**,** 1889-94.

OKUMURA, S., SAITOH, H., ISHIKAWA, T., INOUYE, K. & MIZUKI, E. 2011. Mode of action of parasporin-4, a cytocidal protein from Bacillus thuringiensis. *Biochimica et Biophysica Acta (BBA) - Biomembranes,* 1808**,** 1476-1482.

OKUMURA, S., SAITOH, H., ISHIKAWA, T., MIZUKI, E. & INOUYE, K. 2008. Identification and characterization of a novel cytotoxic protein, parasporin-4, produced by Bacillus thuringiensis A1470 strain. *Biotechnol Annu Rev,* 14**,** 225-52.

OKUMURA, S., SAITOH, H., ISHIKAWA, T., WASANO, N., YAMASHITA, S., KUSUMOTO, K.-I., AKAO, T., MIZUKI, E., OHBA, M. & INOUYE, K. 2005. Identification of a Novel Cytotoxic Protein, Cry45Aa, from Bacillus thuringiensis A1470 and Its Selective Cytotoxic Activity against Various Mammalian Cell Lines. *Journal of Agricultural and Food Chemistry,* 53**,** 6313-6318.

OKUMURA, S., SAITOH, H., WASANO, N., KATAYAMA, H., HIGUCHI, K., MIZUKI, E. & INOUYE, K. 2006. Efficient solubilization, activation, and purification of recombinant Cry45Aa of Bacillus thuringiensis expressed as inclusion bodies in Escherichia coli. *Protein Expression and Purification,* 47**,** 144-151.

OPOTA, O., GAUTHIER, N. C., DOYE, A., BERRY, C., GOUNON, P., LEMICHEZ, E. & PAURON, D. 2011. Bacillus sphaericus Binary Toxin Elicits Host Cell Autophagy as a Response to Intoxication. *PLoS One,* 6**,** e14682.

PACHECO, S., GÓMEZ, I., ARENAS, I., SAAB-RINCON, G., RODRÍGUEZ-ALMAZÁN, C., GILL, S. S., BRAVO, A. & SOBERÓN, M. 2009. Domain II Loop 3 of Bacillus thuringiensis Cry1Ab Toxin Is Involved in a "Ping Pong" Binding Mechanism with Manduca sexta Aminopeptidase-N and Cadherin Receptors. *Journal of Biological Chemistry,* 284**,** 32750-32757.

PALMA, L., MUÑOZ, D., BERRY, C., MURILLO, J. & CABALLERO, P. 2014a. Bacillus thuringiensis Toxins: An Overview of Their Biocidal Activity. *Toxins,* 6**,** 3296-3325.

PALMA, L., MUÑOZ, D., BERRY, C., MURILLO, J., DE ESCUDERO, I. & CABALLERO, P. 2014b. Molecular and Insecticidal Characterization of a Novel Cry-Related Protein from Bacillus Thuringiensis Toxic against Myzus persicae. *Toxins,* 6**,** 3144.

PARDO-LOPEZ, L., SOBERON, M. & BRAVO, A. 2013a. *Bacillus thuringiensis* insecticidal three-domain Cry toxins: mode of action, insect resistance and consequences for crop protection. *FEMS Microbiol Rev* 37**,** 3-22.

PARDO-LOPEZ, L., SOBERON, M. & BRAVO, A. 2013b. Bacillus thuringiensis insecticidal three-domain Cry toxins: mode of action, insect resistance and consequences for crop protection. *FEMS Microbiol Rev,* 37**,** 3-22.

PARK, Y., GONZÁLEZ-MARTÍNEZ, R. M., NAVARRO-CERRILLO, G., CHAKROUN, M., KIM, Y., ZIARSOLO, P., BLANCA, J., CAÑIZARES, J., FERRÉ, J. & HERRERO, S. 2014. ABCC transporters mediate insect resistance to multiple Bt toxins revealed by bulk segregant analysis. *BMC Biology,* 12**,** 1-15.

PETTERSEN, E. F., GODDARD, T. D., HUANG, C. C., COUCH, G. S., GREENBLATT, D. M., MENG, E. C. & FERRIN, T. E. 2004. UCSF Chimera--a visualization system for exploratory research and analysis. *J Comput Chem,* 25**,** 1605-12.

PEYRONNET, O., NIEMAN, B., GÉNÉREUX, F., VACHON, V., LAPRADE, R. & SCHWARTZ, J.-L. 2002. Estimation of the radius of the pores formed by the Bacillus thuringiensis Cry1C δ-endotoxin in planar lipid bilayers. *Biochimica et Biophysica Acta (BBA) - Biomembranes,* 1567**,** 113-122.

PEYRONNET, O., NOULIN, J. F., LAPRADE, R. & SCHWARTZ, J. L. 2004. Patch-clamp study of the apical membrane of the midgut of Manduca sexta larvae: direct demonstration of endogenous channels and effect of a Bacillus thuringiensis toxin. *J Insect Physiol,* 50**,** 791-803.

PEYRONNET, O., VACHON, V., SCHWARTZ, J. L. & LAPRADE, R. 2001. Ion channels induced in planar lipid bilayers by the Bacillus thuringiensis toxin Cry1Aa in the presence of gypsy moth (Lymantria dispar) brush border membrane. *J Membr Biol,* 184**,** 45-54.

PIGOTT, C. R. & ELLAR, D. J. 2007. Role of Receptors in Bacillus thuringiensis Crystal Toxin Activity. *Microbiology and Molecular Biology Reviews,* 71**,** 255-281.

PITELKA, D. R., TAGGART, B. N. & HAMAMOTO, S. T. 1983. Effects of extracellular calcium depletion on membrane topography and occluding junctions of mammary epithelial cells in culture. *The Journal of Cell Biology,* 96**,** 613-624.

POKUTTA, S., HERRENKNECHT, K., KEMLER, R. & ENGEL, J. 1994. Conformational changes of the recombinant extracellular domain of E-cadherin upon calcium binding. *Eur J Biochem,* 223**,** 1019-26.

POORNIMA, K., SELVANAYAGAM, P. & SHENBAGARATHAI, R. 2010. Identification of native Bacillus thuringiensis strain from South India having specific cytocidal activity against cancer cells. *Journal of Applied Microbiology,* 109**,** 348-354.

POPOFF, M. R. 2011. Epsilon toxin: a fascinating pore-forming toxin. *FEBS Journal,* 278**,** 4602-4615.

PORTA, H., CANCINO-RODEZNO, A., SOBERÓN, M. & BRAVO, A. 2011. Role of MAPK p38 in the cellular responses to pore-forming toxins. *Peptides,* 32**,** 601-606.

QI, H., CHEN, B., LE, X. C. & RONG, J. 2012. Concomitant induction of heme oxygenase-1 attenuates the cytotoxicity of arsenic species from lumbricus extract in human liver HepG2 cells. *Chem Biodivers,* 9**,** 739-54.

QIAN, X., KARPOVA, T., SHEPPARD, A. M., MCNALLY, J. & LOWY, D. R. 2004. E-cadherin-mediated adhesion inhibits ligand-dependent activation of diverse receptor tyrosine kinases. *The EMBO Journal,* 23**,** 1739-1748.

QU, X., YU, J., BHAGAT, G., FURUYA, N., HIBSHOOSH, H., TROXEL, A., ROSEN, J., ESKELINEN, E.-L., MIZUSHIMA, N., OHSUMI, Y., CATTORETTI, G. & LEVINE, B. 2003. Promotion of tumorigenesis by heterozygous disruption of the beclin 1 autophagy gene. *Journal of Clinical Investigation,* 112**,** 1809-1820.

QUASTEL, M. R., SEGEL, G. B. & LICHTMAN, M. A. 1981. The effect of calcium chelation on lymphocyte monovalent cation permeability, transport and concentration. *J Cell Physiol,* 107**,** 165-70.

RAJAGOPAL, R., AGRAWAL, N., SELVAPANDIYAN, A., SIVAKUMAR, S., AHMAD, S. & BHATNAGAR, R. K. 2003. Recombinantly expressed isoenzymic aminopeptidases from Helicoverpa armigera (American cotton bollworm) midgut display differential interaction with closely related Bacillus thuringiensis insecticidal proteins. *Biochemical Journal,* 370**,** 971-978.

RAJAGOPAL, R., SIVAKUMAR, S., AGRAWAL, N., MALHOTRA, P. & BHATNAGAR, R. K. 2002. Silencing of Midgut Aminopeptidase N of Spodoptera litura by Double-stranded RNA Establishes Its Role asBacillus thuringiensis Toxin Receptor. *Journal of Biological Chemistry,* 277**,** 46849-46851.

RASKO, D. A., ALTHERR, M. R., HAN, C. S. & RAVEL, J. 2005. Genomics of the Bacillus cereus group of organisms. *FEMS Microbiol Rev,* 29**,** 303-29.

RATNER, A. J., HIPPE, K. R., AGUILAR, J. L., BENDER, M. H., NELSON, A. L. & WEISER, J. N. 2006. Epithelial Cells Are Sensitive Detectors of Bacterial Pore-forming Toxins. *Journal of Biological Chemistry,* 281**,** 12994-12998.

RAUSELL, C., MUNOZ-GARAY, C., MIRANDA-CASSOLUENGO, R., GOMEZ, I., RUDINO-PINERA, E., SOBERON, M. & BRAVO, A. 2004. Tryptophan spectroscopy studies and black lipid bilayer analysis indicate that the oligomeric structure of Cry1Ab toxin from Bacillus thuringiensis is the membrane-insertion intermediate. *Biochemistry,* 43**,** 166-74.

RIBET, D., HAMON, M., GOUIN, E., NAHORI, M.-A., IMPENS, F., NEYRET-KAHN, H., GEVAERT, K., VANDEKERCKHOVE, J., DEJEAN, A. & COSSART, P. 2010. Listeria monocytogenes impairs SUMOylation for efficient infection. *Nature,* 464**,** 1192-1195.

SABIROV, R. Z., KRASILNIKOV, O. V., TERNOVSKY, V. I. & MERZLIAK, P. G. 1993. Relation between ionic channel conductance and conductivity of media containing different nonelectrolytes. A novel method of pore size determination. *Gen Physiol Biophys,* 12**,** 95-111.

SACHDEVA, M., SACHDEVA, N., PAL, M., GUPTA, N., KHAN, I. A., MAJUMDAR, M. & TIWARI, A. 2015. CRISPR/Cas9: molecular tool for gene therapy to target genome and epigenome in the treatment of lung cancer. *Cancer Gene Ther,* 22**,** 509-517.

SAITOH, H., OKUMURA, S., ISHIKAWA, T., AKAO, T., MIZUKI, E. & OHBA, M. 2006. Investigation of a Novel Bacillus thuringiensis Gene Encoding a Parasporal Protein, Parasporin-4, That Preferentially Kills Human Leukemic T Cells. *Bioscience, Biotechnology, and Biochemistry,* 70**,** 2935-2941.

SALAMA, H. S., FODA, M. S. & SHARABY, A. 1985. Potential of some chemicals to increase the effectiveness of Bacillus thuringiensis Berl. against Spodoptera littoralis (Boisd.). *Zeitschrift für Angewandte Entomologie,* 100**,** 425-433.

SANGADALA, S., WALTERS, F. S., ENGLISH, L. H. & ADANG, M. J. 1994. A mixture of Manduca sexta aminopeptidase and phosphatase enhances Bacillus thuringiensis insecticidal CryIA(c) toxin binding and 86Rb(+)-K+ efflux in vitro. *Journal of Biological Chemistry,* 269**,** 10088-92.

SARKAR, A., HESS, D., MONDAL, H. A., BANERJEE, S., SHARMA, H. C. & DAS, S. 2009. Homodimeric Alkaline Phosphatase Located at Helicoverpa armigera Midgut, a Putative Receptor of Cry1Ac Contains α-GalNAc in Terminal Glycan Structure as Interactive Epitope. *Journal of Proteome Research,* 8**,** 1838-1848.

SCHERRER, R. & GERHARDT, P. 1971. Molecular sieving by the Bacillus megaterium cell wall and protoplast. *Journal of Bacteriology,* 107**,** 718-735.

SCHNEPF, E., CRICKMORE, N., VAN RIE, J., LERECLUS, D., BAUM, J., FEITELSON, J., ZEIGLER, D. R. & DEAN, D. H. 1998. Bacillus thuringiensis and Its Pesticidal Crystal Proteins. *Microbiology and Molecular Biology Reviews,* 62**,** 775-806.

SCHOENMAKERS, T. J., VISSER, G. J., FLIK, G. & THEUVENET, A. P. 1992. CHELATOR: an improved method for computing metal ion concentrations in physiological solutions. *Biotechniques,* 12**,** 870-4.

SCHULTZ, S. G. & SOLOMON, A. K. 1961. Determination of the Effective Hydrodynamic Radii of Small Molecules by Viscometry. *The Journal of General Physiology,* 44**,** 1189-1199.

SCHWARTZ, J.-L., GARNEAU, L., MASSON, L. & BROUSSEAU, R. 1991. Early response of cultured lepidopteran cells to exposure to δ-endotoxin from Bacillus thuringiensis: Involvement of calcium and anionic channels. *Biochimica et Biophysica Acta (BBA) - Biomembranes,* 1065**,** 250-260.

SCHWARTZ, J.-L., LU, Y.-J., SÖHNLEIN, P., BROUSSEAU, R., LAPRADE, R., MASSON, L. & ADANG, M. J. 1997. Ion channels formed in planar lipid bilayers by Bacillus thuringiensis toxins in the presence of Manduca sexta midgut receptors. *FEBS Letters,* 412**,** 270-276.

SCHWARTZ, J. L., GARNEAU, L., SAVARIA, D., MASSON, L., BROUSSEAU, R. & ROUSSEAU, E. 1993. Lepidopteran-specific crystal toxins from Bacillus thuringiensis form cation- and anion-selective channels in planar lipid bilayers. *J Membr Biol,* 132**,** 53-62.

SEGEL, G. B., SIMON, W., LICHTMAN, A. H. & LICHTMAN, M. A. 1981. The activation of lymphocyte plasma membrane (Na,K)-ATPase by EGTA is explained better by zinc than calcium chelation. *J Biol Chem,* 256**,** 6629-32.

SHER, D., FISHMAN, Y., ZHANG, M., LEBENDIKER, M., GAATHON, A., MANCHEÑO, J.-M. & ZLOTKIN, E. 2005. Hydralysins, a New Category of β-Pore-forming Toxins in Cnidaria. *Journal of Biological Chemistry,* 280**,** 22847-22855.

SHITOMI, Y., HAYAKAWA, T., HOSSAIN, D. M., HIGUCHI, M., MIYAMOTO, K., NAKANISHI, K., SATO, R. & HORI, H. 2006. A Novel 96-kDa Aminopeptidase Localized on Epithelial Cell Membranes of Bombyx mori Midgut, Which Binds to Cry1Ac Toxin of Bacillus thuringiensis. *Journal of Biochemistry,* 139**,** 223-233.

SIEVERS, F., WILM, A., DINEEN, D., GIBSON, T. J., KARPLUS, K., LI, W., LOPEZ, R., MCWILLIAM, H., REMMERT, M., SÖDING, J., THOMPSON, J. D. & HIGGINS, D. G. 2011. Fast, scalable generation of high-quality protein multiple sequence alignments using Clustal Omega. *Molecular Systems Biology,* 7.

SIMONS, K. & TOOMRE, D. 2000. Lipid rafts and signal transduction. *Nat Rev Mol Cell Biol,* 1**,** 31-39.

SIMPSON, R. M. & NEWCOMB, R. D. 2000. Binding of Bacillus thuringiensis δ-endotoxins Cry1Ac and Cry1Ba to a 120-kDa aminopeptidase-N of Epiphyas postvittana purified from both brush border membrane vesicles and baculovirus-infected Sf9 cells. *Insect Biochemistry and Molecular Biology,* 30**,** 1069-1078.

SIPOS, T. & MERKEL, J. R. 1970. Effect of calcium ions on the activity, heat stability, and structure of trypsin. *Biochemistry,* 9**,** 2766-2775.

SLATIN, S. L., ABRAMS, C. K. & ENGLISH, L. 1990a. Delta-endotoxins form cation-selective channels in planar lipid bilayers. *Biochemical and Biophysical Research Communications,* 169**,** 765-772.

SLATIN, S. L., ABRAMS, C. K. & ENGLISH, L. 1990b. Delta-endotoxins form cation-selective channels in planar lipid bilayers. *Biochem Biophys Res Commun,* 169**,** 765-72.

SOBERÓN, M., LÓPEZ-DÍAZ, J. A. & BRAVO, A. 2013. Cyt toxins produced by Bacillus thuringiensis: A protein fold conserved in several pathogenic microorganisms. *Peptides,* 41**,** 87-93.

SOBERÓN, M., PARDO-LÓPEZ, L., LÓPEZ, I., GÓMEZ, I., TABASHNIK, B. E. & BRAVO, A. 2007. Engineering Modified Bt Toxins to Counter Insect Resistance. *Science,* 318**,** 1640-1642.

SPENCER, C. P. 1958. The Chemistry of ethylenediamine Tetra-Acetic acid in sea water. *Journal of the Marine Biological Association of the United Kingdom,* 37**,** 127-144.

SPRANG, S. R. 1997. G PROTEIN MECHANISMS:Insights from Structural Analysis. *Annual Review of Biochemistry,* 66**,** 639-678.

STRINGARIS, A. K., GEISENHAINER, J., BERGMANN, F., BALSHUSEMANN, C., LEE, U., ZYSK, G., MITCHELL, T. J., KELLER, B. U., KUHNT, U., GERBER, J., SPREER, A., BAHR, M., MICHEL, U. & NAU, R. 2002. Neurotoxicity of pneumolysin, a major pneumococcal virulence factor, involves calcium influx and depends on activation of p38 mitogen-activated protein kinase. *Neurobiol Dis,* 11**,** 355-68.

STUMPFF, F., BONDZIO, A., EINSPANIER, R. & MARTENS, H. 2007. Effects of the Bacillus thuringiensis Toxin Cry1Ab on Membrane Currents of Isolated Cells of the Ruminal Epithelium. *Journal of Membrane Biology,* 219**,** 37-47.

TAM, C., IDONE, V., DEVLIN, C., FERNANDES, M. C., FLANNERY, A., HE, X., SCHUCHMAN, E., TABAS, I. & ANDREWS, N. W. 2010. Exocytosis of acid sphingomyelinase by wounded cells promotes endocytosis and plasma membrane repair. *J Cell Biol,* 189**,** 1027-38.

TANAKA, S., MIYAMOTO, K., NODA, H., JURAT-FUENTES, J. L., YOSHIZAWA, Y., ENDO, H. & SATO, R. 2013. The ATP-binding cassette transporter subfamily C member 2 in

Bombyx mori larvae is a functional receptor for Cry toxins from Bacillus thuringiensis. *FEBS Journal,* 280**,** 1782-1794.

TERRA, W. R. & FERREIRA, C. 1994. Insect digestive enzymes: properties, compartmentalization and function. *Comparative Biochemistry and Physiology Part B: Comparative Biochemistry,* 109**,** 1-62.

TESMER, J. J. G., SUNAHARA, R. K., JOHNSON, R. A., GOSSELIN, G., GILMAN, A. G. & SPRANG, S. R. 1999. Two-Metal-Ion Catalysis in Adenylyl Cyclase. *Science,* 285**,** 756-760.

THASTRUP, O., CULLEN, P. J., DROBAK, B. K., HANLEY, M. R. & DAWSON, A. P. 1990. Thapsigargin, a tumor promoter, discharges intracellular Ca2+ stores by specific inhibition of the endoplasmic reticulum Ca2+-ATPase. *Proceedings of the National Academy of Sciences of the United States of America,* 87**,** 2466-2470.

THOMAS, W. E. & ELLAR, D. J. 1983a. Bacillus thuringiensis var israelensis crystal δ-endotoxin: Effects on insect and mammalian cells in vitro and in vivo. *Journal of Cell Science,* Vol. 60**,** 181-197.

THOMAS, W. E. & ELLAR, D. J. 1983b. Mechanism of action of Bacillus thuringiensis var israelensis insecticidal δ-endotoxin. *FEBS Letters,* 154**,** 362-368.

TSUDA, Y., NAKATANI, F., HASHIMOTO, K., IKAWA, S., MATSUURA, C., FUKADA, T., SUGIMOTO, K. & HIMENO, M. 2003. Cytotoxic activity of Bacillus thuringiensis Cry proteins on mammalian cells transfected with cadherin-like Cry receptor gene of Bombyx mori (silkworm). *Biochemical Journal,* 369**,** 697-703.

TSUZUKI, K., KIMURA, K., FUJII, N., YOKOSAWA, N., INDOH, T., MURAKAMI, T. & OGUMA, K. 1990. Cloning and complete nucleotide sequence of the gene for the main component of hemagglutinin produced by Clostridium botulinum type C. *Infection and Immunity,* 58**,** 3173-3177.

UHLÉN, M., FAGERBERG, L., HALLSTRÖM, B. M., LINDSKOG, C., OKSVOLD, P., MARDINOGLU, A., SIVERTSSON, Å., KAMPF, C., SJÖSTEDT, E., ASPLUND, A., OLSSON, I., EDLUND, K., LUNDBERG, E., NAVANI, S., SZIGYARTO, C. A.-K., ODEBERG, J., DJUREINOVIC, D., TAKANEN, J. O., HOBER, S., ALM, T., EDQVIST, P.-H., BERLING, H., TEGEL, H., MULDER, J., ROCKBERG, J., NILSSON, P., SCHWENK, J. M., HAMSTEN, M., VON FEILITZEN, K., FORSBERG, M., PERSSON, L., JOHANSSON, F., ZWAHLEN, M., VON HEIJNE, G., NIELSEN, J. & PONTÉN, F. 2015. Tissue-based map of the human proteome. *Science,* 347.

UVERSKY, V. N. P. E. A. 2007. *Methods in protein structure and stability analysis,* New York, Nova Biomedical Books.

VACHON, V., LAPRADE, R. & SCHWARTZ, J. L. 2012. Current models of the mode of action of Bacillus thuringiensis insecticidal crystal proteins: a critical review. *J Invertebr Pathol,* 111.

VADLAMUDI, R. K., JI, T. H. & BULLA, L. A. 1993. A specific binding protein from Manduca sexta for the insecticidal toxin of Bacillus thuringiensis subsp. berliner. *Journal of Biological Chemistry,* 268**,** 12334-40.

VADLAMUDI, R. K., WEBER, E., JI, I., JI, T. H. & BULLA, L. A. 1995. Cloning and Expression of a Receptor for an Insecticidal Toxin of Bacillus thuringiensis. *Journal of Biological Chemistry,* 270**,** 5490-5494.

VALAITIS, A. P., MAZZA, A., BROUSSEAU, R. & MASSON, L. 1997. Interaction analyses of Bacillus thuringiensis Cry1A toxins with two aminopeptidases from gypsy moth midgut brush border membranes. *Insect Biochemistry and Molecular Biology,* 27**,** 529-539.

VAN RIE, J., JANSENS, S., HÖFTE, H., DEGHEELE, D. & VAN MELLAERT, H. 1989. Specificity of Bacillus thuringiensisδ-endotoxins. *European Journal of Biochemistry,* 186**,** 239-247.

VILAS-BOAS, G. T., PERUCA, A. P. & ARANTES, O. M. 2007. Biology and taxonomy of Bacillus cereus, Bacillus anthracis, and Bacillus thuringiensis. *Can J Microbiol,* 53**,** 673-87.

VINCZE, T., POSFAI, J. & ROBERTS, R. J. 2003. NEBcutter: a program to cleave DNA with restriction enzymes. *Nucleic Acids Research,* 31**,** 3688-3691.

WALTERS, F. S., SLATIN, S. L., KULESZA, C. A. & ENGLISH, L. H. 1993. Ion Channel Activity of N-Terminal Fragments from CryIA(c) Delta-Endotoxin. *Biochemical and Biophysical Research Communications,* 196**,** 921-926.

WANG, G., WU, K., LIANG, G. & GUO, Y. 2005a. Gene cloning and expression of cadherin in midgut of Helicoverpa armigera and its Cry1A binding region. *Sci China C Life Sci,* 48**,** 346-56.

WANG, P., ZHANG, X. & ZHANG, J. 2005b. Molecular characterization of four midgut aminopeptidase N isozymes from the cabbage looper, Trichoplusia ni. *Insect Biochemistry and Molecular Biology,* 35**,** 611-620.

WARREN, G. W., KOZIEL, M. G., MULLINS, M. A., NYE, G. J., CARR, B., DESAI, N. M., KOSTICHKA, K., DUCK, N. B. & ESTRUCH, J. J. 1998. Auxiliary proteins for enhancing the insecticidal activity of pesticidal proteins. Google Patents.

WILSON, I. A., NIMAN, H. L., HOUGHTEN, R. A., CHERENSON, A. R., CONNOLLY, M. L. & LERNER, R. A. 1984. The structure of an antigenic determinant in a protein. *Cell,* 37**,** 767-778.

WONDERGEM, R., GONG, W., MONEN, S. H., DOOLEY, S. N., GONCE, J. L., CONNER, T. D., HOUSER, M., ECAY, T. W. & FERSLEW, K. E. 2001. Blocking swelling-activated chloride current inhibits mouse liver cell proliferation. *The Journal of Physiology,* 532**,** 661-672.

WOOD, E. J. 1983. Molecular cloning. A laboratory manual by T Maniatis, E F Fritsch and J Sambrook. pp 545. Cold Spring Harbor Laboratory, New York. 1982. $48 ISBN 0-87969-136-0. *Biochemical Education,* 11**,** 82-82.

WOOD, G. S. & WARNKE, R. 1981. Suppression of endogenous avidin-binding activity in tissues and its relevance to biotin-avidin detection systems. *J Histochem Cytochem,* 29**,** 1196-204.

WOOD, H. G. & BARDEN, R. E. 1977. Biotin Enzymes. *Annual Review of Biochemistry,* 46**,** 385-413.

WU, J. H., HONG, L.-C., TSAI, Y.-Y., CHEN, H.-W., CHEN, W.-X. & WU, T. S. 2006. Mitogen-activated protein kinase (MAPK) signalling pathways in HepG2 cells infected with a virulent strain of Klebsiella pneumoniae. *Cellular Microbiology,* 8**,** 1467-1474.

XIE, R., ZHUANG, M., ROSS, L. S., GOMEZ, I., OLTEAN, D. I., BRAVO, A., SOBERON, M. & GILL, S. S. 2005. Single Amino Acid Mutations in the Cadherin Receptor from Heliothis virescens Affect Its Toxin Binding Ability to Cry1A Toxins. *Journal of Biological Chemistry,* 280**,** 8416-8425.

YAMASHITA, S., AKAO, T., MIZUKI, E., SAITOH, H., HIGUCHI, K., PARK, Y. S., KIM, H. S. & OHBA, M. 2000. Characterization of the anti-cancer-cell parasporal proteins of a Bacillus thuringiensis isolate. *Can J Microbiol,* 46**,** 913-9.

YAMASHITA, S., KATAYAMA, H., SAITOH, H., AKAO, T., PARK, Y. S., MIZUKI, E., OHBA, M. & ITO, A. 2005. Typical Three-Domain Cry Proteins of Bacillus thuringiensis Strain A1462 Exhibit Cytocidal Activity on Limited Human Cancer Cells. *Journal of Biochemistry,* 138**,** 663-672.

YAOI, K., NAKANISHI, K., KADOTANI, T., IMAMURA, M., KOIZUMI, N., IWAHANA, H. & SATO, R. 1999. cDNA cloning and expression of Bacillus thuringiensis Cry1Aa toxin binding 120 kDa aminopeptidase N from Bombyx mori1. *Biochimica et Biophysica Acta (BBA) - Gene Structure and Expression,* 1444**,** 131-137.

ZARUBIN, T. & HAN, J. 2005. Activation and signaling of the p38 MAP kinase pathway. *Cell Res,* 15**,** 11-18.

ZHANG, K. & KAUFMAN, R. J. 2004. Signaling the Unfolded Protein Response from the Endoplasmic Reticulum. *Journal of Biological Chemistry,* 279**,** 25935-25938.

ZHANG, R., HUA, G., ANDACHT, T. M. & ADANG, M. J. 2008. A 106-kDa aminopeptidase is a putative receptor for Bacillus thuringiensis Cry11Ba toxin in the mosquito Anopheles gambiae. *Biochemistry,* 47**,** 11263-11272.

ZHANG, X., CANDAS, M., GRIKO, N. B., ROSE-YOUNG, L. & BULLA, L. A. 2005. Cytotoxicity of Bacillus thuringiensis Cry1Ab toxin depends on specific binding of the toxin to the cadherin receptor BT-R1 expressed in insect cells. *Cell Death Differ,* 12**,** 1407-1416.

ZHANG, X., CANDAS, M., GRIKO, N. B., TAUSSIG, R. & BULLA, L. A. 2006. A mechanism of cell death involving an adenylyl cyclase/PKA signaling pathway is induced by the Cry1Ab toxin of Bacillus thuringiensis. *Proceedings of the National Academy of Sciences,* 103**,** 9897-9902.

ZHUANG, M., OLTEAN, D. I., GÓMEZ, I., PULLIKUTH, A. K., SOBERÓN, M., BRAVO, A. & GILL, S. S. 2002. Heliothis virescens and Manduca sextaLipid Rafts Are Involved in Cry1A Toxin Binding to the Midgut Epithelium and Subsequent Pore Formation. *Journal of Biological Chemistry,* 277**,** 13863-13872.

ZIMMERMANN, G., ZHOU, D. & TAUSSIG, R. 1998. Mutations Uncover a Role for Two Magnesium Ions in the Catalytic Mechanism of Adenylyl Cyclase. *Journal of Biological Chemistry,* 273**,** 19650-19655.